UiT The Arctic University of Norway

Faculty of Health Sciences
Department of Clinical Medicine

Molecular aspects of high-risk neuroblastoma and novel therapeutic opportunities

Øyvind Holsbø Hald

A dissertation for the degree of Philosophiae Doctor February 2020

Table of Contents

Acknowledgements 1
Summary 2
List of papers 3
Abbreviations 4
1 Introduction 7
1.1 Neuroblastoma 8
1.1.1 Histology and cellular distinctions 10
1.1.2 Staging and risk stratification of neuroblastomas 10
1.1.3 Current treatment protocols 12
1.2 Genetic aberrations in neuroblastoma 14
1.2.1 The *MYCN* oncogene 14
1.2.2 Chromosomal abnormalities 21
1.2.3 Chromothripsis 22
1.2.4 *ALK* 22
1.2.5 *TERT*, Ras-MAPK and *TP53* 23
1.2.6 Genetic factors predisposing to neuroblastoma 24
1.3 Ribosome biogenesis 24
1.3.1 Inhibitors of ribosome biogenesis: Quarfloxin and CX-5461 26
1.3.2 Other drugs targeting ribosome biogenesis 27
1.4 MicroRNAs 28
1.4.1 MiRNAs in cancer and neuroblastoma 30
1.4.2 MiR-193b 31
1.5 Exosomes 32
1.5.1 The function of exosomes and exosomal miRNAs in cancer 34
2 Aims 36
3 Materials and methods 37
3.1 Bioinformatics using the R2: Genomics Analysis and Visualization Platform 37
3.2 Neuroblastoma xenografts: 37
3.3 XCelligence 38
3.4 Preparation of exosome-free medium and production and isolation of exosomes 39
3.5 Nanosight Tracking Analysis 39
3.6 MiRNA qPCR panels and IPA pathway analysis 40
4 Results 41

Paper 1 41
Paper 2 41
Paper 3 42
5 Discussion 43
5.1 Inhibition of ribosomal RNA production as neuroblastoma therapy 43
5.1.1 Suppression of MycN expression and the role of *TP53* 43
5.1.2 The role of DNA damage 45
5.1.3 Clinical use of quarfloxin and CX-5461 46
5.2 MicroRNA-based neuroblastoma therapy: Overexpression of microRNA-193b 46
5.2.1 MiR-193b –"mechanism of action" 47
5.2.2 Potential of miR-193b as an anti-neuroblastoma drug 48
5.3 The microRNA content of *MYCN*-amplified neuroblastoma exosomes 49
5.3.1 Functional effects of exosomal miRNAs 49
5.3.2 The biomarker potential of exosomal miRNAs 50
6 Conclusions 51
7 References 52

Acknowledgements

The work of this thesis was conducted at the Department of Pediatrics, University Hospital of North Norway (UNN), at the Pediatric Research Group, Department of Clinical Medicine, Faculty of Health Sciences, UiT The Arctic University of Norway and at The Childhood Cancer Research Unit, Department of Women's and Children's Health, Karolinska Institutet (KI), Stockholm. The work was made possible with financial support from the Northern Norway Regional Health Authority (Helse Nord RHF), The Norwegian Childhood Cancer Society (Barnekreftforeningen) and the Simon Fougner Hartmann Family Foundation.

I would like to express my gratitude to several people. First, to my main supervisor, Christer Einvik: Thank you for your excellent guidance. You have introduced me to the world of molecular biology research and I have highly valued your support and mentorship through all phases of this work, and for giving me the freedom to pursue my own ideas. Also, thank you for the many great experiences outside of work, including ski mountaineering, grouse hunting and discussions on the brewing of fine ales. To my co-supervisor, Trond Flægstad: Thank you for taking me in as a member of the research group when I was early in my medical studies. Your ever-present encouragement, good spirits and kindness, has provided a great work environment. My co-supervisor Baldur Sveinbjörnsson: Thank you for great advice and experimental help, your broad knowledge of the cancer research field has been a great source of help to me. To Bjørn Helge Haug, thank you for many fun times and for teaching me the value of never giving up. Cecilie Løkke, thank you for teaching me how to work in a lab, you are always patient, helpful and kind and your company at work has been great. Lotte Olsen, thank you for our collaboration, your contributions and inputs have been highly appreciated: also, thank you for your careful read-through of this thesis. Thanks to Sarah Roth for letting me contribute to her project. Thanks to present and former member of the Pediatric Research Group: Swapnil Bhavsar and Peter Utnes. Also, special thanks to Simon Kranz for strengthening the connection between the Pediatric Oncology Unit at UNN and our lab. To John Inge Johnsen: Thank you for welcoming me into the lab at KI and for all your help. Also thanks to Per Kogner and Lotta Elfmann at KI. Gabriel Gallo-Oller, thank you for your help with the xenograft work, and thank you for all the good times in Stockholm. Thanks to my friends and fellow alumni of The Medical Student Research Program, Sigurd Hald and Marcus Roalsø for many meaningful discussions.

I am grateful to my parents, Laila and Morten, for their encouragements throughout my medical studies and PhD work. Also, thanks to my two sisters and their families.

Finally, thanks to my girlfriend, Liv, for your support in the final stages of this work and for filling my life outside work with meaning.

Øyvind Holsbø Hald Tromsø, February 2020

Summary

Neuroblastoma is a highly heterogeneous cancer of childhood. High-risk disease has a poor prognosis with survival rates below 50% and the majority of cured patients will experience treatment related late effects. Evidently, better therapy is needed for this group of patients. Increasing the knowledge of the molecular biology underlying neuroblastoma is essential to devise new treatment strategies for this disease.

High-risk neuroblastomas are frequently *MYCN*-amplified and *MYCN*-amplification is correlated to enlarged nucleoli due to increased ribosome biogenesis. *MYCN*-amplification leads to overexpression of the MycN protein, which has been shown to upregulate the transcription of genes involved in ribosome biogenesis in neuroblastoma cells. Deregulated microRNA (miRNA)-expression patterns have emerged as a feature of *MYCN*-amplified and high-risk neuroblastoma. Also, in recent years, exosomes, have been shown to provide a way for secretion of miRNAs, but the exosomal miRNA-content in neuroblastoma has not been characterized previously.

We aimed at identifying novel aspects of the molecular biology underpinning high-risk neuroblastomas with an emphasis on *MYCN*, ribosomal RNA and miRNAs. In **paper 1,** we mined several publically available RNA expression datasets of neuroblastoma tumor tissue and found that high-stage and *MYCN* overexpressing neuroblastomas had increased expression levels of genes involved in ribosome biogenesis. We proceeded to investigate the effects of small molecular inhibitors of ribosome biogenesis (RNA polymerase I inhibitors), quarfloxin and CX-5461, in preclinical models. We found that these compounds were cytotoxic to *MYCN*-amplified neuroblastoma cells and led to p53 dependent apoptosis or cell cycle arrest. Both compounds caused DNA damage and reduced the protein levels of MycN**.** CX-5461 also repressed the growth of neuroblastoma xenografts established in nude mice. In **paper 2,** we characterized the tumor suppressor miRNA-193b in neuroblastoma and we found that this miRNA was expressed at a low level in primary tumors. Overexpression of miR-193b in neuroblastoma cell lines induced growth arrest and cell death through direct targeting of *CCND1*, *MCL1* and *MYCN*. In **paper 3,** we investigated the miRNA-content of exosomes derived from two different *MYCN*-amplified neuroblastoma cell lines and discovered that exosomes contained a distinct profile of miRNAs predicted to regulate pathways important in cancer.

In conclusion, the discoveries presented in this thesis, can hopefully lead to future novel therapies and biomarkers in high-risk neuroblastoma.

List of papers

Paper 1: Inhibitors of ribosome biogenesis repress the growth of *MYCN*-amplified neuroblastoma, **Hald ØH**, Olsen L, Gallo-Oller G, Elfman LHM, Løkke C, Kogner P, Sveinbjörnsson B, Flægstad T, Johnsen JI, Einvik C. Oncogene 38**,** 2800–2813 (2019) doi:10.1038/s41388-018-0611-7

Paper 2: MicroRNA-193b-3p represses neuroblastoma cell growth via downregulation of *Cyclin D1*, *MCL-1* and *MYCN*. Roth SA, **Hald ØH**, Fuchs S, Løkke C, Mikkola I, Flægstad T, Schulte J and, Einvik C. Oncotarget. 2018*; 9*: 18160-18179.

Paper 3: Exosome-like Extracellular Vesicles from *MYCN*-amplified Neuroblastoma Cells Contain Oncogenic miRNAs. Haug BH, **Hald ØH**, Utnes P, Roth SA, Løkke C, Flægstad T, Einvik C. Anticancer Res. 2015 May;35(5):2521-30.

Abbreviations

5'-ETS	5' external transcribed spacer
ABCC1	ATP Binding Cassette Subfamily C Member 1 (MRP1; Multidrug Resistance-Associated Protein 1)
ALK	Anaplastic Lymphoma Kinase
ALL	Acute Lymphoblastic Leukemia
AML	Acute Myeloid Leukemia
ATM	Ataxia Telangiectasia Mutated
ATR	Ataxia Telangiectasia And Rad3-Related Protein
ATRX	Alpha Thalassemia/Mental Retardation Syndrome X-linked
BAK	Bcl-2 homologous Antagonist Killer
BAX	Bcl-2-associated X protein
Bcl-2	B-cell lymphoma 2
BH3	Bcl-2 Homology Domain 3
Bim	Bcl-2 Interacting Mediator Of Cell Death
BRCA1/2	Breast And Ovarian Cancer Susceptibility Protein 1/2
CAMTA1	Calmodulin Binding Transcription Activator 1
CASZ1	Castor Zinc Finger 1
CCND1	Cyclin D
CD	Cluster of Differentiation
CDC42	Cell Division Cycle 42
CDK	Cyclin-dependent Kinase
CHD5	Chromodomain Helicase DNA Binding Protein 5
Chk1/2	Checkpoint Kinase 1/2
CLL	Chronic Lymphocytic Leukemia
CRKL	CRK Like Proto-Oncogene, Adaptor Protein
DGCR8	DiGeorge Syndrome Critical Region Gene 8
DKK3	Dickkopf WNT Signaling Pathway Inhibitor 3
DNA	Deoxyribonucleic acid
DUSP6	Dual Specificity Phosphatase 6 (MKP3; Mitogen-Activated Protein Kinase Phosphatase 3)
E-Box	Enhancer box
ERK1/2	Extracellular Signal-Regulated Kinase 1/2
ETS1	ETS Proto-Oncogene 1, Transcription Factor
EZH2	Enhancer Of Zeste 2 Polycomb Repressive Complex 2 Subunit
FBXW7	F-Box And WD Repeat Domain Containing 7
Foxn1	Forkhead Box N1 (mouse)
G-CSF	Granulocyte-Colony Stimulating Factor
GD2	Ganglioside GD2
GLS2	Glutaminase 2
GN	Ganglioneuroma
GNB	Ganglioneuroblastoma
GSK3β	Glycogen Synthase Kinase-3 Beta
H2A.X	H2A.X Variant Histone
HuD	Hu-antigen D

HUVEC	Human Umbilical Vein Endothelial Cells
Huwe1	HECT, UBA And WWE Domain Containing E3 Ubiquitin Protein Ligase 1
IDRFs	Image Defined Risk Factors
Indel	Insertion or deletion
INRG	International Neuroblastoma Risk Group
ITGA5	Integrin Subunit Alpha 5
KIF1B	Kinesin Family Member 1B
KLF4	Kruppel Like Factor 4
KRAS	Kirsten Rat Sarcoma Viral Proto-Oncogene
Let-7	Lethal-7
LIF	LIF (Leukemia Inhibitory Factor), interleukin 6 family cytokine
LIN28B	Lin-28 (Abnormal Cell Lineage Protein 28) Homolog B
LOH	Loss of Heterozygosity
MAPK	Mitogen-activated protein kinase
MAPK	Mitogen-activated protein kinase
Max	Myc-associated factor X
MCM7	Minichromosome Maintenance Complex Component 7
MDM2	Mouse Double Minute 2 Homolog
MET	MET Proto-Oncogene, Receptor Tyrosine Kinase
miRNA	MicroRNA
Miz-1	Myc-Interacting Zinc Finger Protein 1
MNA	*MYCN*-amplification
mRNA	Messenger RNA
MSRA	Methionine Sulfoxide Reductase A
MYC	V-Myc Avian Myelocytomatosis Viral Oncogene Homolog
MYCL	V-Myc Avian Myelocytomatosis Viral Oncogene Lung Carcinoma Derived Homolog
MYCN	V-Myc Avian Myelocytomatosis Viral Oncogene Neuroblastoma Derived Homolog
NGFR	Nerve Growth Factor Receptor (p75NTR)
nt	Nucleotides
NTRK1	Neurotrophic Receptor Tyrosine Kinase 1 (TrkA; Tropomyosin receptor kinase A)
ODC1	Ornithine Decarboxylase 1
$p14^{ARF}$	Protein p14 alternate reading frame
p21	Protein p21
p40	40-kDa protein complex
PLAU	Urokinase-Type Plasminogen Activator
PLK1	Polo Like Kinase 1
POU5F1	POU Class 5 Homeobox 1 (Oct3/4; Octamer-Binding Protein 3/4)
pre-miRNA	Precursor miRNA
pri-miRNA	Primary miRNA
PTK2	Protein tyrosine kinase 2 (FAK; Focal Adhesion Kinase)
Puma	p53-Upregulated Modulator Of Apoptosis
RAN	Ras-Related Nuclear Protein
Ras	Rat sarcoma
RB1	Retinoblastoma 1
RISC	RNA-Induced Silencing Complex

RNA	Ribonucleic Acid
RRN3	RRN3 homolog, RNA polymerase I transcription factor
rRNA	Ribosomal RNA
SMAD3	Mothers Against Decapentaplegic Homolog 3
SNV	Single-nucleotide variant
SP-1/3	Specificity Protein 1/3
SRC	Proto-Oncogene Tyrosine-Protein Kinase Src
TAp63	Isoform encoded by *TP63* (tumor protein p63)
TERF1	Telomeric Repeat Binding Factor 1
TERT	Telomerase Reverse Transcriptase
TGFβ	Transforming Growth Factor Beta
TGM2	Transglutaminase 2
TLR8	Toll-like receptor 8
TP53	Tumor Protein p53
tRNA	Transfer RNA
TSG101	Tumor Susceptibility 101
VEGF	Vascular endothelial growth factor
wt	Wild type

1 Introduction

Pediatric malignancies are rare and account for less than 1% of cancers, with approximately 150 new cases in Norway per year (1). Substantial progress with regards to the survival of pediatric cancer patients has been made over the last 5 decades and today 5-year survival rates exceeds 80% (2). In spite of this, cancer is the second leading cause of death for individuals below 14 years of age in industrialized countries, and in Europe more than 6000 children and adolescents will die from cancer each year (3). In recent years, there has been little or no improvement to the outcomes for difficult-to-treat pediatric cancers with the worst prognosis, including acute myelogenous leukemia, high-risk neuroblastomas, sarcomas and some brain tumors (3, 4). In addition, a substantial proportion of childhood cancer survivors will experience various late effects from their cancer therapy in the months and years after completed treatment (5). For these reasons, novel treatments are needed, both to increase the cure rate of pediatric cancers and to increase the "quality of cure" by reducing the therapy related toxicities.

The causes of childhood cancers are largely unknown, however exposure to high-dose radiation or prior chemotherapy, are accepted as strong external risk factors (6). Some cancer predisposition syndromes may cause malignant disease in childhood, such as Li-Fraumeni (germline *TP53* mutations) and familial retinoblastoma (germline *RB1* mutations) (7). With the increased availability of high-throughput sequencing technologies in recent years, pathogenic germline mutations in cancer predisposition genes have been discovered in a significant proportion pediatric cancers, see section 1.2.

Childhood cancer differs from malignancies in adults in several ways. In contrast to pediatric cancers, specific risk factors are known for several cancers in adults (8). Furthermore, the majority (>90%) of adult cancers are carcinomas (i.e. arising from the epithelial linings of the body), while epithelial derived cancers constitute a minority of the cancers diagnosed in children (9). Cancer development in adults typically happens over several decades, whereas childhood cancers can have a very short latency period (9). This difference in latency is reflected by the findings of large-scale sequencing studies, which have shown that pediatric cancers have a much lower mutational burden as compared to adult neoplasms (8).

The most common malignancy of childhood is leukemia, followed by various tumors of the central nervous system, see figure 1. Also, a large group of childhood cancers consists of embryonal tumors. These are tumors where the putative cell of origin partakes in normal development during embryogenesis and arise in tissues, which are non-self renewing in adults. In order to populate and generate the organs of the body, there is a requirement for tightly regulated phases of embryonal cell

division and subsequent exit from the cell cycle for terminal differentiation. Embryonal tumors are thought to arise from immature cells not exiting this proliferative phase and failing to undergo normal differentiation (10). Thus, these tumors can be looked upon as disorders of normal development.

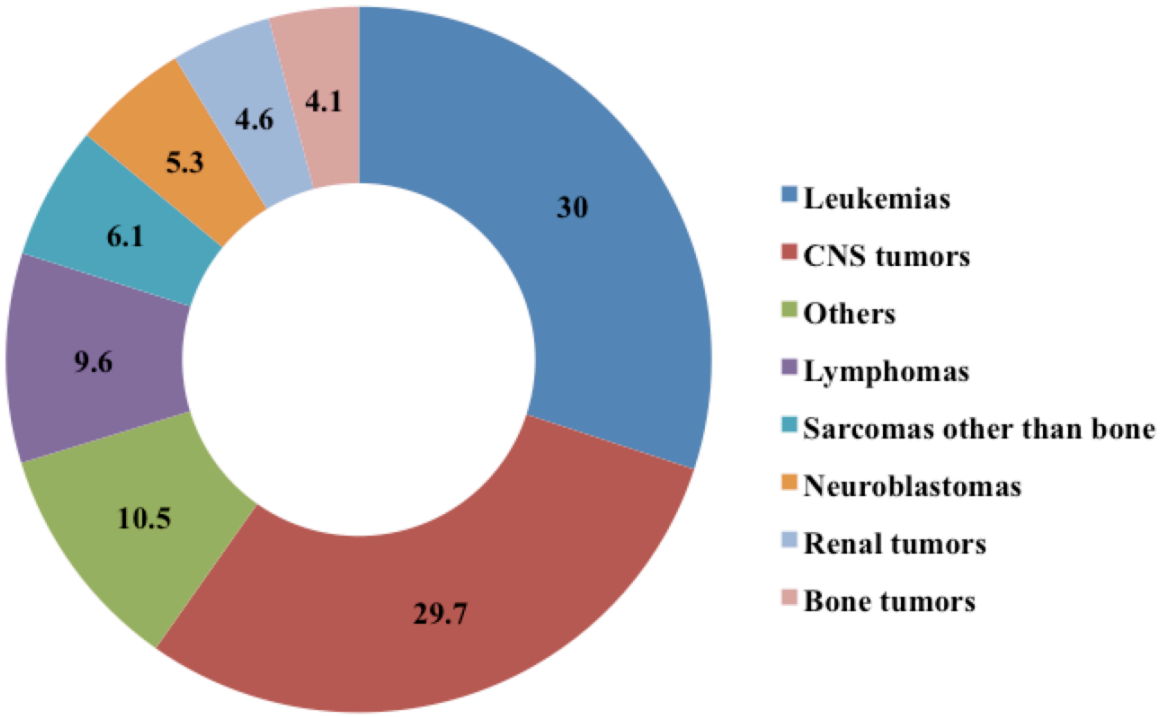

Figure 1. The frequency (%) of different childhood cancers of the 4563 children <15 years of age diagnosed with cancer in Norway 1985-2017 (11). The group "others" comprises retinoblastomas, liver tumors, gonadal tumors, trophoblastic tumors, germinal cell tumors, carcinomas, melanomas and other/unspecified tumors.

1.1 Neuroblastoma

Neuroblastoma is the most frequent cancer diagnosed in the first year of life, and is the most common extracranial solid tumor in children (12). It is an embryonal tumor arising from immature cells of the sympatho-adrenal lineage of the neural crest failing to undergo terminal differentiation and maintaining a proliferative phenotype (13). The developmental origin of neuroblastoma is reflected in the anatomical distributions of primary tumors, which can form anywhere along the sympathetic chains (figure 2). The most common site of primary tumors is the adrenal medulla (65%), but tumors can also occur in the sympathetic ganglia of the chest (20%), neck (5%), and pelvis (5%) (14).

Figure 2. The anatomical distribution of neuroblastic tumors (black and grey). Tumors are seen in the adrenal medulla and along the sympathetic chains. Edited from (15), with permission.

Neuroblastoma accounts for about 7% of pediatric cancers and 15% of oncology deaths below the age of 15 (16). In spite of this disproportionate relationship between morbidity and mortality, a hallmark of neuroblastoma is its extreme heterogeneity. Tumors in low-risk patients have an excellent prognosis with survival rates approaching 100% (17). These patients can often be cured with minimal therapy. In fact, a subset of neuroblastomas have the remarkable capability of decreasing in size or disappearing completely without therapeutic intervention, even in presence of metastatic disease (18). Neuroblastoma has the highest rate of spontaneous regression of all cancers and a substantial proportion of low-risk neuroblastomas will spontaneously regress or differentiate into tumors with benign histopathological features (19). In the other end of the spectrum, high-risk neuroblastoma patients have a poor prognosis. Despite dose-intensive, multimodal treatment including major surgery, chemotherapy with autologous stem cell rescue, ionizing radiation, immunotherapy and treatment with differentiation inducing agents, the 5-year survival rate of high-risk neuroblastoma patients is below 50% (17). Most of the high-risk patients will respond well to the initial therapy, but 50% will relapse with tumors refractory to the presently available therapy (20). Currently, there is no curative approach for patients with recurrent tumors, and today relapsed neuroblastoma is typically fatal. Also, a study has shown that approximately 95% of the patients who are cured of high-risk neuroblastoma experience therapy-related late effects with complications including hearing loss, endocrine dysfunction, infertility, musculoskeletal problems, cardiac and pulmonary problems and secondary neoplasms (21). The poor survival of high-risk patients and the high frequency of late-effects in those who are cured underscore the imminent need for better and less toxic treatment options for this patient group.

1.1.1 Histology and cellular distinctions

Tumors of neuroblastic origin are classified by the International Neuroblastoma Pathology Classification (INPC) (22). This classification takes into account the degree of differentiation of the tumor cells (primitive neuroblasts, maturing neuroblasts, and ganglion cells) and the Schwann-type stromal cells (Schwannian-blasts and mature Schwann cells), and the distribution between these two cell types within the tumor. Tumors are classified as ganglioneuromas, ganglioneuroblastomas or neuroblastomas. The three phenotypes constitute a continuum where ganglioneuromas have a Schwannian-rich stroma with the most differentiated tumor cells, while neuroblastomas consists mainly of undifferentiated malignant cells and a Schwannian-poor stroma. The histological features are important for risk stratifying neuroblastomas (see section 1.1.2).

Neuroblastoma cell lines have been shown to consist of three phenotypically distinct cell types, namely N-type (neuroblastic), S-type (non-neuronal, substrate adherent) and I-type (intermediate between N- and S-type), reviewed in (23). The cell types have distinct morphologies and patterns of growth. N-type cells typically have short neuritic extensions and adhere more strongly to other cells than to the substrate of the growth vessel. S-type cells are large flat cells without neurites. N-type and S-type cells have different biochemical markers. N-type cells express enzymes and receptors, which are present in developing neuroblasts and neurofilaments L, M and H. S-type cells have Schwannian/melanocytic phenotypes with absence of neuronal markers, and produce epidermal growth factor, fibronectin and intermediary filament vimentin. I-type cells have morphological and biochemical features of both cell types. N-type and S-type cells can transdifferentiate into each other. A recent study showed that most neuroblastomas contain two distinct tumor cell types with divergent gene expression profiles, termed adrenergic and mesenchymal (24). Studies of isogenic pairs of patient derived neuroblastoma cell lines showed that the adrenergic and mesenchymal differentiation states were due to distinct super-enhancer-associated transcription factor networks working within each cell type. This was also shown in subclones of the SK-N-SH neuroblastoma cell line; The N-type SH-SY5Y and S-type SH-EP2 cell clones conformed to the adrenergic and mesenchymal cell types, respectively. Cells of the mesenchymal phenotype were inherently more resistant to chemotherapy *in vitro* as compared with adrenergic type cells and mesenchymal type cells were enriched in post-treatment and relapsed tumors, showing a potential clinical relevance of these two differentiation states.

1.1.2 Staging and risk stratification of neuroblastomas

Neuroblastomas are staged according to the International Neuroblastoma Risk Group Staging System (INRGSS) (25, 26). This staging system takes into account various pre-treatment image defined risk factors (IDRFs; table 1), which correlate with the ability to achieve complete surgical resection of the

primary tumor. The IDRFs are in turn combined with the presence or absence of metastatic disease to assign patients to a specific INRG stage (table 2). INRG stage is finally combined with patient age, histological features of the tumor and specific molecular markers in order to place the patient in a specific risk group: low-risk, intermediate- or high-risk, see table 3 (26).

Anatomical region	Image Defined Risk Factor
Neck	Tumor encasing carotid and/or vertebral artery and/or internal jugular vein Tumor extending to base of skull Tumor compressing the trachea
Cervico-thoracic junction	Tumor encasing brachial plexus roots Tumor encasing subclavian vessels and/or vertebral and/or carotid artery Tumor compressing the trachea
Thorax	Tumor encasing the aorta and/or major branches Tumor compressing the trachea and/or principal bronchi Lower mediastinal tumor, infiltrating the costovertebral junctions between T9 and T12
Thoraco-abdominal	Tumor encasing the aorta and/or the vena cava
Abdomen/pelvis	Tumor infiltrating the porta hepatis and/or the hepatoduodenal ligament Tumor encasing branches of the superior mesenteric artery at the mesenteric root Tumor encasing the origin of the coeliac axis and/or of the superior mesenteric artery Tumor invading one or both renal pedicles Tumor encasing the aorta and/or vena cava Tumor encasing the iliac vessels Pelvic tumor crossing the sciatic notch
Intraspinal infiltration whatever the location provided that	More than 1/3 of the spinal canal in the axial plane is invaded and/or the perimedullary leptomeningeal spaces are not visible and/or the spinal cord signal is abnormal
Infiltration of adjacent organs/structures	Pericardium, diaphragm, kidney, liver, duodenal-pancreatic block and mesentery
Ipsilateral tumor extension within two body compartments	Neck-chest, chest-abdomen, abdomen-pelvis
Conditions to be recorded but not considered IDRFs (various anatomical locations)	Multifocal primary tumors Pleural effusion, with or without malignant cells Ascites, with or without malignant cells

Table 1. IDRFs in neuroblastoma, adapted from (25).

INRG Stage	Description
L1	Localized tumor not involving vital structures defined by the list of image-defined risk factors and confined to one body compartment.
L2	Locoregional tumor with presence of one or more image-defined risk factors.
M	Distant metastatic disease (except stage MS).
MS	Metastatic disease in children younger than 18 months with metastases confined to skin, liver and/or bone.

Table 2. INRG stages, adapted from (25)

INRG Stage	Age (months)	Histologic Category	Grade of Tumor Differentiation	*MYCN*	11q Aberration	Ploidy	Pretreatment Risk Group
L1/L2		GN maturing; GN intermixed					A Very low
L1		Any, except GN maturing or GN intermixed		NA			B Very low
				Amp			K High
L2	< 18	Any, except GN maturing or GN intermixed		NA	No		D Low
					Yes		G Intermediate
	≥ 18	GNB nodular; neuroblastoma	Differentiating	NA	No		E Low
					Yes		
			Poorly differentiated or undifferentiated	NA			H Intermediate
				Amp			N High
M	< 18			NA		Hyperdiploid	F Low
	< 12			NA		Diploid	I Intermediate
	12 to < 18			NA		Diploid	J Intermediate
	< 18			Amp			O High
	≥ 18						P High
MS	<18			NA	No		C Very low
					Yes		Q High
				Amp			R High

Table 3. INRG risk groups, adapted from (26).

1.1.3 Current treatment protocols

Neuroblastoma is treated with different protocols according to the INRG risk group of the patient. Norwegian patients are included in clinical trials run by the International Society of Paediatric Oncology Europe Neuroblastoma (SIOPEN) group, see the following two sections. Also, over the last decade a number of smaller clinical trials aiming to identify novel treatments, including targeted therapy, in neuroblastoma have been initiated, some of which are reviewed in (27).

1.1.3.1 Low- and intermediate-risk

Low-risk and intermediate-risk neuroblastoma patients are enrolled in the LINES protocol study (ClinicalTrials.gov identifier: NCT01728155). Patients with the lowest risk are typically observed with follow-up imaging studies due to high rates of spontaneous regression. Intermediate-risk patients will receive various combinations of chemotherapy, radiotherapy and 13-*cis* retinoic acid differentiation inducing treatment.

1.1.3.2 High-risk neuroblastoma treatment

High-risk neuroblastoma patients are currently being enrolled in the High-risk Neuroblastoma Study 1.8 of SIOPEN (ClinicalTrials.gov identifier: NCT01704716). The high-risk protocol consists of three phases; induction, consolidation and maintenance (figure 3). The current induction treatment uses a rapid COJEC regimen. COJEC consists of chemotherapeutic agents cisplatin, vincristine, carboplatin, etoposide and cyclophosphamide. Patients receive supportive treatment with G-CSF to prevent febrile neutropenia. After induction, patients proceed to consolidation therapy beginning with surgical removal of remaining tumor tissue, followed by myeloablative chemotherapy (Busulfan and Melphalan; BuMel) with peripheral blood stem cell rescue and radiotherapy to the site of the primary tumor. At the end of consolidation therapy, patients will receive treatment for minimal residual disease (MRD) consisting of immunotherapy with anti-GD2 antibody (14.18/CHO) with or without the addition of Interleukin-2 (IL-2) and differentiation therapy with 13-*cis* retinoic acid.

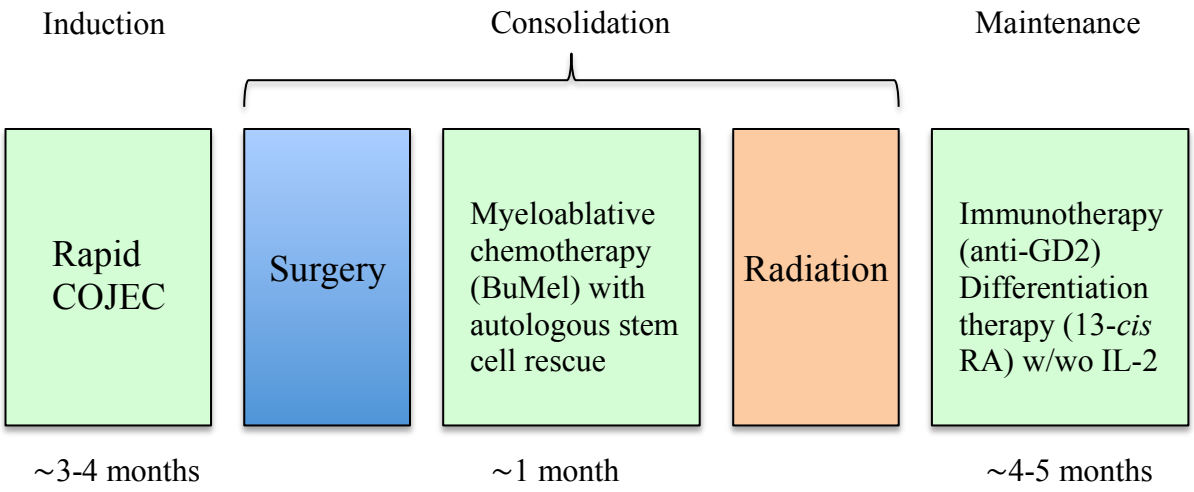

Figure 3. Overview of the timeline for the current high-risk neuroblastoma protocol (1.8) from SIOPEN.

1.2 Genetic aberrations in neuroblastoma

In recent years, our understanding of the genetic underpinnings of pediatric cancer has greatly increased due to large genome wide studies of both tumor tissue and germline. Sequencing of constitutional DNA has revealed that 7-12% of pediatric cancer patients harbor pathogenic or probably pathogenic germline mutations in cancer susceptibility genes (28-31). Most of the germline variants are in genes related to DNA repair mechanisms. Somatic mutations are on average rare in childhood cancers when compared with adults. One study has shown that pediatric cancers on average had 14 times less (coding SNVs and indels) per megabase (Mb) than tumors from adults (0.13 vs. 1.8 mutations per Mb) (31). In spite of the general paucity of somatic mutations, large-scale sequencing efforts across different types of childhood cancer have identified clinically relevant subtypes, increased our knowledge of the drivers of these diseases, and have shown that up to 50% of pediatric cancers harbor genetic events that are potentially druggable (31, 32).

Neuroblastomas generally have a low number of somatic mutations, with a median exonic mutation frequency of 0.60 per Mb (33). However, there are several well characterized recurrent genetic aberrations in neuroblastoma, many of which have well established correlations to prognosis.

1.2.1 The *MYCN* oncogene

Genomic amplification of the *MYCN* gene is a recurrent genetic abnormality in neuroblastoma and is associated with a poor outcome. Due to its clinical importance and central role in this thesis, this section is dedicated to *MYCN*. Thereafter follows descriptions of other recurrent genetic aberrations and genetic predisposition to neuroblastoma (section 1.2.2-1.2.6).

1.2.1.1 Discovery

The road to discovery of cellular proto-oncogenes was paved by pioneering work on avian sarcoma viruses (ASV), which cause tumors in chickens. In 1976 it was shown that the transforming gene in ASV (v-Src) shared homology with DNA present in normal avian cells (34). The homologous DNA in the normal cells was found to be the *SRC* (c-Src) gene, and the term proto-oncogene was coined to describe the normal cellular precursors of transforming viral oncogenes. The *MYC* (c-Myc) gene was found in 1982 as a cellular homolog to the viral myelocytomatosis gene (v-Myc) (35). *MYCN* was subsequently discovered in neuroblastoma cell lines by two different research groups in 1983 as amplified DNA with partial homology to *MYC* and v-Myc (36, 37).

1.2.1.2 Function

The *MYCN* gene encodes the MycN protein and belongs to the MYC family of proto-oncogenes, which also consists of family members *MYC* and *MYCL*, encoding the c-Myc and L-Myc proteins, respectively (38). MycN, like the two other MYC family proteins is a transcription factor containing an N-terminal transactivation domain and C-terminal nuclear localization signal and basic-region/helix-loop-helix/leucine-zipper (bHLHZip) motif. The bHLHZip is involved in protein dimerization and MycN forms a dimer complex with the protein Max (39). This heterodimer activates the transcription of target genes by binding to consensus E-Box sequences (5'-CANNTG-3') in the promoter regions of a wide variety of genes (40). In addition to activating gene transcription, MycN can act as a direct transcriptional repressor in complex with transcription factors Miz-1 and SP-1 (41). MycN can also repress genes indirectly through upregulation of miRNAs, see section 1.4.1. The genes transcribed or repressed by MycN are crucial regulators of processes vital to cellular fate and survival, including differentiation, apoptosis, growth and proliferation (42), see also table 4.

The Myc proteins are frequently overexpressed in cancer. When expressed at high levels in neuroblastoma, MycN leads to a global amplification of transcription through binding active regulatory elements at high affinity canonical E-boxes (5'-CACGTG-3') in promoter regions and to low affinity non-canonical promoter and enhancer E-boxes (43). The ability to increase global transcription, was first shown for c-Myc, which also invades enhancers and promoters of actively transcribed genes when overexpressed (44).

Gene	Function	Regulation by MycN	Mechanism	Reference
ABCC1	Drug efflux	Upregulated	Direct, promoter E-box (luciferase based assay, EMSA)	(45)
ALK	RTK, proliferation	Upregulated	Direct, promoter E-box (ChIP)	(46)
DKK3	Inhibitor of Wnt signaling	Downregulated	Indirect, target of MycN activated miR-92a	(47)
DUSP6	Phosphatase targeting ERK	Downregulated	Direct by SIRT1/Sp-1/MycN complex at *DUSP6* (MKP3) promoter (ChIP)	(48)
EZH2	Histone methylation, gene repression	Upregulated	Direct, promoter E-box (ChIP)	(49)
GLS2	Glutaminolysis	Upregulated	Direct, E-box in intron 1 (ChIP)	(50)
KLF4	Pluripotency signaling	Upregulated	Direct, promoter E-box (ChIP)	(51)
LIF	Inhibitor of angiogenesis, pluripotency signaling.	Contradictory; down- and upregulated	Downregulation: Direct (luciferase based assay). Upregulation: Direct, promoter E-box (ChIP)	(51, 52)
LIN28B	Inhibitor of *MYCN* targeting Let7 miRNA family	Upregulated	Direct, promoter E-box (ChIP)	(53)
MDM2	Negative regulator of p53	Upregulated	Direct, promoter E-box (ChIP)	(54)
MYCN	Transcription factor	Upregulated	Direct, E-box in intron 1 (ChIP)	(55)
NGFR	Neuronal differentiation, NGF signaling	Downregulated	Direct, recruitment of HDAC1 to Miz-1/Sp-1/MycN complex at *NGFR* promoter (ChIP)	(41)
NTRK1	Neuronal differentiation, NGF signaling	Downregulated	Direct, recruitment of HDAC1 to Miz-1/Sp-1/MycN complex at *NTRK1* promoter (ChIP)	(41)
ODC1	Polyamine biosynthesis	Upregulated	Direct, promoter E-box (ChIP)	(56)
PLK1	Trigger of G2/M transition	Upregulated	Direct, promoter E-box (ChIP)	(57)
POU5F1	Pluripotency signaling	Upregulated	Direct, distal enhancer region E-box (ChIP)	(58)
TERT	Telomere maintenance	Upregulated	Direct, promoter E-box (ChIP)	(59)
TGM2	Neuronal differentiation	Downregulated	Direct, recruitment of HDAC1 to Sp-1/MycN complex at *TGM2* (TG2) promoter (ChIP)	(60)
TP53	Cell cycle arrest, apoptosis	Upregulated	Direct, promoter E-box (ChIP)	(61)

Table 4. A selection of genes regulated by MycN, their cellular function and proposed mechanism of regulation.

1.2.1.3 Regulation

MYCN is subject to tight regulation at the transcriptional, translational and post-translational levels. *MYCN* expression is directly stimulated through the binding of the transcription factor Oct4 to the *MYCN* proximal promoter (58). E2F and SP1/SP3 transcription factors can also activate *MYCN* transcription through direct activation of the *MYCN* promoter (62, 63). Also, it has been shown that *MYCN* transcription is the subject of positive auto-regulation, by recruitment of MycN to E-Box motifs found in intron 1 of *MYCN* (55). TGFβ can repress the expression of *MYCN* in neuroblastoma through interaction with E2F binding sites (62). A recent study showed that the p53 family tumor suppressor TAp63 directly repressed *MYCN* transcription through binding exon 1 of *MYCN* (64).

The *MYCN* mRNA can be stabilized through RNA-binding proteins recruited to AU-rich elements in the *MYCN* 3'UTR, including E3 ubiquitin ligase MDM2, p40 and HuD (65-67). *MYCN* transcripts are also subject to miRNA-mediated repression through direct interaction of specific miRNAs with the *MYCN* 3'UTR, including miR-34a, Let-7 and miR-101 (68).

The stability of MycN is regulated by proteins affecting the phosphorylation status of amino acids threonine 58 (Thr58) and serine 62 (Ser62) in the MycN protein sequence. Both epitopes are present in c-Myc and are important for post-translational control of c-Myc protein stability as well (69). Phosphorylation of Ser62 stabilizes MycN and kinases implicated in phosphorylating this epitope include CDK1 and ERK1/2 (48, 70). Thr58 phosphorylation recruits the E3 ubiquitin ligase FBXW7, which ubiqutinates MycN, leading to proteasomal degradation (71). Thr58 phosphorylation is carried out by GSK3β and requires a priming phosphorylation of Ser62. MycN levels are also regulated by factors affecting of FBXW7 stability. One study showed that Plk1 destabilized FBXW7 through direct interaction and that pharmacological inhibition of Plk1 reduced the half-life of MycN by nearly 50% in MNA neuroblastoma cell lines Kelly and BE(2)-C (57). A similar effect on MycN half-life was found after depleting Aurora kinase A in MNA neuroblastoma cells (72). In this study, Aurora kinase A was shown to directly interact with both MycN and FBXW7, leading to an inhibition of FBXW7-mediated proteolysis of MycN. In addition to FBXW7, the E3 ubiquitin ligase Huwe1 can also destabilize MycN through polyubiquitination thereby targeting it for degradation in the proteasome (73).

1.2.1.4 Physiological expression and role in development

MYCN expression is important during normal development, both to induce proliferation during organogenesis and to inhibit premature terminal differentiation. Mice with a targeted homozygous disruption of *Mycn*, die between 10.5 and 12.5 days of gestation, with defective development of several organs, including the heart and cranial and spinal ganglia (74). Most of these defects were consistent with a reduction of embryonal cell proliferation, and not the onset of differentiation. In

another study, targeted *Mycn* knockout in mouse neuronal progenitor cells, led to a 2-fold shrinkage of brain mass and increased neuronal differentiation, underscoring the important role of MycN during the formation of nervous tissue (75). In humans, heterozygous loss-of-function *MYCN* variants in the germline results in Feingold syndrome 1, a developmental disorder characterized by microcephaly, dysmorphic facial features, atresias of the gastrointestinal tract, digital anomalies and learning disabilities (76). This syndrome also demonstrates the importance of *MYCN* during normal development. The physiological expression of *MYCN* is generally absent or very low in adult human tissues (42). A comparison of the expression of *MYCN* in various normal tissues and neuroblastoma is shown in figure 4.

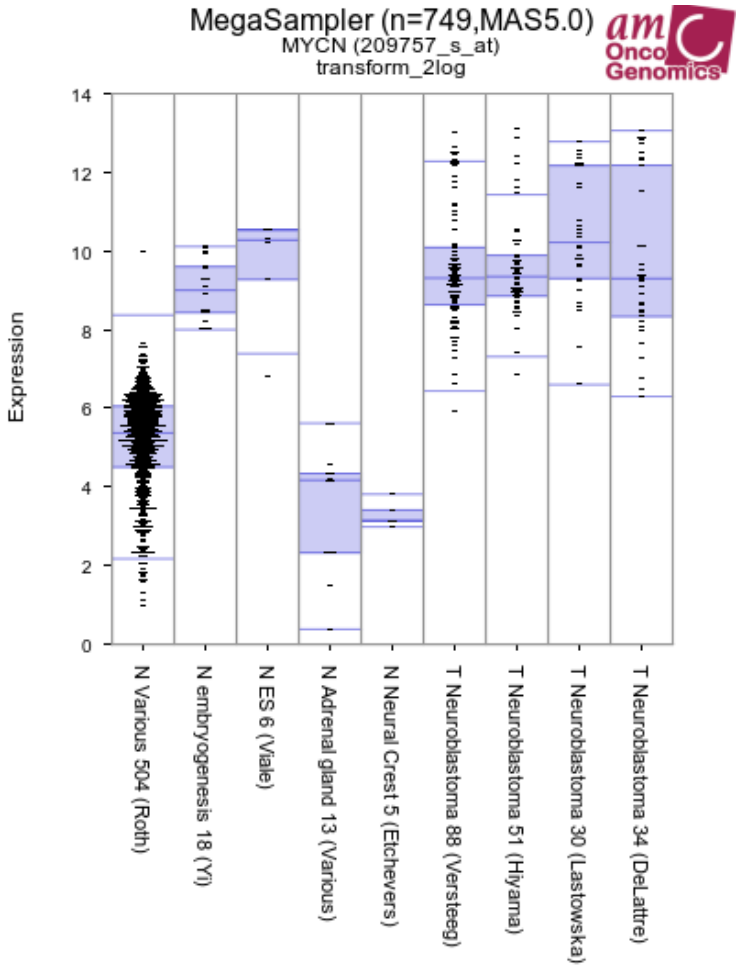

Figure 4. Expression (2log) of *MYCN* transcripts across various datasets of normal human tissues and 4 datasets with tumor tissue from human neuroblastomas. The graph was generated using the MegaSampler across datasets function in the R2: Genomics Analysis and Visualization Platform (r2.amc.nl) with the following normal datasets: N Various 504 (90 distinct tissue types), N embryogenesis 18 (normal human embryos, week 4-9 of development), N ES 6 (neuronal embryonic stem cell rosettes) N Adrenal gland 13 (human adrenal gland tissue), N Neural Crest 5 (human neural crest tissue 26-32 days post fertilization). The following neuroblastoma datasets were included: T Neuroblastoma 88 (Versteeg), T Neuroblastoma 51 (Hiyama), T Neuroblastoma 30 (Lastowska) and T Neuroblastoma 34 (DeLattre), these data sets have expression data from 88, 51, 30 and 34 tumors, respectively.

1.2.1.5 *MYCN* and neuroblastoma

MYCN-amplification (MNA) is present in about 20% of neuroblastomas at diagnosis, and is likely the best described molecular biomarker for risk-stratification of patients (77, 78). When MNA occurs, the neuroblastoma cells contain more than the two copies of the *MYCN* gene normally present in a cell. On the cytogenetic level, MNA manifests as double minute chromosomes (DMs) or as homogenously staining intra-chromosomal regions (HSRs) (79). DMs appear as numerous chromatin bodies in a cytogenetic preparation, these bodies replicate and are therefore "double" in metaphase. HSRs are integrated into chromosomes and are identified in metaphase preparations after chromosomal banding and appear as diffusely staining regions. At the outset, it is thought that *MYCN* becomes amplified as DMs, and this genetic lesion can either persist or the DMs can become linearly integrated into chromosomes to form HSRs (80). It has previously been suggested that MNA is an intrinsic biological property of a subset of aggressive neuroblastomas and that tumors without amplification will rarely if ever develop this aberration (81). However, a recent study comparing the mutational landscape of primary and relapsed neuroblastomas, demonstrated a *de novo* amplification of the *MYCN* locus in one patient at relapse with a non-MNA primary tumor (82).

Copy number of the *MYCN* gene in MNA neuroblastoma is typically 50 to 400 hundred copies per cell and this corresponds with high levels of *MYCN* transcripts and overexpression of the MycN protein (83). The capacity of *MYCN* to act as a bona fide oncogene has been demonstrated by its ability to induce neoplastic transformation of cultured mammalian cells grown *in vitro* (84, 85). Also, it has been shown that sympatho-adrenal restricted overexpression of the human *MYCN* gene (expressed from the tyrosine hydroxylase or dopamine-β-hydroxylase promoters), leads to spontaneous development of neuroblastomas in transgenic mice, demonstrating an *in vivo* functional role of *MYCN* in neuroblastoma tumorigenesis (86, 87). Transgenic zebrafish expressing human *MYCN* under the control of the dopamine-β-hydroxylase promoter also develop neuroblastomas (88). In addition, a recent study demonstrated that enforced overexpression of MycN led to transformation of primary mouse neural crest cells and induced neuroblastomas (89). These tumors showed an accurate morphological phenotype as compared with human neuroblastomas, and also demonstrated molecular aberrations commonly observed in MNA tumors, including 17q gain and 1p36 loss of heterozygosity (LOH).

1.2.1.6 Clinical impact of *MYCN*-amplification

MNA categorizes patients as high-risk, regardless of INRG stage (see table 3). Since 1985 it has been clear that MNA leads to a poor prognosis and rapid tumor progression in neuroblastoma patients (77). The overall probability of survival for patients with MNA is substantially lower than those with non-MNA tumors (figure 5). High *MYCN* levels also correlates with invasive and metastatic behavior (90). Also, aggressive neuroblastomas without MNA often have elevated expression levels of *MYC* signature genes, underscoring the central role of MYC signaling in high-risk neuroblastoma (91, 92).

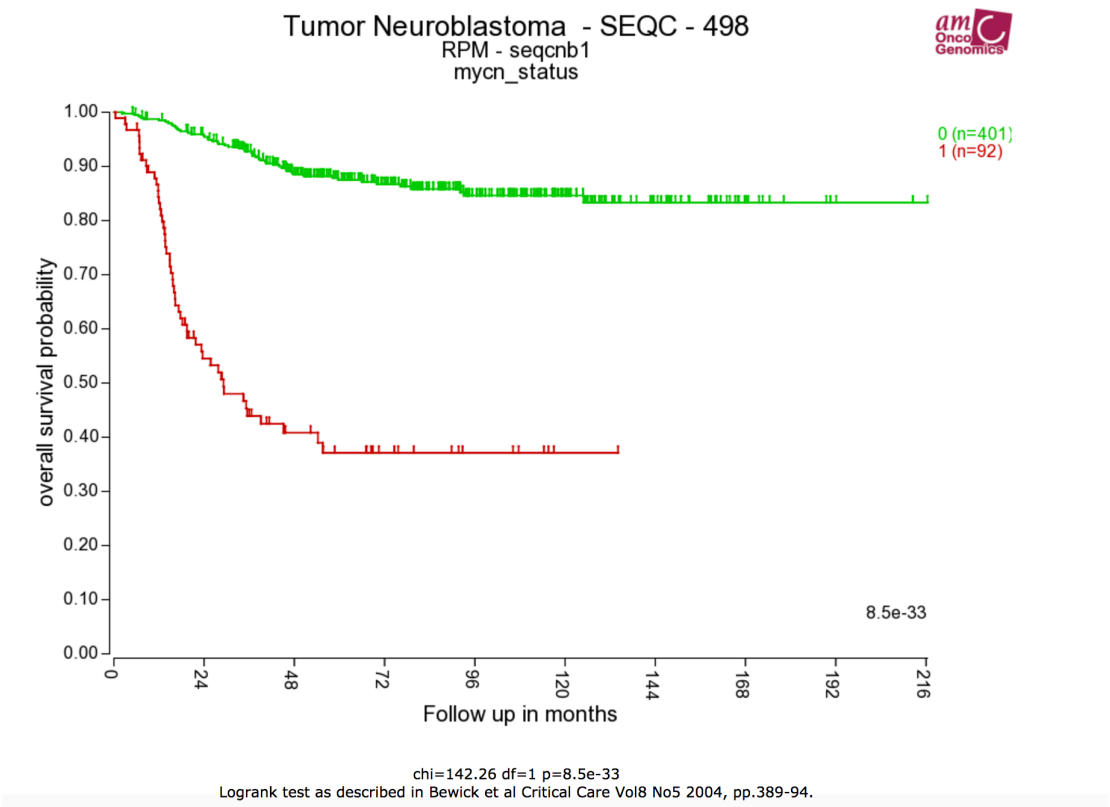

Figure 5. Kaplan Meier plot showing the overall survival of 493 neuroblastoma patients with (red; n=92) or without (green; n=401) MNA. The plot was generated using the Kaplan Meier by annotated parameter function (MYCN status) in R2: Genomics Analysis and Visualization Platform with the dataset 'Tumor Neuroblastoma - SEQC - 498 - RPM - seqcnb1'.

MNA is clearly a strong negative prognostic factor in neuroblastoma, however, a clinical report from 2014 demonstrated that the prognosis of MNA patients is more heterogeneous than previously described (93). In this study of high-risk neuroblastoma patients treated at Memorial Sloan Kettering Hospital between 2000 and 2011, the authors describe a "striking dichotomy" in the outcomes of MNA patients after induction therapy. MNA neuroblastoma patients with a complete response (CR) or a very good partial response (VGPR) to the induction chemotherapy had event-free survival and overall survival rates comparable to non-MNA high-risk patients with CR/VGPR. In contrast to this, progression as a response to induction therapy happened exclusively in the MNA patient population, and early death from progressive disease (<366 days from diagnosis) was significantly more common

in MNA patients compared to the non-MNA group. This study highlights the complexity of the *MYCN* in neuroblastoma at a clinical level, and the authors propose that elucidation of the molecular mechanisms underlying the divergent clinical outcomes amongst MNA patients will yield improvements in prognostication and potentially novel actionable drug targets.

1.2.1.7 *MYCN* in other cancers

In addition to neuroblastoma, genetic aberrations leading to overexpression of *MYCN* can be present in neuroendocrine tumors, such as neuroendocrine prostate cancer (94) and small cell lung cancer (95), in various embryonal tumors of childhood including medulloblastoma (96), retinoblastoma (97), Wilms' tumor (98) and rhabdomyosarcoma (99) and other adult malignancies such as glioblastoma multiforme (100) and various leukemias (AML, ALL, CLL) (101-103).

1.2.2 Chromosomal abnormalities

Chromosomal aberrations are common in neuroblastoma. Tumors with whole chromosome gains, but without segmental changes have an excellent prognosis whereas high-risk tumors are characterized by the presence of segmental chromosomal aberrations (SCAs) (104).

LOH at the 1p36 locus, is a frequent occurrence in neuroblastomas, and a strong predictor of poor prognosis. 1p36 LOH is reported in 20-40% of neuroblastoma patients, and is highly correlated with MNA (105). However, 1p36 LOH can occur in *MYCN* single copy tumors, and one study has shown that monoallelic loss of 1p36 is superior to MNA as a prognostic factor using multivariate analyses with the Cox proportional-hazards model (106). Due to its strong negative prognostic impact, it has been proposed that the 1p36 locus harbors one or more tumor suppressor genes, which are important in neuroblastoma pathogenesis. In fact, several genes have been identified within this genomic region, with tumor suppressive functions in neuroblastoma. The anti-neuroblastoma effects of these genes include repressing *MYCN* expression and inhibiting proliferation (miR-34a (107)), activation of apoptosis (*KIF1B* (108)) and inducing neuronal differentiation (*CDC42* (109), *CAMTA1* (110), *CASZ1*(111) and *CHD5* (112)).

Another frequent SCA in neuroblastoma is gain of the long arm of chromosome 17 (17q gain). The main mechanism for 17q gain is an unbalanced translocation with various different partner chromosomes, and gain of this genetic material is associated with advanced disease stage, MNA and 1p36 deletion (113). It has been proposed that one or more oncogenes reside in 17q and that these contribute to neuroblastoma pathogenesis by an increased gene dosage effect (114).

11q LOH occurs in 35-45% of neuroblastomas and is almost mutually exclusively with MNA (115). 11q-deletion is associated with a poor outcome with regards to long-term survival, and one study has

demonstrated that the prognostic impact of this aberration approaches that of MNA, with 8-year overall survival <35% (116). The same study also showed that patients with 11q-deleted tumors are significantly older at diagnosis (42 vs. 21 months) and have longer median survival after diagnosis (40 vs. 16 months) as compared with MNA. The underpinning of the aggressive phenotype associated with 11q-deleted tumors has not been identified, but haploinsufficiency has been proposed as a potential mechanism (115).

In addition, other frequently occurring SCAs in neuroblastoma are losses of 3p, 4p and distal 6q and gains of 2p and 7q (117)

1.2.3 Chromothripsis

Whole genome sequencing of 87 neuroblastomas of all stages showed few recurrent amino-acid-changing mutations, but revealed chromothripsis in 18% of high-stage neuroblastomas (118). Chromothripsis is a localized shredding of chromosomal material in a particular region followed by a random reassembly of the pieces. The regions affected by chromothripsis frequently involved genes important in neuroblastoma pathogenesis and was associated with MNA and loss of chromosome 1p. Furthermore, this study also demonstrated recurrent mutations in genes involved in neuritogenesis, including regulators of Rho/Rac-signaling such as *ATRX* and *TIAM1* and genes that function in neural growth cones such as *ODZ3*.

1.2.4 *ALK*

Activating point mutations in the anaplastic lymphoma kinase (*ALK*) oncogene are somatically acquired in about 8% of neuroblastoma cases (119). There is a substantial spatiotemporal variation with regards to the presence of *ALK* mutations in neuroblastoma. *ALK* mutations can be present at a subclonal level at the time of diagnosis and show clonal expansion at tumor recurrence, and also *de novo ALK* mutations can emerge at relapse in patients initially diagnosed with wild type (wt) *ALK* disease (120). *ALK* encodes the receptor tyrosine kinase ALK and the majority of the mutations affecting *ALK* in neuroblastoma result in amino acid changes in the tyrosine kinase domain, causing constitutive activation of ALK signaling (121). Several of these mutations have been shown to be oncogenic through their capacity to transform primary cells when they are introduced (122). Targeting mutated *ALK* with ALK specific small molecule inhibitors is possible for some mutations and has shown efficacy in neuroblastoma and ALK inhibitors are currently being evaluated in clinical trials (123). The exact mechanism of how *ALK* exerts its oncogenic effects at the cellular level is not completely understood, but mutant ALK leads to the downstream activation of various signaling pathways including PI3K-AKT-mTOR and Ras-MAPK (124). ALK also stimulates the transcription of *MYCN* in neuroblastoma cell lines (125).

1.2.5 *TERT*, Ras-MAPK and *TP53*

A study from 2015 conducting whole genome sequencing of 56 neuroblastomas from both low-risk and high-risk patients, showed recurrent genomic rearrangements affecting a chromosomal region at 5p15.33 upstream of the telomerase reverse transcriptase (*TERT*) gene (126). These rearrangements were found exclusively in high-risk tumors without MNA or *ATRX* mutations. The genomic rearrangements led to the juxtaposition of *TERT* downstream of powerful enhancer elements and a subsequent massive transcriptional upregulation of *TERT* expression. High *TERT* levels allow tumor cells to avoid cellular senescence by maintaining telomere length, resulting in immortalization and endless replicative potential. The same study also found that telomere maintenance mechanisms were present in all high-risk neuroblastomas, also those without *TERT* rearrangements. In MNA tumors, MycN upregulated the expression of *TERT* through direct interaction with the *TERT* promoter. Also, in a subset of neuroblastomas which harbored loss-of-function *ATRX* mutations, lengthening of telomeres happened through alternative lengthening of telomeres (ALT) mechanisms.

Relapsed neuroblastomas frequently contain mutations predicted to hyperactivate the Ras-MAPK pathway (127). A study which conducted whole-genome sequencing of 23 paired diagnostic and relapsed neuroblastomas showed that 18 (78%) of the relapsed tumors contained mutations predicted to activate Ras-MAPK signaling. In 11 (48%) primary tumors, the same Ras-MAPK pathway mutations as were present in the paired relapsed tumors, were detected. The frequency of Ras-MAPK mutations in primary tumors was much higher than what has been reported previously in neuroblastoma, leading the authors to hypothesize that Ras-MAPK mutations in a diagnostic sample can serve as marker of aggressive disease with a high risk of relapse.

The tumor suppressor gene *TP53* is the most frequently mutated gene in cancer and somatic mutations of this gene occur in at least 50% of human malignancies (128). *TP53* mutations are rare in primary neuroblastomas (~3%) (40). However, changes in *TP53* occur more frequently in relapsed neuroblastomas, one study showed that 15% of relapsed tumors had *TP53* mutations and 49% had abnormalities in p53 pathway genes (129). Also, a study showed that neuroblastoma cell lines established from relapsed tumors frequently had aberrations in the p53-MDM2-p14^{ARF} pathway (130).

In a recent study, Ackermann et al. showed that neuroblastomas containing telomere-maintenance mechanisms (*TERT* gene rearrangements, MNA or ALTs) in addition to Ras-MAPK and/or p53 pathway alterations, had an extremely poor prognosis with the lowest survival rates, underscoring the clinical importance of these molecular events in neuroblastoma (131). They performed whole genome sequencing on 416 untreated primary neuroblastomas and assessed telomere maintenance mechanisms in 208 of these tumors. Tumors lacking telomere-maintenance mechanisms had an excellent prognosis, irrespective of the presence of Ras-MAPK or p53 pathway mutations. The presence of

telomere maintenance without Ras-MAPK/p53 pathway mutations had a poor survival, but was considerably better than the tumors with telomere maintenance and Ras-MAPK/p53 pathway mutations.

1.2.6 Genetic factors predisposing to neuroblastoma

Most neuroblastoma cases are sporadic, however 1-2% are caused by germline mutations, which are inherited in an autosomal dominant fashion (132). Gain-of-function *ALK* variants, and loss-of-function mutations in the homeobox gene *PHOX2B* make up the majority of germline mutations in hereditary neuroblastomas, accounting for 75% and 10%, respectively (133). In recent years, genome-wide association studies (GWAS) have identified several neuroblastoma susceptibility alleles in candidate genes with modest effect sizes, which are associated with tumorigenesis and progression of sporadic neuroblastoma (134).

1.3 Ribosome biogenesis

Ribosomes are an essential part of the protein synthesizing machinery of the cell, facilitating the translation of mRNAs into proteins. The synthesis of ribosomal components, assembly and transport from the nucleolus to the cytoplasm (where protein synthesis takes place) is collectively termed ribosome biogenesis. Ribosome biogenesis requires the coordinated activity of three separate transcription machineries, namely RNA polymerases I, II and III. Ribosomes are generated in the nucleolus, which is the largest subnuclear structure. Human ribosomes consists of four ribosomal RNA (rRNA) molecules (5.8S rRNA, 28S rRNA, 5S rRNA and 18S rRNA) and over 70 different proteins, grouped into two subunits (40S and 60S) (135). The main enzymatic process of the ribosome is the peptidyl transferase reaction, which catalyzes the formation of peptide bonds between adjacent amino acids using amino acid-loaded tRNAs (aminoacyl-tRNAs) during the mRNA translation process. The active site of the peptidyl transferase activity is composed of rRNA (136).

Figure 6 shows an overview of ribosome biogenesis. The synthesis of the majority of rRNA is mediated by RNA polymerase I (RNA pol I), a multiprotein ~590 kDa enzymatic complex consisting of 14 subunits (137). RNA pol I mediated transcription of rRNA occurs at ribosomal DNA (rDNA) repeats present in the nucleolus. The initial transcript produced by RNA Pol I is 47S pre-rRNA (pre-rRNA), which is subsequently processed into 18S, 5.8S and 28S rRNAs (138). The final rRNA transcript, 5S rRNA, is synthesized by RNA pol III, and the mRNAs required for ribosomal proteins are produced by RNA pol II (139). The four rRNA transcripts bind different ribosomal proteins in the nucleolus, a process known as ribosome assembly, to form the pre-40S (containing 18S rRNA) and pre-60S (containing 5S, 5.8S and 28S rRNA) subunits. The pre-40S and pre-60S follow distinct export

routes, and are transported from the nucleolus into the nucleoplasm and subsequently to the cytoplasm, where the mature ribosome can form (140).

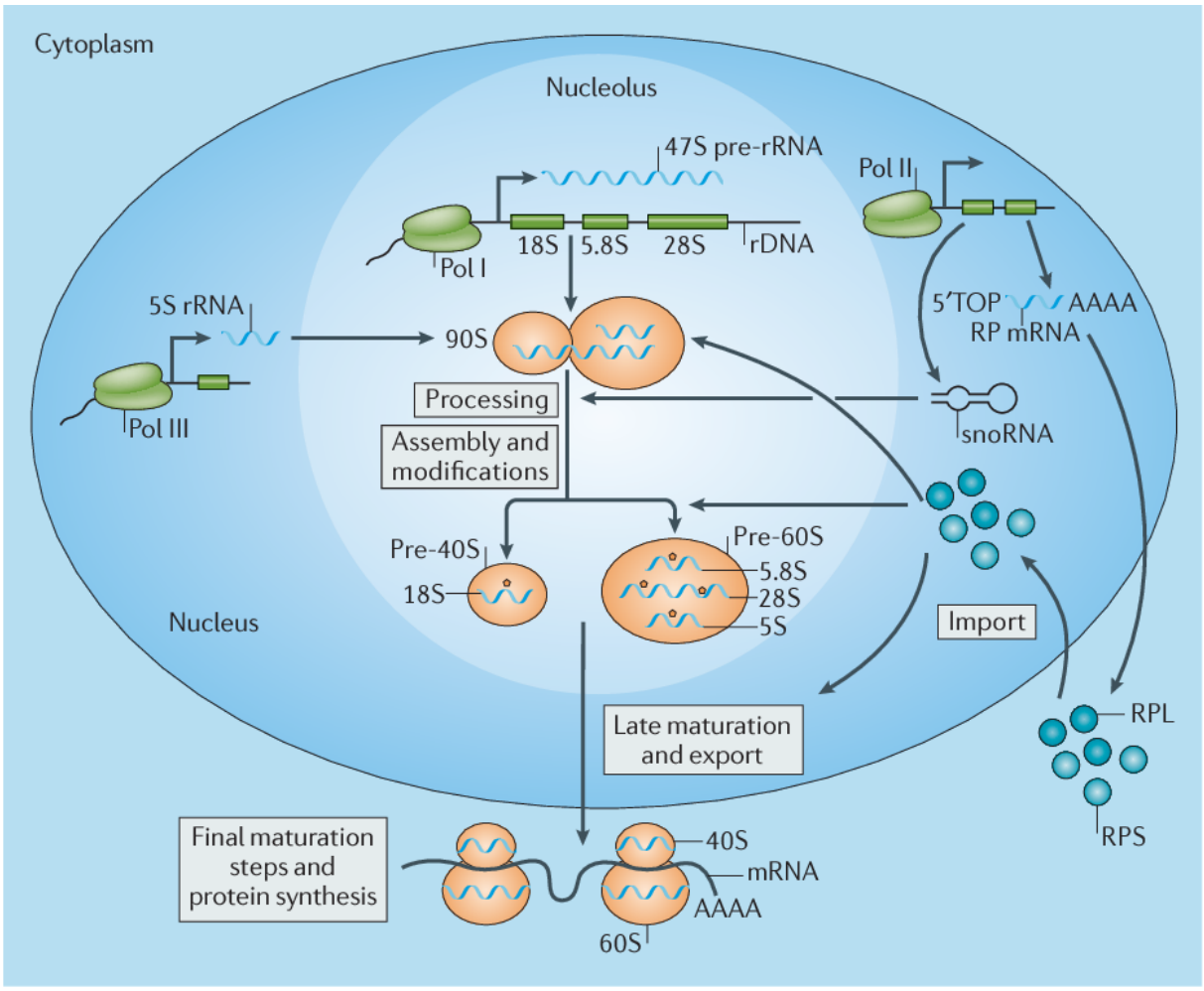

Figure 6. An overview of ribosome biogenesis, see main text for details. From (141), with permission.

The rate of ribosome biogenesis is tightly coupled to cellular growth. Withdrawal of nutrients, especially essential amino acids, leads to a rapid drop of RNA pol I mediated transcription (142). In order to maintain a high proliferative rate, ribosome biogenesis is frequently upregulated in cancers. Upregulated ribosome biogenesis results in increased nucleolar size in tumor cells, and the presence of enlarged nucleoli has been used as a histopathological marker for aggressive cancer for over a century (143). In neuroblastoma, the presence of prominent nucleoli correlates with an undifferentiated phenotype and MNA or c-Myc overexpression (144, 145). It has also been shown that Myc proteins upregulate ribosome biogenesis. c-Myc increases the RNA pol II mediated production of several ribosomal proteins, and also increases RNA pol I activity through direct interaction with rDNA promoter elements (146). MycN has also been shown to enhance the expression of several genes involved in ribosome biogenesis in neuroblastoma cells (147).

The disruption of ribosome biogenesis has been proposed as a target for novel cancer treatment (141). In recent years, two small molecular compounds, quarfloxin and CX-5461 have been characterized as direct and specific inhibitors of ribosome biogenesis (inhibitors of RNA pol I) and have gained attention due to their anti-cancer effects.

1.3.1 Inhibitors of ribosome biogenesis: Quarfloxin and CX-5461

The first characterization of the effects of quarfloxin (CX-3543) and CX-5461 in cancer cells were done by the same group (in 2009 and 2011, respectively) and both compounds were shown to inhibit RNA pol I mediated transcription (148, 149).

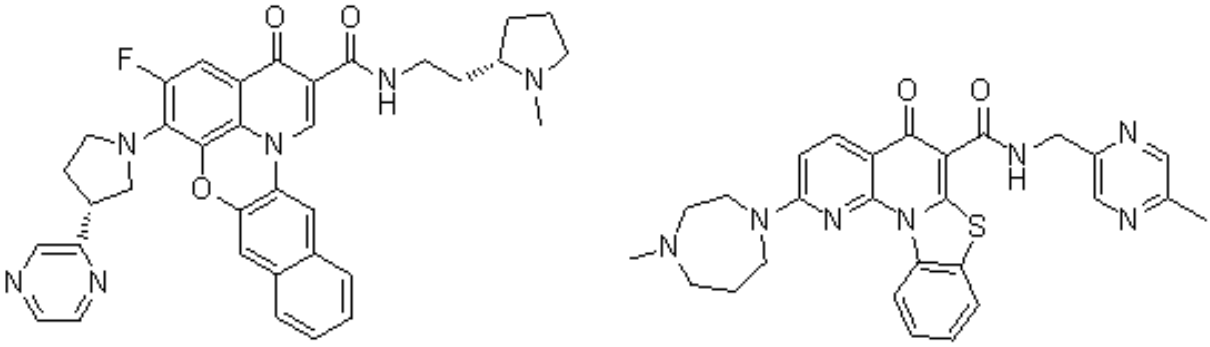

Figure 7. Molecular structure of quarfloxin (left) and CX-5461 (right), available at https://pubchem.ncbi.nlm.nih.gov/.

Quarfloxin was initially characterized due to its ability to stabilize a G-quadruplex structure in the *MYC* promoter (150). G-quadruplexes (G4s) are transient DNA secondary structures, which can form through non-Watson-Crick Hoogsteen base pairing in situations where DNA temporarily becomes single-stranded, for instance during replication and transcription (151). DNA sequences with the propensity to form G4s can be predicted from the pattern $G_{\geq 3}N_{1-7}G_{\geq 3}N_{1-7}G_{\geq 3}N_{1-7}G_{\geq 3}$, where "G" is guanine and "N" is any nucleotide. Genome-wide computational predictions using this pattern have shown that potential G4 forming stretches of DNA are enriched in telomeres, promoter regions and in the first intron of genes (152). G4s are implicated in various biological processes. They are thought to act repressive on both transcription and DNA replication and stabilized G4s trigger genome instability and DNA damage (152). Telomeric G4s have been shown to reduce telomerase function (153), but are also likely important for telomerase recruitment to telomeres (154). Additionally, G4s can form in RNA, which are more thermodynamically stable than their DNA counterparts (155).

Quarfloxin was shown to be concentrated in the nucleoli in A549 lung carcinoma cells treated with this compound *in vitro* (148). The same study demonstrated that quarfloxin reduced rRNA production. By stabilizing G4s in the rDNA, quarfloxin caused disruption between the G4 binding protein Nucleolin and G4s in the rDNA, an interaction absolutely required for rRNA synthesis.

CX-5461 was found to repress the production of rRNA through reducing the affinity of transcription factor Selective factor 1 (SL1) to the rDNA promoter (149). SL1 (consisting of TATA binding protein (TBP) and four TATA box-binding protein-associated factors (TAFs; TAF_I41 TAF_I48, TAF_I63 and TAF_I110 (156)) has the essential function to recruit RNA pol I to the start site of rRNA transcription mediated by the interaction between SL1 subunits TAF_I63 and TAF_I110 and RNA pol I subunit RRN3 (157). CX-5461 has also been shown to be a G4 stabilizer (158).

Both quarfloxin and CX-5461 have been shown to exert growth repressing effects in a wide variety of cancer cell lines and in several xenograft models. Quarfloxin was shown to reduce the viability of a large panel of cell lines grown *in vitro*, induced apoptosis in solid tumor cell lines and reduced tumor growth in a mouse xenograft model (148). CX-5461 had the same effect on cell viability and xenograft growth, and was also shown to induce pro-death autophagy and cellular senescence, but not apoptosis, in cell lines derived from adult solid tumors (149). Subsequent studies have shown that CX-5461 can induce apoptosis and activate p53 signaling in hematological cancers (159-161). The characterization studies of quarfloxin and CX-5461 concluded that these drugs did not result in DNA damage, using both the Ames' and chromosome aberration genotoxicity assays (148, 149). Later reports have contradicted this showing that exposure to these agents induce DNA damage and DNA damage signaling (158, 162, 163), see discussion section 5.1.2.

1.3.2 Other drugs targeting ribosome biogenesis

In a drug screen assaying for compounds with the capacity to induce nucleolar disruption, Morgado-Pallacin et al. showed that the acridine derivate CID-765471 suppressed the transcription of 47S-rRNA, induced nucleolar disruption and a activated a p53 response in the absence of DNA damage (164). Peltonen et al. discovered the compound BMH-21 to be a non-genotoxic p53 activating DNA intercalator (165). Further studies by the same group showed that this chemical possessed inhibitory properties with regards to ribosome biogenesis and had a broad antitumorigenic activity in cancer cell lines and xenograft models (166). They identified that BMH-21 bound to GC-rich sequences in the rDNA and reduced RNA pol I mediated transcription both *in vitro* (using a RNA pol I *in vitro* transcription assay) and *in vivo* (using two different uridine incorporation assays and RT-qPCR of the 5'-ETS of 47S-rRNA in cell lines).

Classical chemotherapeutic drugs often exert their toxic effects on cancer cells by blocking DNA synthesis or causing DNA damage through distinct mechanisms. However, several of these drugs can inhibit ribosome biogenesis in addition to their proposed mechanism of action. Burger et al. demonstrated that chemotherapy agents cisplatin, oxaliplatin, doxorubicin, mitoxanthrone, actinomycin D and methotrexate all led to a strong RNA pol I inhibition (as judged by a decrease in

the levels of 47S-rRNA) and induced morphological changes in the nucleolar structure consistent with a disruption of ribosome biogenesis (167).

In neuroblastoma cell lines, low doses of actinomycin D decreased proliferation and led to a preferential inhibition of RNA pol I mediated transcription (168). The drug also induced apoptosis and transcriptional repression of *MYCN*, both dependent on the presence of functional p53. Actinomycin D is extremely toxic to mammalian cells and blocks RNA synthesis through binding to DNA and interfering with RNA polymerase mediated RNA elongation (169). The compound shows a preference for binding to GC-rich DNA sequences and has been shown to repress oncogene expression through binding to promoter G4s (170).

1.4 MicroRNAs

MicroRNAs (miRNAs) are small (~22 nt) non-coding RNAs that play an important role in the post-transcriptional regulation of gene expression (171). Frequently, miRNA loci are found in close proximity to each other and constitute a polycistronic transcription unit (171). The miRNAs of these clusters are typically transcribed in concert, but can be subjected to individual post-transcriptional regulation. MiRNAs are classified according to their location within the genome as intronic, exonic or intergenic, reviewed in (172). Intronic miRNAs are transcribed from sequence present in introns, exonic miRNAs from sequences within exons, and finally intergenic miRNAs are encoded by genomic regions between annotated genes. Intronic miRNAs can be transcribed from the same promoter as the host gene, but there are examples of intronic miRNAs that are under the control of distinct promoters. Exonic miRNAs are mainly thought to be co-transcribed with their gene of origin. Intergenic miRNAs are expressed independently from their own promoters as monocistrionic or polycistrionic primary-miRNAs (pri-miRNAs).

The canonical pathway for the biogenesis of miRNAs begins with RNA pol II (or RNA pol III) mediated transcription of pri-miRNA molecules in the nucleus (173), see figure 8. Pri-miRNAs contain the miRNA sequence embedded within a local stem-loop structure flanked by single-stranded RNA (ssRNA) at the 5' and 3' sides, which are capped and polyadenylated, respectively (174). The stem-loop structure acts as a substrate for the Microprocessor complex consisting of the nuclear RNase III Drosha and essential cofactor DGCR8. The Microprocessor complex starts the maturation process of the miRNA by cleaving the pri-miRNA into a ~65 nucleotide small hairpin RNA structure containing a 5'-phosphate and a 2 nt 3'-overhang, denoted as a precursor miRNA (pre-miRNA) (174). Mirtrons constitute a group of intronic miRNAs which are matured independent of the Microprocessor complex. In these cases, an intron containing a miRNA sequence is processed by the splicing machinery to yield the pre-miRNA. The pre-miRNA is exported to the cytoplasm by a protein

complex consisting of the GTP-binding Ras-Related Nuclear Protein (Ran-GTP) and Exportin 5 (175). In the cytoplasm, the Ran-GTP is hydrolyzed to Ran-GDP resulting in the dismantling of the transportation complex, and release of the pre-miRNA. Here, the pre-miRNA is cleaved in close proximity to the terminal loop of the hairpin structure by RNaseIII Dicer producing a small RNA duplex (176). Dicer operates in complex with the transactivation-responsive RNA-binding protein (TRBP). The RNA duplex is loaded onto an argonaute (Ago) protein to form the pre-RNA-induced silencing complex (pre-RISC). In order to form the mature RISC, the RNA duplex is unwinded, yielding the mature miRNA guide strand and a passenger strand. The passenger strand is released and degraded, and the mature miRNA now provides specificity for target mRNAs in the mature RISC (176). The canonical mechanism of gene repression by mature miRNAs involves complimentary base pairing between the 3'UTR of a target mRNA and the seed sequence of the miRNA (in the mature RISC), consisting of the 5' 2-8 nucleotides of the miRNA (177). The association of an mRNA with the RISC can then lead to mRNA degradation or translational repression, both resulting in a depletion of the protein encoded by the given mRNA.

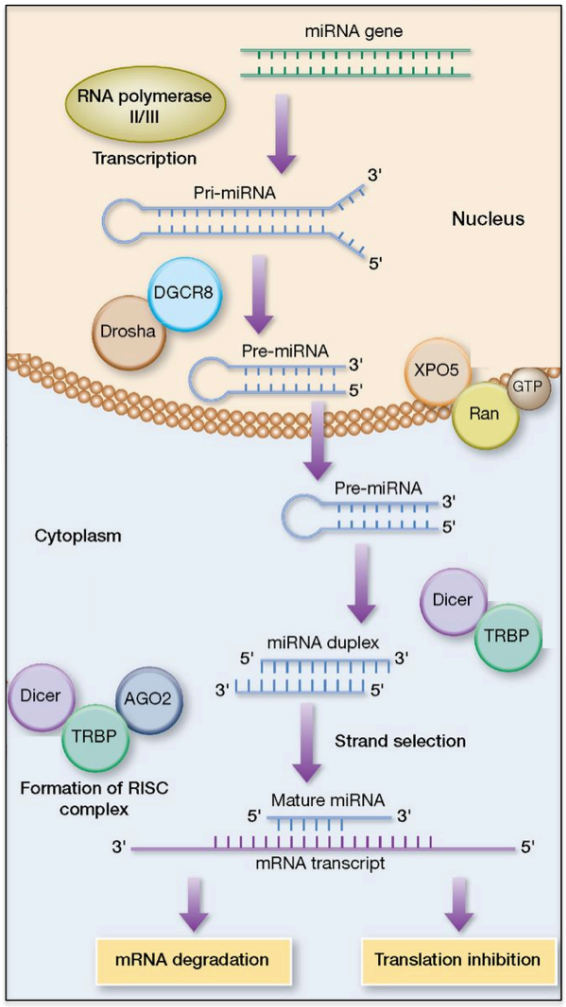

Figure 8. The canonical pathway for miRNA biogenesis, see main text for details. Adapted from (178), with permission.

1.4.1 MiRNAs in cancer and neuroblastoma

The current version of the miRNA database miRBase (version 22) contains 1917 annotated human miRNA precursors, and 2654 mature miRNA sequences (179). The majority of human genes are subject to miRNA regulation and 60% of human protein coding genes are conserved targets of miRNAs (180). Therefore, it is not surprising that deregulated miRNA expression has been implicated in a wide range of diseases, including malignancies (181). Mechanistically, miRNAs may be classified as having tumor suppressive or oncogenic properties with regards to the development and the progression of cancer (182). MiRNAs negatively regulating genes known to drive pro-tumorigenic processes such as increased proliferation, angiogenesis and migration, are denoted as tumor suppressive. In contrast, miRNAs targeting genes involved in the negative regulation of the same processes are classified as oncogenic. However, a given miRNA is not necessarily purely oncogenic or tumor suppressive, and can in theory be both. The same miRNA can target both oncogenes and tumor suppressive genes and the function of miRNAs can have different effects depending on the cellular context (183). For example, miR-193b, which is the focus of paper 2 in this thesis, has been found to have both tumor suppressive and oncogenic properties in different cancer cell types (see section 1.4.2). The basis of miRNA deregulation in cancer can have various molecular etiologies, including amplification or deletion of miRNA genes, changes in the expression of key transcription factors controlling miRNA expression, epigenetic alterations and defects in the miRNA biogenesis pathway (184).

In 2007, Chen and Stallings published the first miRNA expression profiling study in neuroblastoma, assaying 157 miRNAs in 35 primary neuroblastomas (185). This study showed that several miRNAs are differentially expressed between favorable and unfavorable tumors. Since this publication, a large amount of studies have addressed the role of miRNAs in neuroblastoma, and miRNAs have been implicated in various aspects of neuroblastoma pathogenesis, including differentiation, metastasis and chemoresistance, recently reviewed in (186).

MycN has been shown to directly upregulate the transcription of several miRNAs. Fontana et al. showed that MycN upregulated the expression of the polycistrionic miR-17-92 cluster (miRNA cluster located on chromosome 13 and consisting of 6 individual miRNAs; mir-17, mir-18a, mir-19a, mir-19b-1, mir-20a, mir-92a-1) by direct interaction with E-boxes in the miR-17-92 promoter in neuroblastoma cells (187). This study included a functional characterization of this miRNA cluster, showing that it had an oncogenic effect on neuroblastoma cells when overexpressed *in vitro* by increasing proliferation and the capability of clonogenic growth and inhibiting apoptosis (miR-17-5p). The miR-17-92 cluster also acted oncogenic *in vivo* by increasing the growth of xenografts in mice. They finally showed that miR-17-5p directly downregulated the expression the proteins p21 (inhibitor of cell cycle progression) and Bim (pro-apoptotic), thereby providing a mechanism for some of the

observed cellular effects. In a cohort of 95 untreated primary neuroblastoma tumor samples, Mestdagh et al. showed that high expression of the miR-17-92 cluster correlated with poor survival, thereby underscoring the importance of this miRNA cluster in neuroblastoma biology (188). In addition to the miR-17-92 cluster, MycN also upregulates the expression of the paralog clusters miR-106a-363 (chromosome X; miRs 106a, 18b, 20b, 19b-2, 92a-2, 363) and miR-106b-25 (chromosome 7; miRs 106b, 93, 25, host gene *MCM7*) through direct interaction with promoter E-boxes (189). MycN also increases expression of oncogenic miR-9 in neuroblastoma through direct interaction with the miR-9 promoter, and this miRNA was shown to be 2.5 fold higher expressed in tumor tissue from *MYCN*-amplified tumors compared to non-amplified (190). MycN can suppress neuronal differentiation in neuroblastoma through the upregulation of miRNAs. Loven et al. showed that inhibition of miR-17-92 cluster members miR-18a and miR-19a resulted in growth retardation, neurite outgrowth and increased expression of neuronal sympathetic differentiation markers (189). Furthermore, they demonstrated that these miRNAs targeted and downregulated the expression of estrogen receptor-α (*ESR1*) in neuroblastoma cells and that overexpression of *ESR1* led to an onset of neuronal differentiation. Finally, microarray data from neuroblastoma tumor samples showed that high expression of *ESR1* was associated with a favorable outcome in patients. The same group later published a report showing that the miR-17-92 cluster selectively targeted several other members of the nuclear hormone (NHR) superfamily (191). This study found that high NHR gene expression scores in tumors had an inverse correlation with MNA (and *MYC* signaling) and were associated with increased survival in neuroblastoma patients. They further showed that MycN repressed the glucocorticoid receptor (GR; NHR family member) *in vitro* and *in vivo* through miR-17-92 miRNAs and that this correlated to an undifferentiated phenotype in patients and in TH-*MYCN* mice. Finally, *MYCN* inhibition and subsequent reactivation of GR signaling promoted neural differentiation, reduced proliferation and stimulated apoptosis.

MycN also represses the expression of tumor suppressor miRNAs, and several studies show that MycN predominantly acts repressive with regards to the overall expression of miRNAs in MNA neuroblastoma cells, reviewed in (192). *MYCN* is also itself targeted by miRNAs as mentioned in section 1.2.2.

1.4.2 MiR-193b

Most reports on hsa-miR-193b-3p (miR-193b) demonstrate its downregulation in cancerous tissues compared with normal counterparts (193-195) and show its functional ability to suppress cancer growth through the targeting of various oncogenes, including *MCL1*, *KRAS* and *CCND1* (196-198). In hepatocellular carcinoma cells, miR-193b exerts tumor suppression through direct targeting and downregulation of the oncogenes *CCND1* and *ETS1* (199). In one study, miR-193b was found to be downregulated during progression of breast cancer, and overexpression of this molecule resulted in

decreased invasive, migratory and proliferative capacities of breast cancer cells through direct targeting of *PLAU* (200). In contrast to this, it has been demonstrated that miR-193b is overexpressed in glioma patient samples and cell lines compared with normal brain tissues (201). Furthermore, the same study showed that miR-193b increased the proliferative rate of glioma cell lines through direct targeting and downregulation of *SMAD3*, clearly showing an oncogenic role of this miRNA. Another study on head and neck squamous cell carcinomas (HNSCC) also reported on the propensity of miR-193b to act in an oncogenic fashion. In this study, miR-193b expression was shown to be increased in HNSCC relapse-tumors as compared with tumors from non-relapse patients, and this miRNA was also overexpressed in HNSCC cell lines relative to normal oral epithelial cells (202).

1.5 Exosomes

Exosomes are nanosized (typically reported between 30-200 nm in diameter) lipid bilayer vesicles released into the extracellular space by cells and are likely produced by all cell types (203, 204). Exosomes are present in various bodily fluids including urine, blood, saliva, breast milk and cerebrospinal fluid (205). These vesicles are endosomal in origin and are formed by the internal budding of the membrane of late endosomes into multivesicular bodies (MVBs) (206). The MVBs can fuse with the plasma membrane and thereby release their internal vesicles as exosomes. Exosomes are enriched in markers reflecting their endosomal origin including tetraspanins (CD9, CD63, CD37, CD81, and CD82), heat shock proteins, proteins involved in MVB biogenesis (i.e. TSG101) and various membrane fusion proteins (203). In addition to exosomes, the major extracellular vesicles produced by cells are microvesicles and apoptotic bodies, see figure 9 (207). These vesicles are non-endosomal in origin and occur through budding directly from the plasma membrane, they also have a distinct size distribution (microvesicles 50-2000 nm, apoptotic bodies 50-500 nm) and lack exosomal markers.

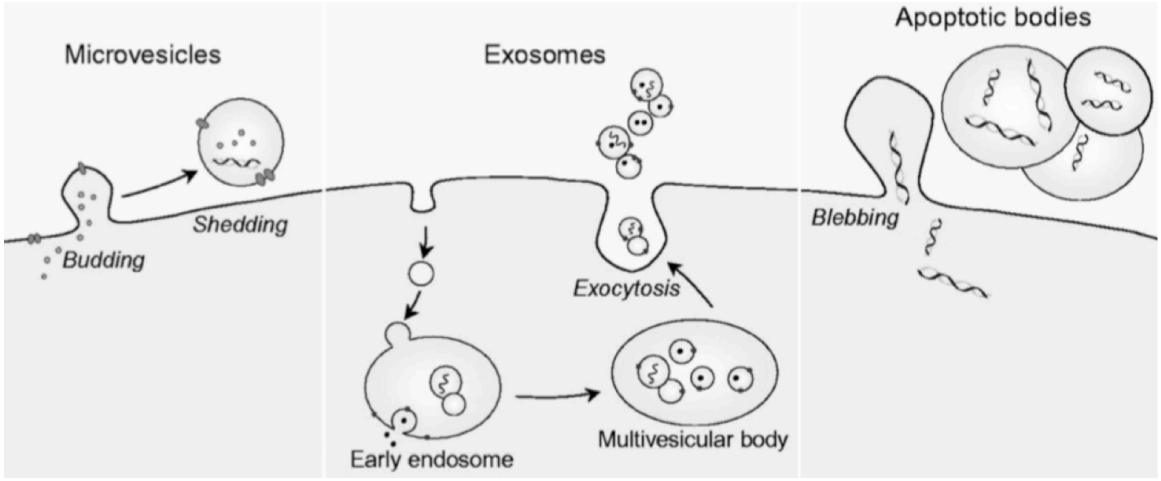

Figure 9. The main types and origin of different extracellular vesicles. Microvesicles (left) are generated by direct budding from the plasma membrane, exosomes (middle) originate from endosomal derived MVBs and apoptotic bodies are arise from the plasma membrane in cells undergoing apoptosis. Adapted from (208), with permission.

Exosomes contain a variety of biomolecules, including lipids, miRNAs, mRNAs, proteins and DNA (figure 10), and their cargo is reflective of the cell of origin (209). Exosomal content is dynamic and the molecular makeup of these vesicles has been shown to change in the transition from health to disease states (210). Exosomes were initially thought to serve as a route of cellular "garbage disposal" by ridding the cell of unnecessary biomolecules (211). In the last decade, the role of exosomes as mediators of cellular communication has emerged, and perhaps the main focus of exosome research in recent years is the role of exosomes as intercellular messengers. Secreted exosomes can be taken up by recipient cells where their cargo can be released (figure 10). The biomolecular cargo of secreted exosomes can allow the cell of origin to regulate cellular processes of surrounding cells in a paracrine fashion or distant cell populations in an endocrine fashion. Exosomes have been shown to have both oncogenic and tumor suppressive functions in in preclinical cancer models (212).

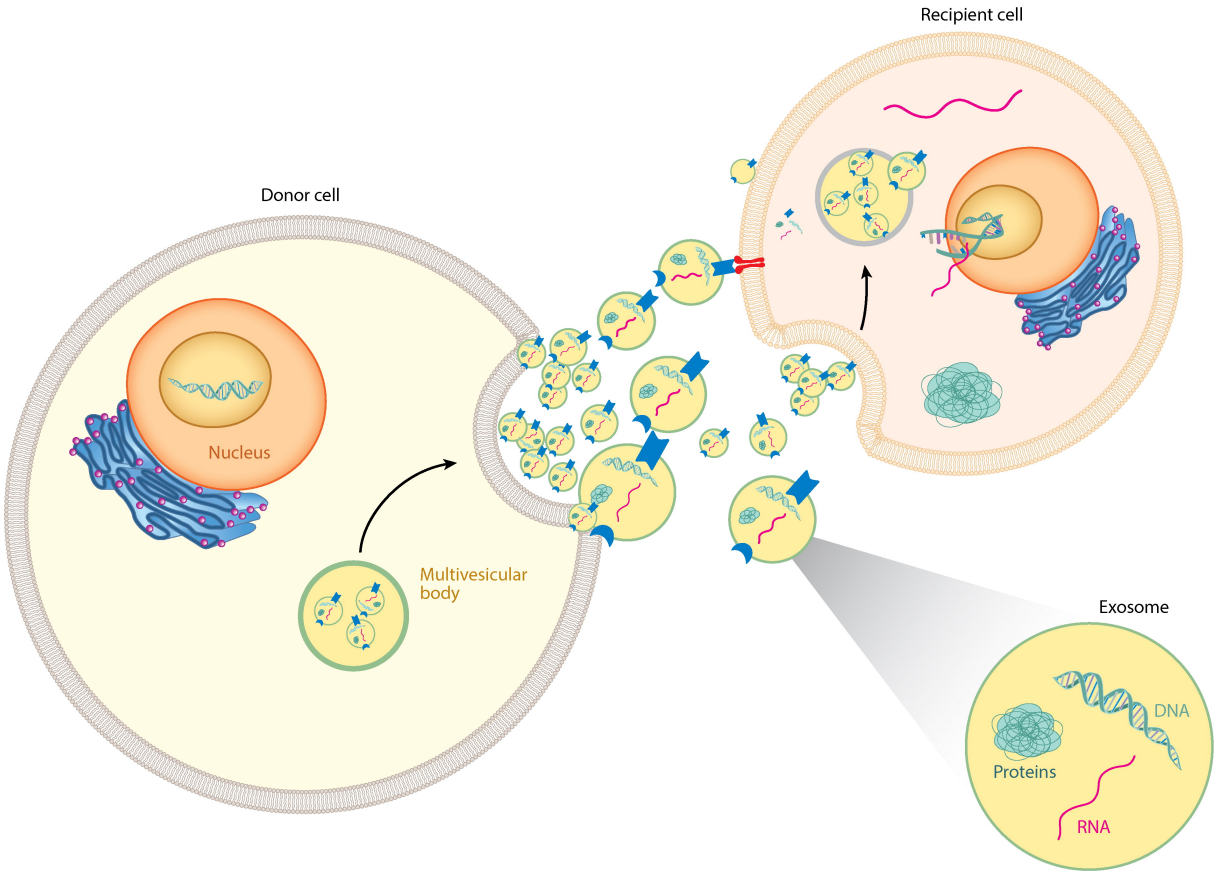

Figure 10. Exosomes as intercellular messengers, from (213), reused with permission. Donor cell (left) releases exosomes into the extracellular space. Exosome cargo includes different DNA- and RNA-molecules and proteins (lower right). Exosomes are internalized by the recipient cell (upper right) where the cargo is released.

1.5.1 The function of exosomes and exosomal miRNAs in cancer

Exosomes released from cancer cells in primary tumors have been demonstrated to condition distant tissues to favor the establishment of metastases and to direct the organotropism of metastatic tumor cells (214-216). This happens through the formation of a pre-metastatic niche. In a mouse model of pancreatic adenocarcinoma (PDAC), PDAC derived exosomes were taken up by Kupffer cells (specialized liver macrophages) and induced Kupffer cell secretion of TGFβ (215). Secreted TGFβ resulted in increased levels of fibronectin in surrounding liver stellate cells. These alterations of the liver microenvironment led to an increase in the PDAC liver metastatic burden. The study revealed that PDAC derived exosomes were enriched in macrophage migration inhibitory factor (MIF) and that blockade of this protein prevented the formation of the pre-metastatic niche and liver metastasis. The same group also published a study demonstrating that melanoma derived exosomes induced a pre-metastatic niche in the lung by increasing lung capillary permeability and recruiting bone marrow derived progenitor cells (216). This was shown to be mediated by MET receptor tyrosine kinase present in melanoma exosomes, and blockade of MET reduced the presence of metastatic disease in the lung.

Several studies have shown that miRNAs in exosomes contribute to tumorigenesis and cancer cell derived exosomal miRNAs have been implicated in inducing a protumorigenic phenotype in recipient cells, both through the canonical mechanism of targeting the 3'UTR of mRNAs and through novel processes. MiR-92a released from leukemia cells was shown to induce angiogenic tube formation of recipient HUVEC cells (217). This study also showed exosomal miR-92a to be functional in HUVEC cells by direct regulation of a miR-92a sensitive luciferase reporter and through downregulation of the protein expression of known target gene *ITGA5*. In a study of breast cancer, extracellular vesicles containing miR-200 released from highly metastatic breast cancer cell lines promoted a metastatic phenotype in non-metastatic cell lines. Also, miR-200 was shown to directly regulate target gene expression in the recipient cells (218). Other studies have revealed a novel mechanism of action of exosomal miRNAs, independent of their ability to directly regulate gene expression. It has been demonstrated that miRNAs present in exosomes can bind to and activate Toll-like receptor 8 (TLR8) in receiver cells. TLR8 is an intracellular receptor present in the endosomal membrane that is important for detecting pathogen-associated molecular patterns in the form of ssRNA, and subsequently eliciting a cytokine response (219). A study of lung cancer showed that activation of TLR8 in immune cells by exosomal miR-21 and miR-29a secreted from lung cancer cells induced a pro-tumorigenic inflammatory environment (220). Exosomal secretion also provides a way for tumor cells to rid themselves of tumor suppressive miRNAs. In a study of ovarian cancer, tumor cells evaded the growth impairing effects of miR-6126 by discarding it into the extracellular environment through exosomal transport (221). The same mechanism was present in liver cancer cells for tumor suppressor miR-198 (222). It is also established that exosomal miRNAs secreted from non-malignant cells can

mediate tumor suppression when taken up by malignant cells. In a study of prostate cancer, the growth of prostate cancer cells was inhibited by the conditioned medium of normal prostate epithelial cells (223). The growth suppression was revealed to be mediated by exosomal secretion of tumor suppressor miR-143.

2 Aims

Increased understanding of the detailed molecular biology underlying various cancers has led to some of the most significant breakthroughs in modern oncology, including the widespread use of targeted therapy with specific receptor tyrosine kinase inhibitors and immunotherapy. Despite large general improvements in cancer therapy, the survival of high-risk neuroblastoma patients is low and the treatment related morbidities for this group of patients remains high. Enhancing the knowledge of the molecular mechanisms present in high-risk neuroblastoma is key to devising new and better therapies. MNA is one of the ”molecular hallmarks” of high-risk neuroblastoma and understanding how MNA impacts neuroblastoma cells and how MycN and MycN regulated processes can be targeted for therapeutic purposes, is a large focus of neuroblastoma research. MycN is a well established regulator of various aspects of the RNA metabolism of the cell. It has been established as a driver of rRNA production. Additionally, MycN has been shown to regulate the expression of several distinct miRNAs and is also itself subject to targeting by several miRNAs. Understanding the aberrancies of rRNA and miRNA expression in high-risk and MNA neuroblastoma and how these aberrancies can be exploited, could lead to new therapeutic opportunities.

The overall aim of the thesis was to identify novel molecular aspects and therapeutic targets in high-risk neuroblastoma, with emphasis on *MYCN*, ribosomal RNA and miRNAs.

Paper 1: The aim was to characterize RNA pol I inhibitors in preclinical models of high-risk and MNA neuroblastoma

Paper 2: Here, we aimed at characterizing tumor suppressive miR-193b as a potential candidate for miR-based repression of neuroblastomas.

Paper 3: In this study, we aimed to profile the miRNAs present in MNA neuroblastoma derived exosomes and to investigate the functionality of exosomal miRNAs in recipient cells.

3 Materials and methods

Most of experimental techniques used in this thesis are regarded as standard methods in molecular biology, and are not described in this section. These methods are presented in the individual articles and include: Western blotting, RT-qPCR, luciferase assay, culturing and propagation of cell lines, siRNA and plasmid transfection (lipofection) into cells, flow cytometric analysis of cell cycle distribution and apoptosis, Alamar blue (Resazurin) cell viability assay and transmission electron microscopy (TEM). In this section, a more detailed description of selected methods used in this thesis is presented.

3.1 Bioinformatics using the R2: Genomics Analysis and Visualization Platform

The R2: Genomics Analysis and Visualization Platform (http://r2.amc.nl) is a freely accessible, web-based tool for analysis and visualization of genomics data developed by Jan Koster and his team at the department of Oncogenomics in Academic Medical Center (AMC) in Amsterdam, the Netherlands. On this platform there are several publicly available neuroblastoma tumor expression datasets, both RNAseq and microarrays. In **paper 1**, we used R2 to perform a *k*-means clustering analysis to partition neuroblastoma tumors from various RNA expression datasets into two groups according to expression of genes defined by the KEGG pathway "Ribosome Biogenesis in Eukaryotes". This resulted in two distinct clusters; "high ribosome biogenesis" (high-RiBi) and low-RiBi. The clusters were in turn correlated to available patient data, including overall and event-free survival, disease stage and *MYCN* expression, also within the R2 platform.

3.2 Neuroblastoma xenografts:

In **paper 1**, we used immunodeficient mice bearing human neuroblastoma xenografts to test the *in vivo* efficacy of orally delivered CX-5461. These studies were conducted at Karolinska Institutet in Stockholm with approval by the regional ethics committee for animal research (approval N304/08 and N391/11) in line with the Animal Protection Law (SFS1988:534), the Animal Protection Regulation (SFS 1988:539) and the Regulation for the Swedish National Board for Laboratory Animals (SFS1988:541). We used 4-6 week old female NMRI nu/nu mice (Scanbur, Stockholm, Sweden). This mouse strain has non-functional *Foxn1*, resulting in thymic aplasia and therefore a lack of T-cells. In addition, this genotype results in a keratinization defect in the skin, rendering the mouse nude. Defective T-cell immunity permits the establishment and growth of human tumor cells (xenografts). Xenografts were established from exponentially growing neuroblastoma cell lines BE(2)-C and IMR-32 by subcutaneous injection into the right flank of mice under isoflurane anesthesia. BE(2)-C were suspended in RPMI-1640 alone and IMR-32 in RPMI-1640 1:1 with Matrigel (Corning, NY). The

addition of Matrigel for IMR-32 xenografts was based upon tumor growth assessment in a pilot experiment showing more consistent tumor take and growth as compared with mice injected with IMR-32 cells without Matrigel. Matrigel is a solubilized basement membrane matrix containing the main proteins of the extracellular matrix and various growth factors, and has been shown to enhance the *in vivo* tumorigenicity of cancer cell lines (224).

Tumors were measured daily using a digital caliper, and tumor volume (cm^3) was calculated using the formula Length (cm) x $Width^2$ (cm) x 0.44. When tumors reached or exceeded 0.15 cm^3, animals were randomized into treatment or no treatment groups. Treatment with CX-5461 (50 mg/kg) was given by oral gavage, and the volume of administrated drug never exceeded 10 mL/kg, as is considered good practice for this route of administration (225). BE(2)-C bearing animals were treated with one dose every three days and sacrificed after 12 days of treatment. Due to no observed side effects as judged by changes in animal behavior and weight at this dosing schedule, it was decided to treat IMR-32 bearing mice with more intensive dosing. IMR-32 bearing mice received 3-6 consecutive doses CX-5461 (50 mg/kg) and then every third day for a total treatment of 10 days. The initial mice included (n=2) received 6 consecutive doses and lost some weight, therefore consecutive day dosing was reduced for the remaining mice (n=8) and these maintained their weight through the remainder of the experiment. Tumor volume was measured every day and normalized to tumor volume at day 0 to yield the tumor volume index (TVI). TVI from treated and untreated tumors for each day were compared in GraphPad Prism 7.0 using repeated measures two-way ANOVA and the Bonferroni post hoc test to correct for multiple comparisons. $p \leq 0.05$ was considered statistically significant.

3.3 XCelligence

The XCelligence system allows for label-free, continuous and real-time monitoring of cellular proliferation using electrical impedance as the readout (226). This system uses special tissue culture plates with gold microelectrode arrays fabricated in the bottom of each well (E-Plates). When cells grown on E-Plates attach to the microelectrodes, there is an increase in the electrical impedance. The larger the number of cells covering the microelectrodes, the larger the increase in impedance. Electrical impedance is displayed in the XCelligence software as cell index values (CI). The CI provides continuous information about the amount of cells present in the E-Plate wells, but can also be affected by changes in cell morphology and adhesion properties. In **paper 2**, we utilized the XCelligence system to measure neuroblastoma cell line growth in response to miR-193b overexpression. Neuroblastoma cell lines were reverse transfected with 25 nM of control or miR-193b mimics in 16-well E-Plates. CI was measured every 30 minutes for a total of 7 days (168 hours).

3.4 Preparation of exosome-free medium and production and isolation of exosomes

To avoid contaminating the exosomes of interest (neuroblastoma derived) with exosomes present in the fetal bovine serum (FBS) which is added to the cell medium, exosome-free FBS was prepared. Tubes containing 25 mL FBS were ultracentrifuged at 170 000 x g at 4°C overnight. The upper 10 mL in each tube was then carefully removed and pooled into a new tube, the remainder of the FBS was discarded. The exosome-free FBS was then passed through a 0.22 μm filter. Exosome-free serum was added to RPMI-1640 at a final concentration of 10% to make exosome-free medium (EFM).
For exosome isolation, BE(2)-C and Kelly cells were grown in Celline Adhere 1000 Bioreactors (CLAD 1000, Sigma-Aldrich). This system was originally designed for monoclonal antibody and cellular protein production, but has also been used for exosome isolation and yields a much higher concentration of exosomes compared with exosomes isolated from the supernatant of a conventional cell flask (227). The vessels consist of a compartment for cell cultivation and a chamber for the growth medium separated by a semi-permeable membrane. The membrane allows for nutrient diffusion and waste elimination, but is impermeable to media constituents >10 kDa. For our studies, suspensions of 25 x 10^6 BE(2)-C or Kelly cells in 15 ml of EFM were added to the cellular compartment of the CLAD 1000s. 550 mL of normal medium (RPMI-1640 containing 10% FBS) was added to the medium compartment. The cells were grown for 10 days before harvesting the medium in the cell chamber for exosome isolation. After harvesting the cell medium, the cell compartment was washed 4x with 1x PBS and fresh EFM was added. The medium in the cell-free compartment was replaced. Subsequent harvesting of medium for exosome isolation was carried out once per week in the same manner as described. Exosomes were isolated by differential ultracentrifugation based on a previously published protocol (228). Briefly, medium harvested from the cell chamber of the CLAD 1000 was centrifuged at 200 x g for 10 minutes at 4°C to remove viable cells. The resulting supernatant was centrifuged for 20 minutes at 2000 x g at 4°C to sediment large cell particles/cell debris. The supernatant was transferred to a new tube and centrifuged for 30 minutes at 10 000 x g at 4°C to remove small cell debris and microvesicles. Finally, the supernatant was ultracentrifuged at 110 000 x g for 70 minutes at 4°C to sediment the exosomes, and the supernatant was removed by careful pouring. The exosome pellet was resuspended in 1x PBS (for TEM and NanoSight), RIPA buffer (for protein extraction) or Qiazol reagent (RNA isolation). Resuspended exosomes were either frozen at -80°C or used directly in the various downstream procedures.

3.5 NanoSight Tracking Analysis

Nanoparticle Tracking Analysis (NanoSight, Salisbury, UK) is a method utilized to assess the size distribution and median diameter of nanosized particles present in a solution, and is commonly used in the characterization of secreted vesicles from mammalian cells (229). Samples containing extracellular

vesicles in liquid suspension are exposed to a laser beam and filmed by a camera attached to a microscope. The resulting video film is analyzed by the Nanoparticle Tracking Analysis software, which calculates the size (diameter) of the individual vesicles present in the laser beam based on their Brownian motion using the two-dimensional Stokes-Einstein equation.

In **paper 3**, extracellular vesicles from Kelly and BE(2)-C in 1x PBS were loaded onto the viewing unit of a NanoSight LM10 (calibrated using 100 nm polystyrene latex beads (NanoSight)) and illuminated with a 405 nm laser. The vesicles were filmed for 90 seconds, recorded at 16.55 frames/second and camera shutter was set to 33 milliseconds. Analysis conditions were set to automatic.

3.6 MiRNA qPCR panels and IPA pathway analysis

For **paper 3,** we used miRCURY LNA microRNA qPCR panels 1+2 V2.M (Exiqon) to profile the miRNA content of neuroblastoma cell line exosomes. These two panels allowed for sensitive and accurate detection of 739 predefined miRNAs in a 384-well format, using a method based on universal reverse transcription and subsequent RT-qPCR with LNA (locked nucleic acids) enhanced primers. In the first step of this system, a polyA tail is added to the mature miRNA template. cDNA is then synthesized through reverse transcription using a PolyT primer with a 3' degenerate anchor and 5' universal tag. The resulting cDNA template is subsequently amplified using miRNA-specific and LNA enhanced forward and reverse primers. LNA are synthetic high-affinity RNA analogs where the ribose ring is engineered to be in an ideal conformation for Watson-Crick binding. This gives LNA-containing oligonucleotides high thermal stability when hybridized to a complementary DNA or RNA strand. Inclusion of LNA into oligonucleotides has been demonstrated to increase the sensitivity and specificity for nucleic acid hybridization-based technologies including PCR. Total RNA from Kelly and BE(2)-C exosomes was extracted using the Trizol method and 40 ng RNA was reverse transcribed with the miRCURY universal cDNA synthesis kit. The cDNA obtained was then used in the miRCURY LNA microRNA qPCR panels 1+2 V2.M. Profiling of RNA from EFM was used to determine the potential interference of bovine RNA molecules remaining in the exosome-depleted serum. CT values <35 were considered detected when the CT of EFM was >35. Samples were also included if (CT EFM)–(CT sample) >6.6, indicating a bovine background of <1% of the sample expression. The 25 most highly expressed miRNAs in Kelly and BE(2)-C exosomes were subjected to bioinformatics using the Ingenuity Pathway Analysis platform (IPA; Qiagen) to determine potential target genes, biological functions and canonical pathways predicted to be affected. This software contains a large database (Ingenuity Knowledge Base) of structured collections of cell line and human tissue genomics data, including observed cause–effect relationships that relate to expression, transcription, activation, molecular modification and transport as well as binding events. This database is the source for the algorithms used in the IPA software predictions.

4 Results

Paper 1

In this paper, we found that tumors from neuroblastoma patients clustered into two groups with regards to high or low expression levels of genes involved in ribosome biogenesis. Furthermore, we showed that high-RiBi tumors had a far worse prognosis both with regards to event-free and overall survival compared with their low-RiBi counterparts. Moreover, high-RiBi tumors correlated with higher expression levels of *MYCN* and more advanced disease stage as opposed to low-RiBi tumors. Due to the negative clinical impact of high ribosome biogenesis in tumors from neuroblastoma patients, we evaluated the effects two small-molecule RNA pol I inhibitors, quarfloxin and CX-5461 in a panel of neuroblastoma cell lines. Both compounds reduced the viability of the cell lines, with absolute IC50 values in the nanomolar range. Neuroblastoma cell lines with MNA or *MYC* overexpression and wild type *TP53* (wt-*TP53*) were the most sensitive. Also, MNA and mutated *TP53* (mut-*TP53*) were more sensitive than non-MNA cell lines with mut-*TP53*. We further analyzed microarray data from MNA IMR-32 cells after siRNA induced *MYCN* knockdown and showed that high *MYCN* (control) samples correlated with high-RiBi and low *MYCN* knockdown samples correlated with low-RiBi. We then demonstrated that neuroblastoma cell lines with MNA or *MYC* overexpression and wt-*TP53* efficiently underwent apoptosis after treatment with quarfloxin or CX-5461, and that this treatment activated p53-signaling. Mut-*TP53* neuroblastoma cell lines failed to undergo apoptosis, but were arrested in the G2/M-phase of the cell cycle. We proceeded to show that pre-treatment depletion of MycN or p53 decreased the loss of cell viability and blocked apoptosis after exposure to quarfloxin and CX-5461. Furthermore, MycN overexpression in a *MYCN* inducible neuroblastoma cell line increased the loss of cell viability after drug treatment. We also found that both quarfloxin and CX-5461 downregulated MycN and that they exerted genotoxicity. In addition, we found that the activity of RNA pol I was inhibited after high dose exposure to both agents. Finally, we showed that oral administration of CX-5461 repressed the growth of two different neuroblastoma xenografts in mice and induced proliferation arrest, DNA damage, apoptosis and MycN downregulation *in vivo*. In conclusion, we have demonstrated the anti-neuroblastoma effect of two small molecular RNA pol I inhibitors, quarfloxin and CX-5461, both *in vitro* and *in vivo*.

Paper 2

In this study, we investigated the potential of tumor suppressive hsa-miR-193b-3p (hereafter miR-193b) as a candidate for miRNA-based anti-neuroblastoma therapy. We assessed the expression levels of miR-193b in 69 neuroblastoma primary tumors and two cell lines, and found that this miRNA was expressed at a similar level as tumor suppressor miR-34a, a miRNA previously shown to be expressed at low levels in aggressive neuroblastomas. Furthermore, miR-193b was expressed at significantly

lower levels compared to established neuroblastoma oncogenic miRNAs, miR-92a and miR-17. We then demonstrated that exogenous introduction of miR-193b mimics into 9 different neuroblastoma cell lines with different cytogenetic aberrations significantly reduced the cell viability and proliferation after 48 hours of all cell lines tested. We also showed that miR-193b caused a G1 cell cycle arrest and induction of apoptosis in several cell lines. Furthermore, we determined that the cell cycle arrest and apoptosis were in part due to downregulation of miR-193b target genes *CCND1* and *MCL1*, respectively. We also revealed for the first time that *MYCN* is a direct target gene of miR-193b using a luciferase based assay and site-directed mutagenesis and that *MYCN* downregulation likely contributed to the cell cycle arrest. In conclusion, we have shown that miR-193b has a low expression in neuroblastoma primary tumors and that this miRNA exerts tumor suppressive activity in a large panel of neuroblastoma cell lines through targeting of oncogenes *CCND1*, *MCL1* and *MYCN*.

Paper 3

In this article, we isolated and characterized exosomes from two MNA-neuroblastoma cell lines (BE(2)-c and Kelly) grown *in vitro*. We demonstrated that we could isolate vesicles present in the cell medium with size distributions, morphologies and biochemical markers consistent with exosomes. The exosomes contained RNAs and were enriched in small RNAs (<200 nt). We profiled the miRNA content of the exosomes using miRNA-arrays, and we identified 11 miRNAs highly expressed in exosomes derived from both cell lines investigated. We found that fluorescently stained exosomes could be taken up by recipient cells using flow cytometry and fluorescent microscopy. However, we failed to demonstrate that three of the highly expressed exosomal miRNAs (miR-9, miR-21 and miR-92a) could regulate target sequence luciferase reporters or activate TLR8 signaling in recipient cells. Finally, we conducted a bioinformatic analysis of the 25 most abundant miRNAs expressed in neuroblastoma exosomes by using the IPA software to predict mRNA targets and performed a functional enrichment analysis on the predicted targets. The functional enrichment analysis indicated that the miRNAs from neuroblastoma exosomes can regulate signaling pathways associated with cancer, including cellular growth, cell survival and cell death. In conclusion, we demonstrated that MNA neuroblastoma cell lines secreted exosomes. Isolated exosomes contained a distinct miRNA population predicted to regulate signaling important in cancer. The exosomes could be taken up by recipient cells, but we could not demonstrate functional effect of the transferred exosomal miRNAs.

5 Discussion

The individual articles in this thesis have detailed discussions and are included in the appendix. In this section I will expand on topics discussed in the publications, address some limitations and outline suggestions for future investigations.

5.1 Inhibition of ribosomal RNA production as neuroblastoma therapy

Targeting ribosome biogenesis through inhibiting RNA pol I has been demonstrated as an efficient strategy to impede the growth of wt-*TP53* and MYC-driven cancers in several studies (160, 161, 230, 231). High-risk neuroblastomas rarely have *TP53*-mutations at diagnosis, are frequently MYC-driven and have nucleolar hypertrophy as a result of hyperactive production of ribosomes (40, 144, 145). These features indicate that neuroblastoma represents a disease likely to respond favorably to inhibition of ribosome production. In **paper 1**, we demonstrated the preclinical efficacy of small molecular inhibitors of RNA pol I, quarfloxin and CX-5461, in neuroblastoma.

5.1.1 Suppression of MycN expression and the role of *TP53*

Our study showed MNA cell lines were more sensitive to the cytotoxic effects of quarfloxin and CX-5461 compared with non-MNA cells. We also observed a prominent reduction of MycN *in vitro* after quarfloxin and CX-5461 treatment in *wt-TP53* IMR-32 and CHP-134. In addition, CX-5461 led to a pronounced MycN depletion *in vivo* in the IMR-32 xenograft model. The ability of CX-5461 to downregulate MycN in neuroblastoma has recently been shown by others (232, 233). CX-5461 has been found to reduce c-Myc levels through enhanced *MYC* mRNA degradation in multiple myeloma cells (230). We have investigated the effects of quarfloxin and CX-5461 on *MYCN* mRNA levels in IMR-32, which were not suppressed by these compounds, in fact we saw a small relative increase in *MYCN* transcripts (unpublished; Appendix, suppl. figure 1). This result implies that quarfloxin and CX-5461 lead to MycN suppression through a post-transcriptional mechanism. We did not observe MycN downregulation in *mut-TP53* Kelly and BE(2)-C cells. P53 has previously been shown to directly activate transcription of *FBXW7*, an ubiquitin E3-ligase known to destabilize MycN (72, 234). Also, reactivation of p53 by the small molecule RITA in neuroblastoma cell lines has been shown to reduce MycN through induction of FBXW7 (235). We saw a robust downregulation of MycN only in wt-*TP53* cells, and we have unpublished results showing an upregulation of *FBXW7* mRNA levels upon quarfloxin or CX-5461 treatment in IMR-32 cells (Appendix, suppl. figure 2). A potential explanation for MycN downregulation could involve a p53-mediated upregulation of *FBXW7*, subsequently leading to ubiquitination and proteasomal degradation of MycN. Further studies assessing the mechanism of MycN downregulation could therefore involve investigating whether the

upregulation of *FBXW7* is in fact p53 dependent and how blocking FBXW7 or the proteasome in the presence of quarfloxin/CX-5461 treatment would affect MycN levels. Another possibility for MycN reduction could involve the G4 stabilizing effects of quarfloxin and CX-5461. Intriguingly, two G4s have been identified in the *MYCN* promoter (236, 237). Promoter G4s have been shown to be repressive on both transcription and translation (152, 238). The function of the *MYCN* promoter G4s are not yet known and is currently being investigated in our lab.

We firmly established that wt-*TP53* sensitized neuroblastoma cells to quarfloxin and CX-5461. Drygin et al. who published the first report characterizing the effects of CX-5461 in a large panel of cancer cell lines and in xenografts, noted that the IC50 value of this drug was significantly lower in cell lines without *TP53* mutations (149). Also, they showed that CX-5461 could stabilize the p53 protein in wt-*TP53* cells, but did not investigate whether a functional activation of the p53 pathway occurred. Several other reports have subsequently demonstrated that CX-5461 induces activation of the p53 signaling pathway (160-162, 239). We showed a clear induction of p53 signaling upon exposure of wt-*TP53* neuroblastoma cell lines to quarfloxin and CX-5461 and knockdown of *TP53* before exposure to the inhibitors, blocked apoptosis. However, when we reconstituted the expression of wt-*TP53* in mut-*TP53* BE(2)-C cells, we did not see an induction of apoptosis or increased loss of cell viability after quarfloxin and CX-5461 exposure. The reason for this is not clear. In our paper, we speculate that this could, at least in part, be an effect of the specific *TP53* mutation (*TP53*mut C135F*)* which BE(2)-C cells harbor. In a study of *TP53*-variants in neuroblastoma cell lines, the C135F-mutant was shown to act in a dominant negative fashion with regards to wt-p53 thereby creating a potential to inhibit the actions of the exogenously expressed wt-protein (240). However, we saw an induction of the protein expression of p53 transcriptional target p21 when transfecting BE(2)-C with a wt-*TP53* expression plasmid, indicating the reconstitution of functional p53 signaling. One study has shown that the level of p21 induced after doxorubicin treatment in MNA/wt-p53 neuroblastoma cells was insufficient to reduce the activity of MycN upregulated CDK4 (241). Active CDK4 promoted S-phase progression and cell death resistance. Elevated CDK4 expression by MycN in BE(2)-C cells could therefore provide a way to avoid cell death after treatment with quarfloxin or CX-5461 in the setting of reactivated wt-*TP53* expression. In order to further understand the role of p53 with regards to RNA pol I inhibitor sensitivity, reestablishing wt-*TP53* in a panel of cell lines with different *TP53* mutations seems reasonable. Furthermore, knockout of the *TP53* C135F variant in BE(2)-C before re-expression of wt-*TP53* is feasible using the CRISPR-Cas9 system. In addition, co-inhibition of CDK4 and RNA pol I after re-expressing wt-*TP53* could address the possibility of CDK4-mediated cell death resistance.

5.1.2 The role of DNA damage

The initial studies on both quarfloxin and CX-5461 reported that these molecules did not cause DNA damage (148, 149). This in contrast to our results and the findings of others. We showed an increase of phosphorylation at serine 139 of histone H2A.X (γ-H2A.X), a commonly used DNA damage marker, in all cell lines tested. DNA damage occurred at the same quarfloxin and CX-5461 dose as p53 dependent apoptosis in wt-*TP53* cell lines. However, we did not see a suppression of RNA pol I at this dosage. This is in line with the results of Xu et al., which showed that both quarfloxin and CX-5461 can cause genotoxicity and cell death independent of their ability to suppress RNA pol I activity (158). In this study, the authors investigated the effects of quarfloxin and CX-5461 in a preclinical model of BRCA1/2 deficient breast and ovarian cancers, and showed that both inhibitors primarily exerted their toxic effects through the induction of replication dependent single-strand breaks and to a lower extent double-strand breaks. They also found that CX-5461 acts as a G4 stabilizer, a property already known to be possessed by quarfloxin (148). Stabilized G4s can cause replication fork arrest by providing a physical hindrance for the replication fork (152). Replication fork arrest leads to replicative DNA damage through the uncoupling of DNA polymerases from the replicative helicase, thereby generating tracts of ssDNA (single-strand breaks) which leads to recruitment of the DNA damage kinase ATR and activation of ATR-Chk-1 signaling (242). If the damage is not sufficiently repaired, replication over single-strand breaks will progress to double-strand breaks and subsequent activation of DNA damage kinase ATM and ATM-Chk-2 signaling (242). Both ATM and ATR are known to phosphorylate H2A.X on ser139 (243). Activation of the ATR/ATM signaling cascade can lead to a variety of downstream effects including activation of specific repair pathways and induction of apoptosis (244). Defective DNA damage signaling has been shown to sensitize cancer cells towards quarfloxin and CX-5461. Xu et al. showed that BRCA1/2 deficient cancer cells were highly sensitive towards both quarfloxin and CX-5461 as compared with cells with functional BRCA1/2 (158). It is well established that BRCA1/2 deficient cells have defective DNA repair. BRCA1 has a diverse role in DNA damage signaling and is important for transducing the signals of several DNA repair pathways including homologous recombination (HR), non-homologous end-joining and single-strand annealing, whereas BRCA2 is restricted to HR and is an essential mediator of this process (245). CX-5461 treatment has been shown to induce signaling through ATR and ATM with subsequent downstream activation of their effector kinases Chk-1 and Chk-2, respectively (162, 163). We have unpublished results investigating the contribution of ATR-Chk1 and ATM-Chk2 signaling in neuroblastoma resistance to CX-5461. Combining CX-5461 with VE-822 (ATR-inhibitor) or MK-8776 (Chk-1 inhibitor) in "CX-5461-resistant" SK-N-AS cells led to an enhancement of viability loss measured by Alamar blue (Appendix, suppl. figure 3A) and to the activation of apoptosis as judged by cleavage of PARP-1 on western blot (Appendix, suppl. figure 3B). These results indicate that activated DNA damage signaling mediates resistance to CX-5461. However, we did not observe induction of apoptosis or an increase in viability loss when co-treating SK-N-AS with CX-5461 and KU-60019

(ATM-inhibitor). In line with our findings, Negi et al. showed a large activation of apoptosis in acute B-lymphoblastic leukemia cell lines SEM and KOPN-8 when combining CX-5461 with VE-822, but not with CX-5461 and KU-60019 (162). One potential explanation could be that the CX-5461 dose used in our experiment (230 nM) and in the study by Negi et al. (250 nM) mainly induces ssDNA breaks (in line with the results of Xu et al.), which results in activation of ATR-Chk1 signaling.

5.1.3 Clinical use of quarfloxin and CX-5461

Our findings and the results from others show that quarfloxin and CX-5461 can induce growth arrest in a variety of cancers, making these compounds interesting candidates for clinical use in cancer patients. One limitation of our study with regards to assessing preclinical therapeutic efficacy is the use of an immunodeficient mouse model. The immune system is known to contribute to the therapeutic effect of chemotherapeutic agents (246). In order to evaluate the role of functional immunity to the response against RNA pol I inhibitors in a preclinical neuroblastoma model, transgenic TH-*MYCN* mice could be used. Another limitation of our study with regards to evaluating the potential of quarfloxin and CX-5461 as future anti-neuroblastoma drugs is the lack of studies on normal cells. These compounds can potentially lead to severe side effects in patients by their effects on the normal cell population both as inhibitors of RNA pol I and due to their genotoxic properties. Several studies have shown that CX-5461 has minimal effects on normal cells and is well tolerated in animal models (149, 158, 160, 161). CX-5461 is currently being evaluated in patients with advanced solid tumors (ClinicalTrials.gov identifier: NCT02719977) and advanced hematological cancer (Australian New Zealand Clinical Trials Registry identifier: ACTRN12613001061729). Preliminary results from the latter, a phase I dose-escalation study, demonstrated tolerability with extended periods of dosing in their patient sample (n=17) (247). In addition, there were patients with sustained and beneficial clinical responses. Quarfloxin has completed a phase 1 trial in patients with advanced solid tumors and lymphomas (ClinicalTrials.gov identifier: NCT00955786) and a phase 2 trials in patients with and neuroendocrine/carcinoid tumors (ClinicalTrials.gov identifier: NCT00780663). No study results from the quarfloxin trials have been published and the reason for discontinuing research of this compound on patients is unknown.

5.2 MicroRNA-based neuroblastoma therapy: Overexpression of microRNA-193b

The capacity of a single tumor suppressive miRNA to simultaneously target and downregulate multiple oncogenes, has drawn attention to these molecules as potential anti-neoplastic agents. In our study, we showed that tumor suppressor miR-193b to be lowly expressed in neuroblastoma tumor samples and that this miRNA acted as a potent tumor suppressor in a large panel of neuroblastoma cell lines.

5.2.1 MiR-193b –"mechanism of action"

Mechanistically, we demonstrated that miR-193b arrested neuroblastoma cells in the G1/S-phase of the cell cycle and induced apoptosis. We showed downregulation of *CCND1*, *MYCN* and *MCL-1* at the mRNA level and also of their protein products. Previous studies have shown interactions between miR-193b and specific binding sites in the 3'UTRs of *CCND1* and *MCL-1* using a luciferase-based assay, confirming these transcripts as direct targets of this miRNA (196, 197). In a study by Beckers et al. utilizing a high-throughput luciferase reporter screen in HEK293T cells, 470 miRNAs were assayed for potential interaction with the 3'UTR of *MYCN*. This paper showed that miR-193b can target the *MYCN* 3'UTR (248). In our study, we corroborated this finding and further identified the exact binding site of miR-193b to be present at position 463-470 in *MYCN* 3'UTR using Targetscan prediction (targetscan.org) and a *MYCN* 3'UTR luciferase reporter system with site directed mutagenesis, thus confirming that *MYCN* as a direct target of this miRNA.

A partial rescue of the miR-193b induced G1/S-phase blockage was observed when re-expressing a *CCND1* expression plasmid lacking the 3'UTR. *CCND1* encodes Cyclin D1, which is a regulatory subunit of the cyclin-dependent kinases CDK4/6. CDK4/6 leads to cell cycle progression from G1 into S-phase by phosphorylation of the retinoblastoma protein thereby releasing E2F transcription factors which activates transcription of various genes required for S-phase entry (249). Deregulation of *CCND1* has been implicated in neuroblastoma tumorigenesis. One study showed two thirds of neuroblastoma tumors and cell lines overexpressed *CCND1* (250). In addition, high levels of *CCND1* and its partner kinase *CDK4* has been found to correlate to an undifferentiated phenotype in neuroblastomas and siRNA mediated knockdown of both these genes in neuroblastoma cell lines induces neuronal differentiation (251). The partial rescue of cell cycle progression implies that other mechanisms contribute to the to the cell cycle arrest induced by miR-193b. A possible way to elucidate the role of *CCND1* could involve CRISPR-Cas9 mediated *in vivo* mutagenesis of the genomic *CCND1* miR-193b seed sequence in a neuroblastoma cell line and subsequently analyzing the effects of miR-193b transfection.

We speculated that *MYCN* repression by miR-193b contributed to the observed cell cycle arrest. We confirmed that *MYCN* depletion using RNA interference led to a G1/S-phase arrest, a finding previously shown by our group (252). Re-expressing a *MYCN* cDNA construct devoid of a 3'UTR (and perhaps also co-expressing *CCND1*) with miR-193b mimics could be a viable strategy to further understand the precise mechanism of the cell cycle arrest.

MiR-193b overexpression induced apoptosis in several neuroblastoma cell lines through downregulating anti-apoptotic gene *MCL-1*. The activation of the apoptosis pathway is triggered by upregulation of BH3-only proteins of the Bcl-2 family such as Noxa, Bim and Puma in response to an

apoptotic stimuli, reviewed in (253). The BH3-only proteins bind to anti-apoptotic Bcl-2 family members (including Bcl-2 and Mcl-1) leading to the release of pro-apoptotic effector proteins BAK and BAX which are sequestered by the anti-apoptotic Bcl-2 family proteins. Freed BAK and BAX can form oligomeric pores in the mitochondrial membrane necessary for cytochrome c release and caspase activation. The initiation of apoptosis is therefore dependent on the balance between the pro- and anti-apoptotic Bcl-2 family members. *MCL-1* is implicated in neuroblastoma and it has been shown that neuroblastoma cell lines are "primed" for cell death through the binding of Bim (the principal BH3-only death activator in neuroblastoma) with either Mcl-1 or Bcl-2 (254). In our study, Mcl-1 primed BE(2)-C and SH-SY5Y cells and Bcl-2 primed CHLA-20 all underwent apoptosis after miR-193b overexpression, whereas siRNAs against *MCL-1* only caused apoptosis in the Mcl-1 primed cell lines. Furthermore, we saw a partial reduction of apoptosis with exogenous *MCL-1* overexpression in Mcl-1-primed but not in Bcl-2 primed neuroblastoma cells after miR-193b overexpression. These results support the notion of a selective dependence on Mcl-1 or Bcl-2 for neuroblastoma cell survival and also show that miR-193b can activate apoptosis independent of Mcl-1. In a study of liposarcoma cells, miR-193b overexpression was shown to induce apoptosis through direct targeting of *CRKL*, *PTK2* and *MSRA* (255). Investigating whether miR-193b also targets these genes in neuroblastoma cell lines would be of value for a deeper understanding of the apoptotic phenotype.

5.2.2 Potential of miR-193b as an anti-neuroblastoma drug

MiR-193b represents an interesting candidate for miR-based therapy in neuroblastoma. It targets three oncogenes important in neuroblastoma pathogenesis and induces a robust antiproliferative and pro-apoptotic phenotype in a large panel of neuroblastoma cell lines with different cytogenetic abnormalities. A limitation of our study with regards to therapeutic efficiency is the lack of testing manipulation of miR-193b in normal cells and *in vivo* studies. Little is known about the role of miR-193b in normal cells and tissues.

In vivo efficacy of miRNA-based therapy in cancer has been investigated in some animal models. Intravenous delivery of tumor suppressive miR-34a in human non-small lung cancer (NSCLC) xenografts and in a spontaneous NSCLC mouse model led to a robust growth inhibition of tumors and was well tolerated by the mice (256). Furthermore, *in vivo* inhibition of oncogenic miR-221 was shown effective in reducing malignant plasma cell proliferation in a mouse model of multiple myeloma (257). In this study, a synthetic 13-mer locked nucleic acid (LNA), which specifically recognizes the complementary sequence of miR-221 and blocks the biological effects of this oncogenic miRNA, was administered intravenously. The treatment did not result in damage to normal organs, weight loss or behavioral changes in the mice, indicating low off-target toxicity.

MiRNA based treatment has been assessed in cancer patients. A promising drug from a mechanistic standpoint, MRX34 containing a mimic of tumor suppressive miR-34, was in phase I clinical trials for patients with primary liver cancer, other selected solid tumors and hematologic malignancies (ClinicalTrials.gov identifier: NCT01829971) (258). In this study, patients were treated intravenously with a liposomal formulation of MRX34. However, the study was terminated prematurely due to serious immune related adverse events in several patients. Whether the adverse events were caused by the liposomal carrier or the miR-34a mimic was not possible to know by the study design.

5.3 The microRNA content of *MYCN*-amplified neuroblastoma exosomes

We showed that neuroblastoma cell lines secrete exosomes with a distinct miRNA profile. The miRNAs present in the exosomes were predicted to regulate cancer associated signaling pathways. To our knowledge, this study was the first characterization of the miRNA content of neuroblastoma exosomes.

5.3.1 Functional effects of exosomal miRNAs

Exosomes allows for the transfer of biomolecules between different cells. Several studies have shown that cancer cell derived exosomal miRNAs are functional in recipient cells, reviewed in (259).
We investigated whether neuroblastoma derived exosomal miRNAs could regulate the expression of known target genes through 3'UTR interaction and their ability to activate TLR8 signaling. However, we were not able to show a functional effect of exosomal miRNA in recipient cells in our study. The failure to show a functional effect in our experiments could be due to several reasons. We showed an uptake of neuroblastoma exosomes when adding them to the media of recipient cells as judged by fluorescence microscopy and flow cytometry. However, we did not address the precise subcellular location of the added exosomes or measure whether we could see an increase in exosomal miRNAs in the recipient cells. If the exosomes were in fact clustered to the outer surface of the recipient cells, this could explain a lacking functional effect of miRNAs in our experiments, as the cellular response to miRNAs require internalization. The exact subcellular location of added exosomes could be addressed by high-resolution microscopy. In addition, measuring an increase of exosome-enriched miRNAs in recipient cells after exosome exposure would indicate an uptake. One study demonstrated that exosomes derived from K562 and MT4 cells were efficiently internalized by phagocytic cells through phagocytosis, but not by various non-phagocytic cell lines where the exosomes adhered to the cell surface (260). Challagundla et al. showed a functional effect of neuroblastoma derived exosomal miR-21 (261). In this study, neuroblastoma cell derived exosomes containing miR-21 led to an activation of TLR8 signaling in recipient monocytes. This resulted in upregulation of miR-155 in the monocytes. Furthermore, exosomes containing miR-155 were secreted from the monocytes and taken up by

neuroblastoma cells, where miR-155 directly targeted *TERF1* (an inhibitor of telomerase), leading to increased cisplatin resistance. TLR8 is an endosomal receptor which recognizes GU-rich single stranded RNA and activation of the receptor requires the internalization of the RNA ligand (262). In our study, we evaluated the activation of TLR8-signaling using HEK-Blue hTLR8 (HEK293 cells transfected with human the *TLR8* gene and an inducible secreted embryonic alkaline phosphatase (SEAP) reporter) as the recipient cell line. HEK293 cells are non-phagocytic and the lack of an activated TLR8 phenotype could therefore be attributed to this. A further study could investigate if a phagocytic receiver cell would result in a functional uptake of exosomal miRNAs and activation of TLR8 signaling.

5.3.2 The biomarker potential of exosomal miRNAs

The miRNAs present in the MNA neuroblastoma derived exosomes isolated in our study were predicted to regulate signaling pathways important in cancer. A limitation of our profiling of exosomal miRNAs is the use of arrays with a fixed number of miRNAs. In order to further characterize the miRNA content of neuroblastoma exosomes an RNA deep sequencing approach could be used.

Exosomes are present in bodily fluids, which are accessible by minimally invasive methods. Therefore, profiling of exosomal miRNA-content from patient blood or other fluids can potentially be useful as clinical biomarkers. A recent study showed downregulation of tumor derived exosomes and their miRNA cargo in blood samples from neuroblastoma patients after induction chemotherapy (263). Furthermore, this study demonstrated that post-induction expression of three exosomal miRNAs (miR-29c, miR-342-3p and Let-7b) could discriminate between different clinical responses. Patients with a minor treatment response showed a significant downregulation of these miRNAs as compared with the pre-treatment levels. The expression was unchanged in patients with a very good partial response when comparing pre- and post-treatment samples. Further profiling of the tumor derived exosomal miRNAs present in the various bodily fluids of neuroblastoma patients, could lead to the discovery of new clinically relevant biomarkers for diagnostics and disease monitoring.

6 Conclusions

The results presented in this thesis have contributed with new insights into aspects of the molecular biology of high-risk neuroblastoma. We have demonstrated that small molecular inhibitors of RNA polymerase I are promising agents for targeting high-risk disease and that these molecules can provide a novel way of depleting MNA neuroblastomas of MycN. Furthermore, we found that the pleiotropically acting miR-193b inhibits the growth of neuroblastoma cells and targets important neuroblastoma oncogenes, including *MYCN*. We also showed that MNA neuroblastoma cells secreted exosomes with a distinct miRNA profile predicted to regulate signaling pathways involved in cancer.

With the current therapy, many high-risk neuroblastoma patients do not survive or have severe treatment related late effects. The discoveries which have been made in this thesis will hopefully be useful for devising better high-risk neuroblastoma biomarkers and therapies in the future.

7 References

1. Cancer Registry of Norway. Cancer in Norway 2017 - Cancer incidence, mortality, survival and prevalence in Norway. Oslo: Cancer Registry of Norway, 2018. 2018.
2. Mogensen H, Modig K, Tettamanti G, Erdmann F, Heyman M, Feychting M. Survival After Childhood Cancer-Social Inequalities in High-Income Countries. Frontiers in Oncology. 2018;8:485.
3. Vassal G, Schrappe M, Pritchard-Jones K, Arnold F, Basset L, Biondi A, et al. The SIOPE strategic plan: A European cancer plan for children and adolescents. Journal of Cancer Policy. 2016;8:17-32.
4. Vassal G, Fitzgerald E, Schrappe M, Arnold F, Kowalczyk J, Walker D, et al. Challenges for children and adolescents with cancer in Europe: the SIOP-Europe agenda. Pediatric Blood & Cancer. 2014;61(9):1551-7.
5. Pritchard-Jones K, Pieters R, Reaman GH, Hjorth L, Downie P, Calaminus G, et al. Sustaining innovation and improvement in the treatment of childhood cancer: lessons from high-income countries. The Lancet Oncology. 2013;14(3):e95-e103.
6. Spector LG, Pankratz N, Marcotte EL. Genetic and nongenetic risk factors for childhood cancer. Pediatric Clinics of North America. 2015;62(1):11-25.
7. Hameed M, Mandelker D. Tumor Syndromes Predisposing to Osteosarcoma. Advances in Anatomic Pathology. 2018;25(4):217-22.
8. Vogelstein B, Papadopoulos N, Velculescu VE, Zhou S, Diaz LA, Jr., Kinzler KW. Cancer genome landscapes. Science. 2013;339(6127):1546-58.
9. Institute of Medicine (US) and National Research Council (US) National Cancer Policy Board; Hewitt M WS, Simone JV, editors. . Childhood Cancer Survivorship: Improving Care and Quality of Life. Washington (DC): National Academies Press (US); 2003. 2, The Epidemiology of Childhood Cancer. Available from: https://www.ncbi.nlm.nih.gov/books/NBK221741/
10. Grimmer MR, Weiss WA. Childhood tumors of the nervous system as disorders of normal development. Current Opinion in Pediatrics. 2006;18(6):634-8.
11. Annual Report of The Norwegian Children's Cancer Registry 2017 ("Årsrapport for barnekreft 2017"). Oslo: Cancer Registry of Norway. 2018.
12. Kushner BH. Neuroblastoma: a disease requiring a multitude of imaging studies. Journal of Nuclear Medicine. 2004;45(7):1172-88.
13. Louis CU, Shohet JM. Neuroblastoma: molecular pathogenesis and therapy. Annual Review of Medicine. 2015;66:49-63.
14. Cheung NK, Dyer MA. Neuroblastoma: developmental biology, cancer genomics and immunotherapy. Nature Reviews Cancer. 2013;13(6):397-411.
15. Johnsen JI, Kogner P, Albihn A, Henriksson MA. Embryonal neural tumours and cell death. Apoptosis. 2009;14(4):424-38.

16. Maris JM. Recent advances in neuroblastoma. The New England Journal of Medicine. 2010;362(23):2202-11.
17. Pinto NR, Applebaum MA, Volchenboum SL, Matthay KK, London WB, Ambros PF, et al. Advances in Risk Classification and Treatment Strategies for Neuroblastoma. Journal of Clinical Oncology. 2015;33(27):3008-17.
18. Brodeur GM. Neuroblastoma: biological insights into a clinical enigma. Nature Reviews Cancer. 2003;3(3):203-16.
19. Brodeur GM, Bagatell R. Mechanisms of neuroblastoma regression. Nature Reviews Clinical Oncology. 2014;11(12):704-13.
20. Cole KA, Maris JM. New strategies in refractory and recurrent neuroblastoma: translational opportunities to impact patient outcome. Clinical Cancer Research. 2012;18(9):2423-8.
21. Laverdiere C, Cheung NK, Kushner BH, Kramer K, Modak S, LaQuaglia MP, et al. Long-term complications in survivors of advanced stage neuroblastoma. Pediatric Blood & Cancer. 2005;45(3):324-32.
22. Shimada H, Ambros IM, Dehner LP, Hata J, Joshi VV, Roald B. Terminology and morphologic criteria of neuroblastic tumors: recommendations by the International Neuroblastoma Pathology Committee. Cancer. 1999;86(2):349-63.
23. Ross RA, Biedler JL, Spengler BA. A role for distinct cell types in determining malignancy in human neuroblastoma cell lines and tumors. Cancer Letters. 2003;197(1-2):35-9.
24. van Groningen T, Koster J, Valentijn LJ, Zwijnenburg DA, Akogul N, Hasselt NE, et al. Neuroblastoma is composed of two super-enhancer-associated differentiation states. Nature Genetics. 2017;49(8):1261-6.
25. Monclair T, Brodeur GM, Ambros PF, Brisse HJ, Cecchetto G, Holmes K, et al. The International Neuroblastoma Risk Group (INRG) staging system: an INRG Task Force report. Journal of Clinical Oncology. 2009;27(2):298-303.
26. Cohn SL, Pearson AD, London WB, Monclair T, Ambros PF, Brodeur GM, et al. The International Neuroblastoma Risk Group (INRG) classification system: an INRG Task Force report. Journal of Clinical Oncology. 2009;27(2):289-97.
27. Johnsen JI, Dyberg C, Fransson S, Wickstrom M. Molecular mechanisms and therapeutic targets in neuroblastoma. Pharmacological Research. 2018.
28. Zhang J, Walsh MF, Wu G, Edmonson MN, Gruber TA, Easton J, et al. Germline Mutations in Predisposition Genes in Pediatric Cancer. The New England Journal of Medicine. 2015;373(24):2336-46.
29. Parsons DW, Roy A, Yang Y, Wang T, Scollon S, Bergstrom K, et al. Diagnostic Yield of Clinical Tumor and Germline Whole-Exome Sequencing for Children With Solid Tumors. JAMA Oncology.2016;2(5):616-624.

30. Chang W, Brohl AS, Patidar R, Sindiri S, Shern JF, Wei JS, et al. MultiDimensional ClinOmics for Precision Therapy of Children and Adolescent Young Adults with Relapsed and Refractory Cancer: A Report from the Center for Cancer Research. Clinical Cancer Research. 2016;22(15):3810-20.
31. Grobner SN, Worst BC, Weischenfeldt J, Buchhalter I, Kleinheinz K, Rudneva VA, et al. The landscape of genomic alterations across childhood cancers. Nature. 2018;555(7696):321-7.
32. Sweet-Cordero EA, Biegel JA. The genomic landscape of pediatric cancers: Implications for diagnosis and treatment. Science. 2019;363(6432):1170-5.
33. Pugh TJ, Morozova O, Attiyeh EF, Asgharzadeh S, Wei JS, Auclair D, et al. The genetic landscape of high-risk neuroblastoma. Nature Genetics. 2013;45(3):279-84.
34. Martin GS. The hunting of the Src. Nature Reviews Molecular Cell Biology. 2001;2(6):467-75.
35. Vennstrom B, Sheiness D, Zabielski J, Bishop JM. Isolation and characterization of c-myc, a cellular homolog of the oncogene (v-myc) of avian myelocytomatosis virus strain 29. Journal of Virology. 1982;42(3):773-9.
36. Schwab M, Alitalo K, Klempnauer KH, Varmus HE, Bishop JM, Gilbert F, et al. Amplified DNA with limited homology to myc cellular oncogene is shared by human neuroblastoma cell lines and a neuroblastoma tumour. Nature. 1983;305(5931):245-8.
37. Kohl NE, Kanda N, Schreck RR, Bruns G, Latt SA, Gilbert F, et al. Transposition and amplification of oncogene-related sequences in human neuroblastomas. Cell. 1983;35(2 Pt 1):359-67.
38. Dang CV. MYC on the path to cancer. Cell. 2012;149(1):22-35.
39. Eilers M, Eisenman RN. Myc's broad reach. Genes & Development. 2008;22(20):2755-66.
40. Chen L, Tweddle DA. p53, SKP2, and DKK3 as MYCN Target Genes and Their Potential Therapeutic Significance. Frontiers in Oncology. 2012;2:173.
41. Iraci N, Diolaiti D, Papa A, Porro A, Valli E, Gherardi S, et al. A SP1/MIZ1/MYCN repression complex recruits HDAC1 at the TRKA and p75NTR promoters and affects neuroblastoma malignancy by inhibiting the cell response to NGF. Cancer Research. 2011;71(2):404-12.
42. Westermark UK, Wilhelm M, Frenzel A, Henriksson MA. The MYCN oncogene and differentiation in neuroblastoma. Seminars in Cancer Biology. 2011;21(4):256-66.
43. Zeid R, Lawlor MA, Poon E, Reyes JM, Fulciniti M, Lopez MA, et al. Enhancer invasion shapes MYCN-dependent transcriptional amplification in neuroblastoma. Nature Genetics. 2018;50(4):515-23.
44. Lin CY, Loven J, Rahl PB, Paranal RM, Burge CB, Bradner JE, et al. Transcriptional amplification in tumor cells with elevated c-Myc. Cell. 2012;151(1):56-67.
45. Manohar CF, Bray JA, Salwen HR, Madafiglio J, Cheng A, Flemming C, et al. MYCN-mediated regulation of the MRP1 promoter in human neuroblastoma. Oncogene. 2004;23(3):753-62.

46. Hasan MK, Nafady A, Takatori A, Kishida S, Ohira M, Suenaga Y, et al. ALK is a MYCN target gene and regulates cell migration and invasion in neuroblastoma. Scientific Reports. 2013;3:3450.
47. Haug BH, Henriksen JR, Buechner J, Geerts D, Tomte E, Kogner P, et al. MYCN-regulated miRNA-92 inhibits secretion of the tumor suppressor DICKKOPF-3 (DKK3) in neuroblastoma. Carcinogenesis. 2011;32(7):1005-12.
48. Marshall GM, Liu PY, Gherardi S, Scarlett CJ, Bedalov A, Xu N, et al. SIRT1 promotes N-Myc oncogenesis through a positive feedback loop involving the effects of MKP3 and ERK on N-Myc protein stability. PLoS Genetics. 2011;7(6):e1002135.
49. Chen L, Alexe G, Dharia NV, Ross L, Iniguez AB, Conway AS, et al. CRISPR-Cas9 screen reveals a MYCN-amplified neuroblastoma dependency on EZH2. The Journal of Clinical Investigation. 2018;128(1):446-62.
50. Xiao D, Ren P, Su H, Yue M, Xiu R, Hu Y, et al. Myc promotes glutaminolysis in human neuroblastoma through direct activation of glutaminase 2. Oncotarget. 2015;6(38):40655-66.
51. Cotterman R, Knoepfler PS. N-Myc regulates expression of pluripotency genes in neuroblastoma including lif, klf2, klf4, and lin28b. PloS One. 2009;4(6):e5799.
52. Hatzi E, Murphy C, Zoephel A, Ahorn H, Tontsch U, Bamberger AM, et al. N-myc oncogene overexpression down-regulates leukemia inhibitory factor in neuroblastoma. European Journal of Biochemistry. 2002;269(15):3732-41.
53. Beckers A, Van Peer G, Carter DR, Gartlgruber M, Herrmann C, Agarwal S, et al. MYCN-driven regulatory mechanisms controlling LIN28B in neuroblastoma. Cancer Letters. 2015;366(1):123-32.
54. Slack A, Chen Z, Tonelli R, Pule M, Hunt L, Pession A, et al. The p53 regulatory gene MDM2 is a direct transcriptional target of MYCN in neuroblastoma. Proceedings of the National Academy of Sciences of the United States of America. 2005;102(3):731-6.
55. Suenaga Y, Kaneko Y, Matsumoto D, Hossain MS, Ozaki T, Nakagawara A. Positive auto-regulation of MYCN in human neuroblastoma. Biochemical and Biophysical Research Communications. 2009;390(1):21-6.
56. Cetinkaya C, Hultquist A, Su Y, Wu S, Bahram F, Pahlman S, et al. Combined IFN-gamma and retinoic acid treatment targets the N-Myc/Max/Mad1 network resulting in repression of N-Myc target genes in MYCN-amplified neuroblastoma cells. Molecular Cancer Therapeutics. 2007;6(10):2634-41.
57. Xiao D, Yue M, Su H, Ren P, Jiang J, Li F, et al. Polo-like Kinase-1 Regulates Myc Stabilization and Activates a Feedforward Circuit Promoting Tumor Cell Survival. Molecular Cell. 2016;64(3):493-506.

58. Kaneko Y, Suenaga Y, Islam SM, Matsumoto D, Nakamura Y, Ohira M, et al. Functional interplay between MYCN, NCYM, and OCT4 promotes aggressiveness of human neuroblastomas. Cancer Science. 2015;106(7):840-7.
59. Mac SM, D'Cunha CA, Farnham PJ. Direct recruitment of N-myc to target gene promoters. Molecular Carcinogenesis. 2000;29(2):76-86.
60. Liu T, Tee AE, Porro A, Smith SA, Dwarte T, Liu PY, et al. Activation of tissue transglutaminase transcription by histone deacetylase inhibition as a therapeutic approach for Myc oncogenesis. Proceedings of the National Academy of Sciences of the United States of America. 2007;104(47):18682-7.
61. Chen L, Iraci N, Gherardi S, Gamble LD, Wood KM, Perini G, et al. p53 is a direct transcriptional target of MYCN in neuroblastoma. Cancer Research. 2010;70(4):1377-88.
62. Strieder V, Lutz W. E2F proteins regulate MYCN expression in neuroblastomas. The Journal of Biological Chemistry. 2003;278(5):2983-9.
63. Kramps C, Strieder V, Sapetschnig A, Suske G, Lutz W. E2F and Sp1/Sp3 Synergize but are not sufficient to activate the MYCN gene in neuroblastomas. The Journal of Biological Chemistry. 2004;279(7):5110-7.
64. Suenaga Y, Yamamoto M, Sakuma T, Sasada M, Fukai F, Ohira M, et al. TAp63 represses transcription of MYCN/NCYM gene and its high levels of expression are associated with favorable outcome in neuroblastoma. Biochemical and Biophysical Research Communications. 2019;518(2):311-8.
65. Gu L, Zhang H, He J, Li J, Huang M, Zhou M. MDM2 regulates MYCN mRNA stabilization and translation in human neuroblastoma cells. Oncogene. 2012;31(11):1342-53.
66. Chagnovich D, Cohn SL. Binding of a 40-kDa protein to the N-myc 3'-untranslated region correlates with enhanced N-myc expression in human neuroblastoma. The Journal of Biological Chemistry. 1996;271(52):33580-6.
67. Manohar CF, Short ML, Nguyen A, Nguyen NN, Chagnovich D, Yang Q, et al. HuD, a neuronal-specific RNA-binding protein, increases the in vivo stability of MYCN RNA. The Journal of Biological Chemistry. 2002;277(3):1967-73.
68. Buechner J, Tomte E, Haug BH, Henriksen JR, Lokke C, Flaegstad T, et al. Tumour-suppressor microRNAs let-7 and mir-101 target the proto-oncogene MYCN and inhibit cell proliferation in MYCN-amplified neuroblastoma. British Journal of Cancer. 2011;105(2):296-303.
69. Hann SR. Role of post-translational modifications in regulating c-Myc proteolysis, transcriptional activity and biological function. Seminars in Cancer Biology. 2006;16(4):288-302.
70. Sjostrom SK, Finn G, Hahn WC, Rowitch DH, Kenney AM. The Cdk1 complex plays a prime role in regulating N-myc phosphorylation and turnover in neural precursors. Developmental Cell. 2005;9(3):327-38.

71. Gustafson WC, Weiss WA. Myc proteins as therapeutic targets. Oncogene. 2010;29(9):1249-59.
72. Otto T, Horn S, Brockmann M, Eilers U, Schuttrumpf L, Popov N, et al. Stabilization of N-Myc is a critical function of Aurora A in human neuroblastoma. Cancer Cell. 2009;15(1):67-78.
73. Zhao X, Heng JI, Guardavaccaro D, Jiang R, Pagano M, Guillemot F, et al. The HECT-domain ubiquitin ligase Huwe1 controls neural differentiation and proliferation by destabilizing the N-Myc oncoprotein. Nature Cell Biology. 2008;10(6):643-53.
74. Charron J, Malynn BA, Fisher P, Stewart V, Jeannotte L, Goff SP, et al. Embryonic lethality in mice homozygous for a targeted disruption of the N-myc gene. Genes & Development. 1992;6(12a):2248-57.
75. Knoepfler PS, Cheng PF, Eisenman RN. N-myc is essential during neurogenesis for the rapid expansion of progenitor cell populations and the inhibition of neuronal differentiation. Genes & Development. 2002;16(20):2699-712.
76. Burnside RD, Molinari S, Botti C, Brooks SS, Chung WK, Mehta L, et al. Features of Feingold syndrome 1 dominate in subjects with 2p deletions including MYCN. American Journal of Medical Genetics. 2018;176(9):1956-63.
77. Seeger RC, Brodeur GM, Sather H, Dalton A, Siegel SE, Wong KY, et al. Association of multiple copies of the N-myc oncogene with rapid progression of neuroblastomas. The New England Journal of Medicine. 1985;313(18):1111-6.
78. Maris JM, Hogarty MD, Bagatell R, Cohn SL. Neuroblastoma. The Lancet.369(9579):2106-20.
79. Schwab M. MYCN Amplification in Neuroblastoma: a Paradigm for the Clinical Use of an Oncogene. Pathology Oncology Research. 1997;3(1):3-7.
80. Moreau LA, McGrady P, London WB, Shimada H, Cohn SL, Maris JM, et al. Does MYCN amplification manifested as homogeneously staining regions at diagnosis predict a worse outcome in children with neuroblastoma? A Children's Oncology Group study. Clinical Cancer Research. 2006;12(19):5693-7.
81. Brodeur GM. Molecular basis for heterogeneity in human neuroblastomas. European Journal of Cancer. 1995;31a(4):505-10.
82. Schramm A, Koster J, Assenov Y, Althoff K, Peifer M, Mahlow E, et al. Mutational dynamics between primary and relapse neuroblastomas. Nature Genetics. 2015;47(8):872-7.
83. Cheung L, Murray J, Haber M, Norris M. The MYCN Oncogene, Oncogene and Cancer - From Bench to Clinic, InTech, DOI: 10.5772/54813. Available from: https://www.intechopen.com/books/oncogene-and-cancer-from-bench-to-clinic/the-mycn-oncogene
84. Small MB, Hay N, Schwab M, Bishop JM. Neoplastic transformation by the human gene N-myc. Molecular and Cellular Biology. 1987;7(5):1638-45.

85. Schwab M, Varmus HE, Bishop JM. Human N-myc gene contributes to neoplastic transformation of mammalian cells in culture. Nature. 1985;316(6024):160-2.
86. Weiss WA, Aldape K, Mohapatra G, Feuerstein BG, Bishop JM. Targeted expression of MYCN causes neuroblastoma in transgenic mice. The EMBO Journal. 1997;16(11):2985-95.
87. Althoff K, Beckers A, Bell E, Nortmeyer M, Thor T, Sprussel A, et al. A Cre-conditional MYCN-driven neuroblastoma mouse model as an improved tool for preclinical studies. Oncogene. 2015;34(26):3357-68.
88. Zhu S, Lee JS, Guo F, Shin J, Perez-Atayde AR, Kutok JL, et al. Activated ALK collaborates with MYCN in neuroblastoma pathogenesis. Cancer Cell. 2012;21(3):362-73.
89. Olsen RR, Otero JH, Garcia-Lopez J, Wallace K, Finkelstein D, Rehg JE, et al. MYCN induces neuroblastoma in primary neural crest cells. Oncogene. 2017.
90. Huang M, Weiss WA. Neuroblastoma and MYCN. Cold Spring Harbor Perspectives in Medicine. 2013;3(10):a014415.
91. Fredlund E, Ringner M, Maris JM, Pahlman S. High Myc pathway activity and low stage of neuronal differentiation associate with poor outcome in neuroblastoma. Proceedings of the National Academy of Sciences of the United States of America. 2008;105(37):14094-9.
92. Westermann F, Muth D, Benner A, Bauer T, Henrich KO, Oberthuer A, et al. Distinct transcriptional MYCN/c-MYC activities are associated with spontaneous regression or malignant progression in neuroblastomas. Genome Biology. 2008;9(10):R150.
93. Kushner BH, Modak S, Kramer K, LaQuaglia MP, Yataghene K, Basu EM, et al. Striking dichotomy in outcome of MYCN-amplified neuroblastoma in the contemporary era. Cancer. 2014;120(13):2050-9.
94. Lee JK, Phillips JW, Smith BA, Park JW, Stoyanova T, McCaffrey EF, et al. N-Myc Drives Neuroendocrine Prostate Cancer Initiated from Human Prostate Epithelial Cells. Cancer Cell. 2016;29(4):536-47.
95. Kim YH, Girard L, Giacomini CP, Wang P, Hernandez-Boussard T, Tibshirani R, et al. Combined microarray analysis of small cell lung cancer reveals altered apoptotic balance and distinct expression signatures of MYC family gene amplification. Oncogene. 2006;25(1):130-8.
96. Pfister S, Remke M, Benner A, Mendrzyk F, Toedt G, Felsberg J, et al. Outcome prediction in pediatric medulloblastoma based on DNA copy-number aberrations of chromosomes 6q and 17q and the MYC and MYCN loci. Journal of Clinical Oncology. 2009;27(10):1627-36.
97. Rushlow DE, Mol BM, Kennett JY, Yee S, Pajovic S, Theriault BL, et al. Characterisation of retinoblastomas without RB1 mutations: genomic, gene expression, and clinical studies. The Lancet Oncology. 2013;14(4):327-34.
98. Williams RD, Al-Saadi R, Chagtai T, Popov S, Messahel B, Sebire N, et al. Subtype-specific FBXW7 mutation and MYCN copy number gain in Wilms' tumor. Clinical Cancer Research. 2010;16(7):2036-45.

99. Williamson D, Lu YJ, Gordon T, Sciot R, Kelsey A, Fisher C, et al. Relationship between MYCN copy number and expression in rhabdomyosarcomas and correlation with adverse prognosis in the alveolar subtype. Journal of Clinical Oncology. 2005;23(4):880-8.
100. Hui AB, Lo KW, Yin XL, Poon WS, Ng HK. Detection of multiple gene amplifications in glioblastoma multiforme using array-based comparative genomic hybridization. Laboratory investigation. 2001;81(5):717-23.
101. Liu L, Xu F, Chang CK, He Q, Wu LY, Zhang Z, et al. MYCN contributes to the malignant characteristics of erythroleukemia through EZH2-mediated epigenetic repression of p21. Cell Death & Disease. 2017;8(10):e3126.
102. Astolfi A, Vendemini F, Urbini M, Melchionda F, Masetti R, Franzoni M, et al. MYCN is a novel oncogenic target in pediatric T-cell acute lymphoblastic leukemia. Oncotarget. 2014;5(1):120-30.
103. Puiggros A, Blanco G, Espinet B. Genetic abnormalities in chronic lymphocytic leukemia: where we are and where we go. BioMed Research International. 2014;2014:435983.
104. Janoueix-Lerosey I, Schleiermacher G, Michels E, Mosseri V, Ribeiro A, Lequin D, et al. Overall genomic pattern is a predictor of outcome in neuroblastoma. Journal of Clinical Oncology. 2009;27(7):1026-33.
105. Caren H, Fransson S, Ejeskar K, Kogner P, Martinsson T. Genetic and epigenetic changes in the common 1p36 deletion in neuroblastoma tumours. British Journal of Cancer. 2007;97(10):1416-24.
106. Caron H, van Sluis P, de Kraker J, Bokkerink J, Egeler M, Laureys G, et al. Allelic loss of chromosome 1p as a predictor of unfavorable outcome in patients with neuroblastoma. The New England Journal of Medicine. 1996;334(4):225-30.
107. Cole KA, Attiyeh EF, Mosse YP, Laquaglia MJ, Diskin SJ, Brodeur GM, et al. A functional screen identifies miR-34a as a candidate neuroblastoma tumor suppressor gene. Molecular Cancer Research. 2008;6(5):735-42.
108. Li S, Fell SM, Surova O, Smedler E, Wallis K, Chen ZX, et al. The 1p36 Tumor Suppressor KIF 1Bbeta Is Required for Calcineurin Activation, Controlling Mitochondrial Fission and Apoptosis. Developmental Cell. 2016;36(2):164-78.
109. Valentijn LJ, Koppen A, van Asperen R, Root HA, Haneveld F, Versteeg R. Inhibition of a new differentiation pathway in neuroblastoma by copy number defects of N-myc, Cdc42, and nm23 genes. Cancer Research. 2005;65(8):3136-45.
110. Henrich KO, Bauer T, Schulte J, Ehemann V, Deubzer H, Gogolin S, et al. CAMTA1, a 1p36 tumor suppressor candidate, inhibits growth and activates differentiation programs in neuroblastoma cells. Cancer Research. 2011;71(8):3142-51.

111. Liu Z, Yang X, Li Z, McMahon C, Sizer C, Barenboim-Stapleton L, et al. CASZ1, a candidate tumor-suppressor gene, suppresses neuroblastoma tumor growth through reprogramming gene expression. Cell Death and Differentiation. 2011;18(7):1174-83.
112. Egan CM, Nyman U, Skotte J, Streubel G, Turner S, O'Connell DJ, et al. CHD5 is required for neurogenesis and has a dual role in facilitating gene expression and polycomb gene repression. Developmental Cell. 2013;26(3):223-36.
113. Bown N, Cotterill S, Lastowska M, O'Neill S, Pearson AD, Plantaz D, et al. Gain of chromosome arm 17q and adverse outcome in patients with neuroblastoma. The New England Journal of Medicine. 1999;340(25):1954-61.
114. Vandesompele J, Michels E, De Preter K, Menten B, Schramm A, Eggert A, et al. Identification of 2 putative critical segments of 17q gain in neuroblastoma through integrative genomics. International Journal of Cancer. 2008;122(5):1177-82.
115. Mlakar V, Jurkovic Mlakar S, Lopez G, Maris JM, Ansari M, Gumy-Pause F. 11q deletion in neuroblastoma: a review of biological and clinical implications. Molecular Cancer. 2017;16(1):114.
116. Caren H, Kryh H, Nethander M, Sjoberg RM, Trager C, Nilsson S, et al. High-risk neuroblastoma tumors with 11q-deletion display a poor prognostic, chromosome instability phenotype with later onset. Proceedings of the National Academy of Sciences of the United States of America. 2010;107(9):4323-8.
117. Depuydt P, Boeva V, Hocking TD, Cannoodt R, Ambros IM, Ambros PF, et al. Genomic Amplifications and Distal 6q Loss: Novel Markers for Poor Survival in High-risk Neuroblastoma Patients. Journal of the National Cancer Institute. 2018;110(10):1084-93.
118. Molenaar JJ, Koster J, Zwijnenburg DA, van Sluis P, Valentijn LJ, van der Ploeg I, et al. Sequencing of neuroblastoma identifies chromothripsis and defects in neuritogenesis genes. Nature. 2012;483(7391):589-93.
119. Bresler SC, Weiser DA, Huwe PJ, Park JH, Krytska K, Ryles H, et al. ALK mutations confer differential oncogenic activation and sensitivity to ALK inhibition therapy in neuroblastoma. Cancer Cell. 2014;26(5):682-94.
120. Schleiermacher G, Javanmardi N, Bernard V, Leroy Q, Cappo J, Rio Frio T, et al. Emergence of new ALK mutations at relapse of neuroblastoma. Journal of Clinical Oncology. 2014;32(25):2727-34.
121. George RE, Sanda T, Hanna M, Frohling S, Luther W, 2nd, Zhang J, et al. Activating mutations in ALK provide a therapeutic target in neuroblastoma. Nature. 2008;455(7215):975-8.
122. Chen Y, Takita J, Choi YL, Kato M, Ohira M, Sanada M, et al. Oncogenic mutations of ALK kinase in neuroblastoma. Nature. 2008;455(7215):971-4.
123. Trigg RM, Turner SD. ALK in Neuroblastoma: Biological and Therapeutic Implications. Cancers. 2018;10(4).

124. Umapathy G, Mendoza-Garcia P, Hallberg B, Palmer RH. Targeting Anaplastic Lymphoma Kinase in neuroblastoma. APMIS : Acta Pathologica, Microbiologica, et Immunologica Scandinavica.2019 May;127(5):288-302.
125. Schonherr C, Ruuth K, Kamaraj S, Wang CL, Yang HL, Combaret V, et al. Anaplastic Lymphoma Kinase (ALK) regulates initiation of transcription of MYCN in neuroblastoma cells. Oncogene. 2012;31(50):5193-200.
126. Peifer M, Hertwig F, Roels F, Dreidax D, Gartlgruber M, Menon R, et al. Telomerase activation by genomic rearrangements in high-risk neuroblastoma. Nature. 2015;526(7575):700-4.
127. Eleveld TF, Oldridge DA, Bernard V, Koster J, Colmet Daage L, Diskin SJ, et al. Relapsed neuroblastomas show frequent RAS-MAPK pathway mutations. Nature Genetics. 2015;47(8):864-71.
128. Cole AJ, Zhu Y, Dwight T, Yu B, Dickson KA, Gard GB, et al. Comprehensive analyses of somatic TP53 mutation in tumors with variable mutant allele frequency. Scientific Data. 2017;4:170120.
129. Carr-Wilkinson J, O'Toole K, Wood KM, Challen CC, Baker AG, Board JR, et al. High Frequency of p53/MDM2/p14ARF Pathway Abnormalities in Relapsed Neuroblastoma. Clinical Cancer Research. 2010;16(4):1108-18.
130. Carr J, Bell E, Pearson AD, Kees UR, Beris H, Lunec J, et al. Increased frequency of aberrations in the p53/MDM2/p14(ARF) pathway in neuroblastoma cell lines established at relapse. Cancer Research. 2006;66(4):2138-45.
131. Ackermann S, Cartolano M, Hero B, Welte A, Kahlert Y, Roderwieser A, et al. A mechanistic classification of clinical phenotypes in neuroblastoma. Science. 2018;362(6419):1165-70.
132. Mosse YP, Laudenslager M, Longo L, Cole KA, Wood A, Attiyeh EF, et al. Identification of ALK as a major familial neuroblastoma predisposition gene. Nature. 2008;455(7215):930-5.
133. Barr EK, Applebaum MA. Genetic Predisposition to Neuroblastoma. Children. 2018;5(9).
134. Ritenour LE, Randall MP, Bosse KR, Diskin SJ. Genetic susceptibility to neuroblastoma: current knowledge and future directions. Cell and Tissue Research. 2018;372(2):287-307.
135. Melnikov S, Ben-Shem A, Garreau de Loubresse N, Jenner L, Yusupova G, Yusupov M. One core, two shells: bacterial and eukaryotic ribosomes. Nature Structural & Molecular Biology. 2012;19(6):560-7.
136. Beringer M, Rodnina MV. The ribosomal peptidyl transferase. Molecular Cell. 2007;26(3):311-21.
137. Engel C, Sainsbury S, Cheung AC, Kostrewa D, Cramer P. RNA polymerase I structure and transcription regulation. Nature. 2013;502(7473):650-5.
138. Goodfellow SJ, Zomerdijk JC. Basic mechanisms in RNA polymerase I transcription of the ribosomal RNA genes. Subcellular Biochemistry. 2013;61:211-36.
139. Tschochner H, Hurt E. Pre-ribosomes on the road from the nucleolus to the cytoplasm. Trends in Cell Biology. 2003;13(5):255-63.

140. Kohler A, Hurt E. Exporting RNA from the nucleus to the cytoplasm. Nature Reviews Molecular Cell Biology. 2007;8(10):761-73.
141. Pelletier J, Thomas G, Volarevic S. Ribosome biogenesis in cancer: new players and therapeutic avenues. Nature Reviews Cancer. 2018;18(1):51-63.
142. Mayer C, Grummt I. Ribosome biogenesis and cell growth: mTOR coordinates transcription by all three classes of nuclear RNA polymerases. Oncogene. 2006;25(48):6384-91.
143. Ruggero D. Revisiting the nucleolus: from marker to dynamic integrator of cancer signaling. Science Signaling. 2012;5(241):pe38.
144. Kobayashi C, Monforte-Munoz HL, Gerbing RB, Stram DO, Matthay KK, Lukens JN, et al. Enlarged and prominent nucleoli may be indicative of MYCN amplification: a study of neuroblastoma (Schwannian stroma-poor), undifferentiated/poorly differentiated subtype with high mitosis-karyorrhexis index. Cancer. 2005;103(1):174-80.
145. Wang LL, Suganuma R, Ikegaki N, Tang X, Naranjo A, McGrady P, et al. Neuroblastoma of undifferentiated subtype, prognostic significance of prominent nucleolar formation, and MYC/MYCN protein expression: a report from the Children's Oncology Group. Cancer. 2013;119(20):3718-26.
146. van Riggelen J, Yetil A, Felsher DW. MYC as a regulator of ribosome biogenesis and protein synthesis. Nature Reviews Cancer. 2010;10(4):301-9.
147. Boon K, Caron HN, van Asperen R, Valentijn L, Hermus MC, van Sluis P, et al. N-myc enhances the expression of a large set of genes functioning in ribosome biogenesis and protein synthesis. The EMBO Journal. 2001;20(6):1383-93.
148. Drygin D, Siddiqui-Jain A, O'Brien S, Schwaebe M, Lin A, Bliesath J, et al. Anticancer activity of CX-3543: a direct inhibitor of rRNA biogenesis. Cancer Research. 2009;69(19):7653-61.
149. Drygin D, Lin A, Bliesath J, Ho CB, O'Brien SE, Proffitt C, et al. Targeting RNA polymerase I with an oral small molecule CX-5461 inhibits ribosomal RNA synthesis and solid tumor growth. Cancer Research. 2011;71(4):1418-30.
150. Balasubramanian S, Hurley LH, Neidle S. Targeting G-quadruplexes in gene promoters: a novel anticancer strategy? Nature Reviews Drug Discovery. 2011;10(4):261-75.
151. Rhodes D, Lipps HJ. G-quadruplexes and their regulatory roles in biology. Nucleic Acids Research. 2015;43(18):8627-37.
152. Hansel-Hertsch R, Di Antonio M, Balasubramanian S. DNA G-quadruplexes in the human genome: detection, functions and therapeutic potential. Nature Reviews Molecular Cell Biology. 2017;18(5):279-84.
153. Zahler AM, Williamson JR, Cech TR, Prescott DM. Inhibition of telomerase by G-quartet DNA structures. Nature. 1991;350(6320):718-20.
154. Moye AL, Porter KC, Cohen SB, Phan T, Zyner KG, Sasaki N, et al. Telomeric G-quadruplexes are a substrate and site of localization for human telomerase. Nature Communications. 2015;6:7643.

155. Fay MM, Lyons SM, Ivanov P. RNA G-Quadruplexes in Biology: Principles and Molecular Mechanisms. Journal of Molecular Biology. 2017;429(14):2127-47.
156. Okuda H, Kanai A, Ito S, Matsui H, Yokoyama A. AF4 uses the SL1 components of RNAP1 machinery to initiate MLL fusion- and AEP-dependent transcription. Nature Communications. 2015;6:8869.
157. Russell J, Zomerdijk JC. The RNA polymerase I transcription machinery. Biochemical Society Symposium. 2006(73):203-16.
158. Xu H, Di Antonio M, McKinney S, Mathew V, Ho B, O'Neil NJ, et al. CX-5461 is a DNA G-quadruplex stabilizer with selective lethality in BRCA1/2 deficient tumours. Nature Communications. 2017;8:14432.
159. Negi SS, Brown P. Transient rRNA synthesis inhibition with CX-5461 is sufficient to elicit growth arrest and cell death in acute lymphoblastic leukemia cells. Oncotarget. 2015;6(33):34846-58.
160. Hein N, Cameron DP, Hannan KM, Nguyen NN, Fong CY, Sornkom J, et al. Inhibition of Pol I transcription treats murine and human AML by targeting the leukemia-initiating cell population. Blood. 2017;129(21):2882-95.
161. Bywater MJ, Poortinga G, Sanij E, Hein N, Peck A, Cullinane C, et al. Inhibition of RNA polymerase I as a therapeutic strategy to promote cancer-specific activation of p53. Cancer Cell. 2012;22(1):51-65.
162. Negi SS, Brown P. rRNA synthesis inhibitor, CX-5461, activates ATM/ATR pathway in acute lymphoblastic leukemia, arrests cells in G2 phase and induces apoptosis. Oncotarget. 2015;6(20):18094-104.
163. Quin J, Chan KT, Devlin JR, Cameron DP, Diesch J, Cullinane C, et al. Inhibition of RNA polymerase I transcription initiation by CX-5461 activates non-canonical ATM/ATR signaling. Oncotarget. 2016;7(31):49800-18.
164. Morgado-Palacin L, Llanos S, Urbano-Cuadrado M, Blanco-Aparicio C, Megias D, Pastor J, et al. Non-genotoxic activation of p53 through the RPL11-dependent ribosomal stress pathway. Carcinogenesis. 2014;35(12):2822-30.
165. Peltonen K, Colis L, Liu H, Jaamaa S, Moore HM, Enback J, et al. Identification of novel p53 pathway activating small-molecule compounds reveals unexpected similarities with known therapeutic agents. PloS One. 2010;5(9):e12996.
166. Peltonen K, Colis L, Liu H, Trivedi R, Moubarek MS, Moore HM, et al. A targeting modality for destruction of RNA polymerase I that possesses anticancer activity. Cancer Cell. 2014;25(1):77-90.
167. Burger K, Muhl B, Harasim T, Rohrmoser M, Malamoussi A, Orban M, et al. Chemotherapeutic drugs inhibit ribosome biogenesis at various levels. The Journal of Biological Chemistry. 2010;285(16):12416-25.

168. Cortes CL, Veiga SR, Almacellas E, Hernandez-Losa J, Ferreres JC, Kozma SC, et al. Effect of low doses of actinomycin D on neuroblastoma cell lines. Molecular Cancer. 2016;15:1.
169. Sobell HM. Actinomycin and DNA transcription. Proceedings of the National Academy of Sciences of the United States of America. 1985;82(16):5328-31.
170. Kang HJ, Park HJ. Novel molecular mechanism for actinomycin D activity as an oncogenic promoter G-quadruplex binder. Biochemistry. 2009;48(31):7392-8.
171. Ha M, Kim VN. Regulation of microRNA biogenesis. Nature Reviews Molecular Cell Biology. 2014;15(8):509-24.
172. Ul Hussain M. Micro-RNAs (miRNAs): genomic organisation, biogenesis and mode of action. Cell and Tissue Research. 2012;349(2):405-13.
173. O'Brien J, Hayder H, Zayed Y, Peng C. Overview of MicroRNA Biogenesis, Mechanisms of Actions, and Circulation. Frontiers in Endocrinology. 2018;9:402.
174. Creugny A, Fender A, Pfeffer S. Regulation of primary microRNA processing. FEBS Letters. 2018;592(12):1980-96.
175. Wu K, He J, Pu W, Peng Y. The Role of Exportin-5 in MicroRNA Biogenesis and Cancer. Genomics, Proteomics & Bioinformatics. 2018;16(2):120-6.
176. Krol J, Loedige I, Filipowicz W. The widespread regulation of microRNA biogenesis, function and decay. Nature Reviews Genetics. 2010;11(9):597-610.
177. Oliveto S, Mancino M, Manfrini N, Biffo S. Role of microRNAs in translation regulation and cancer. World Journal of Biological Chemistry. 2017;8(1):45-56.
178. Mulrane L, McGee SF, Gallagher WM, O'Connor DP. miRNA dysregulation in breast cancer. Cancer Research. 2013;73(22):6554-62.
179. Kozomara A, Birgaoanu M, Griffiths-Jones S. miRBase: from microRNA sequences to function. Nucleic Acids Research. 2019;47(D1):D155-d62.
180. Friedman RC, Farh KK, Burge CB, Bartel DP. Most mammalian mRNAs are conserved targets of microRNAs. Genome Research. 2009;19(1):92-105.
181. Palmero EI, de Campos SG, Campos M, de Souza NC, Guerreiro ID, Carvalho AL, et al. Mechanisms and role of microRNA deregulation in cancer onset and progression. Genetics and Molecular Biology. 2011;34(3):363-70.
182. Zhang B, Pan X, Cobb GP, Anderson TA. microRNAs as oncogenes and tumor suppressors. Developmental Biology. 2007;302(1):1-12.
183. Svoronos AA, Engelman DM, Slack FJ. OncomiR or Tumor Suppressor? The Duplicity of MicroRNAs in Cancer. Cancer Research. 2016;76(13):3666-70.
184. Peng Y, Croce CM. The role of MicroRNAs in human cancer. Signal Transduction and Targeted Therapy. 2016;1:15004.
185. Chen Y, Stallings RL. Differential patterns of microRNA expression in neuroblastoma are correlated with prognosis, differentiation, and apoptosis. Cancer Research. 2007;67(3):976-83.

186. Galardi A, Colletti M, Businaro P, Quintarelli C, Locatelli F, Di Giannatale A. MicroRNAs in Neuroblastoma: Biomarkers with Therapeutic Potential. Current Medicinal Chemistry. 2018;25(5):584-600.
187. Fontana L, Fiori ME, Albini S, Cifaldi L, Giovinazzi S, Forloni M, et al. Antagomir-17-5p abolishes the growth of therapy-resistant neuroblastoma through p21 and BIM. PloS One. 2008;3(5):e2236.
188. Mestdagh P, Bostrom AK, Impens F, Fredlund E, Van Peer G, De Antonellis P, et al. The miR-17-92 microRNA cluster regulates multiple components of the TGF-beta pathway in neuroblastoma. Molecular Cell. 2010;40(5):762-73.
189. Loven J, Zinin N, Wahlstrom T, Muller I, Brodin P, Fredlund E, et al. MYCN-regulated microRNAs repress estrogen receptor-alpha (ESR1) expression and neuronal differentiation in human neuroblastoma. Proceedings of the National Academy of Sciences of the United States of America. 2010;107(4):1553-8.
190. Ma L, Young J, Prabhala H, Pan E, Mestdagh P, Muth D, et al. miR-9, a MYC/MYCN-activated microRNA, regulates E-cadherin and cancer metastasis. Nature Cell Biology. 2010;12(3):247-56.
191. Ribeiro D, Klarqvist MDR, Westermark UK, Oliynyk G, Dzieran J, Kock A, et al. Regulation of Nuclear Hormone Receptors by MYCN-Driven miRNAs Impacts Neural Differentiation and Survival in Neuroblastoma Patients. Cell Reports. 2016;16(4):979-93.
192. Buechner J, Einvik C. N-myc and noncoding RNAs in neuroblastoma. Molecular Cancer Research. 2012;10(10):1243-53.
193. Li H, Xu Y, Qiu W, Zhao D, Zhang Y. Tissue miR-193b as a Novel Biomarker for Patients with Ovarian Cancer. Medical Science Monitor. 2015;21:3929-34.
194. Hu H, Li S, Liu J, Ni B. MicroRNA-193b modulates proliferation, migration, and invasion of non-small cell lung cancer cells. Acta Biochimica et Biophysica Sinica. 2012;44(5):424-30.
195. El-Gewely MR, Andreassen M, Walquist M, Ursvik A, Knutsen E, Nystad M, et al. Differentially Expressed MicroRNAs in Meningiomas Grades I and II Suggest Shared Biomarkers with Malignant Tumors. Cancers. 2016;8(3).
196. Chen J, Zhang X, Lentz C, Abi-Daoud M, Pare GC, Yang X, et al. miR-193b Regulates Mcl-1 in Melanoma. The American Journal of Pathology. 2011;179(5):2162-8.
197. Chen J, Feilotter HE, Pare GC, Zhang X, Pemberton JG, Garady C, et al. MicroRNA-193b represses cell proliferation and regulates cyclin D1 in melanoma. The American Journal of Pathology. 2010;176(5):2520-9.
198. Jin X, Sun Y, Yang H, Li J, Yu S, Chang X, et al. Deregulation of the MiR-193b-KRAS Axis Contributes to Impaired Cell Growth in Pancreatic Cancer. PloS One. 2015;10(4):e0125515.

199. Xu C, Liu S, Fu H, Li S, Tie Y, Zhu J, et al. MicroRNA-193b regulates proliferation, migration and invasion in human hepatocellular carcinoma cells. European Journal of Cancer. 2010;46(15):2828-36.
200. Li XF, Yan PJ, Shao ZM. Downregulation of miR-193b contributes to enhance urokinase-type plasminogen activator (uPA) expression and tumor progression and invasion in human breast cancer. Oncogene. 2009;28(44):3937-48.
201. Zhong Q, Wang T, Lu P, Zhang R, Zou J, Yuan S. miR-193b promotes cell proliferation by targeting Smad3 in human glioma. Journal of Neuroscience Research. 2014;92(5):619-26.
202. Lenarduzzi M, Hui AB, Alajez NM, Shi W, Williams J, Yue S, et al. MicroRNA-193b enhances tumor progression via down regulation of neurofibromin 1. PloS One. 2013;8(1):e53765.
203. Vlassov AV, Magdaleno S, Setterquist R, Conrad R. Exosomes: current knowledge of their composition, biological functions, and diagnostic and therapeutic potentials. Biochimica et Biophysica Acta. 2012;1820(7):940-8.
204. Hannafon BN, Ding WQ. Intercellular communication by exosome-derived microRNAs in cancer. International Journal of Molecular Sciences. 2013;14(7):14240-69.
205. Pant S, Hilton H, Burczynski ME. The multifaceted exosome: biogenesis, role in normal and aberrant cellular function, and frontiers for pharmacological and biomarker opportunities. Biochemical Pharmacology. 2012;83(11):1484-94.
206. Azmi AS, Bao B, Sarkar FH. Exosomes in cancer development, metastasis, and drug resistance: a comprehensive review. Cancer Metastasis Reviews. 2013;32(3-4):623-42.
207. Akers JC, Gonda D, Kim R, Carter BS, Chen CC. Biogenesis of extracellular vesicles (EV): exosomes, microvesicles, retrovirus-like vesicles, and apoptotic bodies. Journal of Neuro-Oncology. 2013;113(1):1-11.
208. Lawson C, Vicencio JM, Yellon DM, Davidson SM. Microvesicles and exosomes: new players in metabolic and cardiovascular disease. The Journal of Endocrinology. 2016;228(2):R57-71.
209. Kalluri R. The biology and function of exosomes in cancer. The Journal of Clinical Investigation. 2016;126(4):1208-15.
210. de la Torre Gomez C, Goreham RV, Bech Serra JJ, Nann T, Kussmann M. "Exosomics"-A Review of Biophysics, Biology and Biochemistry of Exosomes With a Focus on Human Breast Milk. Frontiers in genetics. 2018;9:92.
211. M HR, Bayraktar E, G KH, Abd-Ellah MF, Amero P, Chavez-Reyes A, et al. Exosomes: From Garbage Bins to Promising Therapeutic Targets. International Journal of Molecular Sciences. 2017;18(3).
212. Bae S, Brumbaugh J, Bonavida B. Exosomes derived from cancerous and non-cancerous cells regulate the anti-tumor response in the tumor microenvironment. Genes & Cancer. 2018;9(3-4):87-100.

213. Kourembanas S. Exosomes: vehicles of intercellular signaling, biomarkers, and vectors of cell therapy. Annual Review of Physiology. 2015;77:13-27.
214. Hoshino A, Costa-Silva B, Shen TL, Rodrigues G, Hashimoto A, Tesic Mark M, et al. Tumour exosome integrins determine organotropic metastasis. Nature. 2015;527(7578):329-35.
215. Costa-Silva B, Aiello NM, Ocean AJ, Singh S, Zhang H, Thakur BK, et al. Pancreatic cancer exosomes initiate pre-metastatic niche formation in the liver. Nature Cell Biology. 2015;17(6):816-26.
216. Peinado H, Aleckovic M, Lavotshkin S, Matei I, Costa-Silva B, Moreno-Bueno G, et al. Melanoma exosomes educate bone marrow progenitor cells toward a pro-metastatic phenotype through MET. Nature Medicine. 2012;18(6):883-91.
217. Umezu T, Ohyashiki K, Kuroda M, Ohyashiki JH. Leukemia cell to endothelial cell communication via exosomal miRNAs. Oncogene. 2013;32(22):2747-55.
218. Le MT, Hamar P, Guo C, Basar E, Perdigao-Henriques R, Balaj L, et al. miR-200-containing extracellular vesicles promote breast cancer cell metastasis. The Journal of Clinical Investigation. 2014;124(12):5109-28.
219. Cervantes JL, Weinerman B, Basole C, Salazar JC. TLR8: the forgotten relative revindicated. Cellular & Molecular Immunology. 2012;9(6):434-8.
220. Fabbri M, Paone A, Calore F, Galli R, Gaudio E, Santhanam R, et al. MicroRNAs bind to Toll-like receptors to induce prometastatic inflammatory response. Proceedings of the National Academy of Sciences of the United States of America. 2012;109(31):E2110-6.
221. Kanlikilicer P, Rashed MH, Bayraktar R, Mitra R, Ivan C, Aslan B, et al. Ubiquitous Release of Exosomal Tumor Suppressor miR-6126 from Ovarian Cancer Cells. Cancer Research. 2016;76(24):7194-207.
222. Yu X, Eischeid H, Büttner R, Odenthal M. Tumor suppressor microRNA-198 is actively transported out of liver cancer cells. Zeitschrift für Gastroenterologie. 2016;54(12):A4. 46.
223. Kosaka N, Iguchi H, Yoshioka Y, Hagiwara K, Takeshita F, Ochiya T. Competitive interactions of cancer cells and normal cells via secretory microRNAs. The Journal of Biological Chemistry. 2012;287(2):1397-405.
224. Mullen P. The use of Matrigel to facilitate the establishment of human cancer cell lines as xenografts. Methods in Molecular Medicine. 2004;88:287-92.
225. Diehl KH, Hull R, Morton D, Pfister R, Rabemampianina Y, Smith D, et al. A good practice guide to the administration of substances and removal of blood, including routes and volumes. Journal of Applied Toxicology. 2001;21(1):15-23.
226. Ke N, Wang X, Xu X, Abassi YA. The xCELLigence system for real-time and label-free monitoring of cell viability. Methods in Molecular Biology. 2011;740:33-43.
227. Mitchell JP, Court J, Mason MD, Tabi Z, Clayton A. Increased exosome production from tumour cell cultures using the Integra CELLine Culture System. Journal of Immunological Methods. 2008;335(1-2):98-105.

228. Rani S, O'Brien K, Kelleher FC, Corcoran C, Germano S, Radomski MW, et al. Isolation of exosomes for subsequent mRNA, MicroRNA, and protein profiling. Methods in Molecular Biology. 2011;784:181-95.
229. Bachurski D, Schuldner M, Nguyen PH, Malz A, Reiners KS, Grenzi PC, et al. Extracellular vesicle measurements with nanoparticle tracking analysis - An accuracy and repeatability comparison between NanoSight NS300 and ZetaView. Journal of Extracellular Vesicles. 2019;8(1):1596016.
230. Lee HC, Wang H, Baladandayuthapani V, Lin H, He J, Jones RJ, et al. RNA Polymerase I Inhibition with CX-5461 as a Novel Therapeutic Strategy to Target MYC in Multiple Myeloma. British Journal of Haematology. 2017;177(1):80-94.
231. Kim DW, Wu N, Kim YC, Cheng PF, Basom R, Kim D, et al. Genetic requirement for Mycl and efficacy of RNA Pol I inhibition in mouse models of small cell lung cancer. Genes & Development. 2016;30(11):1289-99.
232. Niemas-Teshiba R, Matsuno R, Wang LL, Tang XX, Chiu B, Zeki J, et al. MYC-family protein overexpression and prominent nucleolar formation represent prognostic indicators and potential therapeutic targets for aggressive high-MKI neuroblastomas: a report from the children's oncology group. Oncotarget. 2018;9(5):6416-32.
233. Taylor JS, Zeki J, Ornell K, Coburn J, Shimada H, Ikegaki N, et al. Down-regulation of MYCN protein by CX-5461 leads to neuroblastoma tumor growth suppression. Journal of pediatric surgery. 2019;54(6):1192-7.
234. Kimura T, Gotoh M, Nakamura Y, Arakawa H. hCDC4b, a regulator of cyclin E, as a direct transcriptional target of p53. Cancer Science. 2003;94(5):431-6.
235. Burmakin M, Shi Y, Hedstrom E, Kogner P, Selivanova G. Dual targeting of wild-type and mutant p53 by small molecule RITA results in the inhibition of N-Myc and key survival oncogenes and kills neuroblastoma cells in vivo and in vitro. Clinical Cancer Research. 2013;19(18):5092-103.
236. Trajkovski M, da Silva MW, Plavec J. Unique structural features of interconverting monomeric and dimeric G-quadruplexes adopted by a sequence from the intron of the N-myc gene. Journal of the American Chemical Society. 2012;134(9):4132-41.
237. Benabou S, Ferreira R, Avino A, Gonzalez C, Lyonnais S, Sola M, et al. Solution equilibria of cytosine- and guanine-rich sequences near the promoter region of the n-myc gene that contain stable hairpins within lateral loops. Biochimica et Biophysica Acta. 2014;1840(1):41-52.
238. Cammas A, Millevoi S. RNA G-quadruplexes: emerging mechanisms in disease. Nucleic Acids Research. 2017;45(4):1584-95.
239. Rebello RJ, Kusnadi E, Cameron DP, Pearson HB, Lesmana A, Devlin JR, et al. The Dual Inhibition of RNA Pol I Transcription and PIM Kinase as a New Therapeutic Approach to Treat Advanced Prostate Cancer. Clinical Cancer Research. 2016;22(22):5539-52.

240. Goldschneider D, Horvilleur E, Plassa LF, Guillaud-Bataille M, Million K, Wittmer-Dupret E, et al. Expression of C-terminal deleted p53 isoforms in neuroblastoma. Nucleic Acids Research. 2006;34(19):5603-12.
241. Gogolin S, Ehemann V, Becker G, Brueckner LM, Dreidax D, Bannert S, et al. CDK4 inhibition restores G(1)-S arrest in MYCN-amplified neuroblastoma cells in the context of doxorubicin-induced DNA damage. Cell Cycle. 2013;12(7):1091-104.
242. Smith J, Tho LM, Xu N, Gillespie DA. The ATM-Chk2 and ATR-Chk1 pathways in DNA damage signaling and cancer. Advances in Cancer Research. 2010;108:73-112.
243. Podhorecka M, Skladanowski A, Bozko P. H2AX Phosphorylation: Its Role in DNA Damage Response and Cancer Therapy. Journal of Nucleic Acids. 2010;2010.
244. Awasthi P, Foiani M, Kumar A. ATM and ATR signaling at a glance. Journal of Cell Science. 2015;128(23):4255-62.
245. Roy R, Chun J, Powell SN. BRCA1 and BRCA2: different roles in a common pathway of genome protection. Nature Reviews Cancer. 2011;12(1):68-78.
246. Zitvogel L, Kepp O, Kroemer G. Immune parameters affecting the efficacy of chemotherapeutic regimens. Nature Reviews Clinical Oncology. 2011;8(3):151-60.
247. Khot A, Brajanovski N, Cameron DP, Hein N, Maclachlan KH, Sanij E, et al. First-in-Human RNA Polymerase I Transcription Inhibitor CX-5461 in Patients with Advanced Hematologic Cancers: Results of a Phase I Dose-Escalation Study. Cancer Discovery. 2019;9(8):1036-49.
248. Beckers A, Van Peer G, Carter DR, Mets E, Althoff K, Cheung BB, et al. MYCN-targeting miRNAs are predominantly downregulated during MYCNdriven neuroblastoma tumor formation. Oncotarget. 2015;6(7):5204-16.
249. Lim S, Kaldis P. Cdks, cyclins and CKIs: roles beyond cell cycle regulation. Development. 2013;140(15):3079-93.
250. Molenaar JJ, van Sluis P, Boon K, Versteeg R, Caron HN. Rearrangements and increased expression of cyclin D1 (CCND1) in neuroblastoma. Genes, Chromosomes & Cancer. 2003;36(3):242-9.
251. Molenaar JJ, Ebus ME, Koster J, van Sluis P, van Noesel CJ, Versteeg R, et al. Cyclin D1 and CDK4 activity contribute to the undifferentiated phenotype in neuroblastoma. Cancer Research. 2008;68(8):2599-609.
252. Henriksen JR, Haug BH, Buechner J, Tomte E, Lokke C, Flaegstad T, et al. Conditional expression of retrovirally delivered anti-MYCN shRNA as an in vitro model system to study neuronal differentiation in MYCN-amplified neuroblastoma. BMC Developmental Biology. 2011;11:1.
253. Singh R, Letai A, Sarosiek K. Regulation of apoptosis in health and disease: the balancing act of BCL-2 family proteins. Nature Reviews Molecular Cell Biology. 2019;20(3):175-93.

254. Goldsmith KC, Gross M, Peirce S, Luyindula D, Liu X, Vu A, et al. Mitochondrial Bcl-2 family dynamics define therapy response and resistance in neuroblastoma. Cancer Research. 2012;72(10):2565-77.
255. Mazzu YZ, Hu Y, Soni RK, Mojica KM, Qin LX, Agius P, et al. miR-193b-Regulated Signaling Networks Serve as Tumor Suppressors in Liposarcoma and Promote Adipogenesis in Adipose-Derived Stem Cells. Cancer Research. 2017;77(21):5728-40.
256. Trang P, Wiggins JF, Daige CL, Cho C, Omotola M, Brown D, et al. Systemic delivery of tumor suppressor microRNA mimics using a neutral lipid emulsion inhibits lung tumors in mice. Molecular Therapy. 2011;19(6):1116-22.
257. Di Martino MT, Gulla A, Gallo Cantafio ME, Altomare E, Amodio N, Leone E, et al. In vitro and in vivo activity of a novel locked nucleic acid (LNA)-inhibitor-miR-221 against multiple myeloma cells. PloS One. 2014;9(2):e89659.
258. Beg MS, Brenner AJ, Sachdev J, Borad M, Kang YK, Stoudemire J, et al. Phase I study of MRX34, a liposomal miR-34a mimic, administered twice weekly in patients with advanced solid tumors. Investigational New Drugs. 2017;35(2):180-8.
259. Wang M, Yu F, Ding H, Wang Y, Li P, Wang K. Emerging Function and Clinical Values of Exosomal MicroRNAs in Cancer. Molecular therapy Nucleic acids. 2019;16:791-804.
260. Feng D, Zhao WL, Ye YY, Bai XC, Liu RQ, Chang LF, et al. Cellular internalization of exosomes occurs through phagocytosis. Traffic. 2010;11(5):675-87.
261. Challagundla KB, Wise PM, Neviani P, Chava H, Murtadha M, Xu T, et al. Exosome-mediated transfer of microRNAs within the tumor microenvironment and neuroblastoma resistance to chemotherapy. Journal of the National Cancer Institute. 2015;107(7).
262. Heil F, Hemmi H, Hochrein H, Ampenberger F, Kirschning C, Akira S, et al. Species-specific recognition of single-stranded RNA via toll-like receptor 7 and 8. Science. 2004;303(5663):1526-9.
263. Morini M, Cangelosi D, Segalerba D, Marimpietri D, Raggi F, Castellano A, et al. Exosomal microRNAs from Longitudinal Liquid Biopsies for the Prediction of Response to Induction Chemotherapy in High-Risk Neuroblastoma Patients: A Proof of Concept SIOPEN Study. Cancers. 2019;11(10).

Appendix

Supplementary figures 1-3

Supplementary figure 1

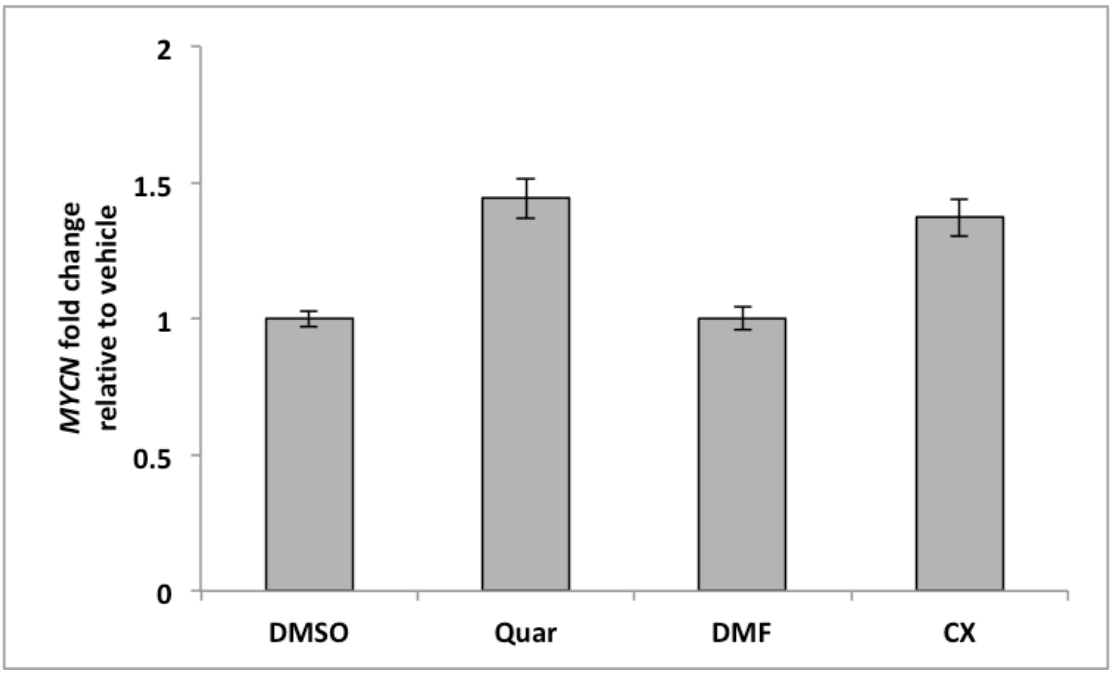

Suppl. figure 1 *MYCN* mRNA levels in IMR-32 after 24 hours treatment with 150 nM quarfloxin (quar) or 230 nM CX-5461 (CX). Treatment with both compounds lead to a slight relative increase in *MYCN* mRNAs. The data represents the mean and SD of two independent experiments performed with two biological replicates pr. condition. Relative expression of transcript levels was evaluated using the ddCT method with the geometric mean of two housekeeping genes (*SDHA* and *ACTB*). Primers: *MYCN*: forward 5'- ACACCCTGAGCGATTCAGAT-3', reverse 5'-TTCTCCACAGTGACCACGTC-3', *SDHA*: forward 5'-CTGATGAGACAAGATGTGGTG-3', reverse 5'-CAATCTCCCTTCAATGTACTCC-3', *ACTB*: forward 5'-CACCATGTACCCTGGCATT-3', reverse 5'-ACGGAGTACTTGCGCTCAG-3'.

Supplementary figure 2

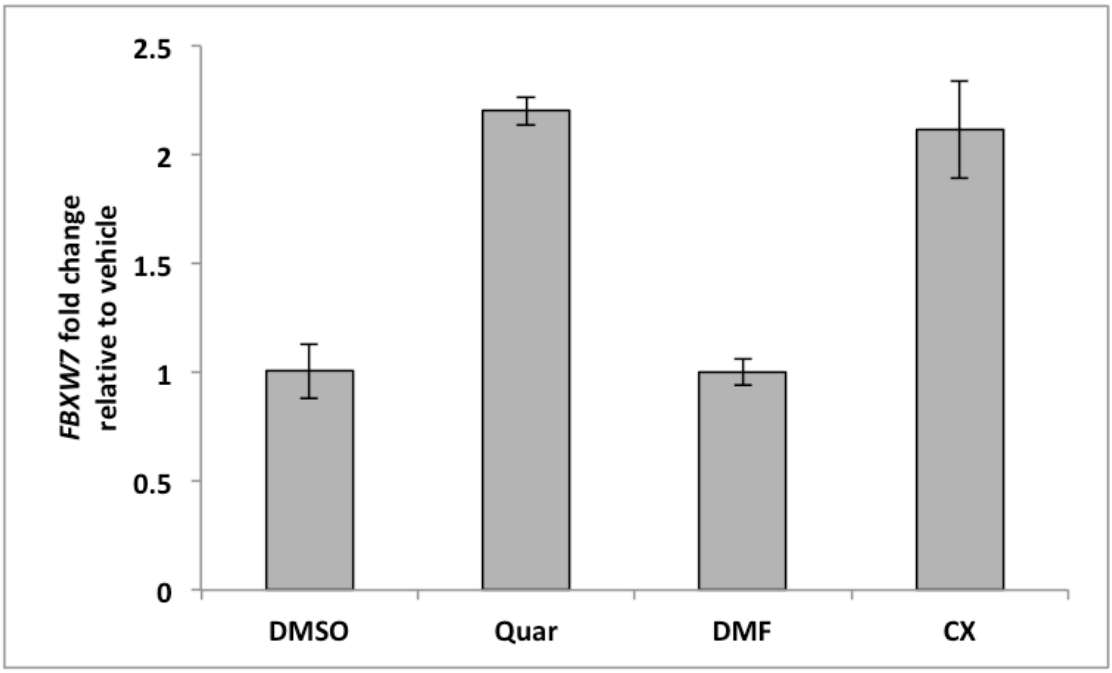

Suppl. figure 2 *FBXW7* mRNA levels in IMR-32 after 24 hours treatment with 150 nM quarfloxin (quar) or 230 nM CX-5461 (CX). Treatment with both compounds led to a distinct relative increase in *FBXW7* mRNAs. The data represents the mean and SD of two independent experiments performed with two biological replicates pr. condition. Relative expression of transcript levels was evaluated using the ddCT method with the geometric mean of two housekeeping genes (*SDHA* and *ACTB*). Primers: *FBXW7*: forward 5'-CCTCCAGGAATGGCTAAAAA-3', reverse 5'-AAGAGTTCATCTAAAGCAAGCAA-3', *SDHA* and *ACTB*: Same primers as in suppl. figure 1.

Supplementary figure 3

A)

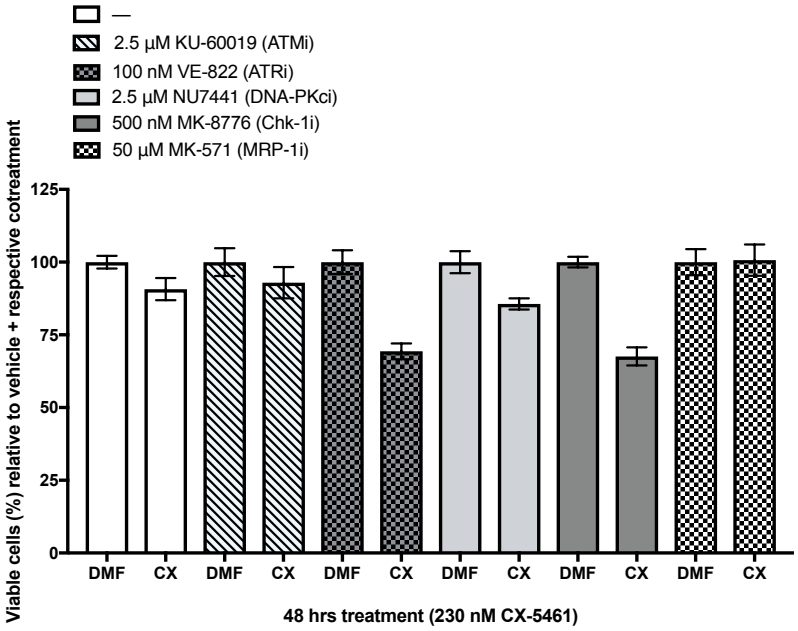

A) Viability (Alamar blue) of neuroblastoma cells 48 hours after exposure to CX-5461 in combination with ATM-inhibitor KU-60019, ATR-inhibitor VE-822, DNA-PKc-inhibitor NU7441, MK-8776 or MK-571. The viability of vehicle + respective drug was set to 100%, against which CX-5461 + respective drug were normalized against. The data represents the mean cell viability and Sc.D. of two individual experiments each performed in duplicate. These results show that the loss of cell viability is most pronounced with the combination of CX-5461 and ATR/Chk-1 inhibitors compared with CX-5461 alone or the combination of CX-5461 and the other compounds. ATM and DNA-PKc inhibition was assessed due to their importance as upstream activators of DNA-damage signaling. MK-571 was included to investigate whether CX-5461 could be subject of MRP-1 mediated drug efflux.

B)

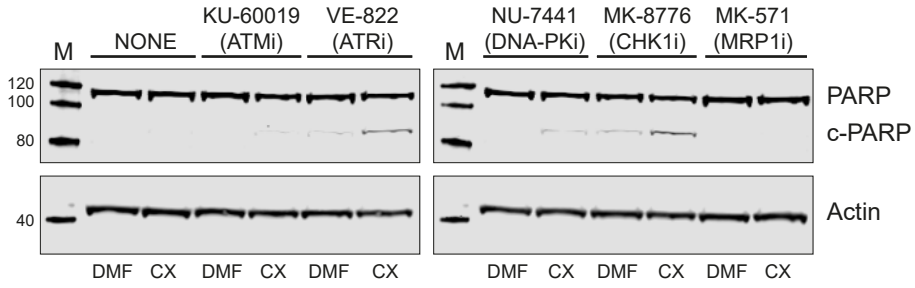

B) Western blot assessing apoptosis in neuroblastoma cells 48 hours after exposure to CX-5461 in combination with ATM-inhibitor KU-60019, ATR-inhibitor VE-822, DNA-PKc-inhibitor NU7441, MK-8776 or MK-571. These results show that the presence of apoptotic marker c-PARP is enhanced with the combination of CX-5461 and ATR/Chk-1 inhibitors compared with CX-5461 alone or the combination of CX-5461 and the other compounds.

Paper 1

Oncogene (2019) 38:2800–2813
https://doi.org/10.1038/s41388-018-0611-7

ARTICLE

Inhibitors of ribosome biogenesis repress the growth of *MYCN*-amplified neuroblastoma

Øyvind H. Hald[1] · Lotte Olsen[2] · Gabriel Gallo-Oller[3] · Lotta Helena Maria Elfman[3] · Cecilie Løkke[2] · Per Kogner[3] · Baldur Sveinbjörnsson[3,4] · Trond Flægstad[1,2] · John Inge Johnsen[3] · Christer Einvik[1,2]

Received: 26 April 2018 / Revised: 27 September 2018 / Accepted: 23 November 2018 / Published online: 12 December 2018

Abstract

Abnormal increases in nucleolar size and number caused by dysregulation of ribosome biogenesis has emerged as a hallmark in the majority of spontaneous cancers. The observed ribosome hyperactivity can be directly induced by the *MYC* transcription factors controlling the expression of RNA and protein components of the ribosome. Neuroblastoma, a highly malignant childhood tumor of the sympathetic nervous system, is frequently characterized by *MYCN* gene amplification and high expression of *MYCN* and *c-MYC* signature genes. Here, we show a strong correlation between high-risk disease, *MYCN* expression, poor survival, and ribosome biogenesis in neuroblastoma patients. Treatment of neuroblastoma cells with quarfloxin or CX-5461, two small molecule inhibitors of RNA polymerase I, suppressed MycN expression, induced DNA damage, and activated p53 followed by cell cycle arrest or apoptosis. CX-5461 repressed the growth of established *MYCN*-amplified neuroblastoma xenograft tumors in nude mice. These findings suggest that inhibition of ribosome biogenesis represent new therapeutic opportunities for children with high-risk neuroblastomas expressing high levels of Myc.

Introduction

Neuroblastoma, a childhood tumor of the peripheral sympathetic nervous system, originates from neural crest cells and usually manifests in the adrenal gland or in a paraspinal location in the abdomen or chest. The clinical features of neuroblastoma are characterized by heterogeneity spanning from spontaneous regression or differentiation with an overall survival of 85–90%, to treatment-refractory progression and metastatic tumors with less than 50% of the patients surviving despite intensive therapies [1]. Currently, no effective therapy exists for patients with recurrent or relapsed neuroblastoma, and new treatment modalities for these patients are urgently needed.

A molecular hallmark of high-risk neuroblastoma is genetic amplification and high expression of the *MYCN* oncogene [2]. Also, single-copy high-risk neuroblastomas frequently show high expression of the *MYCN* homolog *c-MYC* [3]. The MycN and c-Myc proteins are transcription factors, and exert their oncogenic effects through the activation and repression of a wide array of genes controlling fundamental cellular processes, including proliferation, cell growth, metabolism, differentiation, and migration [4].

Ribosomal biogenesis is upregulated in malignant cells, and nucleolar enlargement has been used as a marker for the histopathological diagnosing of cancer for over a century [5]. MycN has been shown to positively regulate the expression of a large set of genes involved in ribosomal biogenesis [6], and also c-Myc is well-established as a driver of this process [7]. In line with these observations, tumor cells from *MYC*-driven neuroblastomas frequently

Supplementary information The online version of this article (https://doi.org/10.1038/s41388-018-0611-7) contains supplementary material, which is available to authorized users.

✉ Christer Einvik
christer.einvik@uit.no

[1] Department of Pediatrics, Division of Child and Adolescent Health, UNN – University Hospital of North-Norway, NO-9038 Tromsø, Norway

[2] Pediatric Research Group, Department of Clinical Medicine, Faculty of Health Science, The Arctic University of Norway – UiT, NO-9037 Tromsø, Norway

[3] Childhood Cancer Research Unit, Department of Women's and Children's Health, Karolinska Institutet, 171 76 Stockholm, Sweden

[4] Molecular Inflammation Research Group, Department of Medical Biology, Faculty of Health Science, The Arctic University of Norway – UiT, NO-9037 Tromsø, Norway

display nucleolar hypertrophy [8, 9]. In recent years, specific inhibitors of ribosomal biogenesis have been developed and characterized. Two small molecular compounds, quarfloxin (CX-3543) and CX-5461, target and inhibit RNA pol I activity. CX-5461 is currently being tested in patients with advanced solid tumors (NCT02719977) and advanced hematological cancer (ACTRN12613001061729) [10]. Quarfloxin has completed phase 1 and 2 trials in patients with advanced solid tumors and lymphomas (NCT00955786) and neuroendocrine/carcinoid tumors (NCT00780663), respectively. Inhibition of RNA pol I activity has been shown to induce apoptosis, nucleolar surveillance signaling, p53 pathway activation, senescence, and pro-death autophagy [11–14].

In this study, we demonstrate a strong correlation between advanced stage disease, high *MYCN* expression levels, and elevated expression of genes involved in ribosome biogenesis in several large neuroblastoma patient cohorts. Based on these observations, we evaluated the effects of quarfloxin and CX-5461, two small molecule inhibitors of ribosome biogenesis in neuroblastoma cell lines and xenografts. Both quarfloxin and CX-5461 are cytotoxic to neuroblastoma cells in nanomolar concentrations and orally administered CX-5461 represses the growth of *MYCN*-amplified neuroblastoma xenografts in mice. Mechanistically, we demonstrate that both compounds induce p53 signaling, cell cycle arrest, DNA damage, and apoptosis of neuroblastoma cells and reduced MycN and RNA pol I activity.

Results

Neuroblastoma tumors with high ribosome biogenesis activity have poor a prognosis

A previous study by Boon et al. showed that the MycN protein enhances the rate of ribosome biogenesis in neuroblastoma cell lines [6]. To investigate how genes regulating ribosome biogenesis correlate with clinical parameters in neuroblastoma, we performed an unsupervised clustering analysis (k-means clustering) to subdivide the tumors in a large neuroblastoma RNAseq dataset (SEQC-498) in two groups according to expression of genes defined by the KEGG pathway "Ribosome Biogenesis in Eukaryotes". The 498 neuroblastoma tumors clustered into two well-defined groups characterized by low (Low-RiBi, $n = 354$) and high (High-RiBi, $n = 144$) expression of ribosome biogenesis genes (Supplementary Figure 1). Eighty-five percent of tumors defined by the High-RiBi group belong to advanced stage disease (INSS 3 and 4) (Fig. 1a). Furthermore, the High-RiBi tumors were characterized by high *MYCN* expression (Fig. 1b). Kaplan–Meier analyses of the two clusters showed that tumors from the High-RiBi group had a very poor overall- and event-free survival (log-rank test, $p = 4.7 \times 10^{-32}$ and $p = 7.4 \times 10^{-20}$, respectively, Figure 1c, d). Similar results were observed for several independent neuroblastoma cohorts investigated (Supplementary Figure 2A–D). These data demonstrate that neuroblastoma tumors with enhanced ribosome biogenesis activity are characterized by high *MYCN* expression, advanced stage disease, and poor prognosis.

Inhibitors of ribosome biogenesis decrease neuroblastoma cell viability

Given that the expression of genes involved in ribosome biogenesis strongly correlated with neuroblastoma high-risk disease and prognosis, we evaluated the effects of two compounds inhibiting RNA polymerase I in a panel of neuroblastoma cells (Supplementary Table 1). Neuroblastoma cells were incubated with an 8-log dose range of CX-5461 (0.0005–5000 nM) or quarfloxin (0.001–10000 nM) for 48 h (Fig. 2a), and absolute IC_{50} values were calculated (Table 1). *MYCN*-amplified (MNA) and wild-type *TP53* (wt-*TP53*) IMR-32 and CHP-134 cells, and *c-MYC* overexpressing/wt-*TP53* CHLA-15 cells, were highly sensitive to the action of both drugs. Also, the IC_{50} of MNA/mut-*TP53* cell lines BE(2)-C and Kelly were substantially lower than those of non-MNA/mut-*TP53* SK-N-AS and SK-N-FI cells.

These data show that quarfloxin and CX-5461 effectively inhibit the growth of neuroblastoma cells in vitro. MNA (or high *c-Myc*) and wt-*TP53* cell lines were found to be more sensitive to these drugs compared with cells with single-copy *MYCN* and inactivating *TP53* mutations.

High MycN expression sensitizes neuroblastoma cell lines to quarfloxin and CX-5461

To further investigate the relationship between MycN expression and ribosome biogenesis in neuroblastoma cell lines, we reanalyzed microarray gene expression data from a previous *MYCN* siRNA experiment on IMR-32 cells performed by Bell et al. [15]. K-means clustering with all genes in the KEGG pathway "Ribosome Biogenesis in Eukaryotes" revealed two distinct clusters defined by a High-RiBi and a Low-RiBi group (Supplementary Figure 3A). The High- and Low-RiBi clusters consisted of samples with high *MYCN* expression (no siRNA, siSCR-16h, and siSCR-48 h) and low *MYCN* expression (siMYCN-16 h and siMYCN-48 h), respectively. The expression of *MYCN* was significantly higher in the High-RiBi cluster compared with the Low-RiBi cluster (Supplementary Figure 3B). These data show that siRNA-mediated knockdown of MycN expression represses the expression of genes involved in ribosome biogenesis.

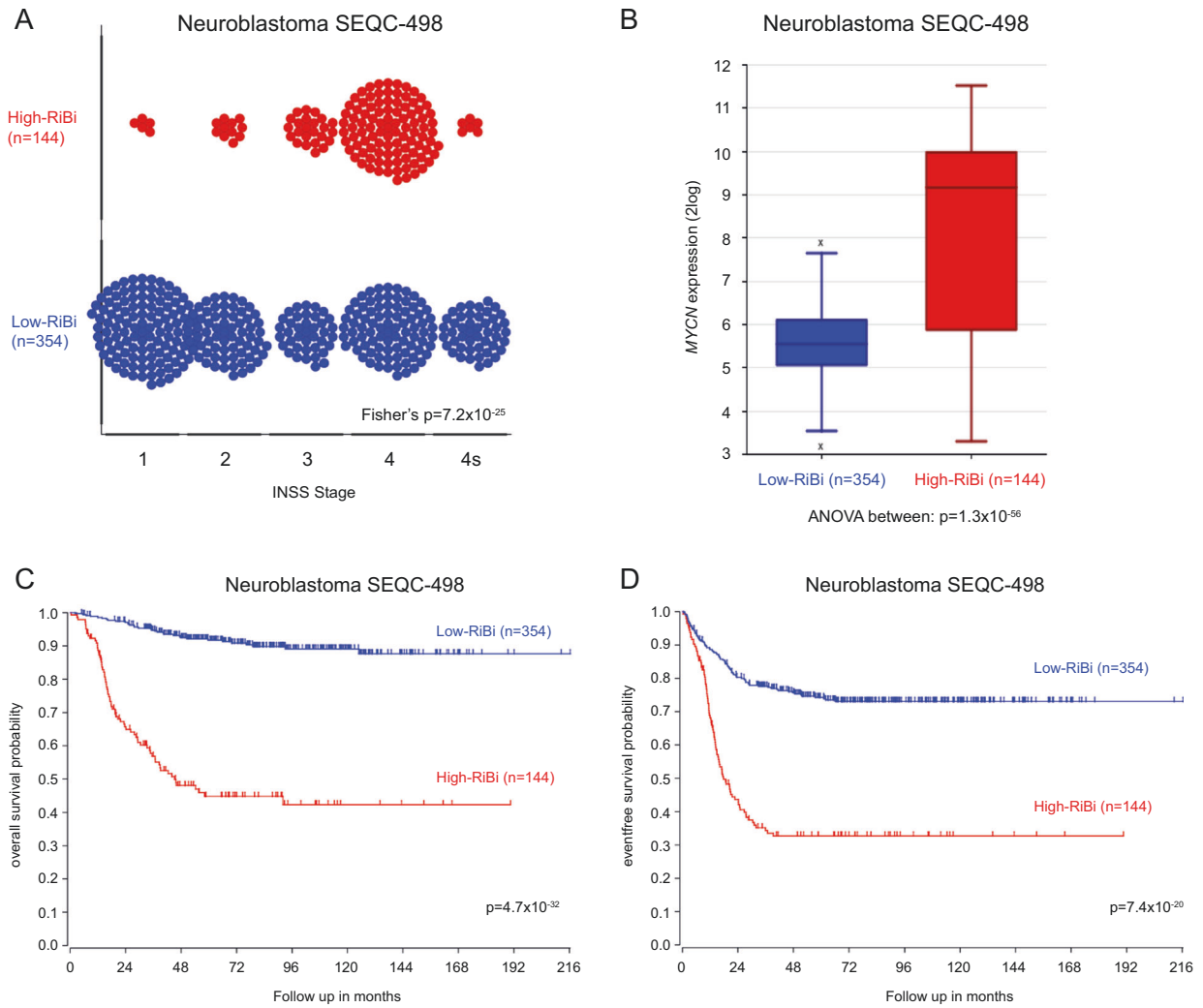

Fig. 1 Neuroblastoma tumors with enhanced ribosome biogenesis activity are characterized by high *MYCN* expression, advanced stage disease, and poor prognosis. **a** Plot showing the distribution of High-RiBi and Low-RiBi neuroblastoma tumors in different INSS stages. **b** Boxplot showing *MYCN* expression in tumors defined by High-RiBi and Low-RiBi. High-RiBi tumors show significantly higher *MYCN* expression. Kaplan–Meier analysis showing overall **c** and event-free **d** survival of neuroblastoma patients defined by High-RiBi and Low-RiBi tumors. The analyses were performed on publically available data (Tumor Neuroblastoma SEQC-498-RNAseq) from R2: Genomic Analysis and Visualization Platform (http://r2.amc.nl)

To functionally investigate the role of MycN on the sensitivity of neuroblastoma cell lines to the ribosome biogenesis inhibitors, we utilized the SHEP-TET21N model system. SHEP-TET21N is a MycN-inducible cell line derived from the parental single-copy *MYCN* human neuroblastoma cell line SHEP [16]. In the presence of 1 µg/mL doxycycline (dox), SHEP-TET21N cells express undetectable levels of MycN, whereas removal of dox induces high MycN expression (Fig. 2b, insert).

High MycN SHEP-TET21N cells grown without dox had a lower IC_{50} value for quarfloxin and CX-5461 compared with their low MycN expressing counterparts treated with 1 µg/mL doxycycline (Fig. 2b, Table 1).

Next, we used two different siRNAs targeting *MYCN* to knockdown MycN expression in the MNA neuroblastoma cell line IMR-32. Cells were transfected with siMYCN-1 and siMYCN-2 (siRNAs targeting *MYCN*) or siNC (a negative control siRNA), and treated with CX-5461 and quarfloxin. Efficient MycN knockdown was confirmed by western blot (Supplementary Figure 4A). After 48 h of drug treatment, both siMYCNs repressed the cytotoxic effect of the drugs when compared with siNC-treated cells (Fig. 2c). Similar results were observed in CHP-134 cells (Supplementary Figure 5).

These data confirm that neuroblastoma cells with high MycN expression are more sensitive to CX-5461 and quarfloxin than cells with low MycN expression.

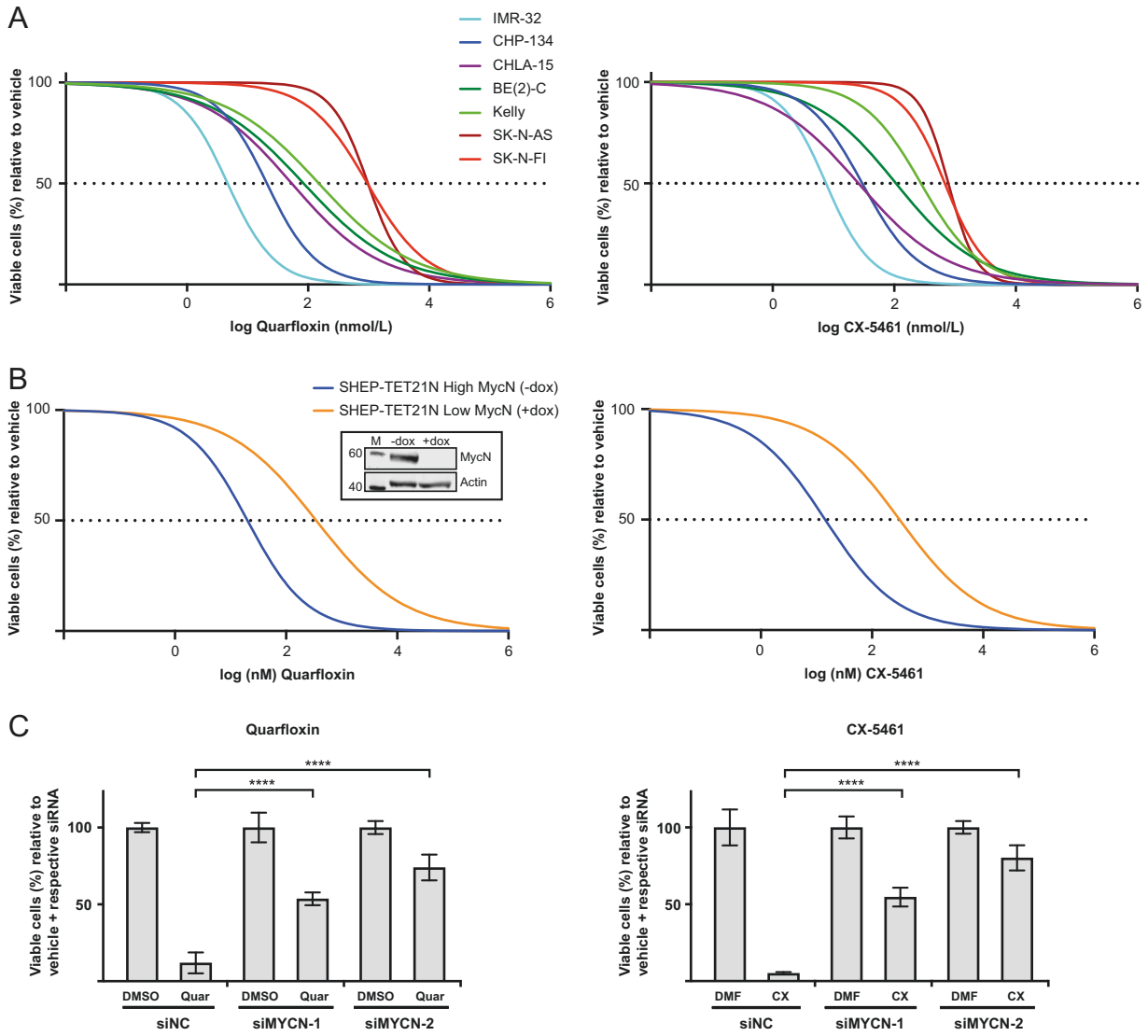

Fig. 2 Cell viability of neuroblastoma cell lines treated with quarfloxin or CX-5461. **a** Cell viability of neuroblastoma cell lines treated with an 8-log fold dose range of quarfloxin (left panel) or CX-5461 (right panel). Absolute half-maximal inhibitory concentrations (IC_{50} values) are shown in Table 1. **b** SHEP-TET21N cells were seeded in the presence (low MycN) or absence (high MycN) of 1 ug/mL doxycycline (dox). On the following day, cells were treated for 48 h with an 8-log fold change dose range of quarfloxin (left panel) or CX-5461 (right panel). IC_{50} values are shown in Table 1. Insert: WB showing MycN expression in absence (-dox) and in presence of dox (+dox). M = marker. Numbers to left indicate MW in kDa. **c** Cell viability of IMR-32 cells transfected with siRNAs (siMYCN-1 and siMYCN-2) targeting *MYCN* or a negative control siRNA (siNC), and treated with 50 nM quarfloxin (left panel) or 75 nM CX-5461 (right panel) for 48 h. The viability of vehicle + respective siRNA was set to 100%, and quarfloxin and CX-5461 treated cells were normalized to their respective controls. DMSO and DMF are vehicle controls to quarfloxin and CX-5461, respectively. For a, b, c; cell viability was measured with the Alamar blue assay. The data represents the mean cell viability and SD of two individual experiments performed in duplicate. (***$p \leq 0.001$; ****$p \leq 0.0001$)

Quarfloxin and CX-5461 induce DNA damage, p53 signaling, cell death, and cell cycle arrest in neuroblastoma cell lines

To investigate the mechanisms underlying the observed growth repression of neuroblastoma cells treated with quarfloxin and CX-5461, we analyzed several cell lines for the presence of apoptotic markers. First, we assessed the presence of the 89 kDa cleaved PARP (c-PARP) fragment and p53 on western blots of protein extracts isolated from cells treated with 150 nM quarfloxin or 230 nM of CX-5461 or 0.1% vehicle (DMSO and DMF, respectively). For all the wt-*TP53* cell lines tested (IMR-32, CHP-134, and CHLA-15), we detected increased presence of c-PARP and induction of the p53 protein after 24 h of treatment (Fig. 3a). On the contrary, mut-*TP53* cells (Kelly, SK-N-AS, and BE(2)-C) showed no significant increase in c-PARP or p53 expression. We further confirmed these observations by

Table 1 Half-maximal inhibitory concentration (IC50 values) from neuroblastoma cell lines treated with quarfloxin and CX-5461

Cell line	*MYCN* status	*TP53* status	IC50 (nM)±SD	
			Quarfloxin	CX-5461
IMR-32	Amp.	Wt	5.0 ± 2.2	7.6 ± 0.21
CHP-134	Amp.	Wt	23.0 ± 14.7	40.1 ± 13.9
CHLA-15	Non-amp.	Wt	54.0 ± 3.7	25.8 ± 2.2
BE(2)-C	Amp.	Mut	84.3 ± 5.0	106.9 ± 2.4
Kelly	Amp.	Mut	150.1 ± 33.7	275.6 ± 29.7
SK-N-AS	Non-amp.	Mut	965.2 ± 122.8	747.5 ± 65.8
SK-N-FI	Non-amp.	Mut	967.6 ± 178.8	618.3 ± 99.1
SHEP-TET21N -dox	Exogenous, high MycN	Wt	20.2 ± 0.03	14.4 ± 2.8
SHEP-TET21N + dox	Exogenous, low MycN	Wt	357.2 ± 151.5	311.8 ± 9.1

Data from two independent experiments each consisting of two biological replicates per concentration. SD is the standard deviation between the individual experiments

showing that two representative wt-*TP53* neuroblastoma cells (IMR-32 and CHLA-15) treated with quarfloxin or CX-5461 had increased expression of the 17/19 kDa cleaved-Caspase-3 (c-Casp-3) and induction of p21 protein and mRNA expression (Fig. 3b, Supplementary Figure 6). Enhanced c-Casp-3 or p21 expression was not observed in the mut-*TP53* neuroblastoma cell lines BE(2)-C and SK-N-AS treated with quarfloxin or CX-5461 (Fig. 3b).

Next, we used flow cytometry to analyze representative wt-*TP53* and mut-*TP53* neuroblastoma cell lines for the apoptotic marker Annexin V after treatment with quarfloxin or CX-5461. As shown in Fig. 3c, an increase in the proportion of Annexin V-positive cells after treatment with quarfloxin or CX-5461 was only observed in the wt-*TP53* cell lines IMR-32 and CHLA-15.

To further confirm the importance of functional p53 on the cytotoxic effect observed upon exposure of neuroblastoma cell lines to quarfloxin and CX-5461, we performed knockdown of *TP53* using two siRNAs (siTP53-1 and siTP53-2, Supplementary Figure 4B). When p53 expression was repressed by siTP53-1 and siTP53-2 in IMR-32 cells, the cytotoxic effect of quarfloxin and CX-5461 was reduced (Fig. 3d) and c-PARP was almost completely abolished (Fig. 3e). A similar, but less prominent, reduction in cell viability upon p53 knockdown was observed in CHP-134 cells (Supplementary Figure 5). Induction of functional p53 signaling by quarfloxin or CX-5461 was validated using a p53-responsive luciferase assay [17]. Only the wt-*TP53* cell lines (IMR-32 and CHLA-15) showed a significant increase in luciferase activity, indicating induction of functional p53 expression in cells exposed to CX-5461 or quarfloxin (Fig. 3f).

However, when we reconstituted functional p53 in BE(2)-C cells by exogenous overexpression of wt-p53, we did not observe a rescue in viability (Supplementary Figure 7A) or increased apoptosis (Supplementary Figure 7B) upon treatment with quarfloxin or CX-5461.

To further understand the growth impairing effects of quarfloxin and CX-5461 in the cell lines failing to undergo apoptosis, we evaluated cell cycle distribution profiles in BE(2)-C and SK-N-AS cells after treatment with these compounds. Both cell lines showed an accumulation in the G2/M-phase of the cell cycle after 24 h exposure to the drugs (Fig. 4a).

Genotoxic stress is a major activator of p53 signaling, therefore we investigated whether quarfloxin and CX-5461 have the propensity to induce DNA damage in neuroblastoma cell lines. In order to assess this, we evaluated the presence of DNA damage biomarker γ-H2A.X on western blots from several neuroblastoma cell lines. In all cell lines tested, we detected an increase of this marker, compared with vehicle-treated cells (Fig. 4b).

Together these results show that CX-5461 and quarfloxin induced DNA damage and impaired growth of neuroblastoma cells by apoptosis in wt-*TP53* cells and G2/M-arrest in mut-*TP53* cells.

Quarfloxin and CX-5461 reduce the expression of MycN and pre-rRNA (47S-rRNA)

To further explore how the RNA pol I inhibitors influence the biology of *MYCN*-amplified neuroblastoma cells, we examined the effect of quarfloxin and CX-5461 on MycN expression in several different *MYCN*-amplified neuroblastoma cell lines. MycN was downregulated in IMR-32 and CHP-134 cells, but not in mut-*TP53* BE(2)-C and Kelly cells after 48 h of drug treatment (Fig. 5a).

As quarfloxin and CX-5461 originally were characterized as direct inhibitors of RNA pol I activity, we assessed the ability of quarfloxin and CX-5461 to suppress the expression of RNA pol I transcript 47S-rRNA. The 47S-rRNA contains the 5'ETS of rDNA genes, which is the first region to be processed with fast kinetics, and is therefore often used as a proxy for the pre-rRNA transcriptional activity of RNA pol I [18]. To our surprise, quarfloxin and CX-5461 concentrations, which effectively induced DNA damage, cell death, p53 signaling, and cell cycle arrest, did not downregulate the expression of 47S-rRNA after 24 h of treatment (Fig. 5b). However, a downregulation of 47S-rRNA was observed after 24 h with a 10-fold increase of the quarfloxin or CX-5461 doses (Fig. 5c). In order to investigate other components of the ribosomal subunits, we measured the expression of mature rRNAs (18S-, 5.8S-, and

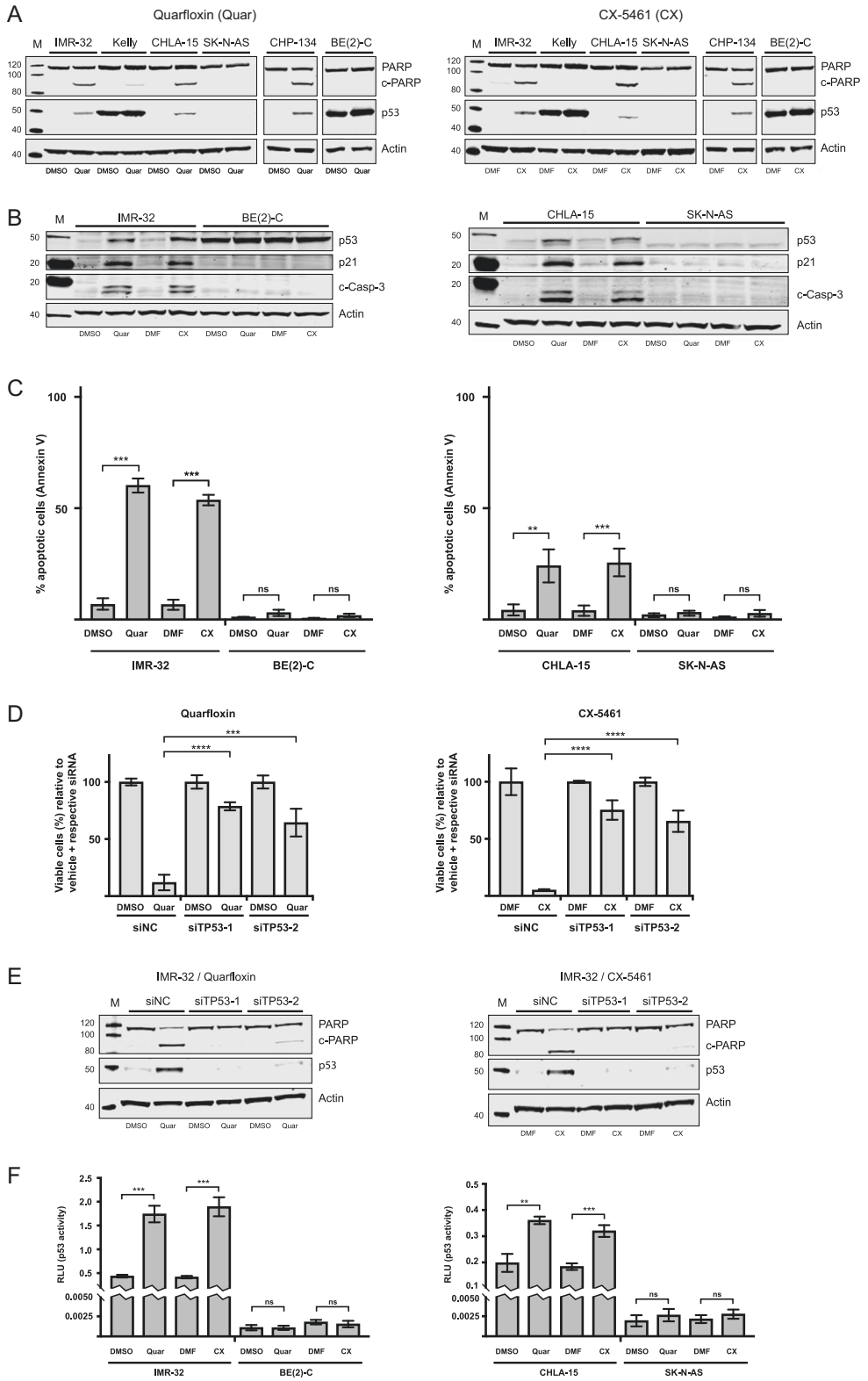

28S-rRNA) and a subset of ribosomal proteins (RPL13A, RPL32, RPS5, and RPS19) in IMR-32 cells exposed to low and high doses of quarfloxin or CX-5461. Similar to our observations of 47S-rRNA expression, no significant changes were observed for the other components of ribosomal subunits when IMR-32 cells were exposed to the low

◀ **Fig. 3** Quarfloxin and CX-5461 induce p53-dependent apoptosis in *TP53*-wt neuroblastoma cells. **a** Representative western blot (WB) for the assessment of cleaved PARP (c-PARP) and p53 expression in neuroblastoma cell lines treated for 24 h with 150 nM quarfloxin (left panel) or 230 nM CX-5461 (right panel) or 0.1% vehicle (DMSO and DMF, respectively). **b** Representative WB evaluation of cleaved-Caspase-3 (c-Casp-3), p53, and p21 expression in neuroblastoma cell lines treated as in **a**. **c** FACS analysis of Annexin V-positive neuroblastoma cells after 24 h treatment with 150 nM quarfloxin or 230 nM CX-5461 or vehicle. The data represents the mean and SD of representative experiments performed with two biological replicates pr. condition (ns, not significant; $^{**}p \le 0.01$; $^{***}p \le 0.001$). **d** p53 induction sensitizes neuroblastoma cells to quarfloxin and CX-5461. The day after transfection with siRNAs targeting *TP53* (siTP53-1 and siTP53-2), 50 nM quarfloxin (left panel) or 75 nM CX-5461 (right panel) were added and cell viability was measured 48 h after treatment. The viability of vehicle + respective siRNA was set to 100%, and quarfloxin and CX-5461 treated cells were normalized against their respective controls. The data represents the mean cell viability and s.d. of two individual experiments performed in duplicate ($^{***}p \le 0.001$; $^{****}p \le 0.0001$). **e** Representative WB assessing c-PARP levels after p53 knockdown. IMR-32 cells were reverse transfected with siTP53-1 and siTP53-2, and treated with 150 nM quarfloxin (left panel) or 230 nM CX-5461 (right panel) for 24 h before harvesting and immunoblotting. **f** Assessment of p53 transcriptional activity. Neuroblastoma cells were co-transfected immediately after seeding with a p53-responsive firefly luciferase reporter (pg13) and CMV-renilla luciferase. 150 nM quarfloxin or 230 nM CX-5461 were added the following day and cells were treated for 24 h before harvesting and analysis. Pg-13 expression was normalized to Renilla expression (RLU) and the data shown represents the mean of one experiment with three biological replicates and is representative of two independent experiments (ns, not significant; $^{**}p \le 0.01$; $^{***}p \le 0.001$)

cytotoxic doses of the inhibitors, except a minor reduction in expression of RPL32. However, when the same cells were exposed to 10-fold higher doses of quarfloxin and CX-5461, we measured increased levels of 18S-rRNA and 28S-rRNA. A similar increase was observed for ribosomal proteins RPL13A and RPS5 (Supplementary Figure 8).

CX-5461 represses the growth of neuroblastoma xenografts

Since quarfloxin and CX-5461 show almost identical effects in all neuroblastoma cell lines tested and because CX-5461 is currently in clinical trials, we decided to limit our preclinical in vivo investigations to CX-5461. In order to evaluate the therapeutic potential of CX-5461 in vivo, NMRI *nu/nu* mice with established IMR-32 or BE(2)-C xenograft tumors were treated by oral administration of CX-5461. In both models, a significant decrease of tumor growth was observed, with treated IMR-32 tumors reduced to 38% (Fig. 6a) and BE(2)-C to 69% (Fig. 6b) at the end of treatment compared with their respective control groups.

Histological analysis of tissue sections from treated tumors revealed a pale appearance with regional necrosis, hemorrhage and significant increase in damaged cells with disintegrated cytoplasm (Fig. 6c, Supplementary Figure 9). In addition, higher number of apoptotic cell bodies and fragmented nuclei were evident as confirmed by immunohistochemical detection of c-Casp-3 (Fig. 6d) and γ-H2A.X (Fig. 6e) levels in tumors from mice treated with CX-5461 compared with control tumors. Furthermore, compared with control tumors, treatment was associated with a prominent reduction in staining of the cell proliferation marker Ki-67 (Fig. 6f) and reduced levels of MycN protein (Fig. 6g). These histological features were in particular evident in tumor tissue from the *MYCN*-amplified IMR-32 xenograft. The data suggest an inhibitory effect of CX-5461 on tumor proliferation by induction of a DNA damage response and apoptosis.

Discussion

Despite intensive treatment modalities, the survival of patients with high-risk neuroblastoma is still around 50%. The major marker attributed to high-risk neuroblastoma is *MYCN* gene amplification and high-risk neuroblastoma patients without *MYCN*-amplification frequently exhibit high expression of either MycN, c-Myc, or Myc signature genes [19]. Our analysis of publicly available gene expression RNAseq and microarray data, show that high-risk neuroblastoma with high *MYCN* expression strongly correlates to elevated expression of genes involved in ribosome biogenesis and poor patient survival. Several observations have shown that c-Myc is an important regulator of ribosome biogenesis by affecting the expression of ribosomal genes as well as auxiliary factors important in ribosome biogenesis [7]. Also, elevated MycN expression has been suggested to augment the expression of several genes involved in ribosome biogenesis and protein synthesis [6]. Similarly, we found that siRNA-mediated down-regulation of MycN expression resulted in reduced expression of genes involved in ribosome biogenesis. Hyperactive ribosome biogenesis, which morphologically can be detected by an increase in nucleolar size and number, is a hallmark for the majority of cancers and is frequently associated with poor prognosis [5]. In neuroblastoma, poorly differentiated cells exhibit increased number of nucleolar organizer regions [20] suggesting increased proliferation and elevated ribosome biogenesis. Furthermore, neuroblastomas with high expression of MycN or c-Myc have been shown to exhibit enlarged nucleoli [8, 9]. Together, these data suggest that inhibition of ribosome biogenesis in neuroblastoma should be tested as a treatment option for neuroblastoma patients expressing high levels of MycN and/or c-Myc. In the present study, we show that treatment with quarfloxin or CX-5461, two small molecule inhibitors of RNA polymerase I, inhibited the growth of neuroblastoma cells with IC_{50} at nanomolar concentrations.

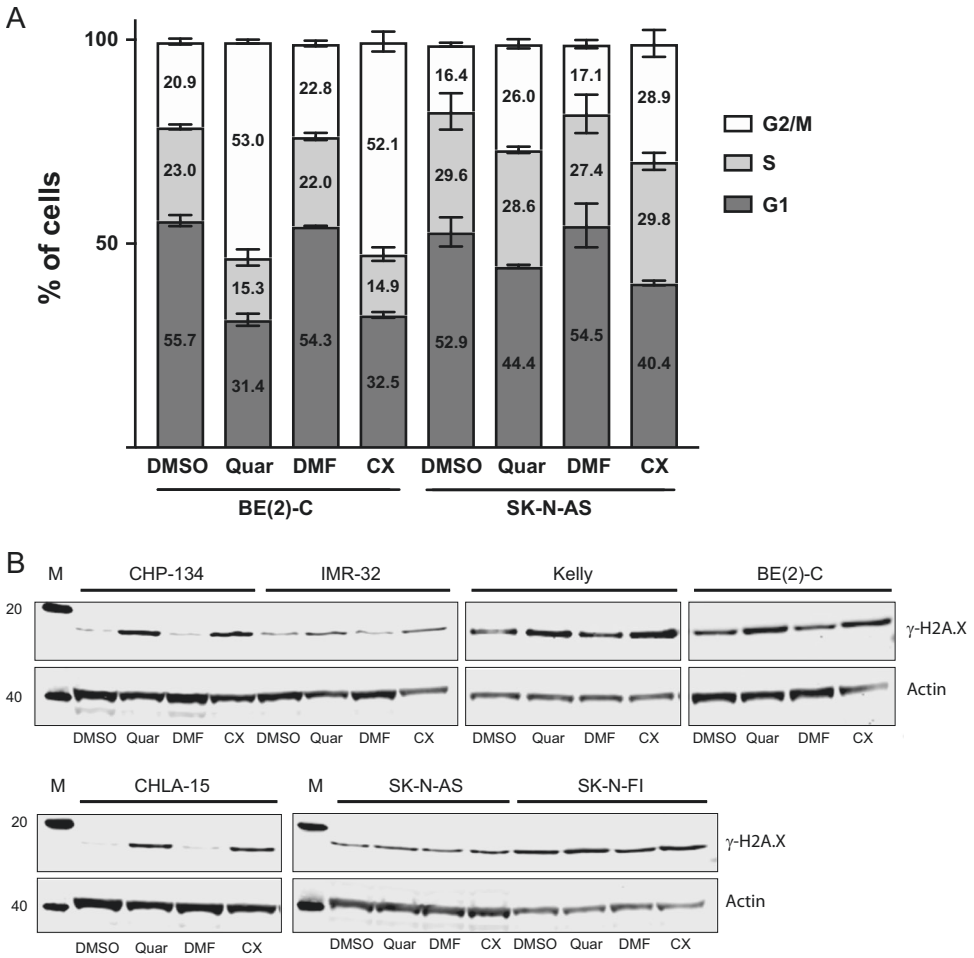

Fig. 4 Analysis of cell cycle distribution and DNA damage in neuroblastoma cell lines. **a** Quarfloxin and CX-5461 induce G2/M-arrest in *TP53*-mutated neuroblastoma cell lines. Flow cytometry analysis of cell cycle distribution in neuroblastoma cell lines BE(2)-C and SK-N-AS after 24 h treatment with 150 nM quarfloxin or 230 nM CX-5461. The data represent the mean percentage and SD of cells in G1, S, and G2/M phases from two individual experiments, each performed with two biological replicates. **b** Quarfloxin and CX-5461 induce DNA damage in neuroblastoma cell lines. Representative western blot of DNA damage marker γ-H2A.X in neuroblastoma cell lines exposed to 150 nM quarfloxin or 230 nM CX-5461 for 24 h

Neuroblastoma cells expressing high levels of *MYCN* or *c-MYC* were significantly more sensitive to treatment with these compounds. We also show that both drugs reduce the levels of MycN protein and that wt-*TP53* neuroblastoma cell lines activate p53 signaling and undergo apoptosis, whereas mut-*TP53* cells undergo cell cycle arrest in the G2/M-phase. Previously, CX-5461 has been shown to prevent initiation of rRNA synthesis by RNA polymerase I through inhibiting the binding of the transcription factor SL1 to the rDNA promoter, with subsequent release of free ribosomal proteins and activation of the nucleolar stress pathway promoting the activation of p53 signaling [21]. Exogenous addition of wt-*TP53* cDNA by transient transfection did not result in increased effects of CX-5461 or quarfloxin in BE(2)-C cells, a neuroblastoma cell line expressing high levels of mutant *TP53* (*TP53mut C135F*). *TP53*-C135F lies within the DNA-binding domain of the p53 protein (UniProt.org) and confers a loss of function to the p53 protein as demonstrated by loss of p53 transactivation activity [22]. In fact, the C135F-mutated version of p53 from SK-N-BE(2) cells has been shown to exert a moderate dominant negative effect on wt-p53 transcriptional activity [23]. Hence, the reason for the lack of increased effects of CX-5461 or quarfloxin in BE(2)-C could be caused by the presence of high levels of endogenous mutant-p53 protein that interferes with the exogenous wt-p53 during complex formation and binding to DNA, resulting in an incomplete restoration of the transactivation activity [24]. This also partly explains that we observed an increase in p21 expression in wt-*TP53* transfected cells but no increase in apoptotic marker (c-PARP) or rescue of cell viability. Together, this can, at least partly, explain the differential effects observed in neuroblastoma cells containing wt-*TP53* versus those cells with mutated *TP53*.

Destabilization of MycN or c-Myc proteins mediated by RNA polymerase I inhibitors has also been established by others [25, 26]. In our study, we did not observe reduction of MycN expression in the *TP53*-mutated cell lines Kelly and BE(2)-C, whereas MycN was robustly downregulated in wt-*TP53* IMR-32 and CHP-134 (Fig. 5a). A similar observation was very recently reported by Niemas-Teshiba et al. [21]. In this study, a low dose of CX-5461 (250 nM) efficiently repressed MycN expression in wt-*TP53* LAN5 cells after 24 h exposure, whereas a fourfold higher dose (1000 nM), only led to a very slight suppression of MycN in *TP53*-mutated Kelly cells. This differential response to the

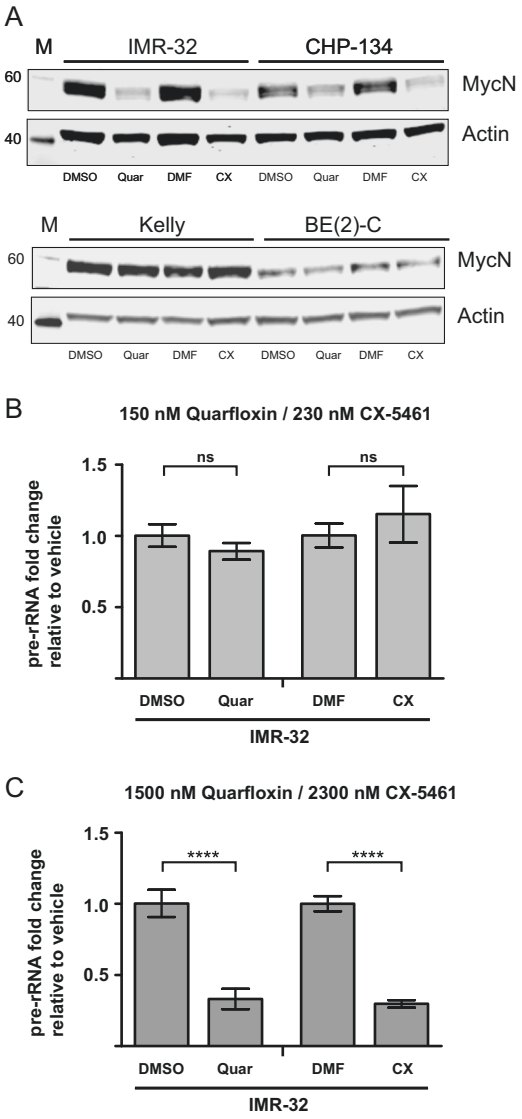

Fig. 5 Analysis of MycN and pre-rRNA expression in neuroblastoma cells treated with quarfloxin and CX-5461. **a** The protein levels of MycN are depleted in neuroblastoma cells with functional p53 upon treatment with quarfloxin or CX-5461. Representative western blot showing MycN protein levels in wt-*TP53* IMR-32 and CHP-134 (upper panel) and *TP53*-mutated Kelly and BE(2)-C (lower panel) cells after 48 h treatment with 150 nM quarfloxin or 230 nM CX-5461. **b** Expression of 47S-rRNA (pre-rRNA) in IMR-32 cells treated for 24 h with low doses of quarfloxin (150 nM) and CX-5461(230 nM). **c** Expression of 47S-rRNA (pre-rRNA) in IMR-32 cells treated for 24 h with high doses of quarfloxin (1500 nM) and CX-5461(2300 nM). ns, not significant; ****$p \le 0.0001$

drugs with regards to MycN expression could be explained by several possible mechanisms. Kelly and BE(2)-C cells have been characterized as drug-resistant cell lines whereas IMR-32 and CHP-134 are drug sensitive [27–29]. Therefore, the difference in MycN downregulation caused by CX-5461 and quarfloxin might be due to enhanced drug efflux caused by high levels of transporter molecules present in Kelly and BE(2)-C cells. In fact, the multifunctional drug transporter protein RALBP1/RLIP76 has been shown to be repressed by p53 in neuroblastoma cells expressing wt-p53. In contrast, SK-N-BE(2) cells expressing mutant-p53 showed overexpression of RALBP1/RLIP76 and increased drug resistance [30]. Another mechanism contributing to the difference in MycN expression could be explained by effects on the MycN degradation machinery. The FBXW7 E3-ubiquitin ligase is an important regulator of MycN stability in neuroblastoma cells [31]. In a study by Burmakin et al., reactivation of p53 by RITA was shown to induce a rapid and substantial downregulation of MycN via FBXW7-mediated proteasomal degradation in neuroblastoma cells [31]. Furthermore, reports from both ovarian and gastric cancers have shown that FBXW7 is downregulated in *TP53*-mutated tumors [32, 33]. When a dominant negative (R175H) p53 was overexpressed in wt-*TP53* ovarian cancer cell lines, the expression of FBXW7 was suppressed.

Interestingly, the *c-MYC* gene contains a G-quadruplex motif in its gene promoter and *MYCN* contains a G-quadruplex in intron 1, a region shown to be important for the transcriptional activation of this gene [34–36]. Quarfloxin has previously been described as a G-quadruplex stabilizer and reduces rRNA synthesis through disruption of the interaction between putative G-quadruplex structures in the rDNA and nucleolin [13]. Stabilization of G-quadruplexes in promoter regions has been shown to inhibit transcription, thereby providing another potential mechanism of *MYC* gene suppression by quarfloxin and CX-5461 [37].

Both quarfloxin and CX-5461 have previously been described as RNA polymerase I inhibitors [12, 13]. In our experiments, we did not observe any change in expression of 47S-rRNA when IMR-32 cells were exposed to quarfloxin and CX-5461 at doses which effectively induced DNA damage, cell death, p53 signaling, and cell cycle arrest (Fig. 5b). In addition, the expression of other components of the ribosomal subunits (mature rRNAs and ribosomal proteins) was also unaffected by this treatment (Supplementary Figure 8A and 8C). We therefore conclude that treatment with low cytotoxic doses of quarfloxin and CX-5461 does not significantly inhibit ribosomal biogenesis in *MYCN*-amplified neuroblastoma cell lines. However, when the cells were exposed to 10-fold higher doses of the drugs, we observed a marked downregulation of 47S-rRNA expression (Fig. 5c). These high concentrations of quarfloxin and CX-5461 also increased the levels of 18S-rRNA, 28S-rRNA, RPL13A, and RPS5 (Supplementary Figure 8B and 8D). We do not have a reasonable biological explanation for the discrepancy observed during exposure of high doses of the drugs. From the raw Cq values, we observe a significant increase, indicating reduced levels, of the mRNA housekeeping genes (*SDHA* and *ACTB*), 5.8S- and 47 S rRNA when cells were exposed to high doses of the drugs. This may explain the apparent increase of 18S- and 28S-rRNA

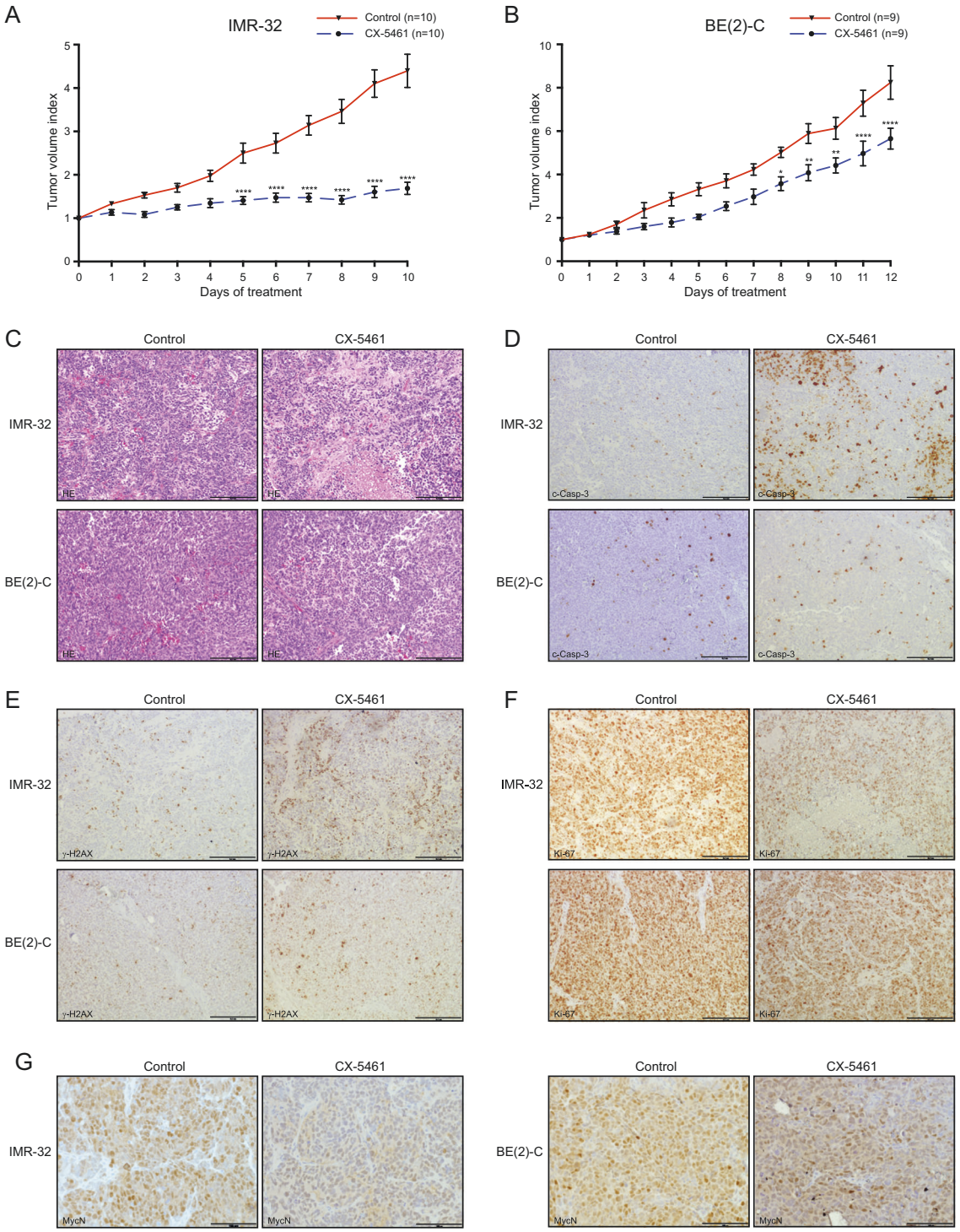

Fig. 6 CX-5461 inhibits neuroblastoma xenograft growth in vivo. **a** Comparison of tumor growth in IMR-32 xenograft bearing mice receiving no treatment ($n = 10$) or CX-5461 ($n = 10$) for 3–6 consecutive days and then every third days for 10 days. Tumor volume index (TVI) means with SEM is displayed (****$p \le 0.0001$). **b** Comparison of tumor growth (tumor volume index; TVI) in BE(2)-C engrafted mice receiving no treatment ($n = 9$) or CX-5461 ($n = 9$) every third day for 12 days. TVI means with SEM is displayed (*$p \le 0.05$; **$p \le 0.01$; ****$p \le 0.0001$). **c** Sections of dissected tumors were analyzed by hematoxylin and eosin (H&E) staining. IMR-32 xenografts sections deriving from mice treated with CX-5461 demonstrated areas with necrotic tissues, which was less evident in corresponding BE(2)-C xenografts, and **d** immunohistochemical staining with antibodies to detect the apoptotic marker c-Casp-3, **e** the DNA damage marker γ-H2A.X, **f** the proliferation marker Ki-67, and **g** MycN. Scalebar = 100 μm

measurements as a normalization artifact, rather than increased expression of these highly expressed and very stable rRNAs. A similar observation was reported in a study by Xu et al., demonstrating that these drugs caused synthetic lethality in BRCA1/2-deficient breast and ovarian cancers at doses which did not inhibit RNA pol I activity [38]. This study uncovered a novel mechanism of action for these drugs through causing replication-dependent ssDNA damage and subsequent growth arrest and apoptosis by stabilization of G-quadruplex structures in the genomic DNA. We demonstrate DNA damage in all neuroblastoma cell lines tested after treatment with quarfloxin and CX-5461, and in vivo DNA damage after CX-5461 treatment of nude mice bearing neuroblastoma xenografts. Our findings suggest that quarfloxin and CX-5461 cause cellular toxicity through a process involving stabilization of G-quadruplexes. The initial characterization studies by Drygin et al. described quarfloxin and CX-5461 as non-genotoxic using the Ames and Comet assay [12, 13]. This is in contrast to our results and the findings of Xu et al. [38] Furthermore, reports by Negi et al. and Quin et al. have shown that CX-5461 induces the ATM/ATR signaling pathway leading to a G2/M-phase cell cycle arrest [39, 40]. ATM and ATR are crucial sensors of DNA damage and activate the DNA damage response upon the presence of dsDNA or ssDNA breaks, respectively [41]. Negi et al. [39] demonstrated the enhancement of apoptosis in leukemia cells when co-treating with VE-822, an ATR inhibitor, and CX-5461. These results suggest that CX-5461 induces ssDNA damage, and show that co-targeting DNA damage response pathways can be utilized to overcome potential resistance to this agent.

CX-5461 significantly inhibited the growth of established *MYCN*-amplified neuroblastoma grown as xenografts in nude mice. Growth suppression was more pronounced in tumors harboring wt-*TP53* (IMR-32) compared with neuroblastoma containing mutated *TP53* (BE(2)-C). These results further support the notion that RNA polymerase I inhibitors activate p53 signaling and that p53 activation is one mechanism for the growth inhibiting effects seen by RNA polymerase I inhibitors in tumor cells.

Taken together, RNA polymerase I inhibitors are promising agents that should be further investigated in clinical studies as a treatment options for neuroblastoma patients with high expression of MycN or c-Myc.

Materials and methods

Cell culture

All cells were grown in a humidified incubator at 37 °C with 5% CO_2. BE(2)-C, SK-N-AS, CHP-134, Kelly and SHEP-TET21N cells were maintained in RPMI-1640 supplemented with 10% sterile-filtered fetal bovine serum (FBS). IMR-32 and SK-N-FI were grown in low glucose DMEM supplemented with 10% FBS and 1% non-essential amino acids (NEAA). CHLA-15 cells were grown in IMDM with 20% FBS, 1x ITS, and 4 nM L-glutamine. All cell identities were confirmed by short tandem repeat analysis, and the cells were regularly checked to be mycoplasma-free.

Chemicals

CX-5461 (Selleckchem) was resuspended in dimethylformamide (DMF) to a 5 mM stock. Quarfloxin (AdooQ) was resuspended in DMSO to a stock of 10 mM as recommended by the manufacturers. Aliquots of both chemicals were kept at −80 °C and were thawed and diluted in their respective vehicles (DMF or DMSO) for working solutions. The concentration of vehicle never exceeded 0.1%. For animal studies, CX-5461 was dissolved in 50 mM NaH_2PO_4 (pH 4.3) at 5 mg/mL.

Viability assays

For IC_{50} experiments, cells grown in 24-well plates were treated with an 8-log dose range of quarfloxin and CX-5461 in a total volume of 500 µL/well for 48 h before the addition of 50 µL Alamar blue reagent (Thermo Fisher) directly to the wells. Cells were incubated at 37 °C for an additional 2 h and 100 µL of media was transferred to a black-walled 96-well plate and fluorescence was measured at 540 nm excitation and 590 nm emission wavelengths using a micro plate reader (CLARIOstar). The raw data was normalized to vehicle treated, and IC_{50} was calculated using the Prism 7 software and the equation: log(inhibitor) vs. normalized response—Variable slope. All experiments were repeated twice with two biological replicates.

Flow cytometry

For cell cycle distribution profiling, cells were treated for 24 h in the presence of vehicle or 150 nM quarfloxin or 230 nM CX-5461. Floating and adherent cells (trypsination) were harvested and subsequently fixed and permeabilized in ice-cold 70% EtOH. Fixed cells were subsequently stained in PBS containing 50 µg/mL Propidium Iodide (PI) and 100 µg/mL RNaseA for 30 min protected from light at room temperature and then placed on ice. PI-stained cells were analyzed using a BD LSR Fortessa, and cell cycle data were further analyzed using FlowJo v.10 with the Watson model for evaluation of cell cycle distribution.

For the Annexin V apoptosis assay, cells were treated for 24 h in the presence of vehicle or 150 nM quarfloxin or 230 nM CX-5461 and analyzed using the FITC Annexin V Apoptosis Detection Kit according to the manufacturer's instructions (BD Biopharmigen). Annexin V-positive cells were detected using a BD LSR Fortessa.

Western blotting

Cells were treated with vehicle, quarfloxin, or CX-5461 as indicated. At harvesting, floating cells and adherent cells (trypsination) were collected for analysis. Protein isolation and blotting were performed essentially as previously described using NuPAGE 4–12% bis-tris precast polyacrylamide gels and Immobilon-PVDF membranes (Millipore) [42]. For western blots containing Caspase-3 and p21, 4–20% Tris-Glycine gels (Lonza) were used for better separation of these low MW proteins. Primary antibodies used in this study were mouse monoclonal anti-MycN (sc-53993, Santa Cruz Biotechnology, CA, USA), mouse monoclonal anti-p53 (sc-126, Santa Cruz Biotechnology, CA, USA), rabbit monoclonal anti-p21 (#2947, Cell Signaling Technology, MA, USA), rabbit polyclonal anti-PARP (#9542, Cell Signaling Technology, MA, USA), rabbit polyclonal anti-Caspase-3 (#9662, Cell Signaling Technology, MA, USA), mouse monoclonal anti-γ-H2A.X (05–636, Merck Millipore, MA, USA), rabbit polyclonal anti-actin (A2066, Sigma-Aldrich, MO, USA) and mouse monoclonal anti-actin (AB3280, Abcam, Cambridge, UK). Membranes were detected using the Odyssey Infrared Imaging system (LI-COR).

RT-qPCR

Floating and adherent cells were lysed in 1 mL of Qiazol (Qiagen), 0.2 mL of chloroform was added for phase separation, and RNA was precipitated overnight from 0.4 mL of the aqueous phase 1:1 in isopropanol at −20 °C. The RNA pellet was washed twice in ice-cold 75% EtOH and resuspended in TE-buffer (10 mM Tris-HCl, 1 mM disodium EDTA, pH 8.0). RNA quality and quantity was assesed using the Nanodrop 2000. In total, 1200 ng of RNA was reverse transcribed using the High Capacity cDNA kit w/RNase inhibitor (Thermo Fisher). Each RT-qPCR reaction (20 µL) contained 12.5 ng of cDNA in 5 µL, 10 µL of Power SYBR (Thermo Fisher), 0.8 µL of 5 µM F+R primers, and 4.2 µL of nuclease-free H_2O. Amplification of cDNA was carried out using a LightCycler 96 SW 1.1 (Roche). Relative expression of transcript levels was evaluated using the ddCT method with the geometric mean of two housekeeping genes (*SDHA* and *ACTB*). Expression of rRNA transcripts was normalized using the geometric mean of all rRNA transcripts according to [43]. Primer sequences were; SDHA: forward 5′-CTGATGAGACAAGATGTGGTG-3′, reverse 5′-CAATCTCCCTTCAATGTACTCC-3′, ACTB: forward 5′-CACCATGTACCCTGGCATT-3′, reverse 5′-ACGGAGTACTTGCGCTCAG-3′, p21: forward 5′-GCAGACCAGCATGACAGATTT-3′, reverse 5′-GGATTAGGGCTTCCTCTTGGA-3′, 47S-rRNA: forward 5′-CCGCGCTCTACCTTACCTAC-3′, reverse 5′-GCATGGCTTAATCTTTGAGACAAG-3′, 5.8S-rRNA: forward 5′-ACTCGGCTCGTGCGTC-3′, reverse: 5′-GCGACGCTCAGACAGG-3′, 18S-rRNA: forward 5′-GTAACCCGTTGAACCCCATT-3′, reverse 5′-CCATCCAATCGGTAGTAGCG-3′, 28S-rRNA: forward 5′-GGGTGGTAAACTCCATCTAAGG-3′, reverse 5′-GCCCTCTTGAACTCTCTCTTC-3′, RPL13A: forward 5′-TAAACAGGTACTGCTGGGCCG-3′, reverse 5′-CTCGGGAAGGGTTGGTGTTC-3′, RPL32: forward 5′-TACGACCCATCAGCCCTTGC-3′, reverse 5′-CATGATGCCGAGAAGGAGATGG-3′, RPS5: forward 5′-ATCATCAACAGTGGTCCCCG-3′, reverse 5′-AGATGGCCTGGTTCACACG-3′, RPS19: forward 5′-AAACCCCGTCGTTCCCTTTC-3′, reverse 5′ GCTTCCCGGACTTTTTGAGG-3′.

p53 activity assays

Cells in 12-well plates were reverse transfected using Lipofectamine 2000 (Thermo Fisher) with 0.5 µg p53 transcriptional reporter (PG13) (Addgene), (originally published in Ref. [17]) and 0.02-µg pCMV-Renilla luc (Promega). On the next day, cells were treated with vehicles or 150 nM quarfloxin or 230 nM CX-5461. After 24 h of treatment, cells were collected in 200 µL 1x PLB buffer, and luciferase activity was measured using the Dual-Luciferase Reporter Assay according to the instructions from the manufacturer (Promega). PG13 firefly activity was normalized to renilla (RLU).

siRNA transfections and *TP53* overexpression

Transfections were carried out using Lipofectamine 2000 and were performed essentially as described [44]. The following siRNAs were used (all from Qiagen): AllStars Negative Control siRNA (siNC), Hs_MYCN_4 FlexiTube siRNA (siMYCN_1), Hs_MYCN_6 FlexiTube siRNA (siMYCN_2), Hs_TP53_3 FlexiTube siRNA (siTP53_1), and Hs_TP53_9 FlexiTube siRNA (siTP53_2). Final concentrations of the respective siRNAs were 20 nM in all the experiments. The wt-p53 overexpression plasmid was a kind gift from Dr. Ugo Moens, University of Tromsø, Norway, empty vector was pCMV-XL4 (Origene). Final DNA plasmid concentration was 1 µg/mL of media.

Xenografts

Four-to-six-week-old female Sca:NMRI *nu/nu* mice (Scanbur, Stockholm, Sweden) were maintained in pathogen-free conditions and given free access to sterile water and food. For BE(2)-C xenografts, 10×10^6 cells were injected subcutaneously on the right flank under isoflurane anesthesia and for IMR-32 9×10^6 cells in 50% Matrigel were injected following the same procedure. Tumors were measured every day with a digital caliper and tumor volume (mL) was calculated as $\text{volume} = \text{width}^2 \times \text{length} \times 0.44$. When

tumors reached ≥ 0.15 ml, mice were randomized into treatment with CX-5461 or control groups (no treatment). Mice in the treatment groups received 50 mg/kg CX-5461 by oral gavage every third day for 12 days for BE(2)-C or 3–6 consecutive days and then every third day for 10 days for IMR-32. Tumor volume index (TVI) was determined by dividing the tumor volume of each day by the starting volume (day 0). TVIs from treated and untreated tumors were compared in GraphPad Prism 7 using repeated measures two-way ANOVA with Bonferroni correction and p-values ≤ 0.05 were considered statistically significant. No significant weight changes were observed in both untreated and treated groups. At autopsy, tumors were fixed in 4% paraformaldehyde (PFA) at 4 °C for 24 h and then kept in 70% EtOH at 4 °C before further analysis. All animal experiments were approved by the regional ethics committee for animal research (N231/14), appointed and under the control of the Swedish Board of Agriculture and the Swedish Court. The animal experiments presented herein were in accordance with national regulations (SFS 1988:534, SFS 1988:539, and SFS 1988:541).

Immunohistochemistry

Formalin-fixed and paraffin-embedded tissue sections were deparaffinized in xylene and graded alcohols, hydrated, and washed in a phosphate-buffered saline (PBS). After antigen retrieval in a sodium citrate buffer (pH 6) in a microwave oven, the endogenous peroxidase was blocked by 0.3% H_2O_2 for 15 min. Sections were incubated overnight at 4 °C with primary antibodies anti-γ-H2A.X (#9718 Cell Signal Technology, MA, USA), anti-cleaved Caspase-3 (Asp175) (Cell signaling Technology, MA, USA) or anti-Ki-67 (SP6, Neomarkers, CA, USA), respectively. As a secondary antibody, the anti-rabbit-horseradish peroxidase (HRP) SignalStain Boost IHC detection kit was used (# 8114, Cell Signaling Technology, MA, USA). For the assessment of MycN expression, a monoclonal mouse anti-MycN antibody was used (sc-53993, Santa Cruz Biotechnology, CA, USA). As a secondary antibody, anti-mouse EnVision-HRP (Dako, Agilent Technologies, Inc., Santa Clara, CA, USA) was used. A matched isotype control was also used as a control for nonspecific background staining.

Statistical analysis

Differences between two groups were compared using the two-sided Student's t test. Differences in treated and untreated xenograft tumor volume indexes were studied using repeated measures two-way ANOVA with Bonferroni correction. All statistical analysis was done using the GraphPad Prism 7 software and a result was considered statistically significant when $p \le 0.05$.

Acknowledgements This work was supported by the Norwegian Childhood Cancer Society (Barnekreftforeningen), The Northern-Norwegian Health Authorities (Helse Nord), the Simon Fougner Hartmanns Familiefond, the Swedish Childhood Cancer Foundation, the Swedish Cancer Foundation, the Swedish Foundation for Strategic Research (www.nnbcr.se) and The Cancer Research Foundations of Radiumhemmet. We wish to thank Dr. Emma Bell for kindly providing the siMYCN IMR-32 microarray data.

Compliance with ethical standards

Conflict of interest The authors declare that they have no conflict of interest.

References

1. Cole KA, Maris JM. New strategies in refractory and recurrent neuroblastoma: translational opportunities to impact patient outcome. Clin Cancer Res. 2012;18:2423–8.
2. Maris JM. Recent advances in neuroblastoma. N Engl J Med. 2010;362:2202–11.
3. Westermann F, Muth D, Benner A, Bauer T, Henrich KO, Oberthuer A, et al. Distinct transcriptional MYCN/c-MYC activities are associated with spontaneous regression or malignant progression in neuroblastomas. Genome Biol. 2008;9:R150.
4. Ruiz-Perez MV, Henley AB, Arsenian-Henriksson M. The MYCN protein in health and disease. Genes. 2017;8:E113
5. Pelletier J, Thomas G, Volarevic S. Ribosome biogenesis in cancer: new players and therapeutic avenues. Nat Rev Cancer. 2018;18:51–63.
6. Boon K, Caron HN, van Asperen R, Valentijn L, Hermus MC, van Sluis P, et al. N-myc enhances the expression of a large set of genes functioning in ribosome biogenesis and protein synthesis. EMBO J. 2001;20:1383–93.
7. van Riggelen J, Yetil A, Felsher DW. MYC as a regulator of ribosome biogenesis and protein synthesis. Nat Rev Cancer. 2010;10:301–9.
8. Kobayashi C, Monforte-Munoz HL, Gerbing RB, Stram DO, Matthay KK, Lukens JN, et al. Enlarged and prominent nucleoli may be indicative of MYCN amplification: a study of neuroblastoma (Schwannian stroma-poor), undifferentiated/poorly differentiated subtype with high mitosis-karyorrhexis index. Cancer. 2005;103:174–80.
9. Wang LL, Suganuma R, Ikegaki N, Tang X, Naranjo A, McGrady P, et al. Neuroblastoma of undifferentiated subtype, prognostic significance of prominent nucleolar formation, and MYC/MYCN protein expression: a report from the Children's Oncology Group. Cancer. 2013;119:3718–26.
10. Harrison SJ, Khot A, Brajanovski N, Cameron D, Hein N, McArthur GA, et al. A phase 1, open-label, dose escalation,

safety, PK and PD study of a first in class Pol1 inhibitor (CX-5461) in patients with advanced hematologic malignancies (HM). J Clin Oncol. 2015;33:e22212-e.
11. Bywater MJ, Poortinga G, Sanij E, Hein N, Peck A, Cullinane C, et al. Inhibition of RNA polymerase I as a therapeutic strategy to promote cancer-specific activation of p53. Cancer Cell. 2012;22:51–65.
12. Drygin D, Lin A, Bliesath J, Ho CB, O'Brien SE, Proffitt C, et al. Targeting RNA polymerase I with an oral small molecule CX-5461 inhibits ribosomal RNA synthesis and solid tumor growth. Cancer Res. 2011;71:1418–30.
13. Drygin D, Siddiqui-Jain A, O'Brien S, Schwaebe M, Lin A, Bliesath J, et al. Anticancer activity of CX-3543: a direct inhibitor of rRNA biogenesis. Cancer Res. 2009;69:7653–61.
14. Li L, Li Y, Zhao J, Fan S, Wang L, Li X. CX-5461 induces autophagy and inhibits tumor growth via mammalian target of rapamycin-related signaling pathways in osteosarcoma. Onco Targets Ther. 2016;9:5985–97.
15. Bell E, Lunec J, Tweddle DA. Cell cycle regulation targets of MYCN identified by gene expression microarrays. Cell cycle (Georgetown, Tex). 2007;6:1249–56.
16. Lutz W, Stohr M, Schurmann J, Wenzel A, Lohr A, Schwab M. Conditional expression of N-myc in human neuroblastoma cells increases expression of alpha-prothymosin and ornithine decarboxylase and accelerates progression into S-phase early after mitogenic stimulation of quiescent cells. Oncogene. 1996;13:803–12.
17. el-Deiry WS, Tokino T, Velculescu VE, Levy DB, Parsons R, Trent JM, et al. WAF1, a potential mediator of p53 tumor suppression. Cell. 1993;75:817–25.
18. Popov A, Smirnov E, Kovacik L, Raska O, Hagen G, Stixova L, et al. Duration of the first steps of the human rRNA processing. Nucleus (Austin, Tex). 2013;4:134–41.
19. Johnsen JI, Dyberg C, Fransson S, Wickstrom M. Molecular mechanisms and therapeutic targets in neuroblastoma. Pharmacol Res. 2018;131:164–76.
20. Egan M, Raafat F, Crocker J, Williams D. Comparative study of the degree of differentiation of neuroblastoma and mean numbers of nucleolar organiser regions. J Clin Pathol. 1988;41:527–31.
21. Hein N, Hannan KM, George AJ, Sanij E, Hannan RD. The nucleolus: an emerging target for cancer therapy. Trends Mol Med. 2013;19:643–54.
22. Gonin-Laurent N, Gibaud A, Huygue M, Lefevre SH, Le Bras M, Chauveinc L, et al. Specific TP53 mutation pattern in radiation-induced sarcomas. Carcinogenesis. 2006;27:1266–72.
23. Goldschneider D, Horvilleur E, Plassa LF, Guillaud-Bataille M, Million K, Wittmer-Dupret E, et al. Expression of C-terminal deleted p53 isoforms in neuroblastoma. Nucleic Acids Res. 2006;34:5603–12.
24. Bykov VJN, Eriksson SE, Bianchi J, Wiman KG. Targeting mutant p53 for efficient cancer therapy. Nat Rev Cancer. 2018;18:89–102.
25. Niemas-Teshiba R, Matsuno R, Wang LL, Tang XX, Chiu B, Zeki J, et al. MYC-family protein overexpression and prominent nucleolar formation represent prognostic indicators and potential therapeutic targets for aggressive high-MKI neuroblastomas: a report from the children's oncology group. Oncotarget. 2018;9:6416–32.
26. Lee HC, Wang H, Baladandayuthapani V, Lin H, He J, Jones RJ, et al. RNA polymerase I inhibition with CX-5461 as a novel therapeutic strategy to target MYC in multiple myeloma. Br J Haematol. 2017;177:80–94.
27. Xue C, Haber M, Flemming C, Marshall GM, Lock RB, MacKenzie KL, et al. p53 determines multidrug sensitivity of childhood neuroblastoma. Cancer Res. 2007;67:10351–60.
28. Keshelava N, Zuo JJ, Chen P, Waidyaratne SN, Luna MC, Gomer CJ, et al. Loss of p53 function confers high-level multidrug resistance in neuroblastoma cell lines. Cancer Res. 2001;61:6185–93.
29. Schroeder U, Bernt KM, Lange B, Wenkel J, Jikai J, Shabat D, et al. Hydrolytically activated etoposide prodrugs inhibit MDR-1 function and eradicate established MDR-1 multidrug-resistant T-cell leukemia. Blood. 2003;102:246–53.
30. Singhal J, Yadav S, Nagaprashantha LD, Vatsyayan R, Singhal SS, Awasthi S. Targeting p53-null neuroblastomas through RLIP76. Cancer Prev Res (Phila, Pa). 2011;4:879–89.
31. Otto T, Horn S, Brockmann M, Eilers U, Schuttrumpf L, Popov N, et al. Stabilization of N-Myc is a critical function of Aurora A in human neuroblastoma. Cancer Cell. 2009;15:67–78.
32. Kitade S, Onoyama I, Kobayashi H, Yagi H, Yoshida S, Kato M, et al. FBXW7 is involved in the acquisition of the malignant phenotype in epithelial ovarian tumors. Cancer Sci. 2016;107:1399–405.
33. Yokobori T, Mimori K, Iwatsuki M, Ishii H, Onoyama I, Fukagawa T, et al. p53-Altered FBXW7 expression determines poor prognosis in gastric cancer cases. Cancer Res. 2009;69:3788–94.
34. Siddiqui-Jain A, Grand CL, Bearss DJ, Hurley LH. Direct evidence for a G-quadruplex in a promoter region and its targeting with a small molecule to repress c-MYC transcription. Proc Natl Acad Sci USA. 2002;99:11593–8.
35. Trajkovski M, da Silva MW, Plavec J. Unique structural features of interconverting monomeric and dimeric G-quadruplexes adopted by a sequence from the intron of the N-myc gene. J Am Chem Soc. 2012;134:4132–41.
36. Suenaga Y, Kaneko Y, Matsumoto D, Hossain MS, Ozaki T, Nakagawara A. Positive auto-regulation of MYCN in human neuroblastoma. Biochem Biophys Res Commun. 2009;390:21–6.
37. Rhodes D, Lipps HJ. G-quadruplexes and their regulatory roles in biology. Nucleic Acids Res. 2015;43:8627–37.
38. Xu H, Di Antonio M, McKinney S, Mathew V, Ho B, O'Neil NJ, et al. CX-5461 is a DNA G-quadruplex stabilizer with selective lethality in BRCA1/2 deficient tumours. Nat Commun. 2017;8:14432.
39. Negi SS, Brown P. rRNA synthesis inhibitor, CX-5461, activates ATM/ATR pathway in acute lymphoblastic leukemia, arrests cells in G2 phase and induces apoptosis. Oncotarget. 2015;6:18094–104.
40. Quin J, Chan KT, Devlin JR, Cameron DP, Diesch J, Cullinane C, et al. Inhibition of RNA polymerase I transcription initiation by CX-5461 activates non-canonical ATM/ATR signaling. Oncotarget. 2016;7:49800–18.
41. Smith J, Tho LM, Xu N, Gillespie DA. The ATM-Chk2 and ATR-Chk1 pathways in DNA damage signaling and cancer. Adv Cancer Res. 2010;108:73–112.
42. Henriksen JR, Haug BH, Buechner J, Tomte E, Lokke C, Flaegstad T, et al. Conditional expression of retrovirally delivered anti-MYCN shRNA as an in vitro model system to study neuronal differentiation in MYCN-amplified neuroblastoma. BMC Dev Biol. 2011;11:1.
43. Karahan G, Sayar N, Gozum G, Bozkurt B, Konu O, Yulug IG. Relative expression of rRNA transcripts and 45S rDNA promoter methylation status are dysregulated in tumors in comparison with matched-normal tissues in breast cancer. Oncol Rep. 2015;33:3131–45.
44. Roth S, Hald Ø, Fuchs S, Løkke C, Mikkola I, Flaegstad T. et al. MicroRNA-193b-3p represses neuroblastoma cell growth via downregulation of Cyclin D1, MCL-1 and MYCN. Oncotarget. 2018;9:18160–79.

Supplementary Table 1: Genetic characteristics of neuroblastoma cell lines used in this study

Cell line	Stage	Origin	Treatment	*MYCN*-amplified	*TP53*	1p del	11q del	17q gain	References
BE(2)-C	4	Bone marrow	YES	YES	MUT	YES	NO	NO	[1, 2]
Kelly	4	Bone marrow	YES	YES	MUT	YES	YES	YES	[3, 4]
IMR-32	unknown	Abdomen	NO	YES	WT	YES	YES	YES	[5]
CHP-134	4	Lymph node (primary: adrenal)	YES	YES	WT	YES	NO	YES	[6]
SK-N-FI		Bone marrow	YES	NO	MUT	NO	?	?	[8]
CHLA-15	4	Primary	NO	NO	WT	?	?	?	[7, 9]
SK-N-AS	4	Bone marrow (primary: adrenal)	YES	NO	MUT	YES	YES	NO	[1, 10, 11]
MYCN-inducible neuroblastoma cell line:									
SHEP-Tet21N		Derived from SHEP (substrate adherent subtype of SK-N-SH)		+dox: OFF -dox: ON	WT				[12]

1. Thiele, C.J., *Neuroblastoma Cell Lines*, in *Neuroblastoma*, J.H.C. Culture. 1998: Lancaster, UK. p. 21-53.

2. Tweddle, D.A., A.J. Malcolm, N. Bown, A.D. Pearson*, et al.*, *Evidence for the development of p53 mutations after cytotoxic therapy in a neuroblastoma cell line*. Cancer Res, 2001. **61**(1): p. 8-13.

3. Gogolin, S., V. Ehemann, G. Becker, L.M. Brueckner*, et al.*, *CDK4 inhibition restores G(1)-S arrest in MYCN-amplified neuroblastoma cells in the context of doxorubicin-induced DNA damage.* Cell Cycle, 2013. **12**(7): p. 1091-104.

4. Piskareva, O., H. Harvey, J. Nolan, R. Conlon*, et al.*, *The development of cisplatin resistance in neuroblastoma is accompanied by epithelial to mesenchymal transition in vitro*. Cancer Lett, 2015. **364**(2): p. 142-55.

5. Tumilowicz JJ, Nichols WW, Cholon JJ, Greene AE. *Definition of a continuous human cell line derived from neuroblastoma*. Cancer Res. 1970 Aug;30(8):2110-8.

6. Schlesinger HR, Gerson JM, Moorhead PS, Maguire H, Hummeler K. *Establishment and characterization of human neuroblastoma cell lines*. Cancer Res. 1976 Sep;36(9 pt.1):3094-100.

7. Keshelava, N., R.C. Seeger, S. Groshen, and C.P. Reynolds, *Drug resistance patterns of human neuroblastoma cell lines derived from patients at different phases of therapy*. Cancer Res, 1998. **58**(23): p. 5396-405.

8. Helson, L., Nisselbaum, J., Helson, C., Majeranowski, A., and Johnson, G. A. *Biological markers in neuroblastoma and other pediatric neoplasias*. In: W. Davis, K. R. Harrap, and G. Stathopoulos (eds.), Human Cancer. Its Characterization and Treatment, pp. 86–94. Princeton: Excerpta Medica, 1980.

9. Keshelava, N., E. Davicioni, Z. Wan, L. Ji*, et al.*, *Histone deacetylase 1 gene expression and sensitization of multidrug-resistant neuroblastoma cell lines to cytotoxic agents by depsipeptide.* J Natl Cancer Inst, 2007. **99**(14): p. 1107-19.

10. Caren, H., H. Kryh, M. Nethander, R.M. Sjoberg*, et al.*, *High-risk neuroblastoma tumors with 11q-deletion display a poor prognostic, chromosome instability phenotype with later onset.* Proc Natl Acad Sci U S A, 2010. **107**(9): p. 4323-8.

11. Goldschneider, D., E. Horvilleur, L.F. Plassa, M. Guillaud-Bataille*, et al.*, *Expression of C-terminal deleted p53 isoforms in neuroblastoma*. Nucleic Acids Res, 2006. **34**(19): p. 5603-12.

12. Lutz W, Stohr M, Schurmann J, Wenzel A, Lohr A, Schwab M. *Conditional expression of N-myc in human neuroblastoma cells increases expression of alpha-prothymosin and ornithine decarboxylase and accelerates progression into S-phase early after mitogenic stimulation of quiescent cells.* Oncogene. 1996;13(4):803-12.

SUPPLEMENTARY FIGURE 1

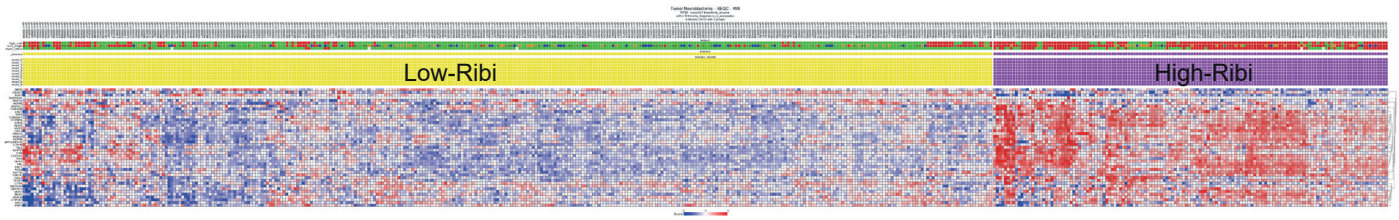

SUPPLEMENTARY FIGURE 2

A

Neuroblastoma Versteeg-88

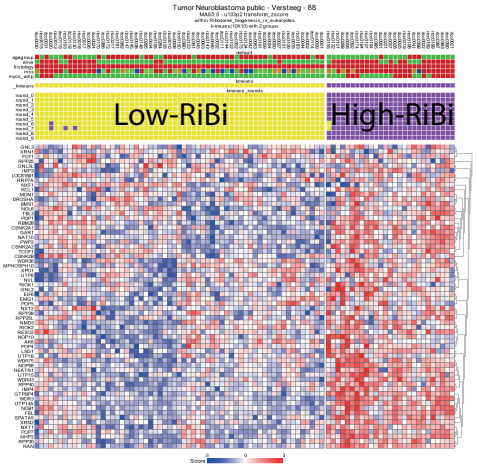

K-means clustering, 2 groups
"ribosome biogenesis in eukaryotes"

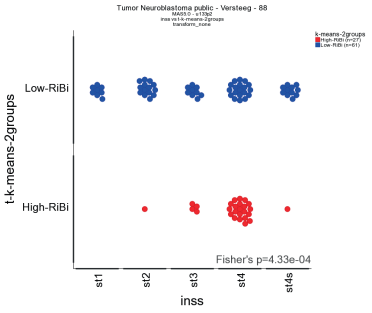

Distribution of High-RiBi and Low-RiBi tumors in INSS tumor stages

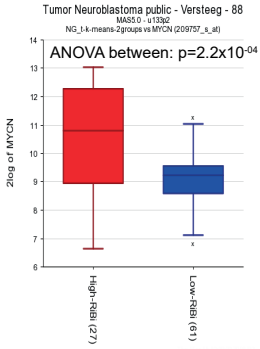

MYCN expression in High-RiBi and Low-RiBi tumors

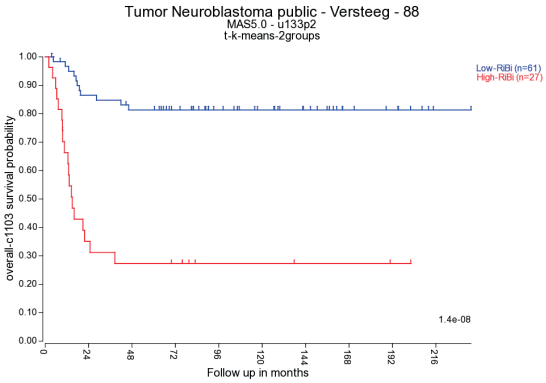

Overall survival between Low-Ribi and High-RiBi tumors

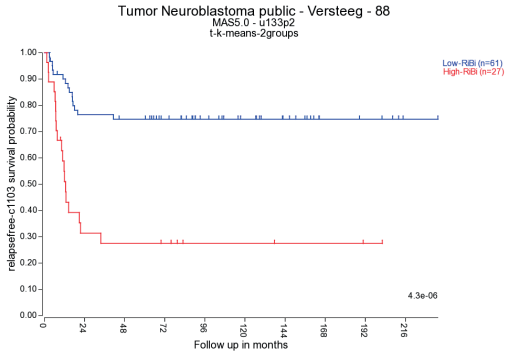

Relapsefree survival between Low-Ribi and High-RiBi tumors

B

Neuroblastoma Maris-101

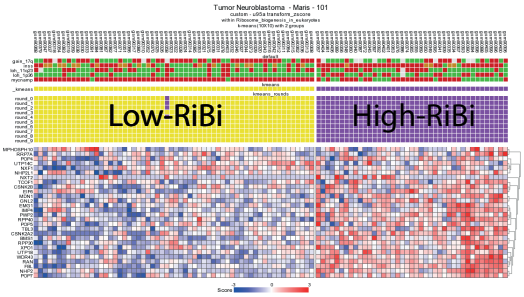

K-means clustering, 2 groups
"ribosome biogenesis in eukaryotes"

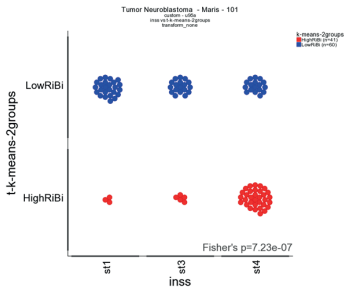

Distribution of High-RiBi and Low-RiBi tumors in INSS tumor stages

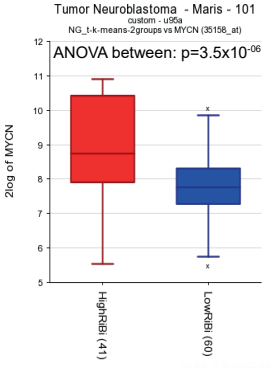

MYCN expression in High-RiBi and Low-RiBi tumors

C

Neuroblastoma Oberthuer-251

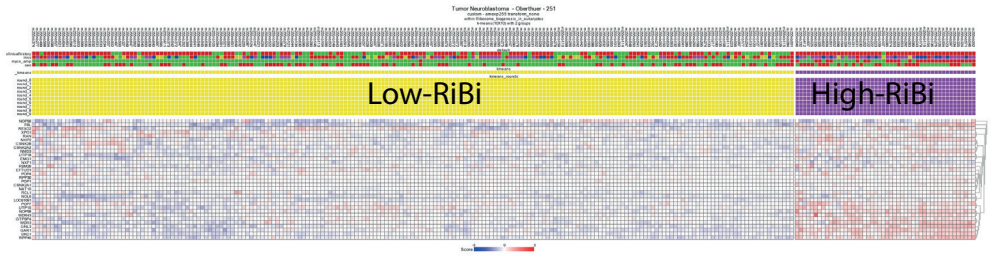

2 color array containing negative values. To avoid filter out, K-mean's settings were as follow:
-floor value: -500
-range: 0
-max exp: -500

K-means clustering, 2 groups
"ribosome biogenesis in eukaryotes"

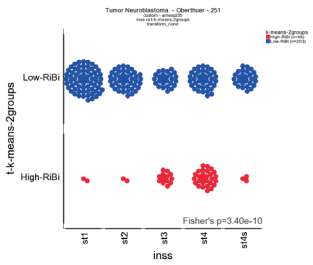

Distribution of High-RiBi and Low-RiBi tumors in INSS tumor stages

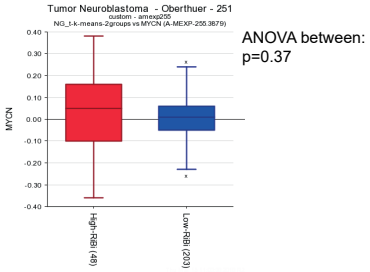

ANOVA between: p=0.37

MYCN expression in High-RiBi and Low-RiBi tumors

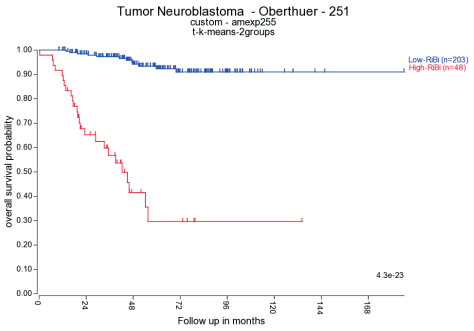

Overall survival between Low-Ribi and High-RiBi tumors

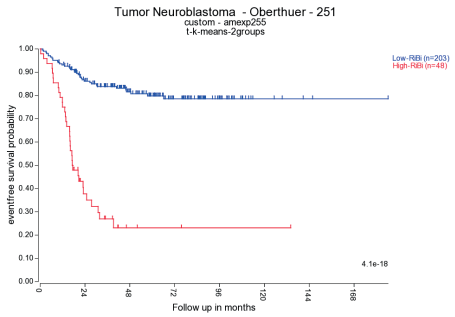

Eventfree survival between Low-Ribi and High-RiBi tumors

D

Neuroblastoma non-*MYCN*-amplified - Seeger-102

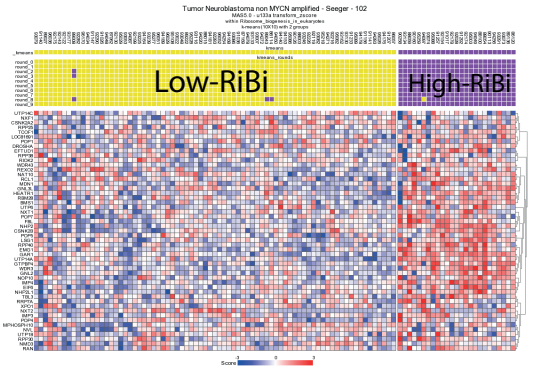

K-means clustering, 2 groups
"ribosome biogenesis in eukaryotes"

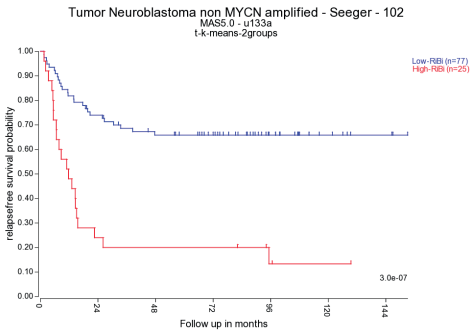

Relapsefree survival between Low-Ribi and High-RiBi tumors

SUPPLEMENTARY FIGURE 4

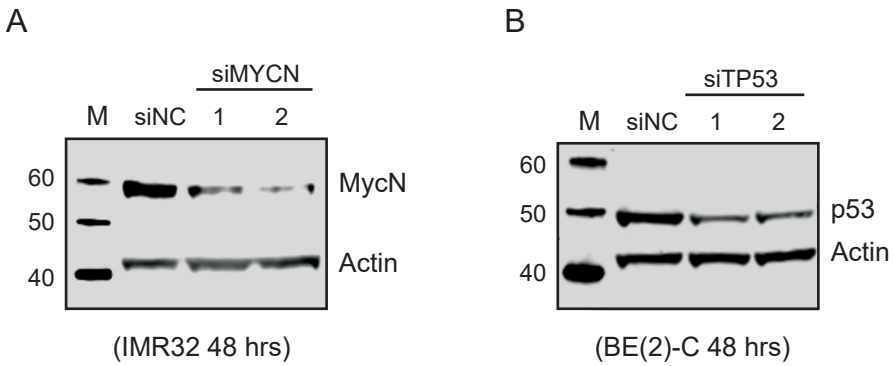

SUPPLEMENTARY FIGURE 5

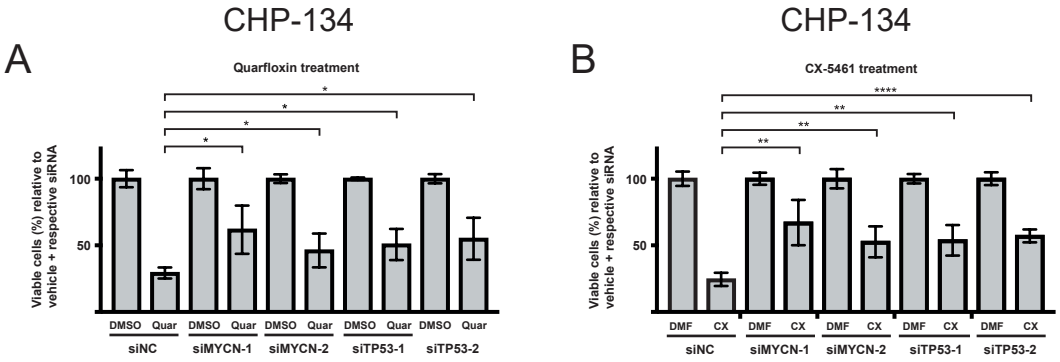

SUPPLEMENTARY FIGURE 6

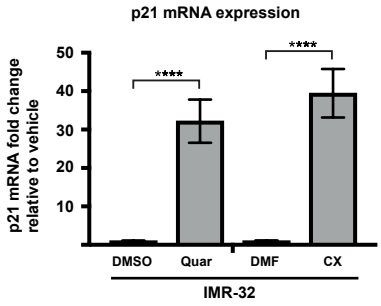

SUPPLEMENTARY FIGURE 7

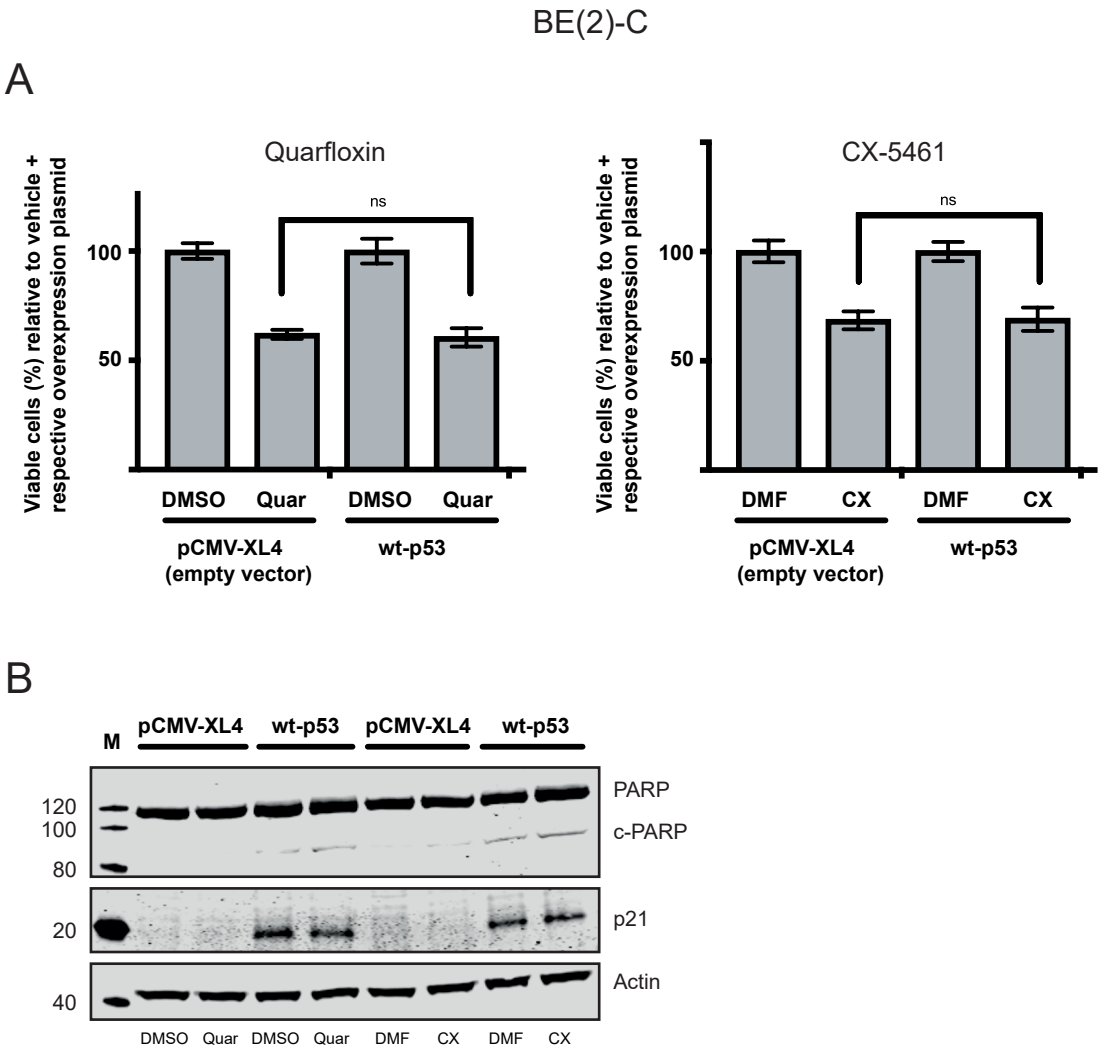

SUPPLEMENTARY FIGURE 8

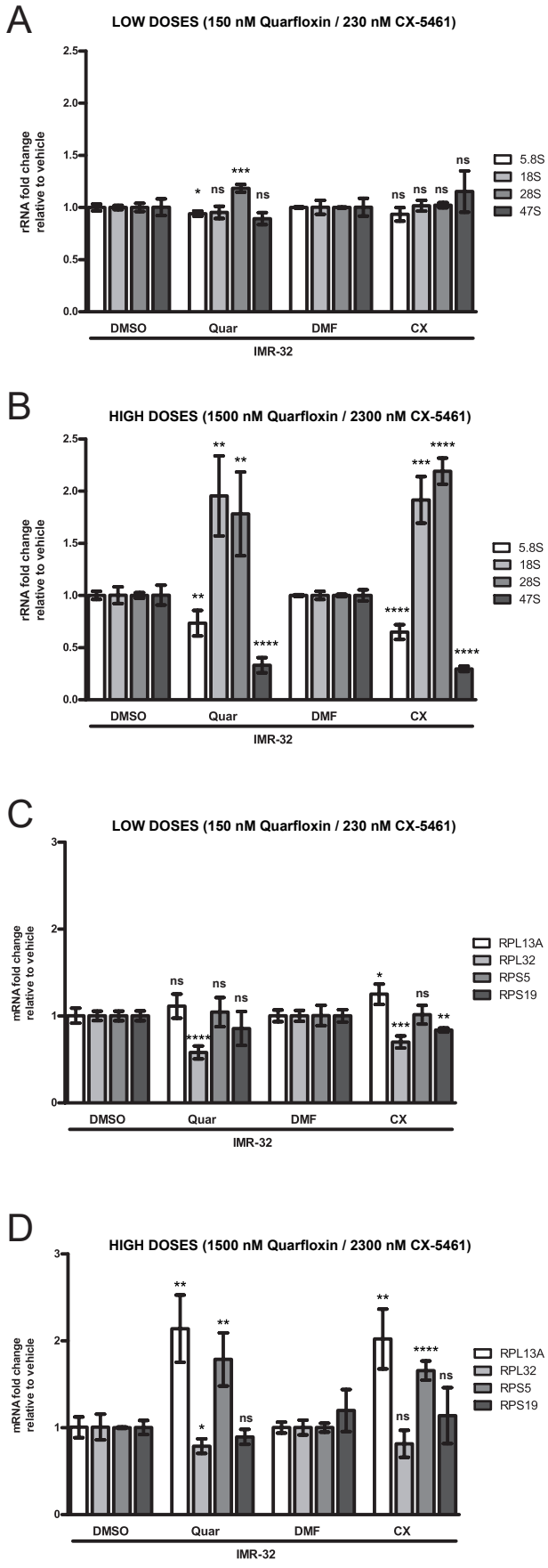

SUPPLEMENTARY FIGURE 9

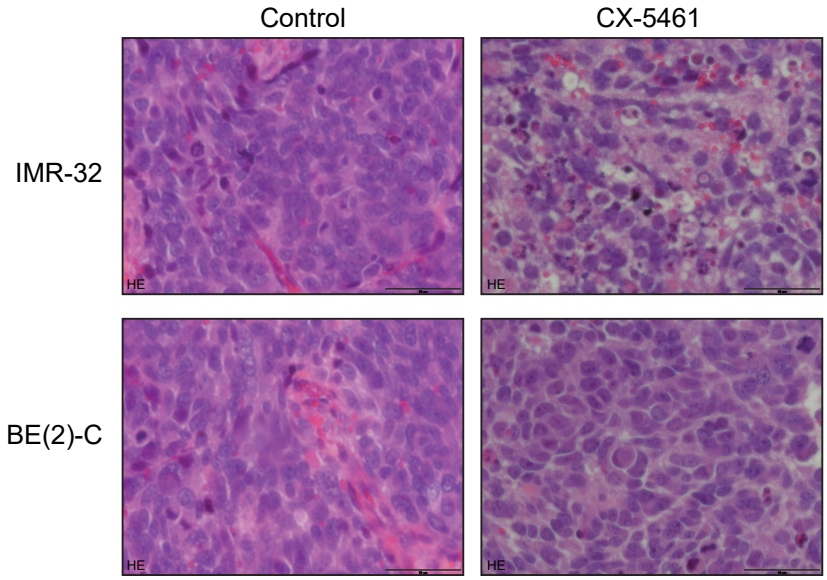

Paper 2

MicroRNA-193b-3p represses neuroblastoma cell growth via downregulation of *Cyclin D1*, *MCL-1* and *MYCN*

Sarah Andrea Roth[1], Øyvind H. Hald[2], Steffen Fuchs[4,5], Cecilie Løkke[1], Ingvild Mikkola[3], Trond Flægstad[1,2], Johannes Schulte[4] and Christer Einvik[1,2]

[1]Pediatric Research Group, Department of Clinical Medicine, Faculty of Health Science, The Arctic University of Norway – UiT, Tromsø NO-9037, Norway

[2]Department of Pediatrics, Division of Child and Adolescent Health, UNN – University Hospital of North-Norway, Tromsø NO-9038, Norway

[3]Research Group of Pharmacology, Department of Pharmacy, The Arctic University of Norway – UiT, Tromsø NO-9037, Norway

[4]Charité – Universitätsmedizin Berlin, corporate member of Freie Universität Berlin, Humboldt-Universität zu Berlin, and Berlin Institute of Health, Department of Pediatric Oncology and Hematology/Bone Marrow Transplantation, Berlin, Germany

[5]Berlin Institute of Health (BIH), Berlin 10178, Germany

Correspondence to: *Christer Einvik,* ***email:*** *christer.einvik@uit.no*

Keywords: *Neuroblastoma; miRNA; tumor suppressor; mir-193b*

Received: *October 26, 2016* ***Accepted:*** *February 28, 2018* ***Published:***

ABSTRACT

Neuroblastoma is the most common diagnosed tumor in infants and the second most common extracranial tumor of childhood. The survival rate of patients with high-risk neuroblastoma is still very low despite intensive multimodal treatments. Therefore, new treatment strategies are needed. In recent years, miRNA-based anticancer therapy has received growing attention. Advances in this novel treatment strategy strongly depends on the identification of candidate miRNAs with broad-spectrum antitumor activity. Here, we identify miR-193b as a miRNA with tumor suppressive properties. We show that miR-193b is expressed at low levels in neuroblastoma cell lines and primary tumor samples. Introduction of miR-193b mimics into nine neuroblastoma cell lines with distinct genetic characteristics significantly reduces cell growth *in vitro* independent of risk factors such as p53 functionality or *MYCN* amplification. Functionally, miR-193b induces a G1 cell cycle arrest and cell death in neuroblastoma cell lines by reducing the expression of *MYCN*, *Cyclin D1* and *MCL-1*, three important oncogenes in neuroblastoma of which inhibition has shown promising results in preclinical testing. Therefore, we suggest that miR-193b may represent a new candidate for miRNA-based anticancer therapy in neuroblastoma.

INTRODUCTION

Neuroblastoma, a neoplasm of the sympathetic nervous system, is the most common diagnosed tumor in infants and the second most common extracranial tumor of childhood [1, 2]. During the last decades, the survival of children with neuroblastoma has significantly improved. New advances and continued research on treatment strategies are contributing to increasing survival rates [2, 3]. Today, the estimated survival of children with low and intermediate-risk neuroblastoma is >98 and 90–95%, respectively. On the contrary, the survival rate of patients with high-risk neuroblastoma is still only 40–50% despite intensive multimodal treatments [2]. More than half of high-risk neuroblastoma patients experience a relapse after treatment with tumors refractory to standard chemotherapeutic agents and there are currently no salvage regimens known to be curative for these patients [2, 4]. These patients have a very poor prognosis with a ten year overall survival rate of less than 20% [5]. Thus, improvements in survival rates for children with high-risk neuroblastoma are dependent on novel treatment approaches.

MicroRNAs (miRNAs) are small (~22 nucleotides), non-coding RNA molecules regulating the expression of their target genes at the post-transcriptional level.

MiRNAs have been implicated to be involved in the regulation of virtually all physiological processes including proliferation, differentiation, apoptosis, and cell survival [6, 7]. Whole-genome miRNA profiling studies revealed that miRNAs are deregulated in most human cancers, indicating that miRNAs have critical functions in carcinogenesis and tumor progression by acting as oncogenes or tumor suppressors [7–9].

In recent years, miRNAs have been reported as valuable biomarkers for diagnosis and prognosis of cancer, and miRNA-based anticancer therapy has emerged as a promising therapeutic strategy for the treatment of human cancers [10–13].

Emerging evidence has demonstrated that miRNAs play a vital role in the initiation and progression of neuroblastoma (reviewed by [14, 15]). A number of studies have demonstrated that miRNAs are differentially expressed between high-risk and low-risk neuroblastomas [16, 17], and also between *MYCN*-amplified and non-*MYCN*-amplified neuroblastomas [18–20]. We have recently demonstrated that several miRNAs have a distinct expression pattern in isogenic neuroblastoma cell lines isolated from patients at diagnosis and at relapse after intensive treatments [21]. In addition to miRNA profiling studies, several studies have focused on individual miRNAs, and performed functional *in vitro* and *in vivo* studies to analyze their specific roles in neuroblastoma. These studies identified a number of tumor suppressive and oncogenic miRNAs involved in proliferation, metastasis and differentiation of neuroblastoma cells (reviewed by [14, 15, 22, 23]).

For instance, miR-34a, which is downregulated in neuroblastoma, exhibits potent tumor suppressive functions in neuroblastoma by inducing apoptosis, cell cycle arrest and differentiation [24–29]. The miR-17-92 cluster, a direct target of N-Myc, exhibits oncogenic functions in neuroblastoma by inhibiting neuronal differentiation, increasing cell proliferation, inhibiting apoptosis, and decreasing cell adhesion (recently reviewed by [15]).

Recent studies in mice have supported the potential of miRNA replacement therapy in neuroblastoma *in vivo* [25, 26, 30–32]. For instance, nanoparticle-based targeted delivery of miR-34a into neuroblastoma tumors in a murine orthotropic xenograft model resulted in decreased tumor growth, increased apoptosis and a reduction in vascularization [26]. Treating nude mice bearing neuroblastoma xenografts with miR-542-3p-loaded nanoparticles also decreased cell proliferation and induced apoptosis *in vivo* [32]. Thus, research on miRNA-based therapy in neuroblastoma offers a chance to develop new drugs to successfully treat high-risk neuroblastoma.

To develop miRNA-based therapeutics for high-risk neuroblastoma, identification of candidate miRNAs with broad-spectrum antitumor activity is needed. In this study, we demonstrated that treatment of neuroblastoma cell lines with miR-193b mimics strongly reduces cell viability and proliferation by inducing a G1 cell cycle arrest and cell death (mainly apoptotic). Our data identified miR-193b as a candidate for miRNA-based anticancer therapy in neuroblastoma.

RESULTS

Low expression of miR-193b in primary neuroblastoma tumors and cell lines

MiR-193b-3p (henceforth referred to as miR-193b) has been described as a tumor suppressor in several cancers. To investigate a potential tumor suppressive role of miR-193b in neuroblastoma, we assessed miR-193b expression in 69 primary neuroblastoma tumors previously profiled for miRNA expression by RT-qPCR [33].

The expression level of miR-193b was significantly lower (p value < 0.0001) as compared to that of the well-defined oncogenic miRNAs miR-92a-3p and miR-17-5p (Figure 1A). In addition, the expression level of miR-193b was found to be comparable to that of miR-34a, a tumor suppressor miRNA that is expressed at low levels in unfavorable primary neuroblastoma tumors and cell lines [24]. Then, to extend the clinical data even more, we also analyzed miR-193b expression compared to miR-92a-3p and miR-17-5p expression in ten primary neuroblastoma samples by deep sequencing (Figure 1B, data from [18]). These data confirmed the RT-qPCR data indicating that miR-193b is downregulated in neuroblastoma, which points to a tumor suppressive function of miR-193b in this tumor entity. In addition, we used RT-qPCR to compare the expression of mir-193b to well established neuroblastoma oncogenic and tumor suppressor miRNAs in two neuroblastoma cell lines, Kelly and SK-N-BE(2)-C (Supplementary Figure 1). As for the tumor samples, the expression of mir-193b was significantly lower as compared to miR-92a and comparable to miR-34a in these cell lines. In concordance to these findings, analysis of miR-193b expression in neuroblastoma cell lines previously profiled by us for miRNA expression by deep sequencing [21] also revealed low expression of miR-193b when compared to known oncogenic miRNAs or tumor suppressor miRNAs, respectively (Supplementary Table 1).

MiR-193b reduces cell viability and proliferation in neuroblastoma cell lines

In order to investigate a potential tumor suppressor role of miR-193b in neuroblastoma cells, miR-193b mimics (mir-193b) or scrambled control miRNA mimics (C) were transfected into nine neuroblastoma cell lines with distinct genetic characteristics. RT-qPCR was performed to validate miR-193b overexpression (Supplementary Figure 2). As shown in Figures 2 and 3, miR-193b had a significant effect on cell viability and proliferation. In all neuroblastoma cell lines tested, a

reduction in cell viability and proliferation was detected within 24 or 48 hours post-transfection, and loss of cell viability by more than 50% was apparent in SK-N-BE(2)-C (BE(2)-C), Kelly, SHSY-5Y and CHLA-20 cells 96 hours after transfection.

MiR-193b induces caspase-dependent and -independent cell death in neuroblastoma

To determine the possible mode of the anti-proliferative activity of miR-193b, the cytotoxic effect of miR-193b was assessed following transfection of miR-193b or control mimics into each cell line. The MultiTox-Fluor Multiplex Cytotoxicity Assay simultaneously measures two protease activities; one is a marker of viability, and the other is a marker of cytotoxicity. As the ratio of viable cells to dead cells is independent of the cell number, the data can be normalized.

High cytotoxic effects were detected in BE(2)-C, Kelly and SHSY-5Y cells by day two. Significant, but lower cytotoxic effects were observed in NBL-S, CHLA-20 and NBL-W cells. MiR-193b had only a modest cytotoxic effect (less than 10%) in SMS-KAN, CHLA-15 and SK-N-AS cells (Figure 4).

Next, to investigate whether the cytotoxic effect of miR-193b is mediated through the induction of apoptosis, activation of caspase-3/7 and PARP-1 cleavage was assessed following transfection of miR-193b into each cell line (Figure 5). In CHLA-15, SMS-KAN, SK-N-AS cells (1.12–1.31-fold relative change) and in NBL-W cells (average fold change 1.65) there was only a small increase in the caspase-3/7 enzymatic activity in miR-193b-transfected cells as compared to control-transfected cells. In BE(2)-C, SHSY-5Y, NBL-S, CHLA-20 and Kelly cells, the caspase-3/7 activity had increased more than two-fold 48 hours post-transfection (Figure 5A). In concordance with this, miR-193b mimic transfection also caused an increase in PARP-1 cleavage in BE(2)-C, Kelly, SHSY-5Y, NBL-S, CHLA-20 and NBL-W cells with a concomitant decrease in total PARP-1, whereas there was only a modest increase in PARP-1 cleavage in SK-N-AS and SMS-KAN cells (Figure 5B). To analyze whether miR-193b may induce secondary cell death, we also analyzed PARP-1 cleavage at 72 hours post-transfection in those cell lines where no PARP-1 cleavage was detected 24 hours post-transfection. 72 hours post-transfection, PARP-1 cleavage had increased in SK-N-AS but not in SMS-KAN cells (Figure 5B). Surprisingly, while miR-193b only slightly increased caspase-3/7 activity in CHLA-15 cells (average fold change 1.26), miR-193b substantially increased PARP-1 cleavage 24 hours post-transfection, which may indicate caspase-independent cell death in this cell line (Figure 5B). To summarize, these results indicate that miR-193b induces both caspase-dependent and -independent cell death in neuroblastoma cell lines.

MiR-193b induces a G1 cell cycle arrest in neuroblastoma

To assess whether mir-193b-induced growth inhibition of cells is mediated via alterations in cell cycle regulation, we analyzed the cell cycle distribution profiles of mir-193b-transfected cells by flow cytometry in six of the nine cell lines. In all neuroblastoma cell lines tested,

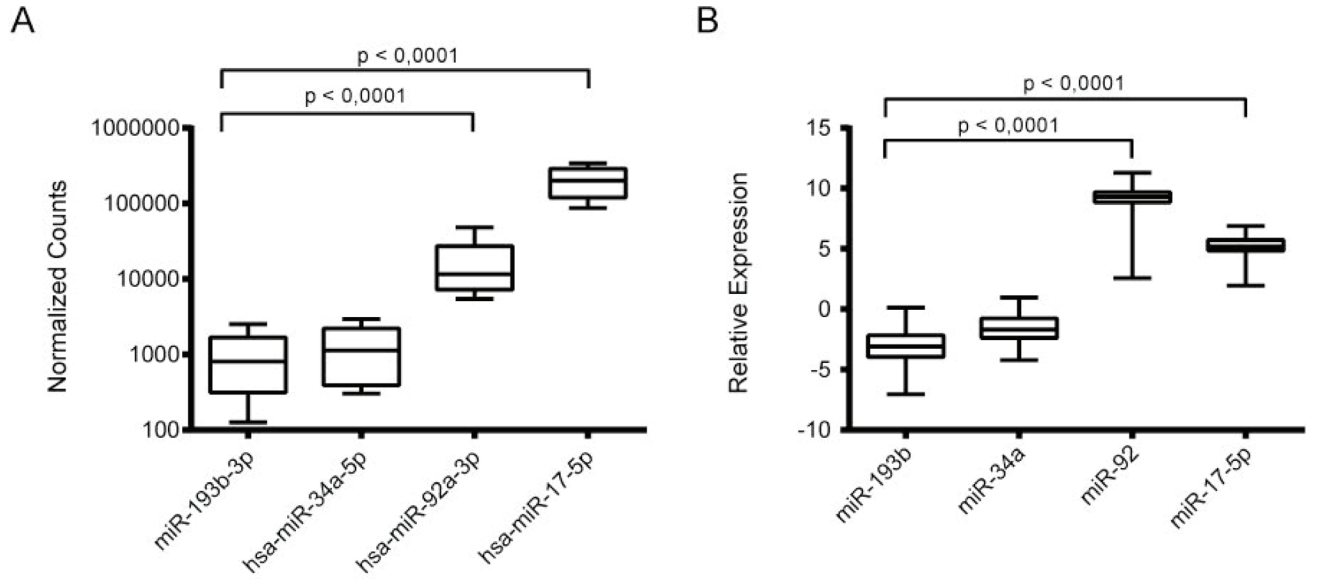

Figure 1: miR-193b is downregulated in primary neuroblastoma tumor samples. (**A**) 10 different neuroblastoma samples were analyzed by RNA sequencing. The expression of miR-193b-3p was comparable to the expression level of the tumor suppressive miR-34a-5p and significantly lower than the expression of the known oncomiRs miR-92a-3p and miR-17-5p ($p < 0.0001$). (**B**) 69 neuroblastoma tumor samples, independent of the first cohort, were analyzed by qRT-PCR. In this cohort we also found a significant downregulation of miR-193b in comparison to the oncomiRs ($p < 0.0001$).

miR-193b increased the number of cells in the G1-phase of the cell cycle by 11.5–22.5% with a concomitant decrease in the number of cells in the Sphase and G2/M-phase (Figure 6). Thus, in addition to apoptosis, miR-193b decreases cell growth in neuroblastoma cell lines by inducing a G1 cell cycle arrest.

MiR-193b targets *Cyclin D1*, *MCL-1* and *MYCN* in neuroblastoma

Next, we investigated the mechanism by which miR-193b may suppress cell growth in neuroblastoma cells. Both *myeloid cell leukemia 1* (*MCL-1*) and *Cyclin D1*, which are associated with apoptosis and cell cycle regulation, respectively, have been found to be direct targets of miR-193b in other cancers [34–42]. We also performed a bioinformatic analysis using TargetScan algorithm [43] to identify further potential target genes of miR-193b associated with cell cycle progression and apoptosis. The analysis revealed a highly evolutionarily conserved miR-193b binding site in the 3′-UTR of the *v-myc avian myelocytomatosis viral oncogene neuroblastoma derived homolog* (*MYCN*) oncogene (Supplementary Figure 4).

To test whether these genes are targeted by miR-193b in neuroblastoma, cells were transfected with either miR-193b or control mimics and the expression levels of the potential target genes were analyzed by Western blot and quantitative RT-PCR. The mRNA and protein levels of MCL-1 and Cyclin D1 were reduced upon miR-193b overexpression in all neuroblastoma cell lines tested (Figure 7A and 7B, Supplementary Figure 5). MiR-193b mimic transfection reduced *MYCN* mRNA expression in the *MYCN*amplified cell lines SMS-KAN, NBL-W and Kelly but there was no reduction in *MYCN* mRNA expression when miR-193b mimics were introduced into BE(2)-C cells (Figure 7B). However, N-Myc protein expression was reduced in all *MYCN*-amplified cell lines tested 24 or 72 hours post-transfection (Figure 7A, Supplementary Figure 5). In BE(2)-C and SMS-KAN cells there was only a slight decrease in N-Myc protein expression 24 hours after transfection, but 72 hours post-transfection, N-Myc protein expression was lower in miR-193b transfected cells as compared to control-transfected cells (Figure 7A, Supplementary Figure 5). Thus, these results indicate that miR-193b targets *MCL-1*, *Cyclin D1* and *MYCN* in neuroblastoma cell lines.

To investigate whether miR-193b directly binds to the predicted 3′UTR binding site of *MYCN*, we used a vector containing the *MYCN* 3`UTR downstream of the firefly luciferase gene (Table 1). In addition, we designed a construct containing mutations at the predicted miRNA-193b seed sequence (Figure 8A). The resulting 3′-UTR-

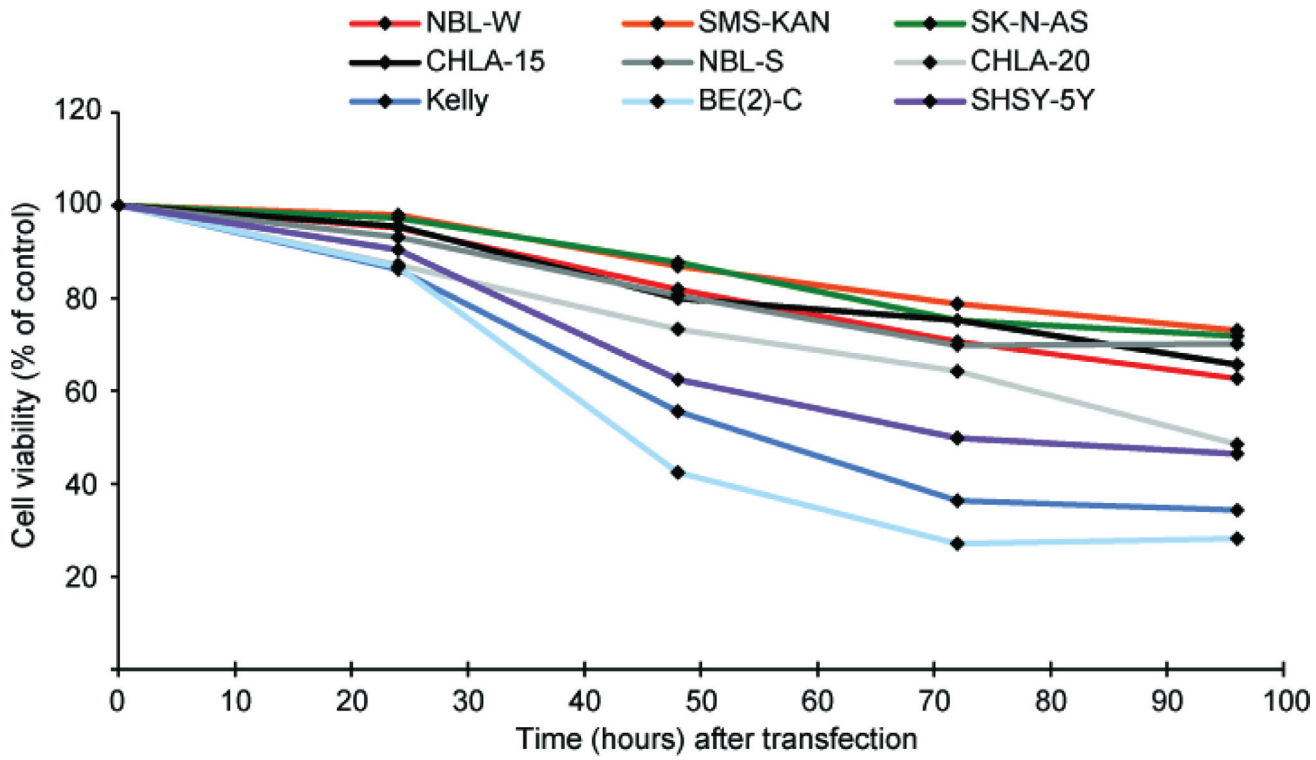

Figure 2: miR-193b reduces cell viability in neuroblastoma cell lines. Neuroblastoma cell lines were transfected with control mimics or miR-193b mimics. Cell viability was analyzed using alamarBlue at indicated time points. The average cell viability of cells transfected with control mimics was set to 100% (not shown) and the cell viability of miR-193b-transfected cells was calculated relative to control-transfected cells. Data are mean of at least three experiments, each performed in triplicate. Standard deviations have been included in Supplementary Figure 3.

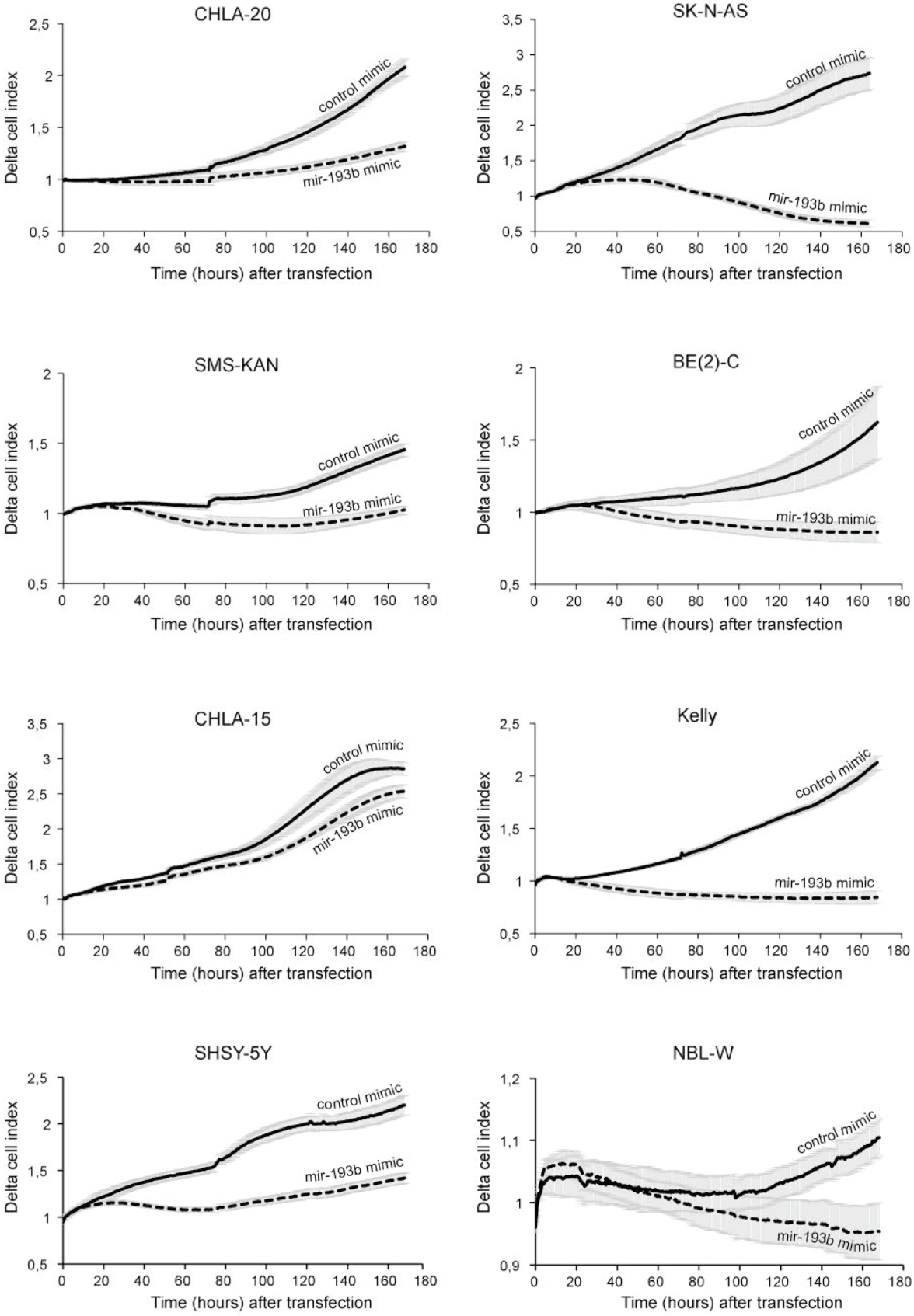

Figure 3: miR-193b reduces proliferation in neuroblastoma cell lines. Neuroblastoma cell lines were transfected with control mimics or miR-193b mimics and cell proliferation was monitored in real time for seven days using xCELLigence. Data are mean of one representative experiment of at least two, each performed in octuplicate. (Solid line: control mimics; Dotted line: miR-193b mimics).

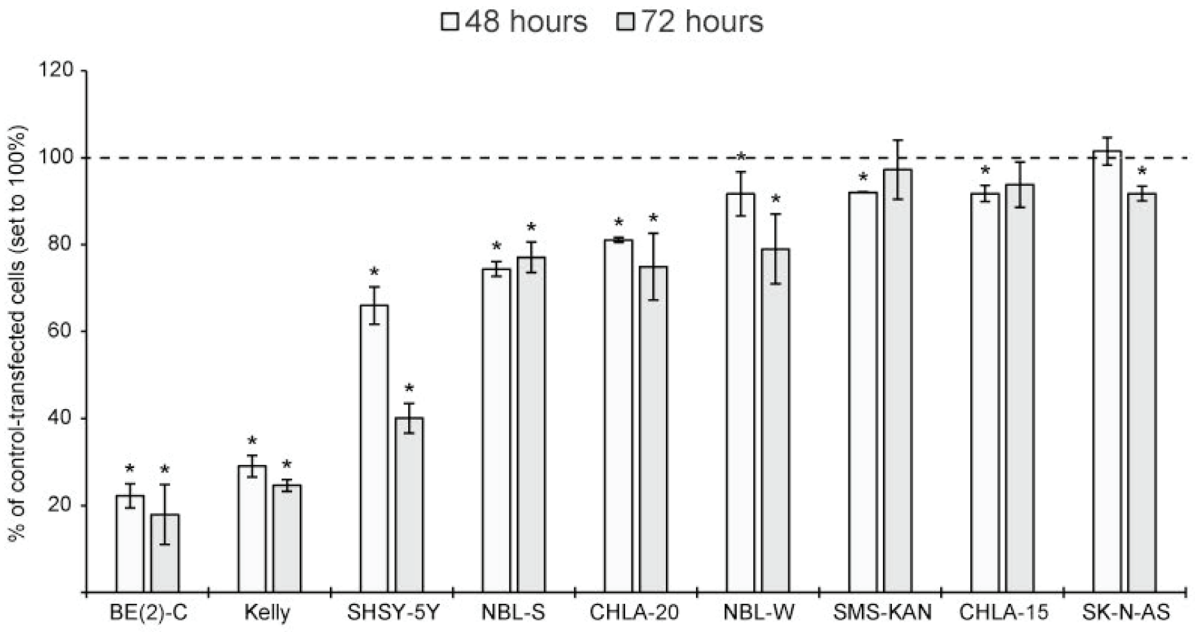

Figure 4: miR-193b is cytotoxic to neuroblastoma cell lines. Cells were transfected with control mimics or miR-193b mimics. Cytotoxicity was analyzed at the indicated time points using the MultiToxFluor Multiplex Cytotoxicity Assay. Cytotoxicity (defined as the ratio of viable cells to dead cells) in miR-193b-transfected cells was calculated in relation to that in control-transfected cells. Data are mean ± SD of at least two independent experiments, each performed in triplicates ($^{*}p < 0.01$ Student`s *t*-test).

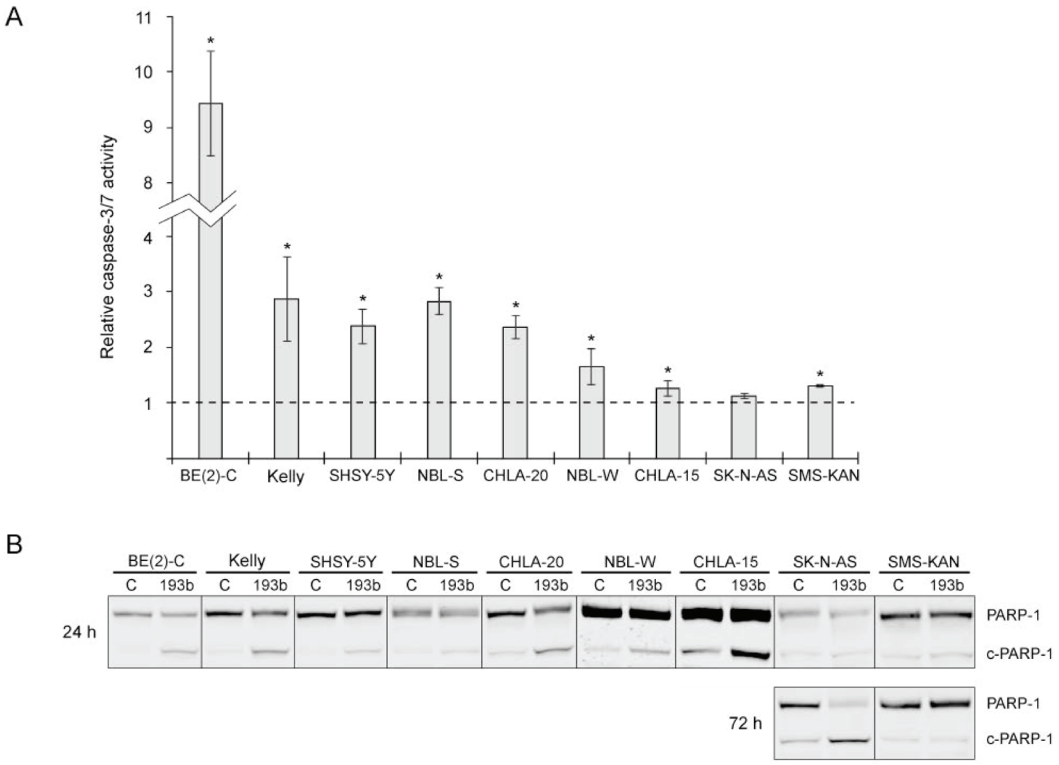

Figure 5 : miR-193b induces apoptosis in neuroblastoma cell lines. (**A**) Cells were transfected with control mimics or miR-193b mimics and caspase activity was measured 48 hours after transfection. The results are expressed as relative caspase activities of miR-193b-transfected cells, which is the ratio between the caspase activity of miR-193b-transfected cells and that measured in control-transfected cells. Data are mean ± SD of at least two independent experiment, each performed in triplicates ($^{*}p < 0.01$ Student`s *t*-test). (**B**) Cells were transfected as in (A). Total PARP1 and PARP-1 cleavage (c-PARP-1) was assessed by Western blot 24 and 72 hours post-transfection, respectively. The experiment was performed at least two times giving similar results, and the result from one representative experiment is shown.

luciferase reporter plasmids were co-transfected with control or miR-193b mimics into several neuroblastoma cell lines (*MYCN*-amplified cell lines: SMS-KAN and BE(2)-C and non-*MYCN* amplified cell line: SK-N-AS). Activity of the luciferase reporter gene carrying the wild-type *MYCN*-3-UTR was significantly lower in cells overexpressing miR-193b, while no repression of luciferase activity was observed in the reporter construct carrying the mutant *MYCN* 3`UTR (Figure 8B). These results confirm that miR-193b repress *MYCN* expression by directly binding to the 3`-UTR sequence of the *MYCN* mRNA.

MiR-193b induces a G1 cell cycle arrest by targeting *Cyclin D1* and *MYCN*

To address whether miR-193b induces a G1 cell cycle arrest by targeting *Cyclin D1*, cells were co-transfected with miRNA mimics and a *Cyclin D1* expression plasmid lacking the 3′UTR.

Overexpression of Cyclin D1 in Kelly, SHSY-5Y and BE(2)-C was confirmed by Western blot analysis (Figure 9A). Unfortunately, we were not able to overexpress Cyclin D1 in SMS-KAN, CHLA-15 and CHLA-20 cells

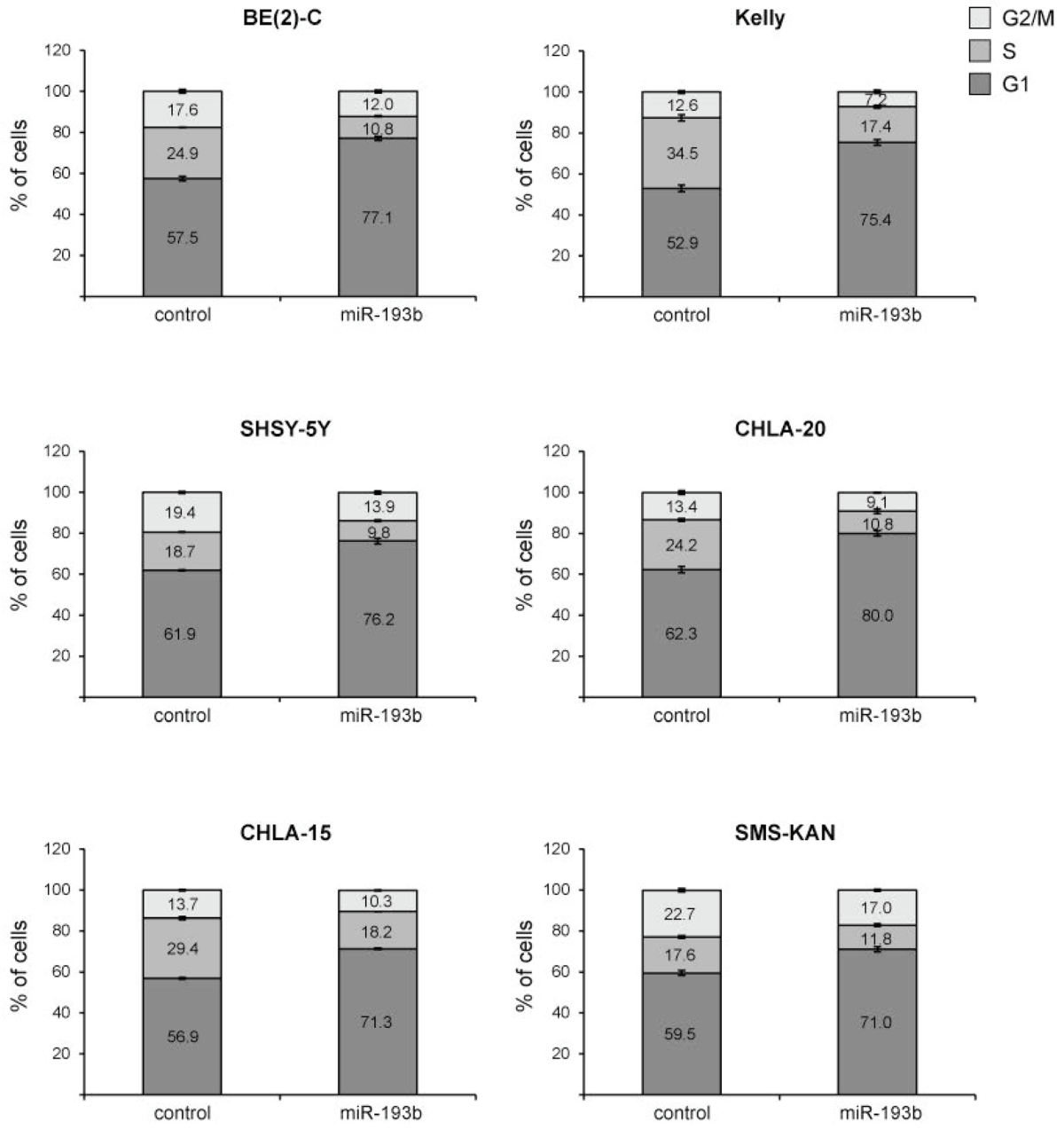

Figure 6: miR-193b induces a G1 cell cycle arrest in neuroblastoma. Cells were transfected with control or miR-193b mimics. 24 hours after transfection, cells were fixed with ethanol and cell-cycle profiles were determined by propidium iodide incorporation and flow cytometry analysis. Results are presented as percentage of cells in a particular phase. Data are mean ± SD of one representative experiment of at least two, each performed in triplicate.

(data not shown). Co-transfection of control mimics and the *Cyclin D1* overexpression plasmid had no (BE(2)-C and Kelly) or only a minor (SHSY-5Y; less than 5%) effect on cell cycle profiles (Figure 9B). *Cyclin D1* overexpression partly rescued cells from miR-193b-mediated G1 cell cycle arrest, confirming an important role of miR-193b in regulating cell cycle progression by targeting *Cyclin D1* (Figure 9B). However, the incomplete rescue by *Cyclin D1* implies that miR-193b may also modulate cell cycle progression by other mechanisms.

We and others have previously shown that downregulation of *MYCN* expression induces a G1 cell cycle arrest in *MYCN*-amplified neuroblastoma cell lines including Kelly and BE(2)-C cell lines [44, 45]. To investigate whether miR-193b-mediated downregulation of *MYCN* may explain the incomplete rescue by *Cyclin D1*, BE(2)-C and Kelly cells were transfected with siRNA against *MYCN* and cell cycle profiles were analyzed. Knockdown of N-Myc was verified by Western blot analysis (Figure 10A). The results confirmed that *MYCN* knockdown causes a G1 phase arrest in Kelly and BE(2)-C cells, although the effect is considerably smaller as compared to that of miR-193b overexpression (Figure 10B). The fraction of cells in the G1 phase of the cell cycle increased from 60.7% (control siRNA) to 65.9% (*MYCN* siRNA) for BE(2)-C cells and from 46.7% (control siRNA) to 56.3% (*MYCN* siRNA) in Kelly cells transfected with 2 nM *MYCN* siRNA.

These results suggest that both *MYCN* and *Cyclin D1* may be important miR-193b targets genes mediating, at least in part, the effects of miR-193b overexpression on proliferation of neuroblastoma cells lines by inducing a G1 cell cycle arrest.

MiR-193b induces cell death by targeting *MCL-1*

Furthermore, we analyzed whether miR-193b induces cell death by targeting *MCL-1*. For this purpose, cells were co-transfected with miRNA mimics and a *MCL-1* expression plasmid lacking the 3′UTR (Table 1). The restoration of MCL-1 expression was confirmed by Western blot analysis (Figure 11). In all cell lines tested, co-transfection of miR-193b and an empty vector resulted

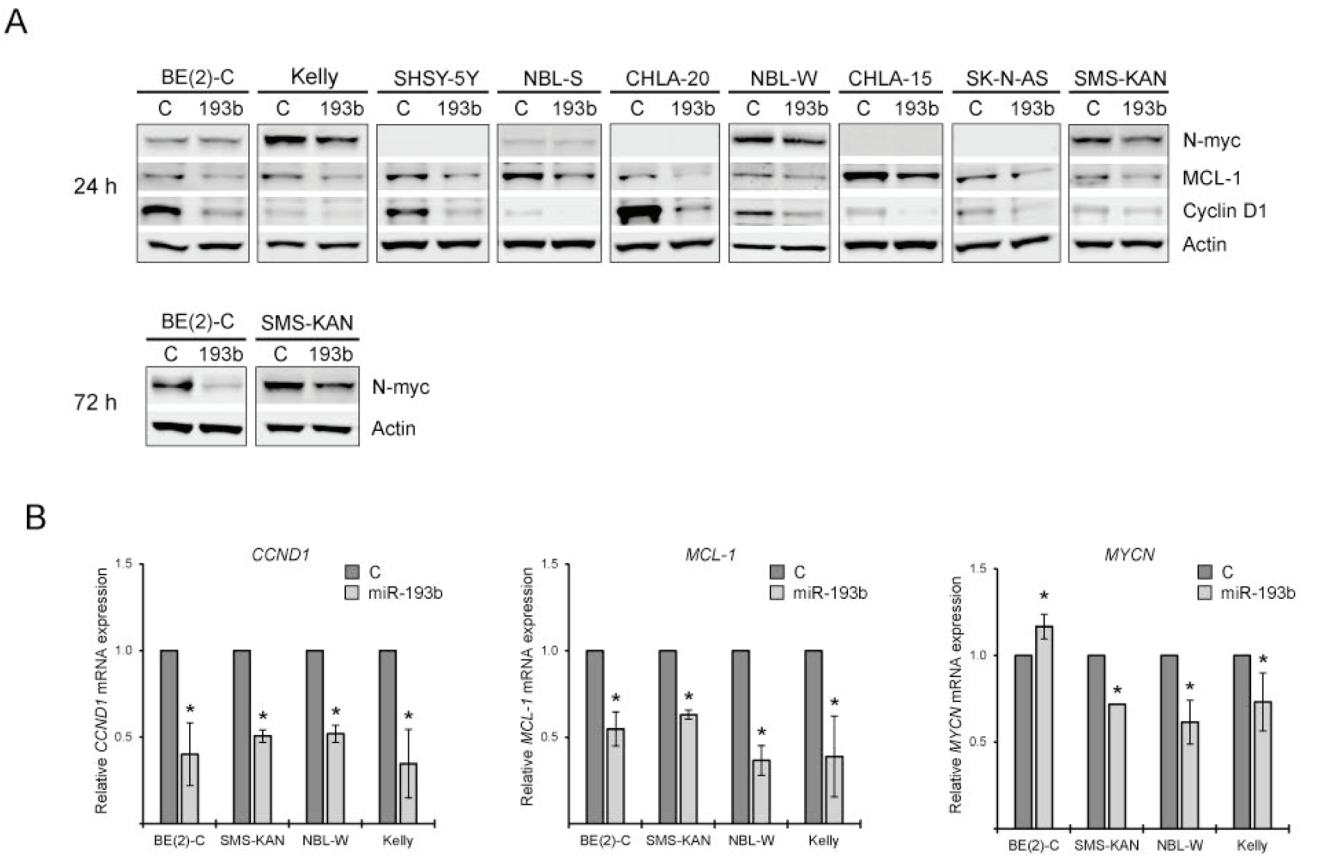

Figure 7 : miR-193b reduces the expression of *Cyclin D1*, *MCL-1* and *MYCN* in neuroblastoma. (**A**) Cells were transfected with miR-193b mimics or control mimics. 24 hours or 72 hours post-transfection, cells were harvested and protein expression was assessed by Western blot. Actin was used to demonstrate equal protein loading. The experiment was performed at least two times giving similar results, and the result from one representative experiment is shown. (**B**) Cells were transfected as in (A). 24 hours post-transfection, the total RNA was isolated, reverse transcribed into cDNA and the expression of genes were analyzed by RT-qPCR. Transcripts levels of individual genes were normalized to SDHA to allow relative quantification of gene expression relative to control-transfected cells by the DDCT method. Data are means ± SD of two independent experiments, each performed in triplicates ($^{*}p < 0.05$ Student`s *t*-test).

in increased PARP-1 cleavage, indicating cell death. Ectopic expression of *MCL-1* partly rescued SHSY-5Y and BE(2)-C cells from miR-193b-induced cell death: When transfected with both miR-193b and a vector overexpressing *MCL-1*, PARP-1- cleavage was reduced as compared to cells co-transfected with miR-193b and an empty vector (Figure 11). These results confirm that miR-193b induces cell death in SHSY-5Y and BE(2)-C cells by targeting *MCL-1*.

However, there was no rescue in CHLA-20 cells when co-transfected with the *MCL-1* expression plasmid (Figure 11). These results indicate that in addition to *MCL-1*, other miR-193b target genes are involved in mir-193b-induced cell death in neuroblastoma cells.

To verify that *MCL-1* downregulation can trigger cell death in neuroblastoma, siRNA against *MCL-1* was transfected into neuroblastoma cell lines. In concordance with the rescue experiments, *MCL-1* downregulation increased PARP-1 cleavage in BE(2)-C and SHSY-5Y whereas there was only a very modest increase in PARP-1 cleavage in CHLA-20 in response to *MCL-1* knockdown (Figure 12).

To summarize, these results indicate that the targeting of *MCL-1* by miR-193b contributes to miR-193b-induced cell death in neuroblastoma cells.

DISCUSSION

Targeted therapy intercepting with a single oncogene is often insufficient due to preexisting or acquired resistance [46, 47]. Therefore, therapeutic approaches should simultaneously affect several targets, e.g. by using miRNAs repressing the expression of multiple targets. MicroRNAs are involved in virtually all cellular processes and exert essential roles in tumorigenesis through acting as oncogenes or tumor suppressors [6, 48]. During the last decade, development of miRNA-based anticancer therapies has received growing attention. However, picking the right miRNA exhibiting a robust

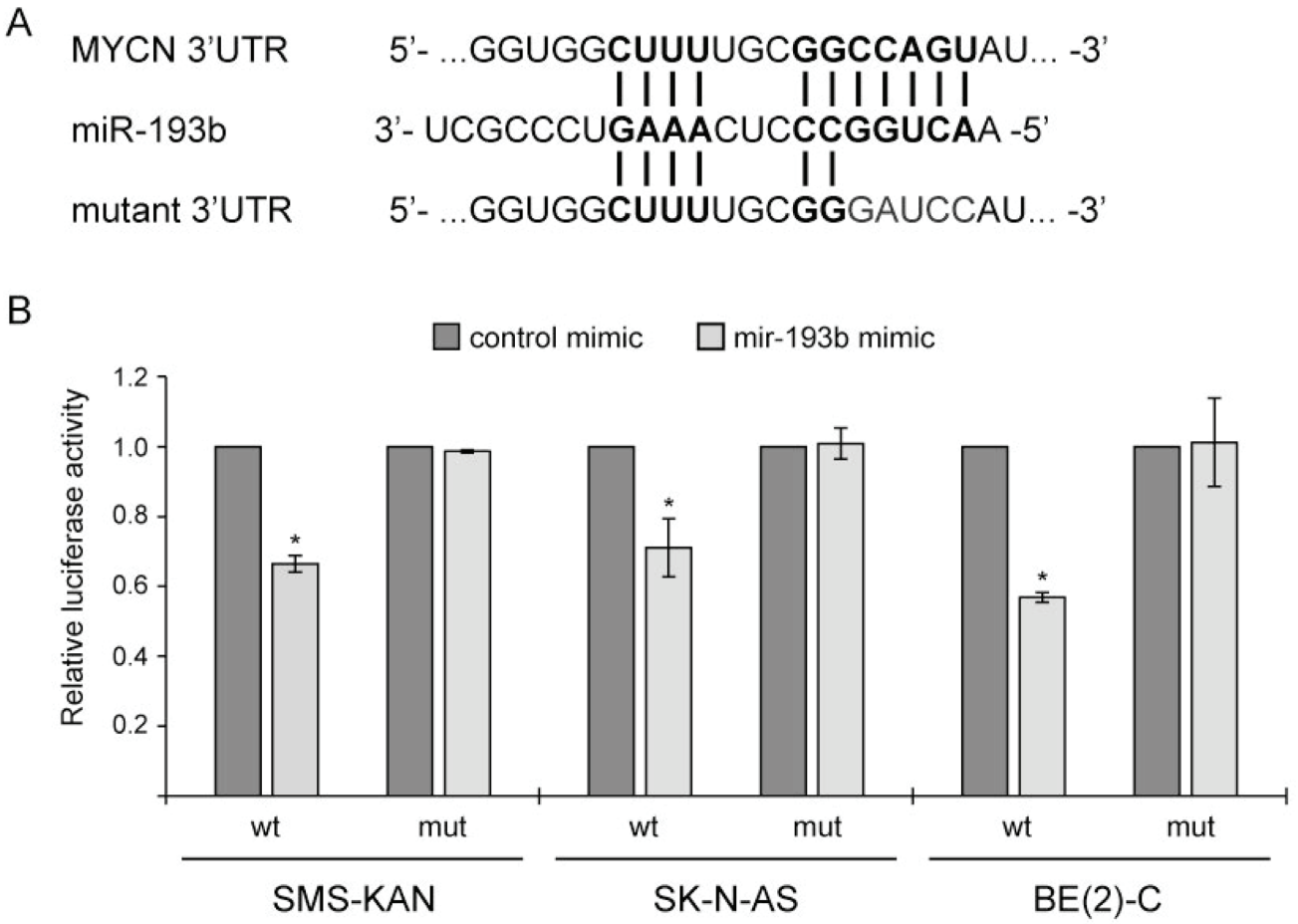

Figure 8: *MYCN* is a direct miR-193b target in neuroblastoma. (**A**) Illustration of the putative target site of miR-193b in the 3′-UTR of *MYCN* according to TargetScan prediction and mutant *MYCN*-3`-UTR sequence. (**B**) Cells were cotransfected with miRNA mimics (either miR-193b or control mimics), a firefly luciferase report plasmids (either pMIR-Report-*MYCN*-UTR-WT or pMIR-Report-*MYCN*-UTR-MUT), and a renilla plasmids. Cells were harvested 24 hours post-transfection. Protein extracts were prepared and assayed for firefly and renilla luciferase activities. Firefly luciferase activity was normalized to renilla luciferase activity. The normalized luciferase activities of miR-193b-transfected cells were calculated relative to those of control-transfected cells (set to one). Data are means ± SD of two independent experiments, each performed in triplicate ($^{*}p < 0.01$ Student`s *t*-test).

phenotype and being potent and safe enough to be used as therapeutics represents a significant challenge [46].

Recent evidence suggests that miR-193b has both oncogenic and tumor suppressor functions in human cancer. MiRNA profiling studies have shown that the expression level of miR-193b is frequently downregulated in human cancer tissues as compared to non-cancerous adjacent tissues. Reduced expression levels of miR-193b as compared to (adjacent) non-cancerous cells were found in ovarian [49], hepatocellular carcinoma [34, 42], non-small cell lung cancer (NSCLC) cells [37], meningioma [50] and endometrioid adenocarcinoma [51], and also in pancreatic [52] and gastric [53, 54] cancer cells. In other cancer types, including glioma [55], multiple myeloma [56] and head and neck squamous cell carcinoma (HNSCC) [57], the expression of miR-193b has been reported to be upregulated compared to non-cancerous cells, and increased miR-193b expression levels were found in relapsed relative to non-relapsed primary HNSCC tissues [57]. Functional studies have identified both tumor suppressive and oncogenic targets of miR-193b regulating proliferation, apoptosis, differentiation, migration and invasion of various cancer

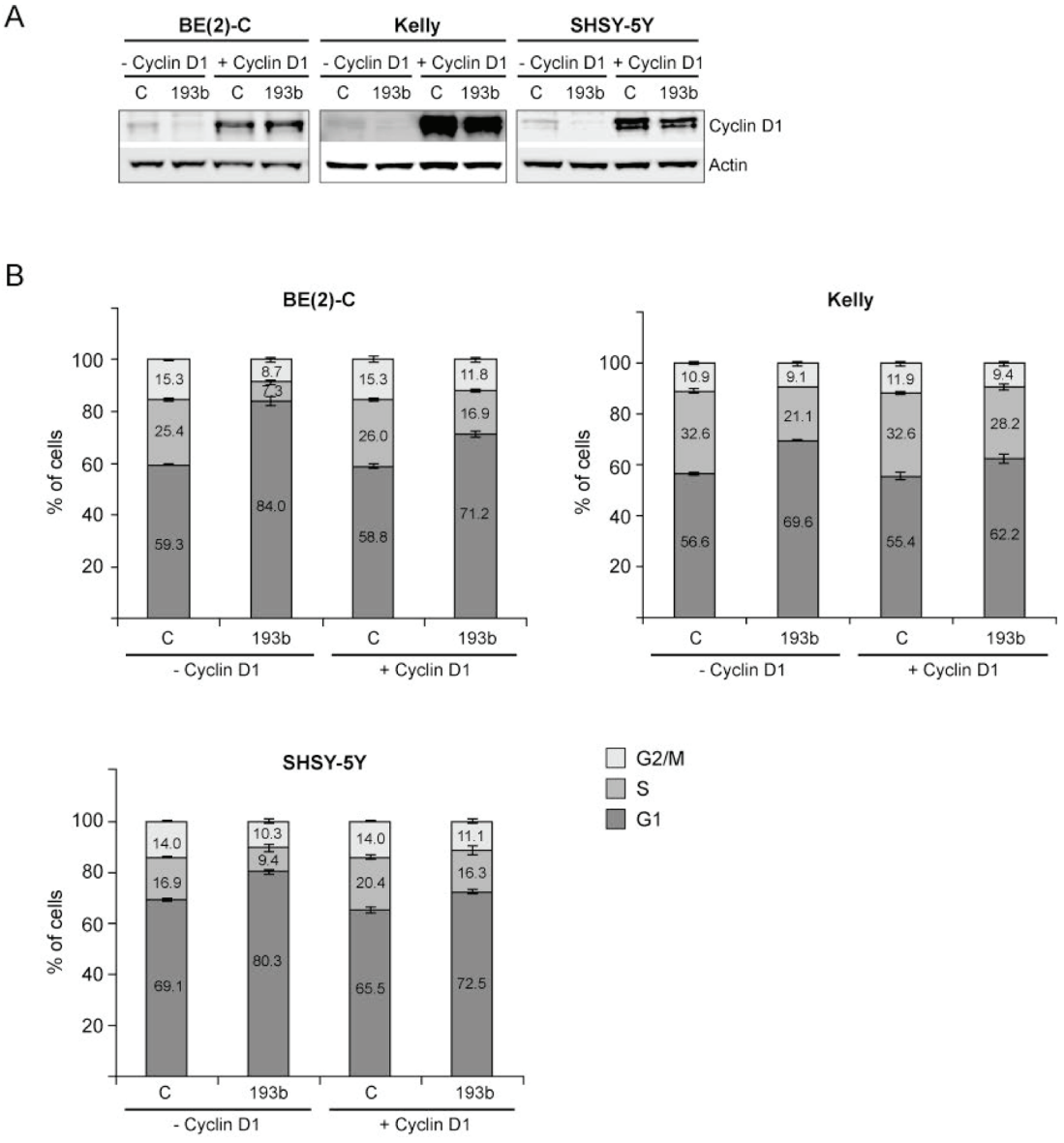

Figure 9: *Cyclin D1* overexpression rescues neuroblastoma cells from miR-193b-induced G1 cell cycle arrest. Cells were co-transfected with control or miR-193b mimics and an empty (– Cyclin D1) or a Cyclin D1 (+ Cyclin D1) overexpression plasmid. 24 hours after transfection, cells were harvested for Western blot analysis to show Cyclin D1 overexpression (**A**) or cells were fixed with ethanol and cell-cycle profiles were determined by propidium iodide incorporation and flow cytometry analysis (**B**). Results from cell cycle analysis are presented as percentage of cells in a particular phase. Cell cycle data are mean ± SD of one representative experiment of at least two, each performed in triplicate. Western blot data show one representative experiment. Actin was used to demonstrate equal protein loading.

cells. Thus, miR-193b regulates multiple hallmarks of cancer by targeting both oncogenes and tumor suppressors (Supplementary Figure 6). It is therefore likely that the miR-193b functions depend on multiple target genes, and both intrinsic and extrinsic factors determine whether this miRNA dominantly exerts tumor suppressive or oncogenic functions in a specific cell type.

The results of this study indicate that miR-193b exhibits tumor suppressive functions in neuroblastoma. We here demonstrated that miR-193b is generally low expressed in primary neuroblastoma samples and cell lines. A previous study revealed higher expression of miR-193b in unfavorable versus favorable neuroblastoma [18], and we recently reported increased expression of miR-193b in post-therapy neuroblastoma cell lines as compared to the matched cell lines isolated at diagnosis before treatment [21]. However, additional analyses (Figure 1B) demonstrated that miR-193b is expressed at low levels in both unfavorable neuroblastoma and in post-therapy neuroblastoma cells (Supplementary Table 1) when compared to the well-defined oncogenic miRNAs miR-92a-3p and miR-17-5p. Analysis of primary neuroblastoma samples by RT-qPCR validated low expression of miR-193b in neuroblastoma. In concordance to these findings, a previous study by Beckers *et al.* indicated that endogenous miR-193b levels do not reach the threshold to exert its tumor suppressive functions in neuroblastoma [58]. Although we and Beckers *et al.* demonstrated that MYCN is directly targeted by miR-193b, Beckers *et al.* found neither a negative correlation between miR-193b and *MYCN* expression nor miR-193b expression and MYCN activity [58]. Thus, the direct miR-193b target *MYCN* is insufficiently counteracted by low endogenous miR-193b expression levels in neuroblastoma. Our *in vitro* data indicate that correcting these deficiencies by miR-193b replacement therapy, effectively represses *MYCN* and two further important oncogenic miR-193b targets, namely *MCL-1* and *cyclin D1* resulting in the activation of anti-proliferative and pro-apoptotic pathways. We thereby showed that the increase

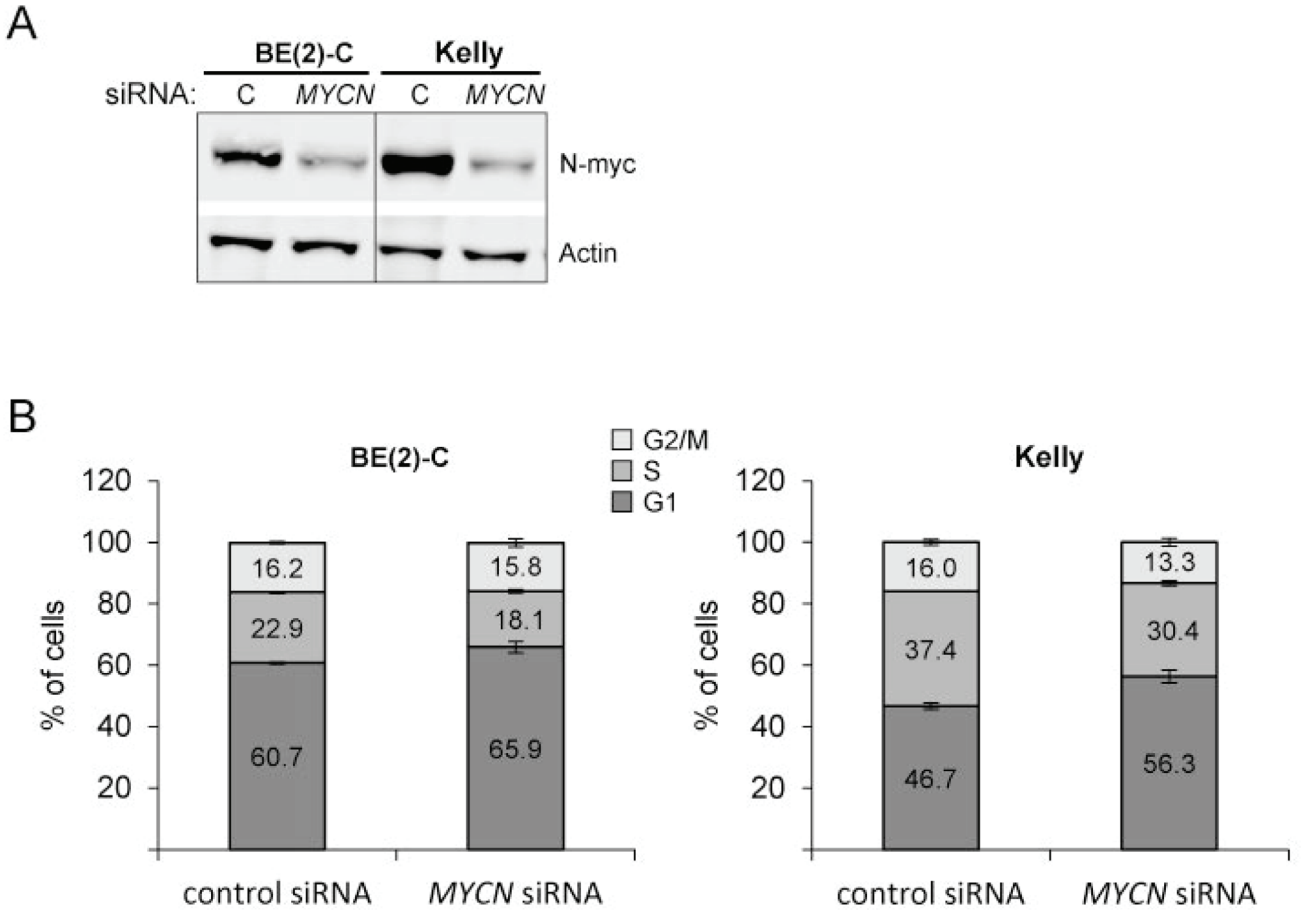

Figure 10 : *MYCN* knockdown increases the number of cells in G1. Cells were transfected with control siRNA or *MYCN* siRNA. 24 hours after transfection, cells were harvested for Western blot analysis to show N-Myc knockdown (**A**) or cells were fixed with ethanol and cell-cycle profiles were determined by propidium iodide incorporation and flow cytometry analysis (**B**). Results from cell cycle analysis are presented as percentage of cells in a particular phase. Cell cycle data are mean ± SD of one representative experiment of at least two, each performed in triplicate. Western blot data show one representative experiment. Actin was used to demonstrate equal protein loading.

Table 1: Plasmids used in this study

Name	Insert/property	Reference
Expression vectors		
pcDNA3.1-Mcl-1	MCL-1 cDNA without 3′UTR Flag-Tag (8aa) between START codon and MCL-1 cDNA	[70]
pCMV-CyclinD1	CyclinD1 cDNA without 3′UTR	[71] (Addgene # 19927)
Luciferase reporter plasmids		
pMIR-Report-*MYCN*-UTR-WT	*MYCN*-3′UTR reporter plasmid	[69]
pMIR-Report-*MYCN*-UTR-MUT	Mutated *MYCN*-3′UTR reporter plasmid	this study
pGL4.75[hRluc/CMV]	Renilla luciferase reporter	Promega

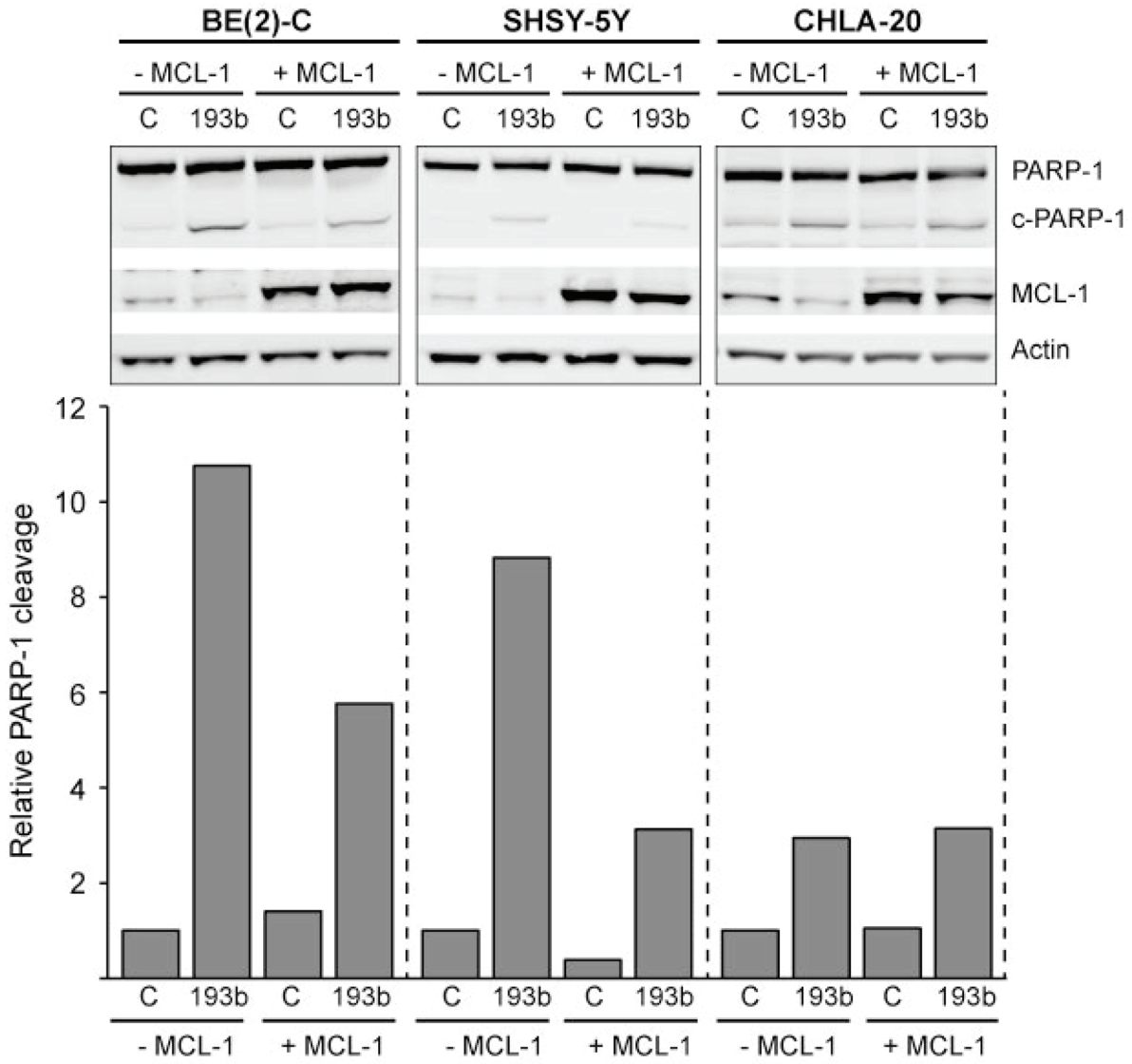

Figure 11: *MCL-1* overexpression partly rescues neuroblastoma cells from miR-193b-induced cell death . Cells were co-transfected with control or miR-193b mimics and an empty (- Mcl-1) or an Mcl-1 (+ Mcl-1) overexpression plasmid. Cells were harvested 24 hours post-transfection. Actin was used to demonstrate equal protein loading. PARP-1 was quantified using ImageJ. Data are expressed as the ratio of cleaved PARP-1 to uncleaved PARP-1 and relative to control + empty-vector- transfected cells (set to 1). The experiment was performed at least two times giving similar results, and the result from one representative experiment is shown.

in miR-193b levels upon mimic transfection significantly augments the antagonizing functions of miR-193b beyond the threshold at which this miRNA becomes dominantly tumor suppressive. Thus, oncogenic pathways, which are insufficiently counteracted by endogenous miR-193b levels, are effectively repressed upon miR-193b mimic transfection. Further studies are required to determine the extent to which *cyclin D1*, *MYCN* and *MCL-1* are actually regulated by endogenous levels of miR-193b.

MicroRNA-193b Induces a G1 Cell Cycle Arrest by Targeting Cyclin D1 and MYCN

Previous studies have shown that deregulation of the cell cycle, in particular G1 entry checkpoint dysregulation, appears to be an important factor in driving neuroblastoma tumorigenesis [59–61]. Several cell cycle regulators, especially those within the cyclin D1/CDK4/CDK6/RB pathway, are hyperactive in neuroblastoma [61]. Recent *in vitro* and *in vivo* studies on the therapeutic utility of inhibitors targeting the cyclin D1-associated kinases CDK4/CDK6 revealed promising results in various cancer types including neuroblastoma [59, 61].

The present study demonstrates that introduction of miR-193b into neuroblastoma cell lines results in a G1 cell cycle arrest via downregulation of *cyclin D1*. However, overexpression of *cyclin D1* only partly rescue miR-193b-mediated G1 cell cycle arrest pointing to additional miR-193b target genes whose inhibition directly or indirectly induces a G1 cell cycle arrest.

Our data indicate that the oncogene *MYCN* is one such target regulated by mir-193b. We have previously shown that downregulation of *MYCN* induces a G1 cell cycle arrest in *MYCN*-amplified neuroblastoma cell lines [44]. In concordance with this, we demonstrated that siRNA-mediated knockdown of *MYCN* increases the proportion of *MYCN*-amplified neuroblastoma cells in the G1 phase of the cell cycle.

Based on these results, we conclude that the observed anti-proliferative effect of miR-193b in neuroblastoma is mediated, at least in part, through targeting both *cyclin D1* and *MYCN*, two oncogenes with

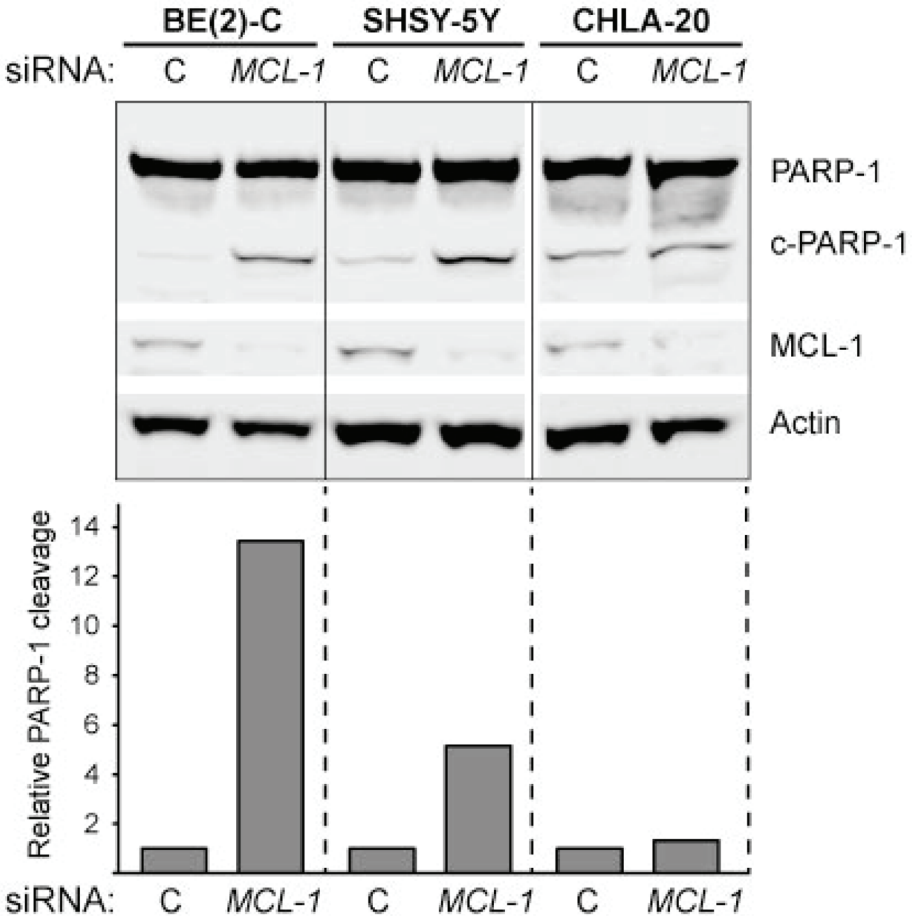

Figure 12: PARP-1 cleavage in response to *MCL-1* knockdown in neuroblastoma. Cells were transfected with control siRNA or *MCL-1* siRNA for 24 hours. Actin was used to demonstrate equal protein loading. PARP-1 was quantified using ImageJ; data are expressed as the ratio of cleaved PARP-1 to uncleaved PARP-1 and relative to control-transfected cells (set to 1). The experiment was performed at least two times giving similar results, and the result from one representative experiment is shown.

essential roles in neuroblastoma tumorigenesis and thereby attractive therapeutic targets.

MicroRNA-193b Induces cell death in neuroblastoma

The functions of miR-193b in the control of the cell cycle are complemented by functions regulating cell death. Apoptosis is the best-characterized mechanism of programmed cell death in which activation of the executioner caspase cascade promotes cell shrinkage, membrane blebbing, chromatin condensation, DNA fragmentation, and finally the formation of apoptotic bodies and cell death [62]. In recent years, a number of non-canonical cell death mechanisms, which are often caspase-independent, have been described. These include caspase-independent apoptosis (CIA), necrosis, mitotic catastrophe, ferroptosis, paraptosis, and pyroptosis [62].

To investigate whether the anti-proliferative effect of miR-193b is also mediated through the induction of apoptosis, we analyzed caspase-3/7 activity and poly(ADP-ribose)-polymerase (PARP)-1 cleavage, which are hallmarks of apoptosis. We found that miR-193b significantly increases both caspase-3/7 activity and PARP-1 cleavage in six of nine investigated neuroblastoma cell lines within 24 hours. Interestingly, while miR-193b only slightly increased caspase-3/7 activity in CHLA-15 cells (1.26 fold), it significantly increased PARP-1 cleavage in this cell line within 24 hours post-transfection, indicating that miR-193b may also induce caspase-independent cell death in neuroblastoma. In SK-N-AS cells, miR-193b-mediated PARP-1 cleavage was not observed before 72 hours post-transfection, suggesting that miR-193b does not directly trigger cell death in this cell line, but rather induces cell death indirectly by modulating signaling cascades, which leads to secondary (delayed) cell death. Thus, these findings suggest that miR-193b may induce directly or indirectly (secondary) cell death in neuroblastoma by several distinct mechanisms.

A number of studies have revealed that miR-193b triggers apoptosis in various cancer cells via downregulation of *MCL-1* [35, 39, 41, 42]. We demonstrated that miR-193b overexpression reduces *MCL-1* mRNA and protein expression in neuroblastoma cells. However, while *MCL-1* overexpression could partly rescue SK-N-BE(2) and SHSY-5Y cells from miR-193b-mediated apoptosis, it could not rescue CHLA-20 cells.

Previous studies established that neuroblastoma cells are primed to death through sequestration of BIM by either MCL-1 or BCL-2 [63, 64]. CHLA-20 is a well-defined BCL-2-primed cell line, whereas SK-N-SH (SHSY-5Y is a subclone of this cell line [65]) and SK-N-BE(2) cells are MCL-1-primed [63]. Goldsmith *et al.* demonstrated that BCL-2-primed cell lines are significantly less sensitive to MCL-1 inhibition by AT-101 (a BH3 mimetic that also binds to BCL-2 but less potently than to MCL-1) as compared to MCL-1-primed cell lines [64]. Concordantly we demonstrated that, while *MCL-1* knockdown by siRNA effectively induces PARP-1 cleavage in MCL-1-primed SHSY-5Y and SK-N-BE(2) cells, it does not trigger PARP-1 cleavage in the BCL-2-primed cell line CHLA-20. These findings support a selective dependence of neuroblastoma cells on either BCL-2 or MCL-1, and explain why *MCL-1* overexpression could rescue BE(2)-C and SHSY-5Y cells, but not rescue the BCL-2-primed neuroblastoma cell line CHLA-20 from miR-193b-induced apoptosis. The mechanisms through which miR-193b may induce apoptosis in BCL-2-primed cell lines remain to be determined.

To summarize, our date provide evidence that miR-193b is capable of inducing cell death by several, distinct mechanisms. Simultaneously targeting several signaling pathways activating cell death may increase the antitumor efficiency of miR-193b-based anticancer therapy and reduce acquired resistance to miR-193b-mediated cell death. Further studies are needed to fully understand the mechanisms by which miR-193b exerts its tumor suppressive function in neuroblastoma.

In summary, miR-193b overexpression induces a cell cycle arrest and apoptosis in neuroblastoma by reducing the expression of *MYCN*, *cyclin D1* and *MCL-1*, three important oncogenes in neuroblastoma whose inhibition by inhibitors have shown promising results in preclinical testing [59, 61, 66, 67]. Our data suggest that miR-193b may be a promising strategy to treat high-risk neuroblastoma resistant to conventional anticancer agents. This is especially supported by the finding that this miRNA has anti-tumor properties in all neuroblastoma cell lines tested. MiR-193b induced a cell cycle arrest and cell death independent on risk factors such as amplification of the *MYCN* oncogene or p53 functionality (Supplementary Table 2). Even cell lines from high-risk neuroblastoma such as BE(2)-C and SK-N-AS, which are highly resistant to most of the currently used neuroblastoma treatment strategies, are sensitive to the treatment with miR-193b. There are clearly certain limitations to our study. First of all, the analyses of mir-193b expression in neuroblastoma tumors were performed in a limited number of tumors. A larger cohort of tumors should be used to validate our finding. And secondly, all the functional analyses were performed in neuroblastoma cell line models. Although cell lines are useful and easily available for *in vitro* analyses, animal models are needed to explore the effect of miR-193b on neuroblastoma tumors *in vivo*.

MATERIAL AND METHODS

Tumor specimens

Previously published expression data by us from primary neuroblastoma tumor specimens representing the whole disease spectrum was reanalyzed for this study [18, 33]. In short, a panel of 69 tumor samples was analyzed by RT-qPCR, and 10 different tumor samples were analyzed

by RNA-Seq. The expression of miR-193b in comparison to tumor suppressor, or oncomiRs was analyzed and statistically evaluated. For technical details please refer to our previous publications.

Cell lines

CHLA-20 and CHLA-15 cells were grown in Iscove's modified Dulbecco's medium supplemented with 20% fetal bovine serum, 4 mM L-Glutamine and 1× ITS (5 µg/ml insulin, 5 µg/ml transferrin, 5 ng/ml selenous acid). The remaining cell lines were grown in RPMI-1640 supplemented with 10% fetal bovine serum and 2 mM L-Glutamine (final concentrations). An overview of the genetic abnormalities for cell lines used in this study is shown in Supplementary Table 2.

All cell lines were cultured at 37° C in a humidified incubator containing a 5% CO_2 atmosphere. The identity of all cell lines was authenticated by short tandem repeat analysis at the Center of Forensic Genetics, The Arctic University of Norway – UiT, Norway. Cells were tested and confirmed negative for mycoplasma contamination.

Transient transfections of miRNAs, plasmids and siRNA

All cell lines were transiently transfected immediately after seeding using Lipofectamine2000 (ThermoFisher Scientific) according to manufacturer's instructions.

To analyze the effect of miR-193b mimics on neuroblastoma cell lines, 25 nM of control mimics or miR-193b-3p mimics (GenePharma) were transfected into neuroblastoma cell lines.

For rescue experiments, cells were co-transfected with 500 or 1 µg of an overexpression plasmid (Table 1) and 40 nM control or miR-193b mimics.

Small inhibitory RNAs (siRNA; OnTargetPLUS SmartPool) directed against *MCL-1* (siMcl-1) and control siRNA were purchased from Dharmacon. SiRNA directed against *MYCN* (si*MYCN*, Hs_*MYCN*_6 FlexiTube siRNA) and negative control siRNA (AllStars Negative Control siRNA) were purchased from Qiagen. Cells were transfected with 20 nM (siMcl-1) or 2 nM (si*MYCN*) siRNA.

Cell viability assay

Cell viability was evaluated using alamarBlue (ThermoFisher Scientific) according to manufacturer's recommendation. Briefly, 1/10th volume of alamarBlue® reagent was directly added to cells in culture medium and cells were incubated at 37° C for three hours. One hundred microliter of supernatant were then collected from each well, transferred to a black-walled 96-well plate and fluorescence was monitored at 540 nm excitation wavelength and 590 nm emission wavelength in a microplate reader (CLARIOstar, BMG LABTECH). Cell viability was calculated as a percentage of control-transfected cells.

xCELLigence

Cells were seeded into a 16-well E-Plate (harboring a high-density gold electrode array to measure electrical impedance) and transfected with control or miR-193b mimics immediately after seeding as described previously. The culture medium was changed 72–96 h post-transfection. Cell proliferation was monitored continuously and recorded as a delta cell index (DCI) every 30 min for 168 hours by the xCELLigence Real-Time Cell Analyzer (RTCA)-DP system (ACEA Biosciences). The DCI was defined as the cell index (CI) at a given time point plus a Delta value. The Delta value is the difference between a reference value (=1) and the cell index at the Delta time point (CI_1 = CI one hour post-transfection): $DCI = CI + (1-CI_1)$.

Cytotoxicity assay

Cytotoxicity was analyzed using the MultiTox-Fluor Multiplex Cytotoxicity Assay (Promega) according to manufacturer`s recommendation. Briefly, one volume of the MultiTox-Fluor reagent was directly added to cells in culture and incubated at 37° C for 30 min. One hundred microliter of supernatant was then collected from each well, transferred to a white-walled 96-well plate and fluorescence was measured in a microplate reader (CLARIOstar, BMG LABTECH). Amounts of cells with intact (living) and disrupted cell membranes (dead) were measured at 400 nm and 485 nm excitation wavelength or 505 and 520 nm emission wavelength, respectively. Normalization involved two steps. First, the number of viable cells was normalized to the number of dead cells, and then the ratio of viable to dead cells of miR-193b-transfected cells was calculated relative to that of control-transfected cells for which the ratio was set to 100%. A decrease in the ratio of viable to dead cells indicates cytotoxicity. Apoptosis assay

Caspase-3/7 activity as an indicator of apoptosis was determined using the Caspase-Glo 3/7 assay (Promega) according to manufacturer`s recommendation. Briefly, one volume of the Caspase-Glo 3/7 reagent was directly added to cells in culture and incubated at room temperature for 90 minutes. One hundred microliter of supernatant were then collected from each well, transferred to a white-walled 96-well plate and luminescence was measured in a microplate reader (CLARIOstar, BMG LABTECH).

Cell cycle analysis

To monitor cell cycle profiles, cells were seeded into 25 cm^2 culture flasks and transfected immediately after seeding as described previously. 24 hours post-transfection, the medium was collected and the cells were

removed from plates using trypsin. Cells in suspension were then added to the collected medium, centrifuged at 200 g and washed twice with phosphate-buffered saline (PBS). The cells were fixed in ice-cold 70% ethanol. After incubation at 4° C overnight, the fixed cells were washed twice with PBS and resuspended in 50 µl PBS containing 100 µg/ml RNase. 200 µl PBS with 50 µg/ml propidium iodide (PI) was added to each sample, incubated in the dark at room temperature for 30 minutes and stored on ice until analyzed by flow cytometry (BD LSRFortessa™ cell analyzer, BD Bioscience). Cell-cycle data were analyzed with the FlowJo 7.6.5 software using the Watson model for cell-cycle evaluation.

Real-time (RT)-PCR

Total RNA was isolated using TRIzol (ThermoFisher Scientific) according to manufacturer's instructions. Purity and concentration of TRIzol-isolated RNA used for reverse transcription was estimated photometrically by calculating the ratio of absorbance at 260 nm to the absorbance at 280 nm, as well as the ratio of absorbance at 260 nm to that of 230 nm using a NanoDrop™ 1000 spectrophotometer (ThermoFisher Scientific).

Complementary DNA (cDNA) from miRNAs was synthesized from isolated total RNA using the miScript II RT Kit (Qiagen). In short, 1 µg of isolated total RNA was brought to a total volume of 12 µl with deionized water. 2 µl of miScript Reverse Transcriptase Mix and 2 µl of miScript Nucleics Mix diluted in 4 µl of 5 × miScript HiSpec buffer were added to each sample. The reverse transcription was performed at 37° C for 60 minutes followed by 95° C for 5 minutes to terminate the reaction. The resulting cDNA was diluted with deionized water to achieve a concentration of 1 ng/µl and stored at -20° C until used in the real-time polymerase chain (RT-PCR) reaction. The miScript SYBR® Green PCR Kit (Qiagen) was used for quantitative RT-PCR. The PCR was performed in a 10 µl reaction volume according to the following protocol: Each 10 µl reaction was composed of 1 µl of cDNA equivalent to 1 ng of cDNA, 2 µl of water, 5 µl of QuantiTect SYBR Green, 1 µl of 10 x Universal primers and 1 µl of 10 × specific miScript primers. The following miScript Primer Assays (Qiagen) were used: Hs_miR-193b_3 (MS00031549), Hs_miR-34a_1 (MS0003318), Hs_miR-92_1 (MS0006594) and Hs_RNU6-2_11 (MS00033740) that was used as an internal control for normalization.

cDNA from mRNAs was synthesized from 1 µg of total isolated RNA by Maxima Reverse Transcriptase (ThermoFisher Scientific) using oligo dT primer: 1 µg of isolated RNA and 1 µl of both oligo dT primer (20 µM) and dNTP (10 mM each) was brought to a total volume of 15.75 µl with deionized water. The mixture was incubated for 5 minutes at 65° C to break down secondary structures and subsequently incubated at 4° C until the reverse transcription mix was added. 0.25 µl Maxima Reverse Transcriptase diluted in 4 µl 5 × RT-Buffer was added to each sample. The reverse transcription was performed at 60° C for 30 minutes followed by 85° C for 5 minutes to terminate the reaction. The resulting cDNA was diluted in 80 µl deionized water to achieve a concentration of 10 ng/µl and stored at –20° C until used in the RT-PCR reaction. The RT-PCR was performed in a 10 µl reaction volume according to the following protocol: Each 10 µl reaction was composed of 1 µl cDNA equivalent to 10 ng cDNA, 3.2 µl water, 5 µl POWER SYBR (ThermoFisher Scientific) and 0.4 µl of 10 µM sense and antisense primer (Table 2).

Amplifications were carried out according to manufacturer's recommendations using the LightCycler 96 SW 1.1 (Roche). To confirm amplification specificity, a melt curve was generated after the completion of the amplification reaction. Expression levels of mRNAs were evaluated using the $2^{-\Delta\Delta CT}$ comparative cycle threshold method [68]. To determine differential expression of mRNAs between control and miR-193b-transfected cells, mRNA expression levels of miR-193b-transfected cells were calculated relative to mRNA expression levels of control-transfected cells whose mean mRNA expression was set to 1.

Western blot analysis

Cells were harvested by standard procedure. Briefly, the culture medium was collected and the cells were washed with PBS. To dissociate adhesive cells from the culture plates, trypsin was added. Cells in suspension were then added to the collected culture medium and centrifuged at 200 g for 5 minutes. After an additional washing step with PBS, cells were lysed in RIPA buffer (50 mM Tris-HCl pH 8, 150 mM NaCl, 1% NP-40, 0.5% sodium deoxycholate, 0.1% SDS) supplemented with 1× Protein Inhibitor Cocktail (Roche) and 1 mM dithiothreitol (DTT). Protein concentrations were determined using the DC™ protein assay kit (Bio-Rad) according to the manufacturer's recommendation. The total protein concentration was calculated based on a bovine serum albumin (BSA) standard curve using a microplate reader (CLARIOstar, BMG LABTECH).

20–40 µg of protein in NuPAGE® LDS Sample Buffer (ThermoFisher Scientific) was separated on NuPAGE® Novex 4–12% Bis-Tris precast polyacrylamide gels (ThermoFisher Scientific) and subsequently electroblotted onto Immobilon-FL PVDF (Millipore). PVDF membranes were blocked in Odyssey blocking buffer (LI-COR Biosciences) for 1 hour at room temperature, and incubated with primary antibodies overnight at 4° C. The membrane was treated with secondary antibodies goat anti-rabbit IRDye800CW (1:5000) (Rockland Immunochemicals) and goat anti-mouse Alexa Fluor 680 (1:5000) (ThermoFisher Scientific) for 1 hour at room temperature. Antibody binding was detected using the Odyssey CLx infrared

Table 2: Oligonucleotides used in this study

Name	Orientation	Sequence (5′ to 3′)
Site directed mutagenesis		
MYCN-3′UTR-193b-f	forward	ATGAGAGGTGGCTTTTGCGGGATCCA TTAGACTGGAAGTTCATAC
MYCN-3′UTR-193b-r	reverse	GTATGAACTTCCAGTCTAATGGATC CCGCAAAAGCCACCTCTCAT
RT-qPCR		
MCL-1-f	forward	GATGCAGCTTTCTTGGTTTATGG
MCL-1-r	reverse	GATGCAGCTTTCTTGGTTTATGG
CCND1-f	forward	CCGTCCATGCGGAAGATC
CCND1-r	reverse	ATGGCCAGCGGGAAGAC
MYCN-f	forward	ACACCCTGAGCGATTCAGAT
MYCN-r	reverse	TTCTCCACAGTGACCACGTC
SDHA-f	forward	CTGATGAGACAAGATGTGGTG
SDHA-r	reverse	CAATCTCCCTTCAATGTACTCC

Oligonucleotides were purchased from Sigma-Aldrich or Invitrogen.

Table 3: Primary antibodies used in this study

Antibody	Epitope	Origin	Dilution	Supplier
MCL-1 (S-19)	Human MCL-1	Rabbit, polyclonal	1:1000	Santa Cruz Biotechnology
Cyclin D1 (H-295)	Human Cyclin D1	Rabbit, polyclonal	1:200	Santa Cruz Biotechnology
PARP-1 (9542)	Human full length and cleaved PARP-1	Rabbit, polyclonal	1:1000	Cell Signalling Technology
N-Myc (B8.4.B)	Human N-Myc	Mouse, monoclonal	1:400	Santa Cruz Biotechnology
Actin (ab3280)	Human actin	Mouse, monoclonal	1:1000	Abcam

imaging system (Li-Cor). Primary antibody specifications are specified in Table 3.

Dual-luciferase reporter assay

The pMIR-Report *MYCN*-UTR vector containing the wildtype putative target site of *MYCN* 3′UTR has been previously generated by our group [69]. QuikChange Multi Site-directed Mutagenesis Kit (Agilent Technologies) was used to mutate the putative miR-193b seed sequence. The sequences of all constructs were confirmed by bidirectional sequencing. Primers used for cloning and site-directed mutagenesis are listed in Table 2.

Cells were co-transfected with 20 ng pGL4.75 [hRluc/CMV] (Promega), 40 nM of either control mimics or miR-193b mimics, and 100 ng of either wild-type *MYCN*-3-UTR construct (pMIR-Report-*MYCN*-UTR-WT) or the mutant variant (pMIR-Report-*MYCN*-UTR-MUT) using Lipofectamine2000. At 24 hours post-transfection, renilla and firefly luciferase activities were analyzed using the Dual-Luciferase Reporter Assay (Promega) according to the manufacturer's instructions. Normalization included two steps: first, the firefly luciferase activity was normalized to the renilla luciferase activity, and second, the luciferase activities of miR-193b-transfected cells were calculated relative to control-transfected cells that were set to one.

Statistical analysis

Statistical analyses were carried out using R (http://www.r-project.org). Statistical differences between means were determined using the parametrical Student`s *t*-test, or where not-applicable, the non-parametric Man-Whitney-*U* test.

ACKNOWLEDGMENTS

The pcDNA3.1-Mcl-1 was kindly provided by Anthony Faber and collegues and the pCMV-Cyclin D1 plasmid by Yue Xiong (Addgene plasmid # 19927).

Steffen Fuchs is participant in the BIH Charité Clinician Scientist Program funded by the Charité – Universitätsmedizin Berlin and the Berlin Institute of Health.

CONFLICTS OF INTEREST

The authors declare that they have no competing interests.

FUNDING

This work was supported by grants from the Northern-Norwegian Health Authorities and the Norwegian Cancer Society.

REFERENCES

1. Park JR, Eggert A, Caron H. Neuroblastoma: biology, prognosis, and treatment. Hematology/oncology clinics of North America. 2010; 24:65–86.
2. Maris JM. Recent advances in neuroblastoma. The New England journal of medicine. 2010; 362:2202–2211.
3. Owens C, Irwin M. Neuroblastoma: the impact of biology and cooperation leading to personalized treatments. Critical reviews in clinical laboratory sciences. 2012; 49:85–115.
4. Fletcher JI, Haber M, Henderson MJ, Norris MD. . Targeting Multidrug Resistance in Neuroblastoma. In: M.A. H, ed. Neuroblastoma: Springer Netherlands). 115–123.
5. Garaventa A, Parodi S, De Bernardi B, Dau D, Manzitti C, Conte M, Casale F, Viscardi E, Bianchi M, D'Angelo P, Zanazzo GA, Luksch R, Favre C, et al. Outcome of children with neuroblastoma after progression or relapse. A retrospective study of the Italian neuroblastoma registry. European journal of cancer (Oxford, England : 1990). 2009; 45:2835–2842.
6. Wilczynska A, Bushell M. The complexity of miRNA-mediated repression. Cell death and differentiation. 2015; 22:22–33.
7. Cho WC. MicroRNAs as therapeutic targets and their potential applications in cancer therapy. Expert opinion on therapeutic targets. 2012; 16:747–759.
8. Kong YW, Ferland-McCollough D, Jackson TJ, Bushell M. microRNAs in cancer management. The lancet oncology. 2012; 13:e249-258.
9. Lin S, Gregory RI. MicroRNA biogenesis pathways in cancer. Nature reviews Cancer. 2015; 15:321–333.
10. Fu X, Han Y, Wu Y, Zhu X, Lu X, Mao F, Wang X, He X, Zhao Y, Zhao Y. Prognostic role of microRNA-21 in various carcinomas: a systematic review and meta-analysis. European journal of clinical investigation. 2011; 41:1245–1253.
11. Ferracin M, Negrini M. Micromarkers 2.0: an update on the role of microRNAs in cancer diagnosis and prognosis. Expert review of molecular diagnostics. 2015; 15:1369–1381.
12. Iorio MV, Croce CM. MicroRNA dysregulation in cancer: diagnostics, monitoring and therapeutics. A comprehensive review. EMBO molecular medicine. 2012; 4:143–159.
13. Thorsen SB, Obad S, Jensen NF, Stenvang J, Kauppinen S. The therapeutic potential of microRNAs in cancer. Cancer journal (Sudbury, Mass). 2012; 18:275–284.
14. Mei H, Lin ZY, Tong QS. The roles of microRNAs in neuroblastoma. World journal of pediatrics : WJP. 2014; 10:10–16.
15. Zhi F, Wang R, Wang Q, Xue L, Deng D, Wang S, Yang Y. MicroRNAs in neuroblastoma: small-sized players with a large impact. Neurochemical research. 2014; 39:613–623.
16. Gattolliat CH, Thomas L, Ciafre SA, Meurice G, Le Teuff G, Job B, Richon C, Combaret V, Dessen P, Valteau-Couanet D, May E, Busson P, Douc-Rasy S, et al. Expression of miR-487b and miR-410 encoded by 14q32.31 locus is a prognostic marker in neuroblastoma. British journal of cancer. 2011; 105:1352–1361.
17. De Preter K, Mestdagh P, Vermeulen J, Zeka F, Naranjo A, Bray I, Castel V, Chen C, Drozynska E, Eggert A, Hogarty MD, Izycka-Swieszewska E, London WB, et al. miRNA expression profiling enables risk stratification in archived and fresh neuroblastoma tumor samples. Clinical cancer research : an official journal of the American Association for Cancer Research. 2011; 17:7684–7692.
18. Schulte JH, Marschall T, Martin M, Rosenstiel P, Mestdagh P, Schlierf S, Thor T, Vandesompele J, Eggert A, Schreiber S, Rahmann S, Schramm A. Deep sequencing reveals differential expression of microRNAs in favorable versus unfavorable neuroblastoma. Nucleic acids research. 2010; 38:5919–5928.
19. Mestdagh P, Fredlund E, Pattyn F, Schulte JH, Muth D, Vermeulen J, Kumps C, Schlierf S, De Preter K, Van Roy N, Noguera R, Laureys G, Schramm A, et al. MYCN/c-MYC-induced microRNAs repress coding gene networks associated with poor outcome in MYCN/c-MYC-activated tumors. Oncogene. 2010; 29:1394–1404.
20. Bray I, Bryan K, Prenter S, Buckley PG, Foley NH, Murphy DM, Alcock L, Mestdagh P, Vandesompele J, Speleman F, London WB, McGrady PW, Higgins DG, et al. Widespread dysregulation of MiRNAs by MYCN amplification and chromosomal imbalances in neuroblastoma: association of miRNA expression with survival. PloS one. 2009; 4:e7850.
21. Roth SA, Knutsen E, Fiskaa T, Utnes P, Bhavsar S, Hald OH, Lokke C, Mestdagh P, Johansen SD, Flaegstad T, Einvik C. Next generation sequencing of microRNAs from isogenic neuroblastoma cell lines isolated before and after treatment. Cancer letters. 2016; 372:128–136.
22. Buechner J, Einvik C. N-myc and noncoding RNAs in neuroblastoma. Molecular cancer research. 2012; 10:1243–1253.

23. Schulte JH, Horn S, Schlierf S, Schramm A, Heukamp LC, Christiansen H, Buettner R, Berwanger B, Eggert A. MicroRNAs in the pathogenesis of neuroblastoma. Cancer letters. 2009; 274:10–15.

24. Welch C, Chen Y, Stallings RL. MicroRNA-34a functions as a potential tumor suppressor by inducing apoptosis in neuroblastoma cells. Oncogene. 2007; 26:5017–5022.

25. Tivnan A, Tracey L, Buckley PG, Alcock LC, Davidoff AM, Stallings RL. MicroRNA-34a is a potent tumor suppressor molecule *in vivo* in neuroblastoma. BMC cancer. 2011; 11:33.

26. Tivnan A, Orr WS, Gubala V, Nooney R, Williams DE, McDonagh C, Prenter S, Harvey H, Domingo-Fernandez R, Bray IM, Piskareva O, Ng CY, Lode HN, et al. Inhibition of neuroblastoma tumor growth by targeted delivery of microRNA-34a using anti-disialoganglioside GD2 coated nanoparticles. PLoS One. 2012; 7:e38129.

27. Cole KA, Attiyeh EF, Mosse YP, Laquaglia MJ, Diskin SJ, Brodeur GM, Maris JM. A functional screen identifies miR-34a as a candidate neuroblastoma tumor suppressor gene. Molecular cancer research : MCR. 2008; 6:735–742.

28. Chen Y, Tsai YH, Tseng SH. Inhibition of cyclin-dependent kinase 1-induced cell death in neuroblastoma cells through the microRNA-34a-MYCN-survivin pathway. Surgery. 2013; 153:4–16.

29. Agostini M, Tucci P, Killick R, Candi E, Sayan BS, Rivetti di Val Cervo P, Nicotera P, McKeon F, Knight RA, Mak TW, Melino G. Neuronal differentiation by TAp73 is mediated by microRNA-34a regulation of synaptic protein targets. Proceedings of the National Academy of Sciences of the United States of America. 2011; 108:21093–21098.

30. Xiang X, Mei H, Qu H, Zhao X, Li D, Song H, Jiao W, Pu J, Huang K, Zheng L, Tong Q. miRNA-584-5p exerts tumor suppressive functions in human neuroblastoma through repressing transcription of matrix metalloproteinase 14. Biochimica et biophysica acta. 2015; 1852:1743–1754.

31. Xiang X, Mei H, Zhao X, Pu J, Li D, Qu H, Jiao W, Zhao J, Huang K, Zheng L, Tong Q. miRNA-337-3p suppresses neuroblastoma progression by repressing the transcription of matrix metalloproteinase 14. Oncotarget. 2015.

32. Althoff K, Lindner S, Odersky A, Mestdagh P, Beckers A, Karczewski S, Molenaar JJ, Bohrer A, Knauer S, Speleman F, Epple M, Kozlova D, Yoon S, et al. miR-542-3p exerts tumor suppressive functions in neuroblastoma by downregulating Survivin. International journal of cancer Journal international du cancer. 2015; 136:1308–1320.

33. Schulte JH, Schowe B, Mestdagh P, Kaderali L, Kalaghatgi P, Schlierf S, Vermeulen J, Brockmeyer B, Pajtler K, Thor T, de Preter K, Speleman F, Morik K, et al. Accurate prediction of neuroblastoma outcome based on miRNA expression profiles. International journal of cancer Journal international du cancer. 2010; 127:2374–2385.

34. Xu C, Liu S, Fu H, Li S, Tie Y, Zhu J, Xing R, Jin Y, Sun Z, Zheng X. MicroRNA-193b regulates proliferation, migration and invasion in human hepatocellular carcinoma cells. European journal of cancer (Oxford, England : 1990). 2010; 46:2828–2836.

35. Mao K, Zhang J, He C, Xu K, Liu J, Sun J, Wu G, Tan C, Zeng Y, Wang J, Xiao Z. Restoration of miR-193b sensitizes Hepatitis B virus-associated hepatocellular carcinoma to sorafenib. Cancer letters. 2014; 352:245–252.

36. Long J, Ji Z, Jiang K, Wang Z, Meng G. miR-193b Modulates Resistance to Doxorubicin in Human Breast Cancer Cells by Downregulating MCL-1. BioMed research international. 2015; 2015:373574.

37. Hu H, Li S, Liu J, Ni B. MicroRNA-193b modulates proliferation, migration, and invasion of non-small cell lung cancer cells. Acta biochimica et biophysica Sinica. 2012; 44:424–430.

38. Chen J, Feilotter HE, Pare GC, Zhang X, Pemberton JG, Garady C, Lai D, Yang X, Tron VA. MicroRNA-193b represses cell proliferation and regulates cyclin D1 in melanoma. The American journal of pathology. 2010; 176:2520–2529.

39. Chen J, Zhang X, Lentz C, Abi-Daoud M, Pare GC, Yang X, Feilotter HE, Tron VA. miR-193b Regulates Mcl-1 in Melanoma. The American journal of pathology. 2011; 179:2162–2168.

40. Kaukoniemi KM, Rauhala HE, Scaravilli M, Latonen L, Annala M, Vessella RL, Nykter M, Tammela TL, Visakorpi T. Epigenetically altered miR-193b targets cyclin D1 in prostate cancer. Cancer medicine. 2015; 4:1417–1425.

41. Braconi C, Valeri N, Gasparini P, Huang N, Taccioli C, Nuovo G, Suzuki T, Croce CM, Patel T. Hepatitis C virus proteins modulate microRNA expression and chemosensitivity in malignant hepatocytes. Clinical cancer research. 2010; 16:957–966.

42. Yin W, Nie Y, Zhang Z, Xie L, He X. miR-193b acts as a cisplatin sensitizer via the caspase-3-dependent pathway in HCC chemotherapy. Oncol Rep. 2015; 34:368–374.

43. Agarwal V, Bell GW, Nam JW, Bartel DP. Predicting effective microRNA target sites in mammalian mRNAs. eLife. 2015; 4.

44. Henriksen JR, Haug BH, Buechner J, Tomte E, Lokke C, Flaegstad T, Einvik C. Conditional expression of retrovirally delivered anti-MYCN shRNA as an *in vitro* model system to study neuronal differentiation in MYCN-amplified neuroblastoma. BMC developmental biology. 2011; 11:1.

45. Bell E, Premkumar R, Carr J, Lu X, Lovat PE, Kees UR, Lunec J, Tweddle DA. The role of MYCN in the failure of MYCN amplified neuroblastoma cell lines to G1 arrest after DNA damage. Cell cycle (Georgetown, Tex). 2006; 5:2639–2647.

46. Bader AG. miR-34 - a microRNA replacement therapy is headed to the clinic. Frontiers in genetics. 2012; 3:120.

47. Kasinski AL, Kelnar K, Stahlhut C, Orellana E, Zhao J, Shimer E, Dysart S, Chen X, Bader AG, Slack FJ. A combinatorial microRNA therapeutics approach to suppressing non-small cell lung cancer. Oncogene. 2015; 34:3547–3555.

48. Zhang B, Pan X, Cobb GP, Anderson TA. microRNAs as oncogenes and tumor suppressors. Dev Biol. 2007; 302:1–12.

49. Li H, Xu Y, Qiu W, Zhao D, Zhang Y. Tissue miR-193b as a Novel Biomarker for Patients with Ovarian Cancer. Medical science monitor : international medical journal of experimental and clinical research. 2015; 21:3929–3934.

50. El-Gewely MR, Andreassen M, Walquist M, Ursvik A, Knutsen E, Nystad M, Coucheron DH, Myrmel KS, Hennig R, Johansen SD. Differentially Expressed MicroRNAs in Meningiomas Grades I and II Suggest Shared Biomarkers with Malignant Tumors. Cancers. 2016; 8.

51. Wu W, Lin Z, Zhuang Z, Liang X. Expression profile of mammalian microRNAs in endometrioid adenocarcinoma. European journal of cancer prevention. 2009; 18:50–55.

52. Jin X, Sun Y, Yang H, Li J, Yu S, Chang X, Lu Z, Chen J. Deregulation of the MiR-193b-KRAS Axis Contributes to Impaired Cell Growth in Pancreatic Cancer. PLoS One. 2015; 10:e0125515.

53. Wang L, Zhang Y, Zhao L, Liu S, Yu S, Ma Y, Sun G. MicroRNA-193b inhibits the proliferation, migration and invasion of gastric cancer cells via targeting cyclin D1. Acta histochemica. 2016.

54. Mu YP, Tang S, Sun WJ, Gao WM, Wang M, Su XL. Association of miR-193b down-regulation and miR-196a up-regulation with clinicopathological features and prognosis in gastric cancer. Asian Pacific journal of cancer prevention. 2014; 15:8893–8900.

55. Zhong Q, Wang T, Lu P, Zhang R, Zou J, Yuan S. miR-193b promotes cell proliferation by targeting Smad3 in human glioma. Journal of neuroscience research. 2014; 92:619–626.

56. Unno K, Zhou Y, Zimmerman T, Platanias LC, Wickrema A. Identification of a novel microRNA cluster miR-193b-365 in multiple myeloma. Leukemia & lymphoma. 2009; 50:1865–1871.

57. Lenarduzzi M, Hui AB, Alajez NM, Shi W, Williams J, Yue S, O'Sullivan B, Liu FF. MicroRNA-193b enhances tumor progression via down regulation of neurofibromin 1. PloS one. 2013; 8:e53765.

58. Beckers A, Van Peer G, Carter DR, Mets E, Althoff K, Cheung BB, Schulte JH, Mestdagh P, Vandesompele J, Marshall GM, De Preter K, Speleman F. MYCN-targeting miRNAs are predominantly downregulated during MYCNdriven neuroblastoma tumor formation. Oncotarget. 2015; 6:5204–5216.

59. Rihani A, Vandesompele J, Speleman F, Van Maerken T. Inhibition of CDK4/6 as a novel therapeutic option for neuroblastoma. Cancer cell international. 2015; 15:76.

60. Molenaar JJ, Ebus ME, Koster J, van Sluis P, van Noesel CJ, Versteeg R, Caron HN. Cyclin D1 and CDK4 activity contribute to the undifferentiated phenotype in neuroblastoma. Cancer research. 2008; 68:2599–2609.

61. Rader J, Russell MR, Hart LS, Nakazawa MS, Belcastro LT, Martinez D, Li Y, Carpenter EL, Attiyeh EF, Diskin SJ, Kim S, Parasuraman S, Caponigro G, et al. Dual CDK4/CDK6 inhibition induces cell-cycle arrest and senescence in neuroblastoma. Clinical cancer research : an official journal of the American Association for Cancer Research. 2013; 19:6173–6182.

62. Ranjan A, Iwakuma T. Non-Canonical Cell Death Induced by p53. International journal of molecular sciences. 2016; 17.

63. Goldsmith KC, Gross M, Peirce S, Luyindula D, Liu X, Vu A, Sliozberg M, Guo R, Zhao H, Reynolds CP, Hogarty MD. Mitochondrial Bcl-2 family dynamics define therapy response and resistance in neuroblastoma. Cancer research. 2012; 72:2565–2577.

64. Goldsmith KC, Lestini BJ, Gross M, Ip L, Bhumbla A, Zhang X, Zhao H, Liu X, Hogarty MD. BH3 response profiles from neuroblastoma mitochondria predict activity of small molecule Bcl-2 family antagonists. Cell death and differentiation. 2010; 17:872–882.

65. Biedler JL, Helson L, Spengler BA. Morphology and growth, tumorigenicity, and cytogenetics of human neuroblastoma cells in continuous culture. Cancer research. 1973; 33:2643–2652.

66. Barone G, Anderson J, Pearson AD, Petrie K, Chesler L. New strategies in neuroblastoma: Therapeutic targeting of MYCN and ALK. Clinical cancer research. 2013; 19:5814–5821.

67. Tanos R, Karmali D, Nalluri S, Goldsmith KC. Select Bcl-2 antagonism restores chemotherapy sensitivity in high-risk neuroblastoma. BMC cancer. 2016; 16:97.

68. Livak KJ, Schmittgen TD. Analysis of relative gene expression data using real-time quantitative PCR and the 2(-Delta Delta C(T)) Method. Methods (San Diego, Calif). 2001; 25:402–408.

69. Buechner J, Tomte E, Haug BH, Henriksen JR, Lokke C, Flaegstad T, Einvik C. Tumour-suppressor microRNAs let-7 and mir-101 target the proto-oncogene MYCN and inhibit cell proliferation in MYCN-amplified neuroblastoma. British journal of cancer. 2011; 105:296–303.

70. Ham J, Costa C, Sano R, Lochmann TL, Sennott EM, Patel NU, Dastur A, Gomez-Caraballo M, Krytska K, Hata AN, Floros KV, Hughes MT, Jakubik CT, et al. Exploitation of the Apoptosis-Primed State of MYCN-Amplified Neuroblastoma to Develop a Potent and Specific Targeted Therapy Combination. Cancer cell. 2016; 29:159–172.

71. Watanabe H, Pan ZQ, Schreiber-Agus N, DePinho RA, Hurwitz J, Xiong Y. Suppression of cell transformation by the cyclin-dependent kinase inhibitor p57KIP2 requires binding to proliferating cell nuclear antigen. Proceedings of the National Academy of Sciences of the United States of America. 1998; 95:1392–1397.

MicroRNA-193b-3p represses neuroblastoma cell growth via downregulation of *Cyclin D1*, *MCL-1* and *MYCN*

SUPPLEMENTARY MATERIALS

Supplementary Table 1: Low expression of miR-193b in neuroblastoma cell lines. Total RNA was isolated from cell lines, enriched for small RNAs and small RNA sequencing was performed according to Roth *et al*. 2016. See Supplementary_Table_1

Supplementary Table 2: Genetic characteristics of neuroblastoma cell lines used in this study

Cell line	Stage	Origin	Treatment	MYCN-amplified	p53	1p del	11q del	17q gain	References
BE(2)-C	4	Bone marrow (primary: unknown)	YES	YES	MUT	YES	NO	NO	[1, 2]
Kelly	4	Bone marrow	YES	YES	MUT	YES	YES	YES	[3, 4]
SHSY-5Y*	?	Bone marrow (primary: thorax)	YES	NO	WT	NO	NO	YES	[1, 5, 6]
CHLA-20	4	Primary, progressive	YES	NO	WT	?	?	?	[7, 8]
NBL-W	4S	Adrenal (primary)	NO	YES	WT	YES	?	NO	[1, 9]
CHLA-15	4	Primary	NO	NO	WT	?	?	?	[7, 10]
NBL-S	3	Adrenal (primary)	NO	NO	WT	NO	?	NO	[1, 11]
SK-N-AS	4	Bone marrow (primary: adrenal)	YES	NO	MUT	YES	YES	NO	[1, 12, 13]
SMS-KAN	4	Pelvis (primary)	NO	YES	WT	YES	YES	YES?	[1, 14, 15]

*parental cell line: SK-N-SH

1. Thiele CJ. Neuroblastoma Cell Lines, in Neuroblastoma, J.H.C. Culture. 1998: Lancaster. UK. 21–53.
2. Tweddle DA, Malcolm AJ, Bown N, Pearson AD, Lunec J. Evidence for the development of p53 mutations after cytotoxic therapy in a neuroblastoma cell line. Cancer Res. 2001; 61:8–13.
3. Gogolin S, Ehemann V, Becker G, Brueckner LM, Dreidax D, Bannert S, Nolte I, Savelyeva L, Bell E, Westermann F. CDK4 inhibition restores G(1)-S arrest in MYCN-amplified neuroblastoma cells in the context of doxorubicin-induced DNA damage. Cell Cycle. 2013; 12:1091–104.
4. Piskareva O, Harvey H, Nolan J, Conlon R, Alcock L, Buckley P, Dowling P, Henry M, O'Sullivan F, Bray I, Stallings RL. The development of cisplatin resistance in neuroblastoma is accompanied by epithelial to mesenchymal transition *in vitro*. Cancer Lett. 2015; 364:142–55.
5. Djos A, Fransson S, Kogner P, Martinsson T. Aneuploidy in neuroblastoma tumors is not associated with inactivating point mutations in the STAG2 gene. BMC Med Genet. 2013; 14:102.
6. Tweddle DA, Malcolm AJ, Cole M, Pearson AD, Lunec J. p53 cellular localization and function in neuroblastoma: evidence for defective G(1) arrest despite WAF1 induction in MYCN-amplified cells. Am J Pathol. 2001; 158:2067–77.
7. Keshelava N, Seeger RC, Groshen S, Reynolds CP, Drug resistance patterns of human neuroblastoma cell lines derived from patients at different phases of therapy. Cancer Res. 1998; 58:5396–405.
8. Goto H, Yang B, Petersen D, Pepper KA, Alfaro PA, Kohn DB, Reynolds CP. Transduction of green fluorescent protein increased oxidative stress and enhanced sensitivity to cytotoxic drugs in neuroblastoma cell lines. Mol Cancer Ther. 2003; 2:911–7.
9. Carr-Wilkinson J, Griffiths R, Elston R, Gamble LD, Goranov B, Redfern CP, Lunec J, Tweddle DA. Outcome of the p53-mediated DNA damage response in neuroblastoma is determined by morphological subtype and MYCN expression. Cell Cycle. 2011; 10:3778–87.
10. Keshelava N, Davicioni E, Wan Z, Ji L, Ji L, Sposto R, Triche TJ, Reynolds CP. Histone deacetylase 1 gene expression and sensitization of multidrug-resistant neuroblastoma cell lines to cytotoxic agents by depsipeptide. J Natl Cancer Inst. 2007; 99:1107–19.
11. Cohn SL, Salwen H, Quasney MW, Ikegaki N, Cowan JM, Herst CV, Kennett RH, Rosen ST, DiGiuseppe JA, Brodeur GM. Prolonged N-myc protein half-life in a neuroblastoma cell line lacking N-myc amplification. Oncogene. 1990; 5:1821–7.
12. Caren H, Kryh H, Nethander M, Sjoberg RM, Träger C, Nilsson S, Abrahamsson J, Kogner P, Martinsson T. High-risk neuroblastoma tumors with 11q-deletion display a poor prognostic, chromosome instability phenotype with later onset. Proc Natl Acad Sci U S A. 2010; 107:4323–8.
13. Goldschneider D, Horvilleur E, Plassa LF, Guillaud-Bataille M, Million K, Wittmer-Dupret E, Danglot G, de Thé H, Bénard J, May E, Douc-Rasy S. Expression of C-terminal deleted p53 isoforms in neuroblastoma. Nucleic Acids Res. 2006; 34:5603–12.

14. Van Maerken T, Rihani A, Dreidax D, De Clercq S, Yigit N, Marine JC, Westermann F, De Paepe A, Vandesompele J, Speleman F. Functional analysis of the p53 pathway in neuroblastoma cells using the small-molecule MDM2 antagonist nutlin-3. Mol Cancer Ther. 2011; 10:983–93.
15. Michels E, Hoebeeck J, De Preter K, Schramm A, Brichard B, De Paepe A, Eggert A, Laureys G, Vandesompele J, Speleman F. CADM1 is a strong neuroblastoma candidate gene that maps within a 3.72 Mb critical region of loss on 11q23. BMC Cancer. 2008; 8:173.

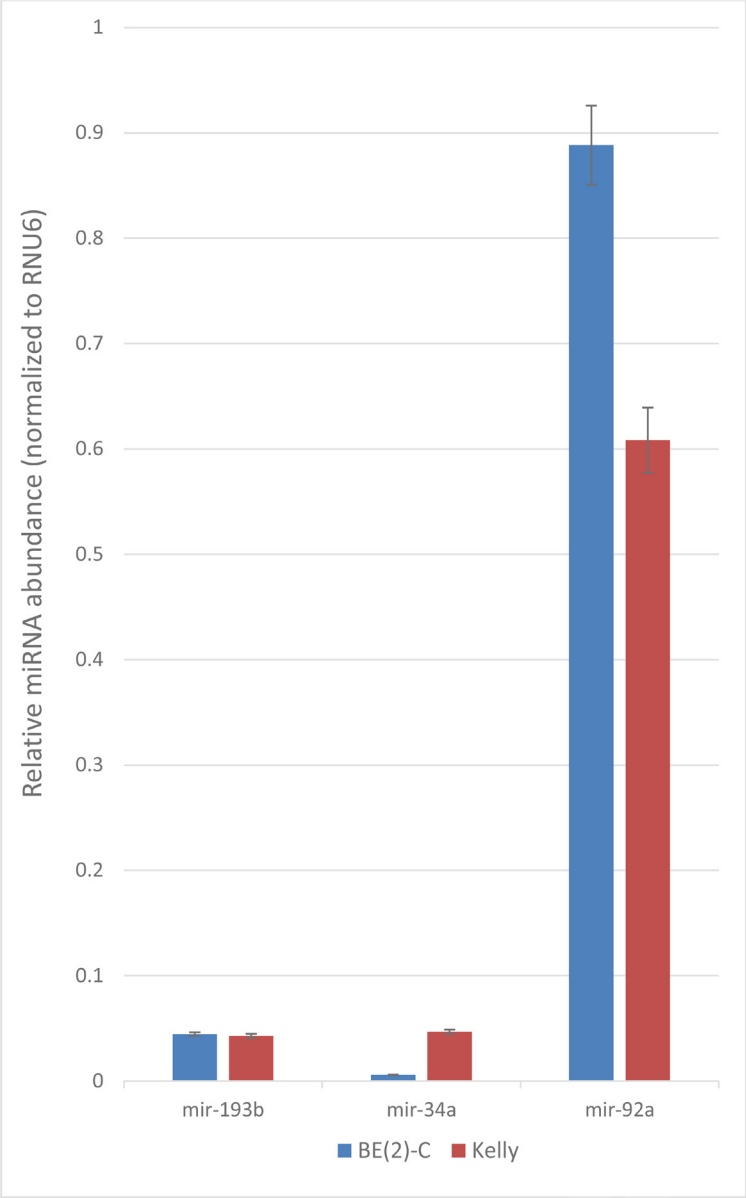

Supplementary Figure 1: Relative expression of selected miRNAs (mir-193b, mir-34a and mir-92a) in BE(2)-C and Kelly cells. RT-qPCR was performed on RNA isolated from BE(2)-C and Kelly according to description in Materials and Methods section. Raw fluorecence values (non-baseline corrected) were used to calculate mean PCR efficiencies in the LinRegPCR software [1]. PCR efficiency corrected Cq values were used to calculate the relative miRNA abundance according to 2^-Cq(MiR)/2^-Cq(RNU6). qPCR reactions were performed in triplicates on 3 independent biological replicates. Standard deviations were calculated taking into account the principle of error propagation (including technical and biological replicated and standard deviations from PCR efficiency determinations).

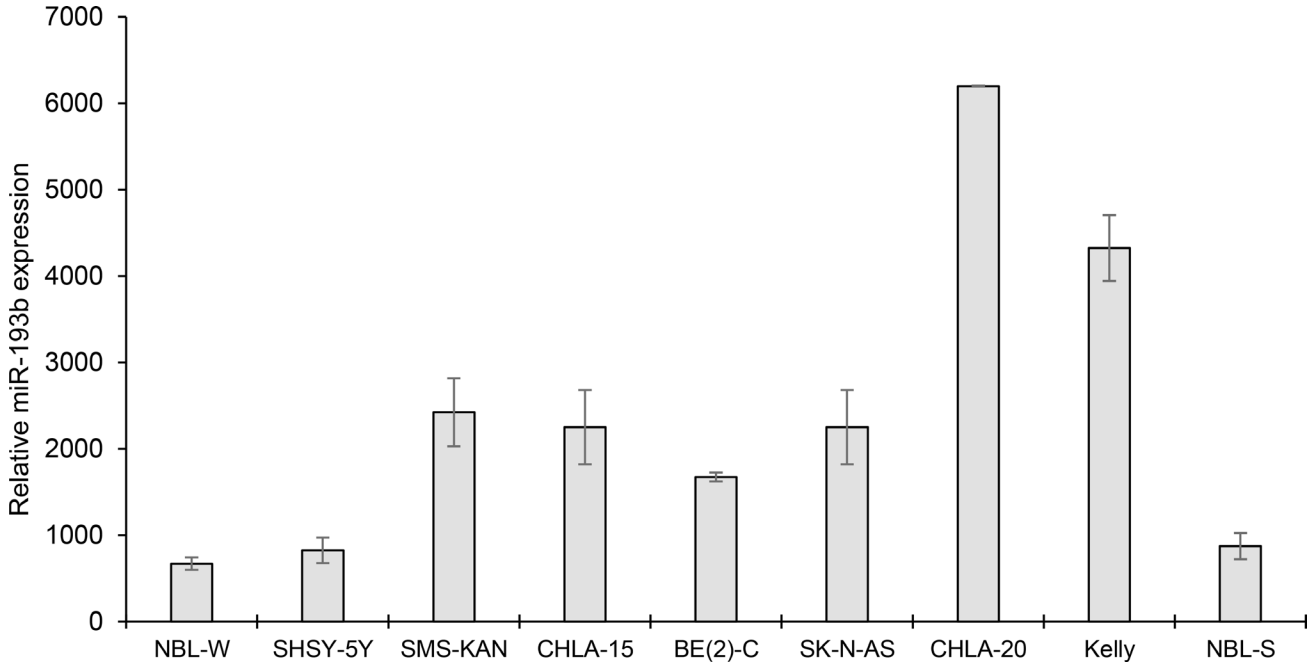

Supplementary Figure 2: MicroRNA-193b expression in neuroblastoma cell lines transfected with control or miR-193b mimics. 24 hours post-transfection, the total RNA was isolated, reverse transcribed into cDNA and the expression of miR-193b was analyzed by qRT-PCR. The expression levels of mature miR-193b were evaluated using the ΔΔCT comparative cycle threshold method. MiRNA expression levels of miR-193b mimic-transfected cells were calculated relative to miRNA expression levels of cells transfected with control mimics whose mean miRNA concentrations were set to 1. RNU6 was used as housekeeping genes. The experiment was performed at least two times giving similar results, and the result from one representative experiment is shown. Results are given as mean ± STDV from three independent samples and triplicate qPCR reactions.

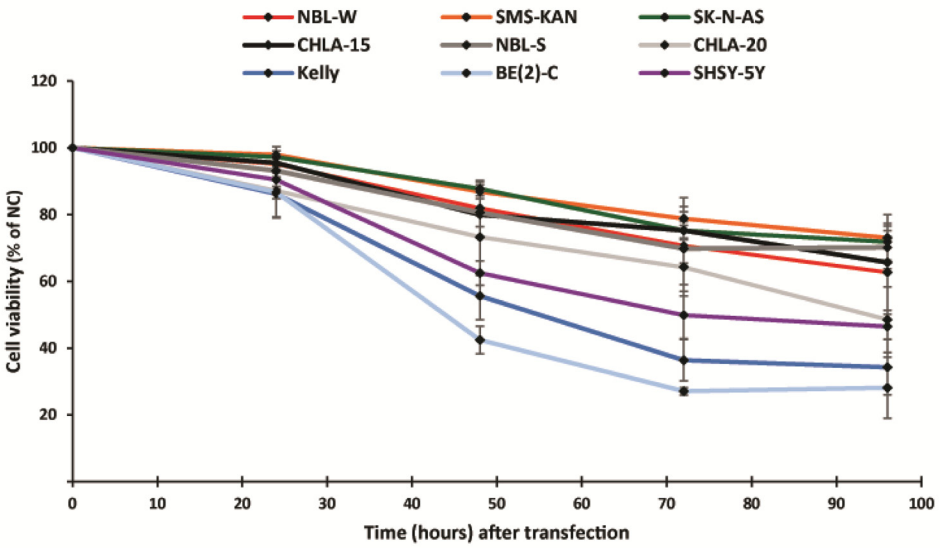

Supplementary Figure 3: miR-193b reduces cell viability in neuroblastoma cell lines. Data from Figure 2 including standard deviations.

```
Human              UAAUGAGAGGUGGCUUUUGCGGCCAGUAUUAGACUGG-AAGUUCAUACCUAAGUACUGUAAUAA
Chimp              UAAUGAGAGGUGGCUUUUGCGGCCAGUAUUAGACUGG-AAGUUCAUACCUAAGUACUGUAAUAA
Gorilla            UAAUGAGAGGUGGCUUUUGCGGCCAGUAUUAGACUGG-AAGUUCAUACCUAAGUACUGUAAUAA
Orangutan          UAAUGAGAGGUGGCUUUUGUGGCCAGUAUUAGACUGG-AAGUUCAUACCUAAGUACUGUAAUAA
Gibbon             UAAUGAGAGGUGGCUUUUGCGGCCAGUAUUAGACUGG-AAGUUCAUACCUAAGUACUGUAAUAA
Rhesus             UAAUGAGAGGUGGCUUUUGCGGCCAGUAUUAGACUGG-AAGUUCAUACCUAAGUACUGUAAUAA
Macaqee            UAAUGAGAGGUGGCUUUUGCGGCCAGUAUUAGACUGG-AAGUUCAUACCUAAGUACUGUAAUAA
Baboon             UAAUGAGAGGUGGCUUUUGCGGCCAGUAUUAGACUGG-AAGUUCAUACCUAAGUACUGUAAUAA
Green monkey       UAAUGAGAGGUGGCUUUUGCGGCCAGUAUUAGACUGG-AAGUUCAUACCUAAGUACUGUAAUAA
Marmoset           UAAUGAGAGGUGGCUUUUGCGGCCAGUAUUAGACUGG-AAGUUCAUACCUAAGUACUGUAAUAA
Squirrel monkey    UAAUGAGAGGUGGCUUUUGCGGCCAGUAUUAGACUGG-AAGUUCAUACCUAAGUACUGUAAUAA
Mouse              UAAUGAGAGGUGGCUCUUGCGGCCAGUAUUAGACUGG-AAGUUCACACCUAAGUACUGUAAGAA
Rat                UAAUGAGAGGUGGCUCUCG-GGCCAGUAUUAGACUGG-AAGUUCACACCUAAGUACUGUAAGAA
Rabbit             UAAUGCGCGGUGGCUUUCGCGGCCAGUGGUAGGCUGGCCCGUUCACACCUGAGUACUGUAAUAA
```

Supplementary Figure 4: The miR-193b binding site in the 3′-UTR of MYCN (highlighted in yellow) is highly conserved.

A

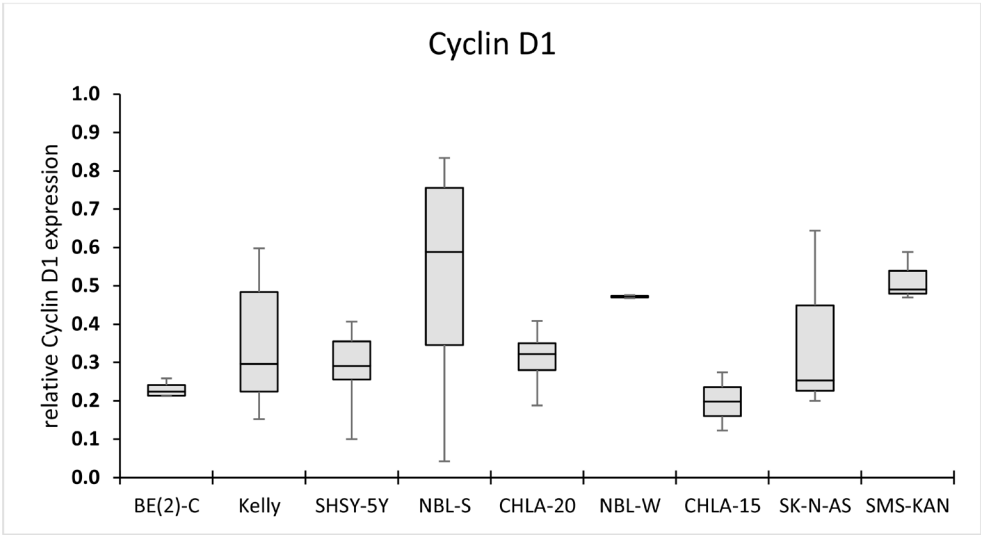
Cyclin D1
relative Cyclin D1 expression
1.0
0.9
0.8
0.7
0.6
0.5
0.4
0.3
0.2
0.1
0.0
BE(2)-C
Kelly
SHSY-5Y
NBL-S
CHLA-20
NBL-W
CHLA-15
SK-N-AS
SMS-KAN

B

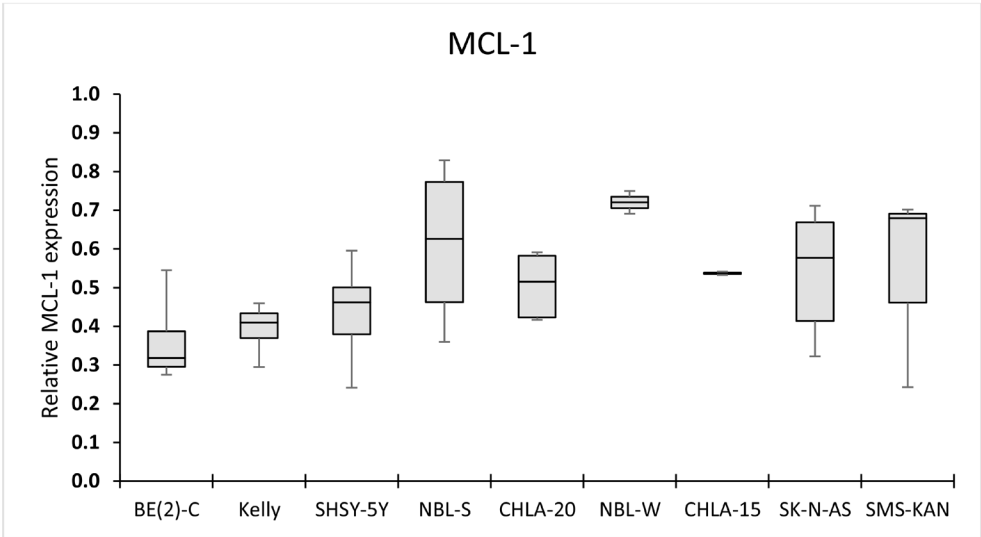
MCL-1
Relative MCL-1 expression
1.0
0.9
0.8
0.7
0.6
0.5
0.4
0.3
0.2
0.1
0.0
BE(2)-C
Kelly
SHSY-5Y
NBL-S
CHLA-20
NBL-W
CHLA-15
SK-N-AS
SMS-KAN

C

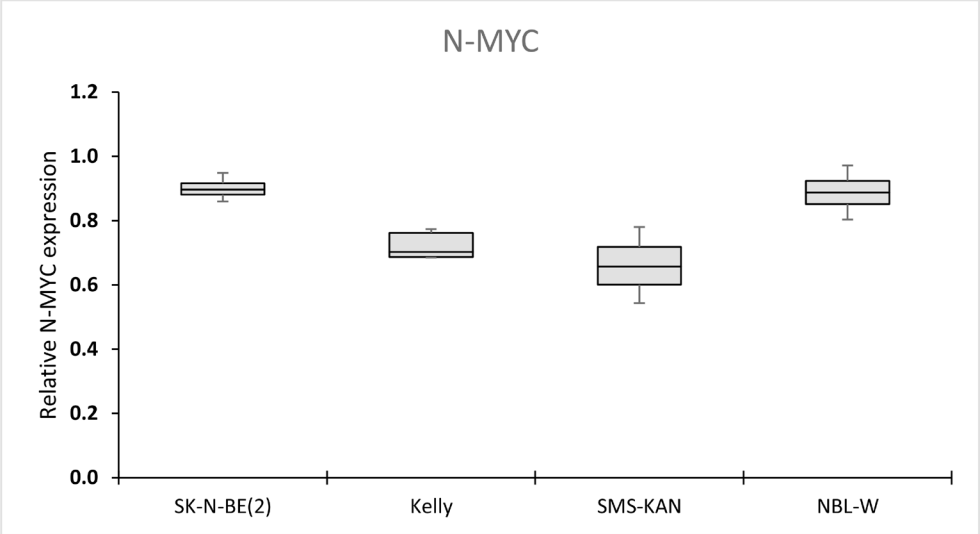

D

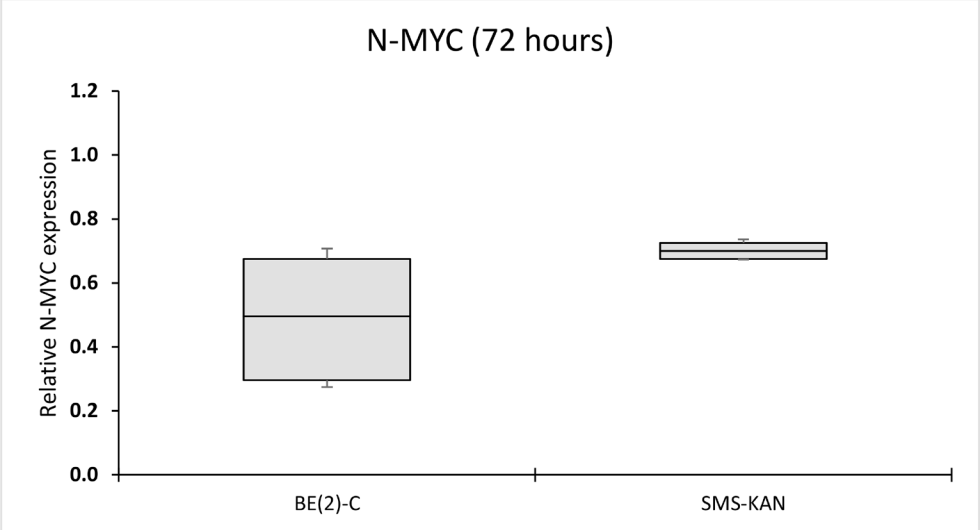

Supplementary Figure 5: MicroRNA-193b reduces the expression of cyclin D1 (**A**), MCL-1 (**B**) and N-MYC (**C** and **D**). Cells were transfected with miR-193b mimics or control mimics. 24 or 72 hours post-transfection, cells were harvested and protein expression was assessed by Western Blot. Blot intensities were quantified using ImageJ. The densitometric values were normalized to Actin. The boxplots (with median, 1st quantiles, 3rd quantile, maximum and minimum from at least two independent experiments) show protein expression of miR-193b-transfected cells relative to control-transfected cells (normalized values set to 1).

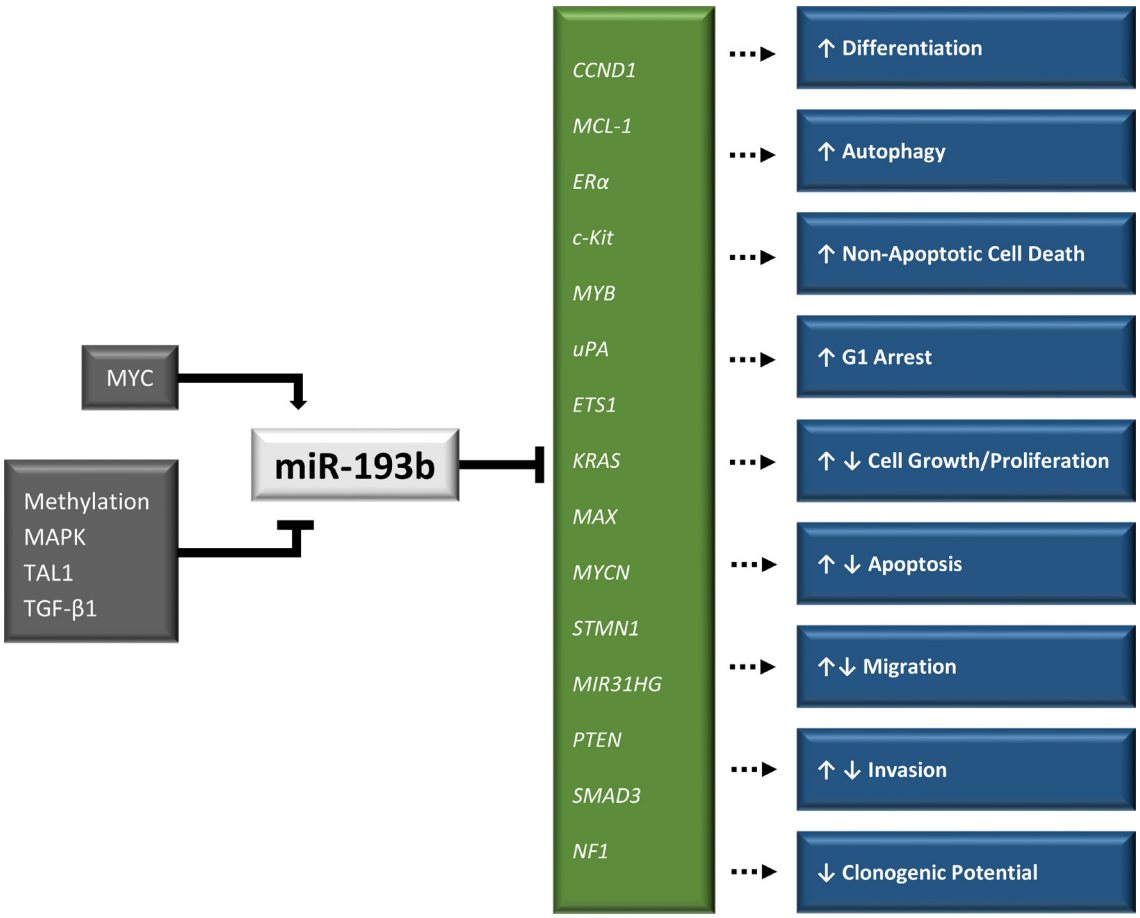

Supplementary Figure 6: Overview of miR-193b regulation and functions. MiR-193b expression is negatively regulated by gene methylation, MAPK and TGF-β1 signaling, and by TAL1, and positively regulated by MYC. MiR-193b affects multiple hallmarks of cancer by targeting numerous tumor suppressors and oncogenes.

REFERENCE

1. Ruijter JM, Ramakers C, Hoogaars WMH, Karlen Y, Bakker O, van den Hoff MJB, Moorman AFM. Amplification efficiency: linking baseline and bias in the analysis of quantitative PCR data. Nucleic Acids Res. 2009; 37:e45.

Supplementary Table 1: Low expression of miR-193b in neuroblastoma cell lines. Total RNA was isolated from cell lines, enriched for small RNAs and small RNA sequencing was performed according to Roth et al 2016.

Normalized expression values:

		SMS-KAN	SMS-KANR	CHLA-15	CHLA-20	SK-N-NE(1)	SKN-BE(2)	CHLA-122	CHLA-136	NBL-W	NBL-WR
hsa-mir-193b-3p		209,26	787,16	190,33	209,37	27,70	130,76	129,63	376,96	202,91	550,48
hsa-mir-34a-5p		1274,74	28,97	604,67	113,19	49,46	9,37	959,85	231,32	2168,31	484,34
	fold of miR-193b	6,09	0,04	3,18	0,54	1,79	0,07	7,40	0,61	10,69	0,88
hsa-miR-17-5p		38367,77	28670,41	55151,28	51455,46	8334,59	49489,85	28917,54	11829,72	4216,08	9916,90
	fold of miR-193b	183,35	36,42	289,76	245,76	300,90	378,49	223,07	31,38	20,78	18,01
hsa-miR-92a-3p		930,94	1096,73	967,22	905,83	2457,33	1022,78	551,11	3804,53	3258,26	2157,89
	fold of miR-193b	4,45	1,39	5,08	4,33	88,72	7,82	4,25	10,09	16,06	3,92

Roth SA, Knutsen E, Fiskaa T, Utnes P, Bhavsar S, Hald OH, Lokke C, Mestdagh P, Johansen SD, Flaegstad T and Einvik C. Next generation sequencing of microRNAs from isogenic neuroblastoma cell lines isolated before and after treatment. Cancer letters. 2016; 372(1):128-136

Paper 3

Exosome-like Extracellular Vesicles from *MYCN*-amplified Neuroblastoma Cells Contain Oncogenic miRNAs

BJØRN HELGE HAUG[1], ØYVIND H. HALD[2], PETER UTNES[1], SARAH A. ROTH[2], CECILIE LØKKE[2], TROND FLÆGSTAD[1,2] and CHRISTER EINVIK[1,2]

[1]*Department of Pediatrics, University-Hospital of Northern-Norway (UNN), Tromsø, Norway;*
[2]*Pediatric Research Group, Department of Clinical Medicine, University of Tromsø, Tromsø, Norway*

Abstract. *Background: In recent years, evidence has accumulated indicating that both normal and cancer cells communicate via the release and delivery of macromolecules packed into extracellular membrane vesicles. Materials and Methods: We isolated nano-sized extracellular vesicles from MYCN-amplified neuroblastoma cell lines using ultracentrifugation and exosome precipitation (Exoquick) protocols. These vesicles were characterized by transmission electron microscopy (TEM), nanoparticle tracking analysis and western blotting. Exosomal miRNA profiles were obtained using a reverse transcription-polymerase chain reaction (RT-PCR) ready-to-use panel measuring a total of 742 miRNAs. Results: In this study, we showed that MYCN-amplified neuroblastoma cell lines secrete populations of miRNAs inside small exosome-like vesicular particles. These particles were shown to be taken-up by recipient cells. By profiling the miRNA content, we demonstrated high expression of a group of established oncomirs in exosomes from two MYCN-amplified neuroblastoma cell lines. Despite the fact that other studies have demonstrated the ability of exosomal miRNAs both to repress mRNA targets and to stimulate Toll-like receptor-8 (TLR8) signaling in recipient cells, we did not observe these effects with exosomes from MYCN-amplified neuroblastoma cells. However, functional enrichment analysis reveals that mRNA targets of highly expressed exosomal miRNAs are associated with a range of cellular and molecular functions related to cell growth and cell death. Conclusion: MYCN-amplified neuroblastoma cell lines secrete exosome-like particles containing oncogenic miRNAs. This work showed for the first time that neuroblastoma cells secrete exosome-like particles containing miRNAs with potential roles in cancer progression. These findings indicate a new way for MYCN-amplified neuroblastoma cells to interact with the tumor environment.*

Correspondence to: Christer Einvik, Department of Pediatrics, University-Hospital of Northern-Norway, 9037 Tromsø, Norway, Tel: +47 77669726, e-mail: christer.einvik@uit.no

Key Words: Exosome, neuroblastoma, microRNA, miRNA.

Neuroblastoma is the most common solid tumor in children and comprises 7% of pediatric cancers. It has a clinical behavior ranging from spontaneous regression to progressive and fatal disease resistant to currently known treatments (1). In order to develop more effective treatments, a broader knowledge of neuroblastoma pathogenesis and tumor biology is needed. One of the most important prognostic factors in neuroblastoma is amplification of the *MYCN* oncogene, present in 20% of cases (1, 2). *MYCN* encodes a transcription factor (N-Myc), which contributes to a malignant phenotype through transcriptional regulation of several genes (3).

Micro-RNAs (miRNAs) are a group of small, non-coding RNAs of great importance in normal gene regulation. Aberrant miRNA expression patterns have been linked to development of many diseases, including cancer. These molecules function primarily by post-transcriptionally down-regulating gene expression by binding to the 3' untranslated region (UTR) of messenger-RNAs (mRNAs), either by inhibiting their translation or through facilitating mRNA degradation (4). *MYCN* has been demonstrated to both increase and decrease the expression of oncogenic and tumor suppressive miRNAs, respectively. Several studies have investigated the role of *MYCN* in regulating miRNAs using RNAi-based approaches in *MYCN*-amplified neuroblastoma cell lines (5, 6). Other studies have used experimental over-expression of *MYCN* as a system for differential profiling of miRNAs (7-9). While different studies suggest that *MYCN* primarily functions as a suppressor of miRNA expression, it can also trans-activate the 17-92, 106a-363, 106b-25 clusters, as well as mir-9 and mir-421 through direct promoter binding (10).

Exosomes are nano-sized extracellular membrane vesicles containing several RNA species, including mRNAs and miRNAs, as well as proteins and DNA (11). Recent studies revealed that these biological macromolecules can function in intercellular communication through exosomal trafficking

from immune cells, fibroblast and cancer cells to a range of different recipient cells (12). Exosomes originate by intraluminal budding in endosomes to form multivesicular bodies and are further transported to the cell membrane where they are released extracellularly (13). MiRNAs transported in exosomes are protected against degradation by RNases in the extracellular space and in the circulation. Exosomal miRNAs have been demonstrated not only to function through classical negative gene regulation by binding to mRNAs 3'UTR but also through stimulation of the Toll-like receptor 8 (TLR8) in humans and TLR7 in mice (14). This receptor is known to activate nuclear factor-κB (NF-kB) signaling in response to pathogen-associated RNA sequences (15). Recent investigations suggest that miRNAs, to a greater extent, allocate to multivesicular bodies with subsequent extracellular secretion when intracellular target-transcripts are scarce. In an abundance of target transcripts, miRNAs tend to favor sites associated with intracellular gene silencing (16).

Cancer cell-derived exosomes can modulate a diverse array of processes, including angiogenesis (17-19), anti-tumor immune responses (11) and metastatic potential (20-22). On the other hand, non-cancer cell-derived exosomes can also act by promoting growth inhibition of malignant cells (23).

The aim of the present study was to investigate whether miRNA-containing exosomes are secreted from *MYCN*-amplified neuroblastoma cells. We also wanted to test if exosomes could function as intercellular players in tumorigenesis by affecting gene expression in recipient cells.

In the present study, we utilize an improved protocol for culturing cells, which yield large amounts of exosomes (24). The miRNA content of exosome-like particles from two *MYCN*-amplified neuroblastoma cell lines was profiled and validated. The potency of exosomes to associate with different recipient cells and regulate target seed sequences or stimulate TLR8 signaling within recipient cells was investigated. Finally, we performed functional enrichment analyses on targets of highly expressed exosomal miRNAs. Our results indicate that exosomes derived from *MYCN*-amplified neuroblastoma cells may have important roles in tumor development.

Materials and Methods

Cell culture. All cells were cultured at 37˚C and 5% CO_2. The *MYCN*-amplified Kelly (ECACC, Porton Down, Salisbury, UK) and SK-N-BE(2)-C (kindly provided by Dr John Inge Johnsen, Karolinska Institutet, Stockholm, Sweden) neuroblastoma cell lines, as well as the non *MYCN*-amplified SK-N-AS (ATCC, Manassas, VA, USA) cell line were cultured in Roswell Park Memorial Institute medium (RPMI)-1640 containing L-glutamine and non-essential amino acids (Sigma-Aldrich, St. Luis, MO, USA). Similarly, HEK-293T (ATCC) cells were cultured in Dulbecco's modified Eagle's medium (DMEM; Sigma-Aldrich). The medium was supplemented with 10% fetal bovine serum (FBS). HEKblue-TLR8 cells (InvivoGen, San Diego, USA), stably expressing TLR8 and a reporter construct responsive to activator protein 1 (AP-1) and NF-kB activation as a readout for TLR8 stimulation, were cultured in high-glucose DMEM supplemented with 10% heat-inactivated FBS. Commercially provided HUVEC cells pooled from donors in accredited institutions (Life technologies, Carlsbad, CA, USA) were grown in medium-200 with low serum growth supplement (LSGS) (Life technologies). Consent for use of the cells in research applications was obtained from next of kin (25). Cells were split and subcultured before confluency.

The identity of the neuroblastoma cell lines used in this study was verified by short tandem repeat (STR) analysis at Center of Forensic Genetics, University of Tromsø, Tromsø, Norway. All cells used in this study were tested for mycoplasma contamination.

Isolation of exosomes. Exosome-depleted FBS was prepared by centrifugation at 4˚C over night at 170,000 ×g, followed by sterile filtration using 0.2 μm filters (Millipore Corporation, Billerica, MA 01821, USA). Exosome-free media (EFM) was prepared by addition of 10% exosome-depleted serum to RPMI-1640.

SK-N-BE(2)-C and Kelly cells were grown in Celline Adhere 1000 bioreactors (CLAD 1000) (Sigma-Aldrich) as previously described (24). The flasks have a small compartment for cells and a large compartment for media. A 10-kDa semi-permeable membrane that retains cells, exosomes and larger proteins, but allows exchange of nutrients and waste products, separates the two compartments. During exosome production, the medium compartment contained 500 ml complete RPMI-1640 and the cell compartment 15 ml EFM. Media from the cell compartment was collected for exosome isolation once a week. The compartment was then flushed vigorously 4 times using sterile 1× PBS, removing floating cells and other debris, before addition of fresh growth media to both compartments. After 4 isolations, adherent cells were trypsinized and checked for viability using PBS/0.4% Trypan blue staining. Exosomes were isolated by ultracentrifugation according to previously described protocols (26). Briefly, conditioned media was centrifuged at 200×g for 10 minutes, 2,000×g for 20 minutes, 10,000×g for 30 minutes and 110,000×g for 70 minutes to remove cells, debris and microvesicles, respectively. Unconditioned exosome-free media (EFM) was treated in parallel as a negative control. The amounts of exosomes isolated were measured using the Bio-Rad DC protein assay (Bio-Rad, Hercules, CA, USA) and stored at –80˚C or directly used in experiments.

Western blotting. Cells and exosomes were lysed in RIPA buffer (50mM Tris HCl, pH 8, 150 mM NaCl, 1% NP-40, 0.5% sodium deoxycholate, 0.1% SDS) supplemented with protease inhibitor cocktail (Roche Applied Science, Indianapolis, IN, USA). Thirty μg proteins were separated on NuPAGE 4-12% Bis-Tris Gels (Life technologies). Proteins were transferred onto Immobilon-FL polyvinylidene difluoride (PVDF) membranes (Millipore Corp., Bedford, MA, USA), blocked for 1 hour at room temperature in Odyssey Blocking Buffer (LI-COR, Lincoln, NE, USA) before incubation at 4˚C overnight with the primary antibodies CD9 sc-13118, CD63 sc-5275, GAPDH sc-25778, N-MYC sc-53113 (Santa Cruz, Dallas, TX, USA), TSG101 ab83 (Abcam, Cambridge, UK), GRP78 G8918, Actin A2066 (Sigma-Aldrich). Secondary antibodies were goat anti-rabbit IRDye800CW (Rockland, Gilbertsville, PA, USA) and goat anti-mouse Alexa Fluor 680 (Life technologies). Antibody binding was detected using the Odyssey Infrared Imaging System (LI-COR).

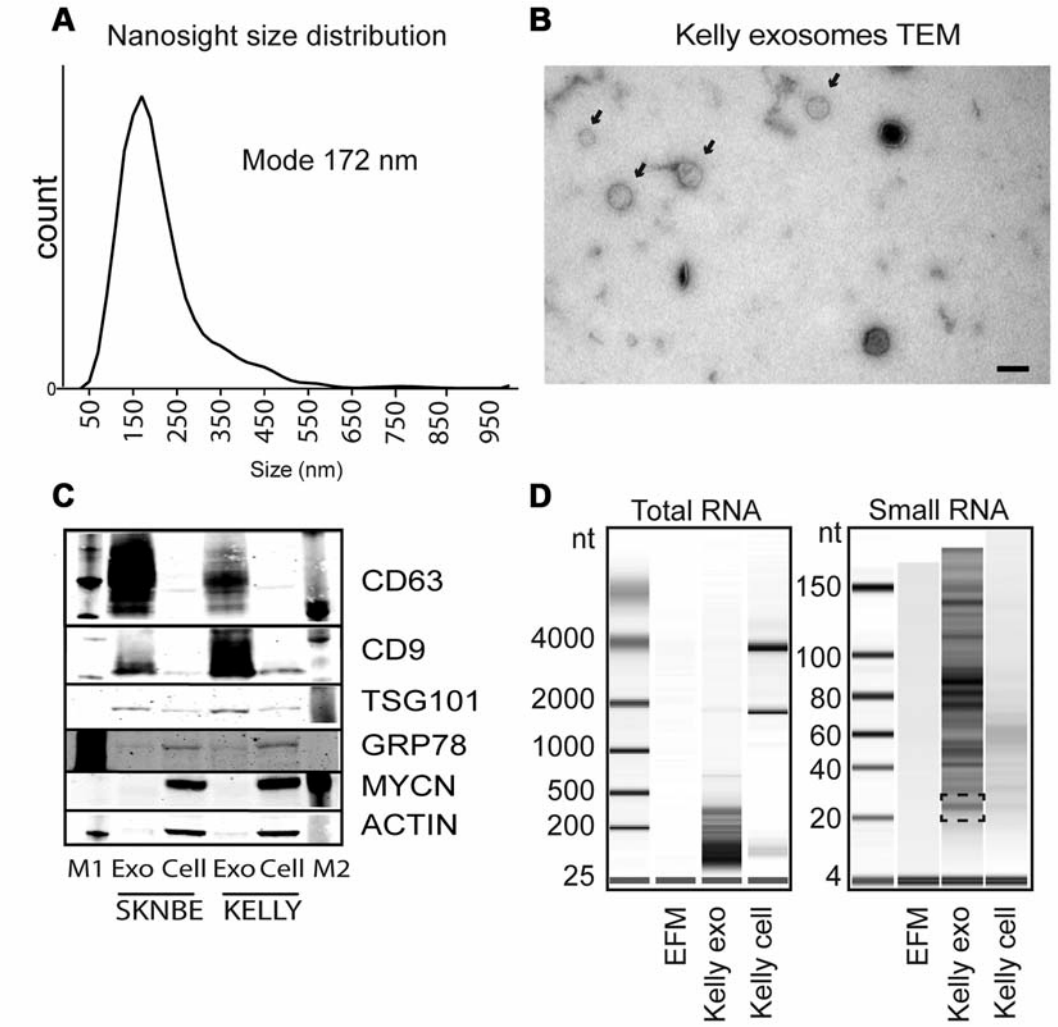

Figure 1. *Characterization of exosome isolates. A) Nanosight (nanoparticle-tracking analysis). Size distribution of isolated Kelly exosomes. B) Transmission electron microscopy (TEM) of PFA fixed exosomes on formvar grids at 80,000× magnification. The scale bar measures 100 nanometers. C) Western blotting of lysed exosomes and cells from the MYCN-amplified neuroblastoma cell lines SK-N-BE(2)–C and Kelly. The blot shows the exosomal markers CD63, CD9 and TSG101, as well as cellular GRP78, N-Myc and β-actin proteins. M1 and M2, markers. D) Analysis of total (left) and small (right) RNA fractions using the Agilent Bioanalyzer. The marker indicates nucleotide (nt) size.*

Characterization of the size and morphology of isolated particles using transmission electron microscopy (TEM) and Nanosight analysis. Exosome samples isolated by ultracentrifugation were washed, re-suspended in PBS and fixed in 2% paraformaldehyde (PFA). Subsequently, samples were loaded on formvar-coated electron microscopy (EM) grids. After washing, the samples were post-fixated in 1% gluteraldehyde. They were washed once more and, subsequently, stained in methyl cellulose-uranyl acetate for 10 min on ice. Grids were dried and examined using TEM at 80,000× magnification.

Isolated exosomes were further analyzed using the Nanosight LM10 system equipped with a 405 nm blue laser (Nanosight Ltd, Wiltshire, UK). The laser illuminated the isolated vesicles and the software recorded their movement under Brownian motion. Videos were subjected to nanoparticle tracking analysis using the provided software to acquire size distribution. All analysis parameters were kept constant within the experiments.

Profiling of exosomal miRNAs. Exosomal miRNA content was profiled from SK-N-BE(2)-C and Kelly cells. All miRNA assays were run in at least two biological isolates. Exosomes were isolated as specified and lysed in Qiazol reagent (Qiagen, Valencia, CA, USA). RNA was precipitated using isopropanol. RNA concentration was determined using the Qubit 2.0 RNA assay kit (Life technologies). The content and quality of the exosomal RNA was determined using the 2100 Bioanalyzer instrument with the small RNA and Eukaryote total RNA kits (Agilent technologies, Santa Clara, CA, USA). Forty ng total RNA was reverse transcribed using the miRCURY universal cDNA synthesis kit (Exiqon, Copenhagen, Denmark). RNA from exosomes and cells was profiled with the

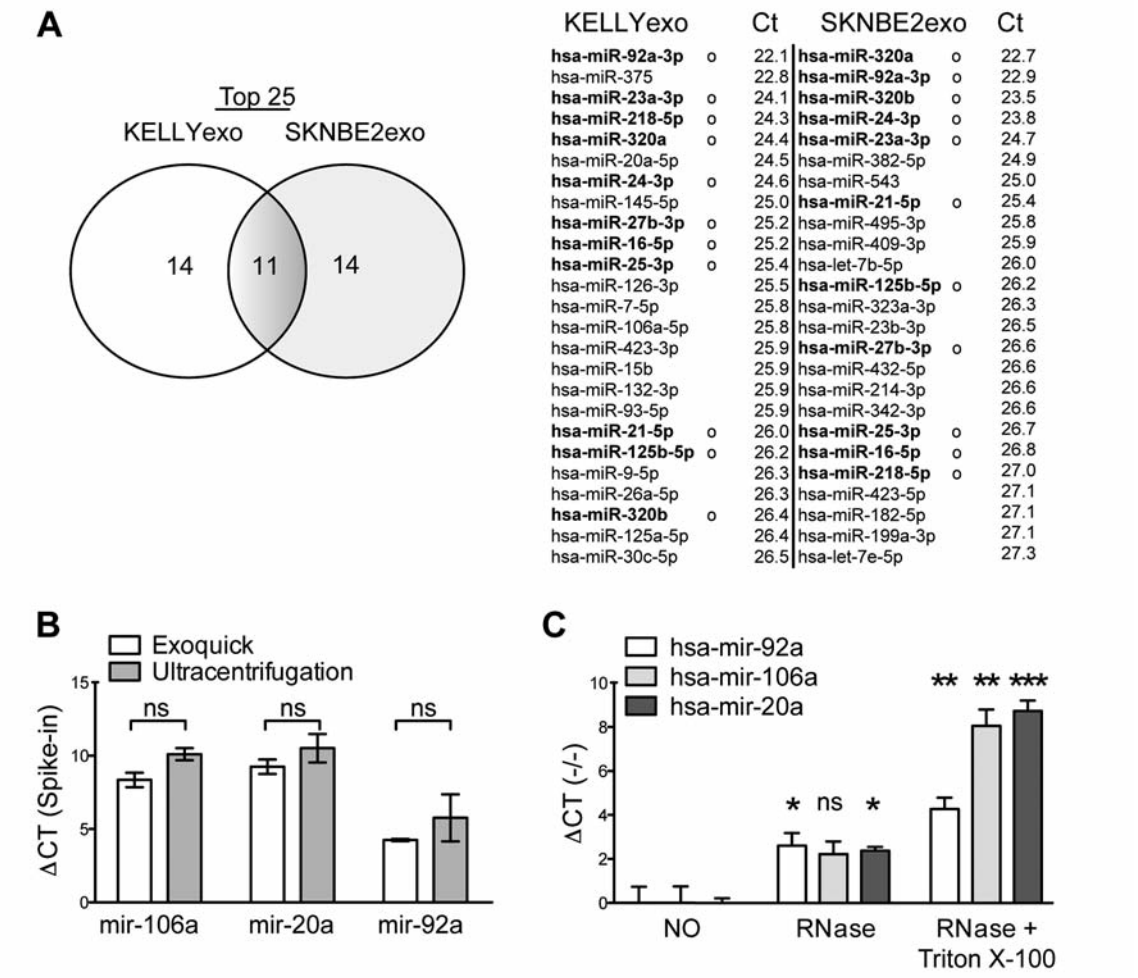

Figure 2. *miRNA expression in neuroblastoma exosome-like extracellular particles. A) Venn diagram of miRNAs expressed in exosomes from Kelly and SK-N-BE(2)-C cells (left). Average C_T values of miRNA assays in exosomal samples (right) from Kelly and SK-N-BE(2)-C cells. miRNAs commonly expressed among the top 25 in both cell lines constitute the overlapping fraction in the Venn diagram and are marked by a circle (o) in the table. B) The relative expression of three different miRNAs were measured in exosomal isolates from Kelly cell using two different isolation protocols (Exoquick and ultracentrifugation). $\Delta C_T = (C_{T\ miRNA\ assay} - C_{T\ spike\text{-}in})$. C) ΔC_T values in untreated samples (NO-set to 0), RNAse and RNase+Triton X-100 treated samples. Untreated samples were used as calibrators and set to zero. Increases in ΔC_T (compared to untreated samples-NO) indicate degradation in response to the treatment. Exosomes isolated from Kelly cells. Error bars indicate standard deviation. ns illustrates $^{*}p>0.05$, $^{**}p<0.05$, 0.01 and $^{***}p<0.001$.*

miRCURY qPCR panels 1+2 V2.M (Exiqon, Copenhagen, Denmark). ROX was included as a passive reference dye. Variations between plates were normalized using interplate calibrators and cycle threshold (C_T) values were, then, averaged between replicates. Unconditioned EFM was also profiled to determine background signal. C_T values <35 were considered detected. We included miRNA assays where the C_T value of the EFM control was >35, indicating no interfering bovine miRNAs. However, samples were included if (C_T EFM)–(C_T sample) >6.6, indicating a bovine background of less than 1% of the sample expression.

To further validate the origin of the isolated miRNAs, Kelly exosome preparations were obtained in parallel using both differential centrifugation and the Exoquick-TC polymer-based exosome precipitation solution. Exoquick isolation was performed according to the manufacturer's protocol (System Biosciences, Mountain View, CA, USA). Equal amounts of RNA were used as input and a spike in control was added before cDNA synthesis. The relation between the different isolation methods were compared and presented as ΔC_T normalized to the spike in ($C_{T\ spike\text{-}in}$-$C_{T\ miRNA}$). Individual miRNA primer assays (Exiqon) for mir-106a, mir-20a, mir-92a and a spike-in control were used to measure miRNA expression. Student's *t*-test statistics was used when comparing the isolation methods.

RNase A/Triton X-100 experiments. Equal amounts of exosomes were treated with 5 U/ml RNase A (Qiagen) in the presence or absence of 1% Triton X-100. Samples were incubated at 37˚C for 30 minutes followed by addition of Qiazol reagent. RNA was isolated and reverse transcribed as for profiling experiments. mir-

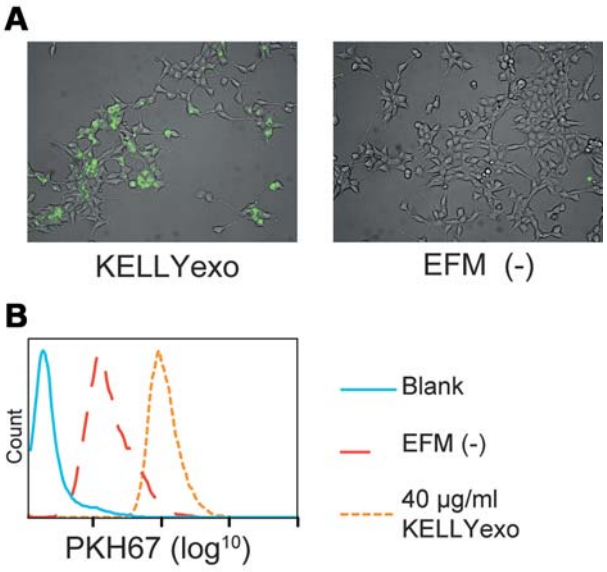

Figure 3. *Uptake of labeled exosomes in recipient cells. A) HEK-293T cells exposed to PKH67 (green)-labeled Kelly exosomes (KELLYexo) and EFM control. Pictures were taken at 400x magnification. B) Flow cytometry analysis of SK-N-AS cells exposed to fluorescent exosomes (KELLYexo) or controls (Blank=no treatment, EFM=exosome-free media).*

106a, mir-20a ,mir-92a were assayed as previously mentioned. Data are presented as ΔC_T ($C_{T\ sample}$–$C_{T\ untreated}$) using non-treated samples as calibrators. Statistical comparison of the treatments was performed using one-way ANOVA and Tukeys post-test.

Exosomal fluorescence staining and uptake. Kelly and SK-N-BE(2)-C-derived exosomes were isolated and washed in serum free RPMI-1640 to remove dye-binding proteins. The pelleted exosomes were resuspended in the provided buffer and stained with the lipophilic dye PKH67 (Sigma-Aldrich). Excess dye was inactivated using ten volumes exosome-depleted, serum containing media (EFM) and re-pelleted. Subsequently, the exosomes were washed twice in PBS, resuspended in unsubstituted medium, analyzed for protein concentration and added to recipient HEK-293T and SK-N-AS cells. Cells for microscopy and flow cytometry were exposed to 40 µg/ml exosomes. Twenty-four hours after addition, cells subjected to exosomes were examined using immunofluorescence microscopy and flow cytometry.

miRNA responsive luciferase assays. HEK-293T and SK-N-AS cells were used to measure uptake of functional miRNAs. For transfection, we used 1 µl/ml Lipofectamine 2000 (Life sciences) according to the manufacturer's instructions. Cells were co-transfected with the pMIR-report firefly-luciferase reporter vector (Promega, Madison, WI, USA) containing miRNA responsive seed sequences and the constitutively Renilla luciferase expressing vector pRL-TK (Promega). miRNA mimics targeting the relevant seed in the reporter vector and a scrambled control miRNA was used as positive and negative controls, respectively (Shanghai genepharma, Shanghai, China). The mir-92a insert was created by annealing the primers 5'-CTAGTATCTGG ACCAGGCTGTGGGTAGATGTGCAATAGAAATAGCTA-3'(sense) and 5'-AGCTTAGCTATTTCTATTGCACATCTACCCACAGCCTG GTCCAGATA-3' (antisense), corresponding to the mir-92a binding

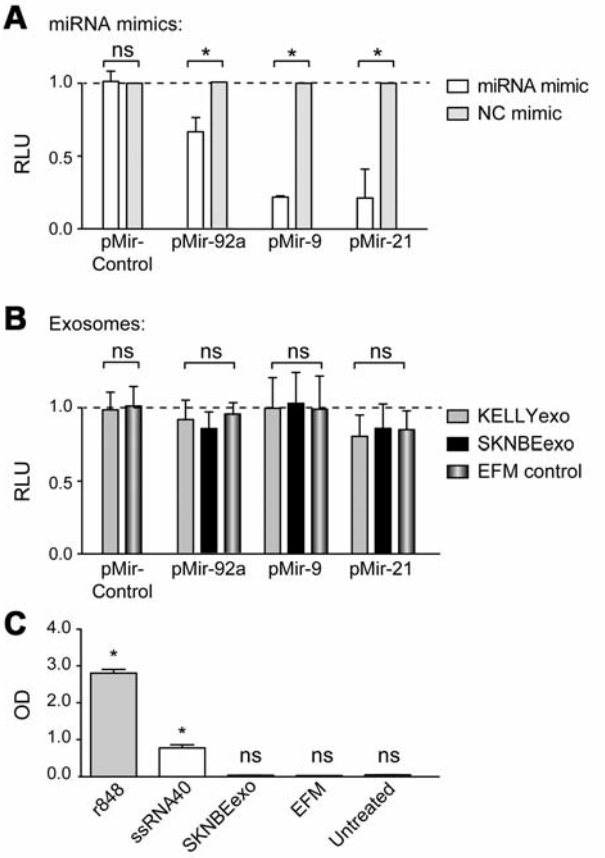

Figure 4. *Reporter activity for different exosomal miRNAs and ELISA for the mir-92 target DKK3 after treatment with exosomes. A) SK-N-AS cells expressing reporter constructs containing binding sites for no human miRNAs (pMir-Control), mir-92 (pMir-92a), mir-9 (pMir-9) and mir-21(pMir-21) were incubated with the corresponding miRNA mimics (40 pmols). Mimics without human targets (NC) (40 pmols) were used as negative controls. Luciferase activity was measured 24 h after transfection. RLU=relative luciferase units. B) Same as A, except 40 µg/ml isolated exosomes from Kelly (KELLYexo), SK-N-BE(2)-C (SKNBEexo) or control isolates (EFM control) were added to the transfected cells instead of miRNA mimics. C) Optical density (OD) measurements of culture media from HEKblue-TLR8 cells containing AP-1 and NF-kB responsive SEAP-expressing elements. Ccells were stimulated with positive controls r848 (5µg) or ssRNA40 (5µg), SK-N-BE(2)-C exosomes (SKNBEexo), EFM exosome control and untreated. Error bars indicate standard deviation. ns indicates $p>0.05$, $^{*}p<0.05$.*

site of the DKK3-3'UTR (27). The annealed primers were ligated into SpeI/HindIII-treated pMIR-Report vector to generate a mir-92a responsive firefly luciferase construct (pMIR-92a). Similarly, the pMIR-report-derived pMIR-9 (18) and pMIR-21-luc (kindly provided gift From Dr. Anders H. Lund, Copenhagen) vectors contain 3'UTR binding sites for mir-9 and mir-21 downstream of the firefly luciferase coding sequence. One-way ANOVA with Tukeys post-test was used when comparing the treatments.

TLR8 activation assay. One hundred thousand human HEKblue-TLR8 cells (Invivogen) were seeded in each 4 cm^2 well. Twenty-four hours

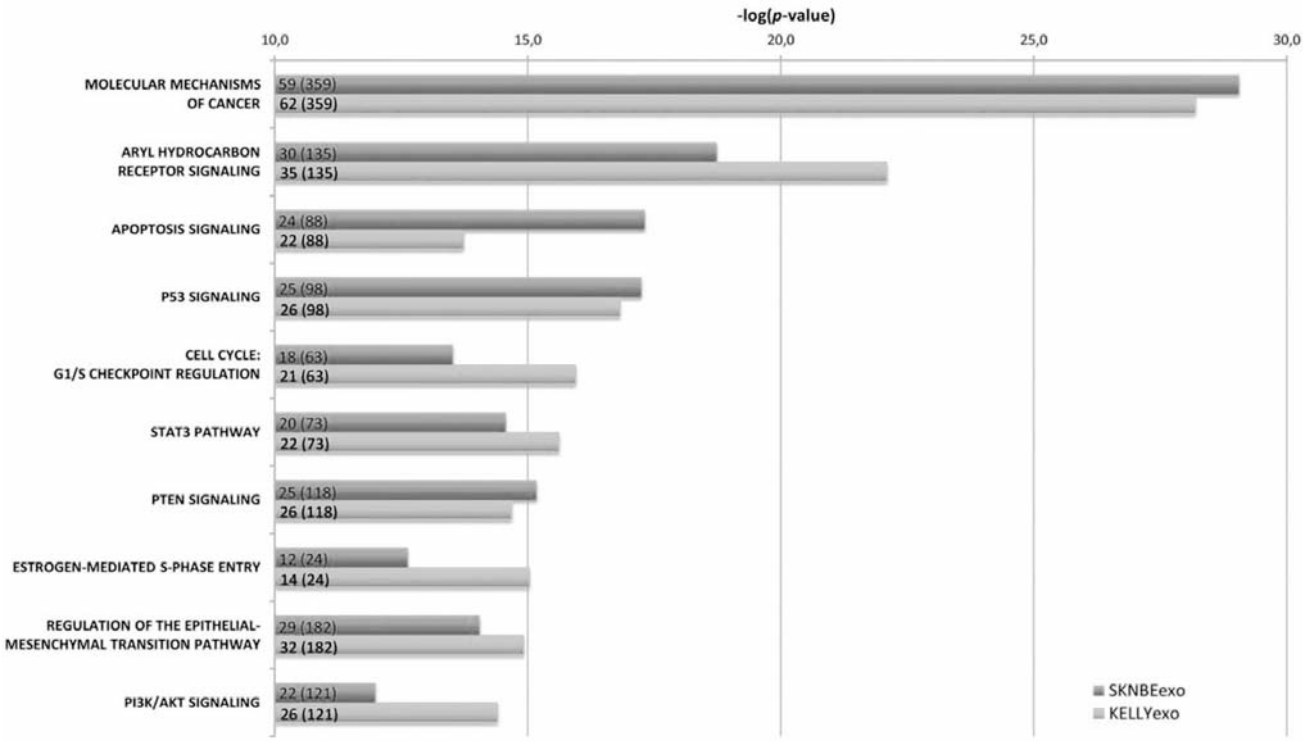

Figure 5. *Canonical pathways potentially affected by neuroblastoma exosomal miRNAs. Ingenuity pathway analysis (IPA) showing the canonical pathways that are most significantly affected by the target genes for the 25 highest expressed miRNAs isolated from SK-N-BE(2)-C and Kelly cells. The pathways are indicated on the y-axis. The x-axis indicates the significance score as negative log of p-values calculated using the Fisher's exact test. Numbers within the bars indicate identified predicted target genes to the pathway (of total genes in the pathway).*

after seeding, the cells were treated with exosomes (50 μg/ml) from SK-N-BE(2)-C cells . As positive controls, parallels were either transfected with 5 μg/ml of the viral ssRNA40 using 2 μL/ml Lipofectamine 2000 (Life sciences) or maintained in the presence of the molecular agonist R848 (5μg/ml). Twenty hours after treatment, the media was harvested and centrifuged at 21,100×g for 5 min to remove debris and secreted embryonic alkaline phosphatase (SEAP) levels in the supernatant was quantified using the QuantiBlue assay (InvivioGen, San Diego, CA 92121, USA). The data were statistically analyzed using one-way ANOVA with Tukeys post-test.

Functional enrichment analysis. Potential targets for the 25 highest expressed exosomal miRNAs were predicted using the Ingenuity Pathway Analysis (IPA) software (Ingenuity Systems, Redwood City, CA, USA). Here, three miRNA-mRNA interaction algorithms were used (TargetScan, TarBase and miRecords) and, to limit the total number of predicted mRNA targets, only the experimentally validated targets were selected for further analysis. The relationships among the predicted targets were also analyzed using IPA. Core analyses, filtered to use the Ingenuity Knowledge Base reference set with all human tissue and cell lines, were performed separately on each set of predicted miRNA targets. Finally, a comparison analysis was performed to identify common biological functions and canonical pathways predicted to be affected by exosomal miRNAs isolated from both SK-N-BE(2)-C and Kelly neuroblastoma cell lines.

Results

MYCN-amplified neuroblastoma-derived particles exhibit exosome-like characteristics. To determine if *MYCN*-amplified neuroblastoma cells secrete exosome-like vesicles, we isolated extracellular vesicles by a standard ultracentrifugation protocol from *in vitro* cultured Kelly and SK-N-BE(2)-C cells. Transmission electron microscopy and Nanosight size distribution analysis demonstrated a population of small circular particles between 50 to 350 nm, with a mode of 172 nm (Figure 1A and B). The EFM control media did not contain measurable levels of particles (data not shown). Western blot analysis demonstrated a striking enrichment of the tetraspanin exosomal markers CD63 and CD9. A more modest enrichment of another exosomal marker, TSG101, was seen. In contrast, the endoplasmic reticulum marker GRP78, the cytoskeletal component β-actin and the N-myc protein were almost exclusively detected in cellular lysates (Figure 1C). RNA composition analysis using a Bioanalyzer revealed that the exosome-like particles were highly enriched in small RNAs less than 300-400 nucleotides (nt). In contrast to cellular RNA, they also lacked cellular 18S and 28S ribosomal peaks, identifying the RNA composition

Table I. *IPA pathway analysis of neuroblastoma exosomal miRNA targets genes. Enriched functional categories as reported by IPA from the target genes for the 25 highest expressed miRNAs isolated from SK-N-BE(2)-C and Kelly cells. Number of molecules indicates potential miRNA target genes linked to each category. Range p-value shows the lowest and highest p-values from all under-categories.*

Category	Analyzed exosomal miRNAs	Molecules	Range *p*-values
Cellular development	KELLYexo	226	1.6E-53-1.2E-07
	SKNBEexo	185	8.6E-42-4.2E-07
Cellular growth and proliferation	KELLYexo	242	1.6E-53-1.2E-07
	SKNBEexo	206	8.6E-42-3.5E-07
Cell death and survival	KELLYexo	227	2.8E-47-1.4E-07
	SKNBEexo	191	1.2E-35-4.5E-07
Cellular movement	KELLYexo	161	5.6E-37-1.2E-07
	SKNBEexo	123	2.7E-26-3.9E-07
Cell cycle	KELLYexo	134	1.8E-32-1.6E-07
	SKNBEexo	123	4.2E-32-3.5E-07

as fundamentally different from their cells of origin (Figure 1 D, left panel). Analysis of small RNAs revealed a population of RNAs at about 23 nt, consistent with the expected size of miRNAs. In combination, these results confirm successful isolation of exosome-like particles from neuroblastoma cells.

MYCN-amplified neuroblastoma cells secrete exosome-like particles with a distinct miRNAs content. The miRNA content of exosome-like particles from *MYCN*-amplified neuroblastoma cell lines Kelly and SK-N-BE(2)-C was investigated using LNA-qPCR arrays. The top 25 expressed exosomal miRNAs isolated from both cell lines were compared and 11 of the exosomal miRNAs identified (mir-16, 125b, 21, 23a, 24, 25, 27b, 218, 320a, 320b and 92a) were common to both cell lines (Figure 2A, marked by circles).

To validate the origin of the assayed miRNAs, we compared the expression of three different miRNAs from Kelly exosomes using two different exosome isolation protocols. The Exoquick-TC and the ultracentrifugation exosome-isolates had almost identical expression of the three assayed miRNAs, mir-20a, mir-92a and mir-106b (Figure 2B). Furthermore, we investigated whether the secreted miRNAs were in fact resistant to RNase mediated degradation. Kelly-derived exosomes were treated with RNase in the presence or absence of Triton X-100 and the levels of mir-20a, mir-92a and mir-106b were quantified. A similar level of partial degradation across all samples was present when adding RNase A to the exosome suspension, while the degradation was further enhanced by addition of the detergent 1% Triton-×100 (Figure 2C).

Collectively, these results strongly suggest that the miRNAs investigated are indeed present within the isolated exosome-like particles.

Neuroblastoma exosomes associate with various recipient cells. To investigate if recipient cells take-up the isolated exosome-like particles, fluorescently labeled exosomes were added to cultured HEK-293T cells and tracked by microscopy. HEK-293T cells displayed significant uptake of labeled Kelly-derived exosomes after 24 h co-incubation (Figure 3A). Flow cytometry analysis of SK-N-AS (Figure 3B) cells similarly demonstrated exosome uptake, as measured by increased recipient cell fluorescence. Similar uptake in other cell lines tested, including HUVEC, SK-N-BE(2)-C and Kelly cell lines, was verified by both fluorescence microscopy and flow cytometry suggesting a wide range of potential recipient cells, including an autocrine uptake.

Exosomal miRNAs do not repress target gene expression or activate the endosomal TLR8 receptor in recipient cells. Mir-92a was the most highly expressed miRNA when considering exosomes from both cell lines examined. To investigate whether miRNA-containing exosomes could regulate established 3'UTR target seed-sequences in recipient cells, we transfected cells with miRNA sensing luciferase reporter vectors. Luciferase activity was significantly reduced after co-transfection with purified miRNA mimics (Figure 4A). However, we did not observe any significant differences in luciferase activity using mir-92a (pMIR-92a), mir-9 (pMIR-9) and mir-21 (pMIR-21-luc) responsive constructs when exposing SK-N-AS or HEK-293T cells to 40 μg/ml Kelly or SK-N-BE(2)-C exosomes. (Figure 4A).

Finally, we tested the recent finding that exosomal miRNAs may induce NF-kB activation through TLR8 activation. We stimulated HEKblue-TLR8 cells stably transfected with TLR8 and NF-kB/AP-1 SEAP reporter constructs with exosomes and controls. In contrast to the positive controls ssRNA40 and r848, SK-N-BE(2)-C exosomes did not give significant increases in SEAP levels compared to untreated cells (Figure 4C).

Functional enrichment analysis indicates that miRNAs from neuroblastoma exosomes are associated with signal pathways important for cell growth, survival and death. To evaluate the functions of miRNAs from neuroblastoma cell-derived exosomes, we used the IPA software to predict mRNA targets and performed a functional enrichment analysis on these predicted targets.

The 25 most abundantly expressed miRNAs from Kelly and SK-N-BE(2)-C exosomes were predicted to target 565 and 499 experimentally observed mRNAs, respectively. Furthermore, when these mRNAs were analyzed for functional categories, a range of cellular and molecular functions related to cell development, growth and death were identified (Table I).

When IPA was further used to analyze canonical pathways, we identified "Molecular Mechanisms of Cancer" (SKNBE2exo: $p=8.8\times10^{-30}$ n=59, KELLYexo: $p=6.4\times10^{-29}$ n=62), in addition to several well-characterized pathways like

aryl hydrocarbon receptor- (SKNBE2exo: $p=1.9\times10^{-19}$ n=30, KELLYexo: $p=8.0\times10^{-23}$ n=35), apoptosis- (SKNBE2exo: $p=4.9\times10^{-18}$ n=24, KELLYexo: $p=1.9\times10^{-14}$ n=22), p53- (SKNBE2exo: $p=5.7\times10^{-18}$ n=25, KELLYexo: $p=1.5\times10^{-17}$ n=26), cell cycle (G1/S checkpoint)- (SKNBE2exo: $p=3.0\times10^{-14}$ n=18, KELLYexo: $p=1.1\times10^{-16}$ n=21), STAT3- (SKNBE2exo: $p=2.7\times10^{-15}$ n=20, KELLYexo: $p=2.4\times10^{-16}$ n=22) and PTEN- (SKNBE2exo: $p=6.7\times10^{-16}$ n=25, KELLYexo: $p=2.1\times10^{-15}$ n=26) signaling, to be the most significantly enriched pathways by the predicted miRNA targets (Figure 5). The full list of putative targets related to all significant pathways for both SK-N-BE(2)-c and Kelly exosomal miRNAs can be provided upon request.

Discussion

The aim of our study was to identify and profile exosomal miRNAs from *MYCN*-amplified neuroblastoma cells and to investigate their role in intercellular signaling by tumor cells.

The present data show that *MYCN*-amplified neuroblastoma cells secrete a population of small vesicles exhibiting the characteristics of exosomes. Enrichment of established exosomal markers like CD63, CD9 and TSG101, and absence of intracellular GRP78, β-actin and N-myc proteins provide further support for this conclusion. Previously, a full proteomic analysis of neuroblastoma-derived exosomes showed that, in addition to the exosomal markers, exosomes from neuroblastoma cells, also express proteins involved in defense response, cell differentiation, cell proliferation and regulation of other important biological processes, including the neuroblastoma specific marker GD2 disialoganglioside (28).

To further characterize the secreted vesicles, we performed nanoparticle tracking analysis using Nanosight and TEM and showed a size distribution of these particles similar to that found in exosome isolates (29-31). In addition, the enrichment in small RNAs and relatively low content of ribosomal RNA is also a previously described trait of exosomes. The RNA profiles identified in our samples match the findings in the two most in-depth descriptions of exosomal RNA content (32, 33). The authors of these articles used deep sequencing approaches and identified significant enrichments of small RNAs not restricted to and, in fact, not dominated by miRNAs. They also observed large amounts of Y-RNAs in the exosomes. We incidentally discovered high expression of a Y-RNA, previously believed to be a miRNA (mir-1979) (34) in exosomes from both Kelly and SK-N-BE(2)-C (average C_T of 22.2 and 21.1, respectively). The RNA distribution profiles of our exosome preparations clearly indicate larger populations of small RNAs in addition to the observed band corresponding to the size of miRNAs (20-25 nt). These different RNAs may have yet un-identified important functions. Deep sequencing approaches could be utilized in order to map for the complete transcriptome of these small vesicles.

By profiling the exosomal miRNA content, we identified a population of 11 miRNAs highly expressed from both screened cell lines. These miRNAs included several known oncogenic miRNAs. Recipient cells were associated with fluorescently stained exosomes after 24 h co-incubation, indicating uptake. However, luciferase reporter studies on mir-92a, mir-9 and mir-21 in cells exposed to exosomes did not yield any reduction in reporter activity in recipient cells. This was the case, even after addition of 40 μg/ml neuroblastoma exosomes, compared to 12.5 μg/ml exosomes in a comparable study (35).

Our experiments indicate that exosomal mir-92a, mir-9 and mir-21 do not have functional effects on established mRNA 3'UTR seed targets in the tested recipient cells, at least not without some co-stimulatory factor not yet identified. The recent finding that exosomal miRNAs can stimulate NF-kB signaling through binding and activating TLR8 in cellular endosomal compartments does not seem to be relevant with exosomes from *MYCN*-amplified neuroblastoma cells.

In order to obtain information regarding the potential role of the neuroblastoma-derived exosomal miRNAs, we performed a functional enrichment analysis using predicted mRNA target genes from the 25 highest expressed miRNAs. One of the highest scores was obtained for AHR signaling, shown to be involved in multiple aspects of cancer like survival, proliferation, differentiation, apoptosis, angiogenesis and invasion, reviewed in Feng *et al*. (36). Very recent data suggest that AHR is inversely correlated to *MYCN* expression in neuroblastoma tissue. Ectopic over-expression of AHR suppressed *MYCN* promoter activity resulting in down-regulation of *MYCN* expression, while AHR shRNA promoted the expression of *E2F1* and *MYCN* in neuroblastoma cells. AHR was suggested to be an important upstream regulator of *MYCN* (37).

The analyses further revealed that several canonical pathways known to be deregulated in most cancers are potentially impacted by the exosomal miRNAs. These include apoptosis-, p53- and G_1/S checkpoint regulation signaling. Aberrant STAT3 signaling is well-known to promote initiation and progression of several human cancers by either promotion of cell proliferation, survival, invasion, metastasis and angiogenesis, or inhibiting apoptosis (38). Recently, a critical role for STAT3 in metastatic drug resistant neuroblastoma was documented (39). Several reports during the last years have also established the importance of PTEN/PI3K/Akt signaling, including its relation to *MYCN*, in neuroblastoma survival, proliferation, invasion and angiogenesis (40-43).

The trophism and uptake of exosomes into different cells have been debated, but is believed to involve surface receptors (13). In contrast to other studies demonstrating direct seed interaction by exosomal miRNAs, we were not able to show any significant effects in recipient cells using our miRNA

reporter assays. A recent study performed on immune cells demonstrated that exosome substitution alone was not enough for effects on miRNA reporters in recipient cells. Cell-to-cell contact and the subsequent formation of an immunological synapse were required for functional transmission of functionally active miRNA contents (44). Another recent study demonstrates that the lipid raft-associated Caveolin1 (CAV1) can inhibit uptake and function of exosomes by inhibiting ERK1/2 (29). It has also been demonstrated that phagocytic cells have a high uptake of exosomes, while the non-phagocytic cells only associate with exosomes without internalizing them (45). Considering these observations, it is not unlikely that the cell systems used in our studies lack the specific prerequisite conditions for exosomal miRNA function.

Conclusion

In this article, we present data demonstrating the secretion of exosome-like particles from two well-studied *MYCN*-amplified neuroblastoma cell lines. The exosomes are internalized into recipient cells and contain miRNAs with known oncogenic properties. Exosomal miRNAs may have roles in cell-to-cell signaling in neuroblastoma pathogenesis. However, our data do not support the theory that this happens through miRNA-seed sequence interaction or by activating the TLR8 receptor, as previously described in model systems of other cancers.

Acknowledgements

This work was supported by grants from the Northern-Norwegian Health Authorities (gene therapy program) and the Norwegian Cancer Society (Ragnvarda F. Sørvik and Håkon Starheims Foundation).

References

1 Maris JM, Hogarty MD, Bagatell R and Cohn SL: Neuroblastoma. Lancet *369*: 2106-2120, 2007.
2 Schwab M, Alitalo K, Klempnauer KH, Varmus HE, Bishop JM, Gilbert F, Brodeur G, Goldstein M and Trent J: Amplified DNA with limited homology to myc cellular oncogene is shared by human neuroblastoma cell lines and a neuroblastoma tumour. Nature *305*: 245-248, 1983.
3 Cheung L, Murray JE, Haber M and Norris MD: The MYCN Oncogene. *In*: Oncogene and Cancer-From Bench to Clinic. Siregar Y (ed.). InTech, pp 437-454, 2013.
4 Bartel DP: MicroRNAs: target recognition and regulatory functions. Cell *136*: 215-233, 2009.
5 Chen Y and Stallings RL: Differential patterns of microRNA expression in neuroblastoma are correlated with prognosis, differentiation, and apoptosis. Cancer Res *67*: 976-983, 2007.
6 Buechner J, Henriksen JR, Haug BH, Tømte E, Flaegstad T and Einvik C: Inhibition of mir-21, which is up-regulated during MYCN knockdown-mediated differentiation, does not prevent differentiation of neuroblastoma cells. Differentiation *81*: 25-34, 2011.
7 Lovén J, Zinin N, Wahlström T, Müller I, Brodin P, Fredlund E, Ribacke U, Pivarcsi A, Påhlman S and Henriksson M: MYCN-regulated microRNAs repress estrogen receptor-alpha (ESR1) expression and neuronal differentiation in human neuroblastoma. Proc Natl Acad Sci USA *107*: 1553-1558, 2010.
8 Shohet JM, Ghosh R, Coarfa C, Ludwig A, Benham AL, Chen Z, Patterson DM, Barbieri E, Mestdagh P, Sikorski DN, Milosavljevic A, Kim ES and Gunaratne PH: A genome-wide search for promoters that respond to increased MYCN reveals both new oncogenic and tumor suppressor microRNAs associated with aggressive neuroblastoma. Cancer Res *71*: 3841-3851, 2011.
9 Ma L, Young J, Prabhala H, Pan E, Mestdagh P, Muth D, Teruya-Feldstein J, Reinhardt F, Onder TT, Valastyan S, Westermann F, Speleman F, Vandesompele J and Weinberg R a: miR-9, a MYC/MYCN-activated microRNA, regulates E-cadherin and cancer metastasis. Nat Cell Biol *12*: 247-256, 2010.
10 Buechner J and Einvik C: N-myc and Noncoding RNAs in Neuroblastoma. Mol Cancer Res: 1243-1253, 2012.
11 Bobrie A, Colombo M, Raposo G and Théry C: Exosome secretion: molecular mechanisms and roles in immune responses. Traffic *12*: 1659-1668, 2011.
12 Valadi H, Ekström K, Bossios A, Sjöstrand M, Lee JJ and Lötvall JO: Exosome-mediated transfer of mRNAs and microRNAs is a novel mechanism of genetic exchange between cells. Nat Cell Biol *9*: 654-659, 2007.
13 Raposo G and Stoorvogel W: Extracellular vesicles: Exosomes, microvesicles, and friends. J Cell Biol *200*: 373-383, 2013.
14 Fabbri M, Paone A, Calore F, Galli R, Gaudio E, Santhanam R, Lovat F, Fadda P, Mao C, Nuovo GJ, Zanesi N, Crawford M, Ozer GH, Wernicke D, Alder H, Caligiuri MA, Nana-Sinkam P, Perrotti D and Croce CM: MicroRNAs bind to Toll-like receptors to induce prometastatic inflammatory response. Proc Natl Acad Sci USA *109*: E2110-2116, 2012.
15 Cervantes JL, Weinerman B, Basole C and Salazar JC: TLR8: the forgotten relative revindicated. Cell Mol Immunol 9: 434-438, 2012.
16 Squadrito ML, Baer C, Burdet F, Maderna C, Gilfillan GD, Lyle R, Ibberson M and De Palma M: Endogenous RNAs Modulate MicroRNA Sorting to Exosomes and Transfer to Acceptor Cells. Cell Rep: 1-15, 2014.
17 Nazarenko I, Rana S, Baumann A, McAlear J, Hellwig A, Trendelenburg M, Lochnit G, Preissner KT and Zöller M: Cell surface tetraspanin Tspan8 contributes to molecular pathways of exosome-induced endothelial cell activation. Cancer Res *70*: 1668-1678, 2010.
18 Zhuang G, Wu X, Jiang Z, Kasman I, Yao J, Guan Y, Oeh J, Modrusan Z, Bais C, Sampath D and Ferrara N: Tumour-secreted miR-9 promotes endothelial cell migration and angiogenesis by activating the JAK-STAT pathway. EMBO J: 1-11, 2012.
19 Umezu T, Ohyashiki K, Kuroda M and Ohyashiki JH: Leukemia cell to endothelial cell communication *via* exosomal miRNAs. Oncogene: 1-9, 2012.
20 Peinado H, Alečković M, Lavotshkin S, Matei I, Costa-Silva B, Moreno-Bueno G, Hergueta-Redondo M, Williams C, García-Santos G, Ghajar CM, Nitadori-Hoshino A, Hoffman C, Badal K, Garcia B a, Callahan MK, Yuan J, Martins VR, Skog J, Kaplan RN, Brady MS, Wolchok JD, Chapman PB, Kang Y, Bromberg J and Lyden D: Melanoma exosomes educate bone marrow progenitor cells toward a pro-metastatic phenotype through MET. Nat Med *18*: 883-891, 2012.

21 Luga V, Zhang L, Viloria-Petit AM, Ogunjimi AA, Inanlou MR, Chiu E, Buchanan M, Hosein AN, Basik M and Wrana JL: Exosomes mediate stromal mobilization of autocrine Wnt-PCP signaling in breast cancer cell migration. Cell *151*: 1542-1556, 2012.

22 Kogure T, Lin W-L, Yan IK, Braconi C and Patel T: Intercellular nanovesicle-mediated microRNA transfer: a mechanism of environmental modulation of hepatocellular cancer cell growth. Hepatology *54*: 1237-1248, 2011.

23 Kosaka N, Iguchi H, Yoshioka Y, Hagiwara K, Takeshita F and Ochiya T: Competitive interactions of cancer cells and normal cells *via* secretory microRNAs. J Biol Chem *287*: 1397-1405, 2012.

24 Mitchell JP, Court J, Mason MD, Tabi Z and Clayton A: Increased exosome production from tumour cell cultures using the Integra CELLine Culture System. J Immunol Methods *335*: 98-105, 2008.

25 Life Technologies: Certificate of analysis. 887799: 1, 2011. Available from: http://tools.lifetechnologies.com/Content/SFS/COAPDFs/2011/887799_C0155C.pdf.

26 Rani S, Brien KO, Kelleher FC, Corcoran C, Germano S, Radomski MW, Crown J and Driscoll LO: Isolation of Exosomes for Subsequent mRNA, MicroRNA, and Protein Profilin. *In*: Methods. O'Driscoll L (ed.). Totowa, NJ, Humana Press, pp 181-195, 2011.

27 Haug BH, Henriksen JR, Buechner J, Geerts D, Tømte E, Kogner P, Martinsson T, Flægstad T, Sveinbjørnsson B and Einvik C: MYCN-regulated miRNA-92 inhibits secretion of the tumor suppressor DICKKOPF-3 (DKK3) in neuroblastoma. Carcinogenesis *32*: 1005-1012, 2011.

28 Marimpietri D, Petretto A, Raffaghello L, Pezzolo A, Gagliani C, Tacchetti C, Mauri P, Melioli G and Pistoia V: Proteome profiling of neuroblastoma-derived exosomes reveal the expression of proteins potentially involved in tumor progression. PLoS One *8*: e75054, 2013.

29 Svensson KJ, Christianson HC, Wittrup A, Bourseau-Guilmain E, Lindqvist E, Svensson LM, Morgelin M and Belting M: Exosome uptake depends on ERK1/2-heat shock protein 27 signalling and lipid raft-mediated endocytosis negatively regulated by caveolin-1. J Biol Chem *288*: 17713-17724, 2013.

30 Garnier D, Magnus N, Lee TH, Bentley V, Meehan B, Milsom C, Montermini L, Kislinger T and Rak J: Cancer cells induced to express mesenchymal phenotype release exosome-like extracellular vesicles carrying tissue factor. J Biol Chem *287*: 43565-43572, 2012.

31 Kucharzewska P, Christianson HC, Welch JE, Svensson KJ, Fredlund E, Ringnér M, Mörgelin M, Bourseau-Guilmain E, Bengzon J and Belting M: Exosomes reflect the hypoxic status of glioma cells and mediate hypoxia-dependent activation of vascular cells during tumor development. Proc Natl Acad Sci USA *110*: 7312-7317, 2013.

32 Bellingham S a, Coleman BM and Hill AF: Small RNA deep sequencing reveals a distinct miRNA signature released in exosomes from prion-infected neuronal cells. Nucleic Acids Res *40*: 10937-10949, 2012.

33 Nolte-'t Hoen ENM, Buermans HPJ, Waasdorp M, Stoorvogel W, Wauben MHM and 't Hoen P a C: Deep sequencing of RNA from immune cell-derived vesicles uncovers the selective incorporation of small non-coding RNA biotypes with potential regulatory functions. Nucleic Acids Res *40*: 9272-9285, 2012.

34 Meiri E, Levy A, Benjamin H, Ben-David M, Cohen L, Dov A, Dromi N, Elyakim E, Yerushalmi N, Zion O, Lithwick-Yanai G and Sitbon E: Discovery of microRNAs and other small RNAs in solid tumors. Nucleic Acids Res *38*: 6234-6246, 2010.

35 Montecalvo A, Larregina AT, Shufesky WJ, Stolz DB, Sullivan MLG, Karlsson JM, Baty CJ, Gibson G a, Erdos G, Wang Z, Milosevic J, Tkacheva O a, Divito SJ, Jordan R, Lyons-Weiler J, Watkins SC and Morelli AE: Mechanism of transfer of functional microRNAs between mouse dendritic cells *via* exosomes. Blood *119*: 756-766, 2012.

36 Feng S, Cao Z and Wang X: Role of aryl hydrocarbon receptor in cancer. Biochim Biophys Acta *1836*: 197-210, 2013.

37 Wu P-Y, Liao Y-F, Juan H-F, Huang H-C, Wang B-J, Lu Y-L, Yu I-S, Shih Y-Y, Jeng Y-M, Hsu W-M and Lee H: Aryl hydrocarbon receptor downregulates MYCN expression and promotes cell differentiation of neuroblastoma. PLoS One *9*: e88795, 2014.

38 Siveen KS, Sikka S, Surana R, Dai X, Zhang J, Kumar AP, Tan BKH, Sethi G and Bishayee A: Targeting the STAT3 signaling pathway in cancer: role of synthetic and natural inhibitors. Biochim Biophys Acta *1845*: 136-154, 2014.

39 Ara T, Nakata R, Sheard MA, Shimada H, Buettner R, Groshen SG, Ji L, Yu H, Jove R, Seeger RC and DeClerck YA: Critical role of STAT3 in IL-6-mediated drug resistance in human neuroblastoma. Cancer Res *73*: 3852-3864, 2013.

40 Peirce SK, Findley HW, Prince C, Dasgupta A, Cooper T and Durden DL: The PI-3 kinase-Akt-MDM2-survivin signaling axis in high-risk neuroblastoma: a target for PI-3 kinase inhibitor intervention. Cancer Chemother Pharmacol *68*: 325-335, 2011.

41 Hogarty MD and Maris JM: PI3King on MYCN to improve neuroblastoma therapeutics. Cancer Cell *21*: 145-147, 2012.

42 Megison ML, Gillory LA and Beierle EA: Cell survival signaling in neuroblastoma. Anticancer Agents Med Chem *13*: 563-575, 2013.

43 Qiao J, Lee S, Paul P, Qiao L, Taylor CJ, Schlegel C, Colon NC and Chung DH: Akt2 regulates metastatic potential in neuroblastoma. PLoS One *8*: e56382, 2013.

44 Mittelbrunn M, Gutiérrez-Vázquez C, Villarroya-Beltri C, González S, Sánchez-Cabo F, González MÁ, Bernad A and Sánchez-Madrid F: Unidirectional transfer of microRNA-loaded exosomes from T cells to antigen-presenting cells. Nat Commun *2*: 282, 2011.

45 Feng D, Zhao W-L, Ye Y-Y, Bai X-C, Liu R-Q, Chang L-F, Zhou Q and Sui S-F: Cellular internalization of exosomes occurs through phagocytosis. Traffic *11*: 675-687, 2010.

Received January 26, 2015
Revised February 6, 2015
Accepted February 9, 2015